Investigating mitochondrial trafficking within dopaminergic neurons of the nigrostriatal pathway

Nishani Jeyapalan

This thesis is submitted for the degree of Doctor of Philosophy at Newcastle University

Institute of Neuroscience

Wellcome Trust Centre of Mitochondrial Research Group

October 2019

For Dad and Grandad, thank you for everything.

Abstract

Parkinson's disease (PD) is an age-related neurodegenerative disorder affecting more than 1% of the population aged over 60 years of age. PD is characterised by the loss of dopaminergic (DAergic) neurons from the substantia nigra pars compacta (SNpc), with mitochondrial dysfunction believed to be a contributor to this degeneration. The finding that complex I deficits can trigger Parkinsonism in the 1980s, has resulted in growing evidence of mitochondrial impairment in PD and ageing. Alongside the finding that SNpc neurons exhibit increased mtDNA deletion levels, these data suggest mitochondrial defects render them highly vulnerable in PD. These large scale mtDNA deletions have also been associated with the DAergic neuronal loss seen in normal ageing.

Mitochondria are dynamic organelles, whose distribution is regulated by organelle transport to balance the energy needs of neurons. Axonal mitochondria travel long and short distances and genetic mutations in the machinery which controls these movements have been identified in early onset PD. Fundamental insight into the mitochondrial transport system has arisen from yeast and fly models, the effects however of altered mitochondrial movement on neuronal function still remain unanswered with a mammalian PD model.

Hence, this study investigated mitochondrial trafficking within neurons via two disease models. The first involved the optimisation of a method to observe the movements of fluorescently tagged mitochondria within DAergic neurons in *ex vivo* nigrostriatal brain slices. Young and old mice were studied to understand the effects of age on these movements. Changes in these movements in the presence of PD pathology were studied in human wild type alpha-synuclein expressing mice.

The second study utilised induced pluripotent stem cells (IPSCs) to compare modifications in mitochondrial trafficking in SNpc neurons from IPSCs derived from a mitochondrial disease patient harbouring a large scale mtDNA deletion. Mitochondrial movement was first observed within low and high mtDNA deletion cell lines, to ascertain the effect of mitochondrial dysfunction on the movement of these organelles. Following this initial study, the effect of mitochondrial Ca^{2+} extrusion into the cytoplasm was investigated, alongside how this mediated mitochondrial motility.

This study successfully managed to obtain videos of mitochondrial motility, from cell body to synapse, allowing the observation of speed, directionality and membrane potential of mitochondria within neurons of these disease models. These models have collectively provided information on the movements and trafficking of mitochondria in both culture and in a mouse model, presenting a promising method to comprehend the consequences of mitochondrial dysfunction in PD.

Acknowledgements

There are many people I would like to thank for helping me get to where I am now. Firstly, my supervisors for providing me with this opportunity: Doug for constantly making sure the story was always told and Chris for ensuring I was well read and up to date with the current literature (and biscuits!). To Amy, thank you for helping with the scientific brainstorming and for allowing complete flexibility and originality throughout this project. I hope together we've bought some of our wacky ideas to life.

To everyone who's helped with overcoming the logistical and practical hurdles of this project, Felix, Clare, Mark, Brigid, Alex and Rolando, this would have been impossible to achieve without your input. To all the MRG postgraduate students, post-docs and research technicians, past and present, you've all been a great team to work with. To the Kretins, thank you for enabling procrastination (when deserved) as we're all in this together, and to the badminton squad, for coaching me through healthy anger management.

I'd like to give a special shout out to a few individuals, without whom this journey would have been a lonely one. To Liz (or Nish? Who knows…), Tazza and Lottie who have set the office entertainment bar extremely high from day one. From mispronounced ethnical names, making up Disney dwarves and to the very overdue geography lessons, you guys have really been an absolute joy to be around. To Pav, who has become my personal motivational speaker, Carla, for keeping me company during the crying and/or Netflix & chilling, and finally Shane, the only PhD student who shares my love for mini lops bunnies and mitophagy, I've appreciated it all.

I'd like to thank all my friends at home who made sure I kept going during some particularly difficult times. To the OG girl clan, Ahreni, Thanusha and Maj, you've allowed me to lean on you during my ups, but mostly downs, and for that safe space, I am so thankful. To the actual banes of my life; Rat, Vasima and Tauqeer, thank you for always checking up on me, and for constantly reminding me of why I embarked on this journey in the first place. To all my family, who probably won't understand a single page of this thesis (except this one!), I know you've been cheering me on in the background and I can't wait to come home!

To my aunt and grandparents, who have always spoiled me rotten, I am so lucky to be surrounded by your unconditional love and unwavering belief in my abilities, even when I've doubted myself. You're my favourite people.

To my not so little sister, who always gives it to me straight, reminds me that momma didn't raise a quitter, buys me my favourite nibbles, and has chauffeured me to Kings Cross on way too many occasions. Thank you for swapping roles and taking care of me over the last three years…I've really needed it. You'll always be my best friend.

To the people who raised me, thank you for letting me take off the big girl cape every now and then... you keep my inner child gleaming, always. Dad, I miss you. Not a day goes by where I don't think about you, our daily calls and our singalong road-trips. I'll be taking the words from your stories and I'll carry them with me every day. And finally, thank you mum for being the best role model a little girl could have ever asked for. You've single handedly shown me how to be strong and how to persevere. We've been each other's rock over the last three years and that will never change. You guys are my favourite people and I hope I have made you proud.

Author's Declaration

This thesis is submitted for the degree of Doctor of Philosophy at Newcastle University. The research was conducted in the Wellcome Trust Centre for Mitochondrial Research, Institute of Neuroscience, Newcastle University under the supervision of Dr Amy K Reeve, Dr Christopher M Morris, and Professor Sir D M Turnbull. All work is my own unless otherwise stated. I certify that none of the material presented here in this thesis has previously been submitted by me for a degree or qualification at this or any other university.

Chapter specific Declarations

Chapter Four, Section 4.1.7.2, Figure 4.2. Alpha–synuclein neuropathology in human α-synuclein expressing transgenic mice (Masliah et al., 2000).

Chapter Six Section 6.1.2, Figure 6.2. Overexpression of Wild-type and familial PD mutation carrying synuclein decreases ER–mitochondrial contacts (Paillusson *et al.,* 2017)

TABLE OF CONTENTS

LIST OF TABLES

LIST OF FIGURES

TABLE OF ABBREVIATIONS

µl	Microliter
µm	Micromolar
•OH	hydroxyl radical
ΔΨm	Mitochondrial membrane potential
8-oxoG	Oxoguanine
A	Adenine
AC	Adenylyl cyclase
ACSF	Artificial cerebrospinal fluid
AD	Alzheimer's disease
ADP	Adenosine diphosphate
AIF	Apoptosis inducing factor
ALS	Aamyotrophic lateral sclerosis
APP	Amyloid precursor protein
APs	Action potentials
AR	Anterograde
ATP	Adenosine Triphosphate
ATPase	Adenosine Triphosphate synthase
Aβ	β-amyloid
Bcl2-L-13	Bcl-2-like protein 13
BDNF	Brain derived neurotrophic factor
BER	base excision repair
bFGF	Basic fibroblast growth factor
bH	High affinity haem
bL	Low affinity haem

BNIP3	B-cell lymphoma 2 19 kDa interacting protein 3
bp	Base pairs
$Ca2^{+}$	Calcium ion
$CaCl_2$	Calcium Chloride
CAG	Cytomegalovirus/β-actin
c-AMP	Cyclic adenosine monophosphate
CCCP	Carbonyl cyanide m-chlorophenyl hydrazine
CFP	Cyan fluorescent protein
CI	Complex I
CII	Complex II
CIII	Complex III
CIV	Complex IV
C-KIFs	C-terminal motor domain kinesin superfamily proteins
Cl^{-}	Chloride ion
CNS	Central nervous system
CO_2	Carbon Dioxide
CoA	Acetyl-Coenzyme
COMT	catechol O-methyl transferase
COX	Cytochrome c Oxidase
CV	Complex V
DA	Dopamine
DAergic	Dopaminergic
DAT	Dopamine active transporter
DIC	Dynein intermediate chains
DLBs	Dementia with LBs

DLC	Dynein light chains
DLIC	Dynein light intermediate chains
DNA	Deoxyribonucleic Acid
dNTP	Deoxynucleotide
DOPAL	3,4-dihydroxyphenyl-acetaldehyde
DP	Dynamic pause
Drp1	Dynamin related protein 1
Dync1h1	Cytoplasmic dynein heavy chain 1
Dync1h2	Cytoplasmic dynein heavy chain 2
EAE	Encephalomyelitis
ECAR	Extracellular acidification rate
EDTA	Ethylenediaminetetraacetic acid
EM	Electron microscopy
ENK	enkephalin
EP	entopeduncular nucleus
ER	Endoplasmic Reticulum
ERRα	Oestrogen related receptor alpha
ES	embryonic stem cells
ETC	Electron transport chain
FADH2	Flavin adenine dinucleotide
Fe-S	Iron-sulphur
FGF8	Fibroblast growth factor 8
Fis1	Mitochondrial fission protein1
fMet	Formylated methionine
FMN	Flavin mononucleotides

FXN	Frataxin
G	Guanine
GABA	γ-aminobutyric acid
GDNF	Glial cell line derived neurotrophic factor
GFP	Green Flourescent Protein
GP	Globus pallidus
H strand	Heavy strand
H^+	Proton
H_2O	Water
H_2O_2	Hydrogen peroxide
HD	Huntington's disease
Het	Heterozygous
HIF-1	Hypoxia-inducible factor-1
Hom	Homozygous
IMM	Inner mitochondrial membrane
IMS	Intermembrane space
iPSCs	Induced pluripotent stem cells
ISCU	iron sulphur cluster enzyme
Kb	Kilobase
KCL	Potassium Chloride
KDa	Kilo Daltons
KHC	Kinesin-1 heavy chain
KIFs	Kinesin superfamily proteins
KSS	Kearn-Sayre Syndrome
L strand	Light strand

LAMP2A	lysosome-associated membrane glycoprotein 2A
LBs	Lewy bodies
LC3	Microtubule-associated proteins 1A/1B light chain 3B
LIR	LC3-interacting region
LSP	light strand promoter
LUHMES	Lund Human Mesencephalic
MAO	Monoamine oxidases
MAP2	Microtubule associated Protein
$_{m}Ca^{2+}$	Mitochondrial Calcium
MCU	Mitochondrial calcium uniporter
Mff	Mitochondrial fission factor
MFN	Mitofusin
$MgCl_2$	Magnesium Chloride
$MgSO_4$	Magnesium Sulfate
MiD49	Mitochondrial dynamics proteins of 49
MiD50	Mitochondrial dynamics proteins of 50
Miro	Mitochondrial Rho
M-KIFs	M-terminal motor domain kinesin superfamily proteins
mL	Millilitre
mM	Millimolar
MMP	Mitochondrial membrane potential
MOPS	3-(N-morpholino)propanesulfonic acid
MPP	Mitochondrial processing peptidase
MPP^+	1-methyl-4-phenylpyridinium
mPTP	mitochondrial permeability transition pore

MPTP	1-methyl-4-phenyl-1,2,3,6-tetrahydropyridine
mRNA	Messenger Ribonucleic Acid
MS	Multiple sclerosis
MTCO1	Mitochondrially encoded cytochrome c oxidase
mtDNA	Mitochondrial DNA
mt-EFG2	Mitochondrial elongation factor G2
mt-EFTu	Mitochondrial elongation factor Tu
mTERF	Mitochondrial termination factor
MtHtt	Mutant Huntingtin
mt-LSU	Mitochondrial ribosomal large subunit
mtPAP	Mitochondrial poly (A) polymerase
mt-RF1a	Mitochondrial release factor 1a
mt-RRF1	Mitochondrial release factor 1
mtSSB	Mitochondrial Single Strand Binding protein
mt-SSU	Mitochondrial ribosomal small subunit
mt-tRNA	Mitochondrial transfer Ribonucleic Acid
Na+	Sodium ion
NAC	Non-amyloidogenic component
NaCl	Sodium Chloride
NADH	Nicotinamide adenine dinucleotide
NaH_2PO_4	Monosodium phosphate
$NaHCO_3$	Sodium Hydrogen Carbonate
NaOH	Sodium Hydroxide
NBR1	Neighbour of BRCA1 gene
NCLX	$Na^+/Ca^{2+}/Li^+$ exchanger

NCX	Na^{+}/Ca^{2+} exchanger
nDNA	Nuclear DNA
NDUFA9	NADH dehydrogenase [ubiquinone] 1 alpha subcomplex subunit 9
NDUFA13	NADH dehydrogenase [ubiquinone] 1 alpha subcomplex subunit 13
NDUFB8	NADH dehydrogenase [ubiquinone] 1 beta subcomplex subunit 8
NFS1	Cysteine desulfurase
Ngn2	Neurogenin2
N-KIFs	N-terminal motor domain kinesin superfamily proteins
nm	Nanometer
NPCs	Neuronal progenitor cells
NRF-1	Nuclear respiratory factor-1
O_2	Oxygen
O_2^{2-}	Superoxide anion radical
OCR	Oxygen consumption rate
OH	Origin of heavy strand replication
OL	Origin of light strand replication
OMM	Outer mitochondrial membrane
OPA1	Optic Atrophy 1
OPTN	Optineurin
OSCP	Oligomycin sensitivity-conferring protein
OXPHOS	Oxidative phosphorylation
PARL	Presenilin-associated rhomboid-like protease
PBS	Phosphate buffered saline
PCR	Polymerase chain reaction
PD	Parkinson's disease

PDGF-b	Platelet-derived growth factor–b
PFA	Paraformaldehyde
PGC-1α	Peroxisome proliferator-activated receptor gamma coactivator 1-alpha
PHB2	Prohibitin 2
PINK1	PTEN induced putative kinase
PKA	Protein Kinase A
POLG	Polymerase Gamma
RGC	Retinal ganglion cells
RIMS	Refractive Index Matching Solution
RITOLS	Ribonucleotides are Incorporated ThroughOut the Lagging Strand
RNA	Ribonucleic Acid
ROCKi	Y-27632
ROS	Reactive oxygen species
RR	Retrograde
SDHA	Succinate Dehydrogenase
SDS	Sodium Dodecyl Sulfate
SHH	Sonic hedgehog
SMI	Phosphorylated Neurofilament
SNCA	Alpha-synuclein gene
SNpc/SNc	Substantia nigra pars compacta
Snph	Syntaphilin
SNr	Substantia nigra pars reticula
SNV	Selective neuronal vulnerability
ST	Stationery
STN	Subthalamic nucleus

TBST	Tris Buffered Saline with Tween
TCA	Tricarboxylic acid
TFAM	Transcriptional factor A
TG	Thymine glycol
TH	Tyrosine Hydroxylase
TIM	Translocase of the inner membrane
TMRM	Tetramethylrhodamine, methyl ester
TNF	Tumour necrosis factor
TOM	Translocase of the outer membrane
Tom20	Translocase of outer membrane 20 homolog
Tris-HCL	Tris(hydroxymethyl)aminomethane – Hydrogen Chloride
tRNA	Transfer ribonucleic acid
TSFM	Mitochondrial translation factor Ts
TWNK	Twinkle
UBD	Ubiquitin binding domain
UCH	Ubiquitin C-terminal hydrolase
VDAC	Voltage Dependant Anion Channel
VGCC	Voltage-dependent Ca^{2+}channels
VGLUT	Vesicular glutamate transporter
VTA	Ventral tegmental area
α–syn	Alpha synuclein protein

CHAPTER ONE

Introduction

1.1 MITOCHONDRIAL ORIGIN

Mitochondria are rod-shaped intracellular organelles that are located within the cytosol of nucleated eukaryotic cells. Though their primary function is to produce cellular energy in the form of adenosine triphosphate (ATP), mitochondria also partake in a myriad of biological processes which include iron-sulphur (Fe-S) cluster formation, sequestering calcium, ROS generation and removal, and haem biogenesis.

Mammalian mitochondria were thought to originate through endosymbiotic relationships approximately 2 billion years ago (Sagan, 1967, Gray *et al.,* 1999). The theories surrounding mitochondrial origin involve two mechanisms i) the archezoan and ii) the symbiogenesis methods (Gray *et al.,* 2012). In the archezoan model, the host of the mitochondrial endosymbiont was thought to be a primitive eukaryote, whilst the symbiogenesis model describes that alpha-proteobacteria were engulfed *by* a primordial eukaryotic cell causing mitochondrial production (Koonin, 2010). The archezoan scenario describes a typical endosymbiotic relationship (Margulis 1970, Doolittle 1980) and the symbiogenesis model is referred to as the hydrogen hypothesis (Martin and Müller 1998). The theories differ in whether mitochondria and nuclear formation occurred simultaneously (symbiogenesis model) or whether the nuclear components of the mitochondria appeared later (archezoan scenario) (Martin & Müller 1998, Gray *et al.,* 2001).

Scientists suggest that it is following these biological phenomena's that mitochondrion to nuclear gene transfer occurred. This reaction was found to trigger a reduction in the eubacterial genome, instigating the unique morphology of mitochondria to appear within their host cells (Martin and Herrman, 1998, Gray *et al.,* 2001). Importantly, not all mitochondrial genes were transferred, as during the nuclear transfer, mitochondrial DNA (mtDNA) could not recombine and genetic information was lost. Consequently, many mitochondrion-based genes were degraded, leaving them to only exist in the nucleus (Blanchard and Lynch, 2000, Selosse *et al.,* 2001).

Mitochondria-related organelles (MROs) have been identified (Embley and Hirt, 1998), comprising two double membrane bound organelles, hydrogenosomes and mitosomes, with their prominent functional divergence being that hydrogenosomes harbour the ability to generate ATP whilst mitosomes cannot.

Hydrogenosomes (sighted first within non-mammalian eukaryotes), do not contain their own genomic DNA and do not house the sufficient OXPHOS and ETC components. Instead, particular enzymes are involved in this anaerobic ATP production, where H_2 is produced as an end product, hence hydrogenosomes (Whatley *et al.,* 1979). Mitosomes however do partake in aerobic processes though harbour an evolution that is more reduced than that of hydrogenosomes. Iron-sulphur (Fe-S) cluster formation is an important function of this organelle (Gray, 2012), a key function which appears consistently conserved within mitochondria, mitosomes and hydrogenosomes (Gray, 2012), regarding it as a mitochondrial function equally important as oxidative phosphorylation.

1.2 THE STRUCTURE AND FUNCTION OF MITOCHONDRIA

1.2.1 Mitochondrial structure

Mitochondria retained structural features that support their origin from a bacterial endosymbiotic relationship. These organelles are double membraned and contain their own genome, circular in shape and are referred to as mtDNA. Palade (1953) and Sjostrand (1956) indicate that the mitochondrial double membrane comprises an inner (IMM) and outer mitochondrial membrane (OMM) (Palade, 1953, Sjostrand, 1956).

The first model described by Palade in 1953, indicates that baffles (referred to as cristae) are produced by the matrix, where the later Sjostrand model, describes an additional membrane, known as the septa which separates the mitochondrial matrix (Palade, 1953, Sjostrand, 1956). Research revealed that this was actually IMM invaginations that created a structure called *crista mitochondriales*, commonly referenced to as cristae (Frey and Manella, 2000).

The IMM is less permeable than the OMM encompassing a larger protein to phospholipid ratio (Fleischer *et al.,* 1961), due to the increased level of proteins that are required for metabolic pathways (Wilkens *et al.,* 2013, Cogliati *et al.,* 2016). The IMM is divided into i) the inner boundary membrane (IBM), localised near the OMM and creates cristae junctions and ii) and the cristae membrane (CM), which holds relevant proteins for OXPHOS (Perkins and Frey, 2000). The mitochondrial matrix is the central region for mito-biochemical processes i.e. iron-sulphur (Fe-S) cluster formation and the tricarboxylic acid (TCA) cycle. MtDNA copies are found here, alongside the components required for mtDNA transcription and translation. Nuclear encoded proteins with a mitochondrial targeting sequence (MTS) enter the mitochondria via the outer (TOM) and inner (TIM) mitochondrial translocases (Herrmann and Neupert, 2000, Rehling *et al.,* 2004). These proteins are directed accordingly towards to the matrix, IMS or inserted into the OMM or IMM (Rehling *et al.,* 2004).

A)

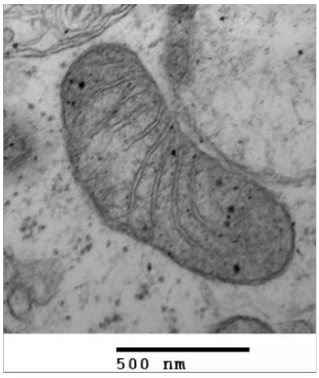

B)

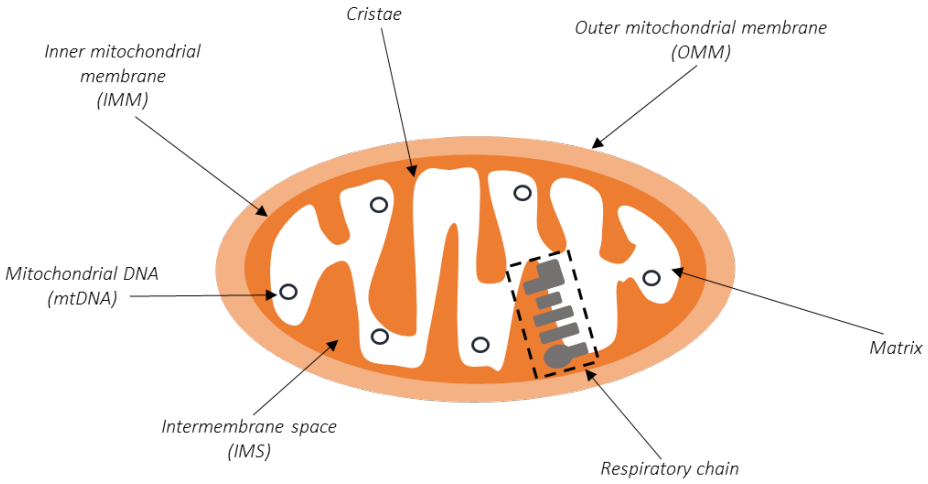

Figure 1.1. Mitochondrial structure. A) Electron microscopy image of a mitochondrion and **B)** labelled ultrastructure of the mitochondria. (Electron microscopy image courtesy of Dr Amy Reeve, WCMR)

1.2.2 Oxidative phosphorylation (OXPHOS) reactions

Mitochondria contain OXPHOS proteins which generate cellular energy in the form of ATP, embedded within the IMM of the mitochondrion. The OXPHOS system is composed of the electron transport chain (ETC), which houses Complexes I- IV and ATP synthase (complex V) (Sheratt.,1991) (Figure 1.2). The mitochondrial complexes facilitate electron transfer and proton movement within the matrix to the IMS, creating a proton motive force which promotes ATP synthesis from ADP via complex V (Boyer *et al.,* 1975).

The chemiosmotic theory describes the process of electron transfer from a reduced donor to the terminal electron acceptor oxygen and the coupling of these reactions to generate ATP. Protons that are translocated across the IMM into the IMS have been shown to create an electrochemical gradient (Mitchell, 1961), termed as OXPHOS. This process is described as follows: the glycolysis or fatty acid oxidation by-product, pyruvate, is imported into the mitochondria via the mitochondrial pyruvate carrier. Pyruvate then undergoes decarboxylation into acetyl-coenzyme (CoA), which is then transferred to the tricarboxylic acid (TCA) or the Kreb's cycle (Krebs, 1940). In the TCA cycle, carbon atoms of the acetyl component of CoA are oxidised, generating high energy electrons. These electrons are then transferred to electron carriers, nicotinamide adenine dinucleotide (NADH) and Flavin adenine dinucleotide ($FADH_2$), and are distributed to Complex I and II respectively. From here on, electrons are transferred to ubiquinone, a soluble electron carrier found within the IMS. Ubiquinone is reduced to ubiquinol by CIII, with electron transfer to cytochrome *c*, a water-soluble carrier. The final step in this reaction, describes Complex IV as a generator of molecular oxygen (O_2) and water (H_2O), through ATP synthase driven ADP phosphorylation, producing ATP (Mitchell, 1961)

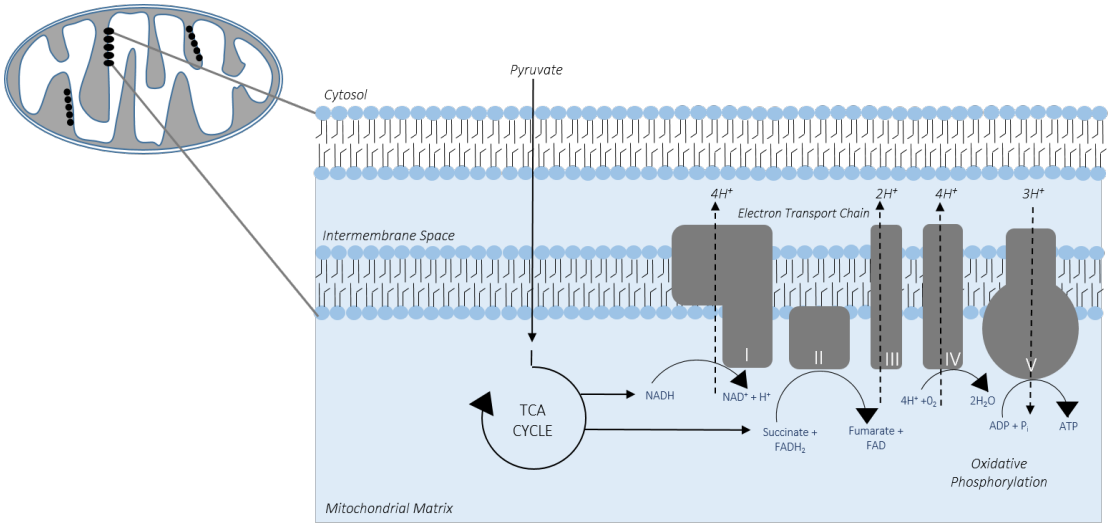

Figure 1.2. Oxidative phosphorylation. Respiratory chain complexes I-IV comprise the ETC. Complex V couples the oxidation of reduced equivalents with ADP phosphorylation to generate ATP and H_2O molecules. Electrons enter the ETC via complex I or II and are transferred to complex II and IV before reaching the terminal acceptor, O_2. (Figure adapted from Stefely and Pagliarini, 2017)

1.2.2.1 The OXPHOS system – Glycolysis

Before ATP is produced, anaerobic glycolysis reactions occur that link into the TCA cycle within the mitochondrial matrix. Glucose metabolism generates two pyruvates via the glycolytic pathway (Berg *et al.,* 2012). In addition to ATP, two NADH molecules are also generated.

$$\text{Glucose} + 2[NAD^+] + 2[ADP] + 2[P_i] \rightarrow 2\ [\text{Pyruvate}] + 2[NADH] + 2[H^+] + 2[ATP] + 2[H_2O]$$

Equation 1.1. Glycolysis reactions

1.2.2.2 The OXPHOS system – The Links Reaction

Pyruvate dehydrogenase regulates the movement of cytosolic pyruvate to the mitochondrial matrix for further metabolism via the oxidative carboxylation of pyruvate to acetyl CoA (Henderson *et al.,* 2000).

$$\text{Pyruvate} + CoA + NAD^+ \rightarrow \text{Acetyl-CoA} + NADH + H^+ + CO_2$$

Equation 1.2. The Links Reactions

1.2.2.3 The OXPHOS system – The TCA cycle

The TCA cycle encompasses the formation of ATP, NADH and FAD electron carriers, which are transferred into the mitochondrial matrix for the final stages of metabolism in the OXPHOS system (Berg *et al.,* 2012). Acetyl-CoA is then converted to citrate catalysed by citrate synthase. The TCA cycle generates reduced equivalents in the form of NADH and $FADH_2$, where one cycle of the pathway yields four reduced equivalents, one GTP molecule and two CO_2 molecules.

$$\text{Acetyl-CoA} + 3[NAD^+ + FAD + ADP + P_i + 2[H_2O] \rightarrow CoA + 3[NADH] + 2[H^+] + FADH_2 + ATP + 2[CO_2]$$

Equation 1.3. The TCA cycle

Reduced coenzymes enable the delivery of electrons to the ETC and initiates OXPHOS.

1.2.2.4 The OXPHOS system – Complex I (NADH: Ubiquinone Oxidoreductase)

Complex 1 is the largest complex (1000kDa) of the respiratory chain (Zhu *et al.,* 2016), containing 45 subunits encoded by both nuclear (38 subunits) and mitochondrial (7 subunits) genomes. 14 of the 45 subunits (7 nDNA and 7 mtDNA encoded) have been rendered as crucial for mitochondrial function and are highly conserved with the remaining 31 being mammalian supernumery (Letts *et al.,* 2016). This L-shaped structure comprises a hydrophobic arm embedded in the IMM and the other arm extended into the matrix (Sousa *et al.,* 2018) (Figure 1.3) and houses 3 functional segments. These segments are known as: the N (NADH oxidation), Q (quinone reduction) and P-(proximal and distal pumping) modules (Hunte *et al.,* 2010). The N module binds NADH and is followed by electron transfer to Flavin mononucleotide (FMN), forming FMH_2. Electrons are then transferred via the Fe-S clusters in the Q module to the quinone pool, following which, the QH_2 product is released into the IMS. The P-module, embedded in the IMM, functions as a proton pump allowing proton translocation (Zhu *et al.,* 2016).

$$NADH + Q + 5[H^+]\ matrix \rightarrow NAD^+ + QH_2 + 4[H^+]\ IMS$$

Equation 1.4. Complex I reactions (Berg et al., 2012b).

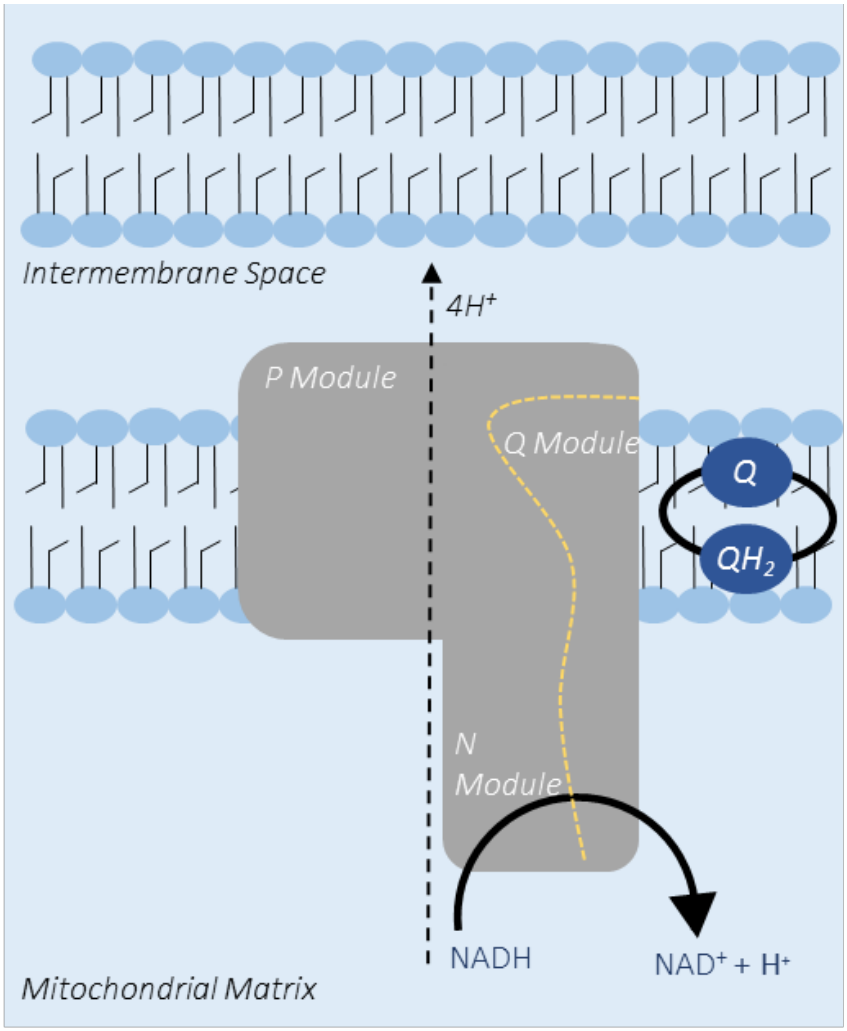

Figure 1.3. Complex I. Electrons are passed from NADH to FMN and through Fe-S clusters (yellow dotted line) to the quinone pool. Meanwhile, four protons are pumped from the matrix into the IMS. (Figure adapted from Kühlbrandt 2015, Stefely and Pagliarini, 2017).

1.2.2.5 The OXPHOS system – Complex II (Succinate ubiquinone oxidoreductase)

Complex II is the secondary and last site of electron entry into the ETC. It is a 124kDa structure, and its enzymatic module is succinate dehydrogenase or (SDH) and does not partake in proton translocation across the IMM (Cecchini *et al.,* 2003). Complex II is made of 4 nuclear encoded subunits, and catalyses the conversion of succinate to fumarate, generating an oxidised $FADH_2$. This oxidation reaction reduces FAD to $FADH_2$, triggering electron transfer to the quinone pool via Fe-S clusters (Bezawork-Geleta *et al.,* 2017) (Figure 1.4).

Succinate +FAD +2[H^{+}] +Q → Fumarate +$FADH_2$ + Q → Fumarate +FAD +QH_2

Equation 1.5. Complex II reaction (Berg et al., 2012b)

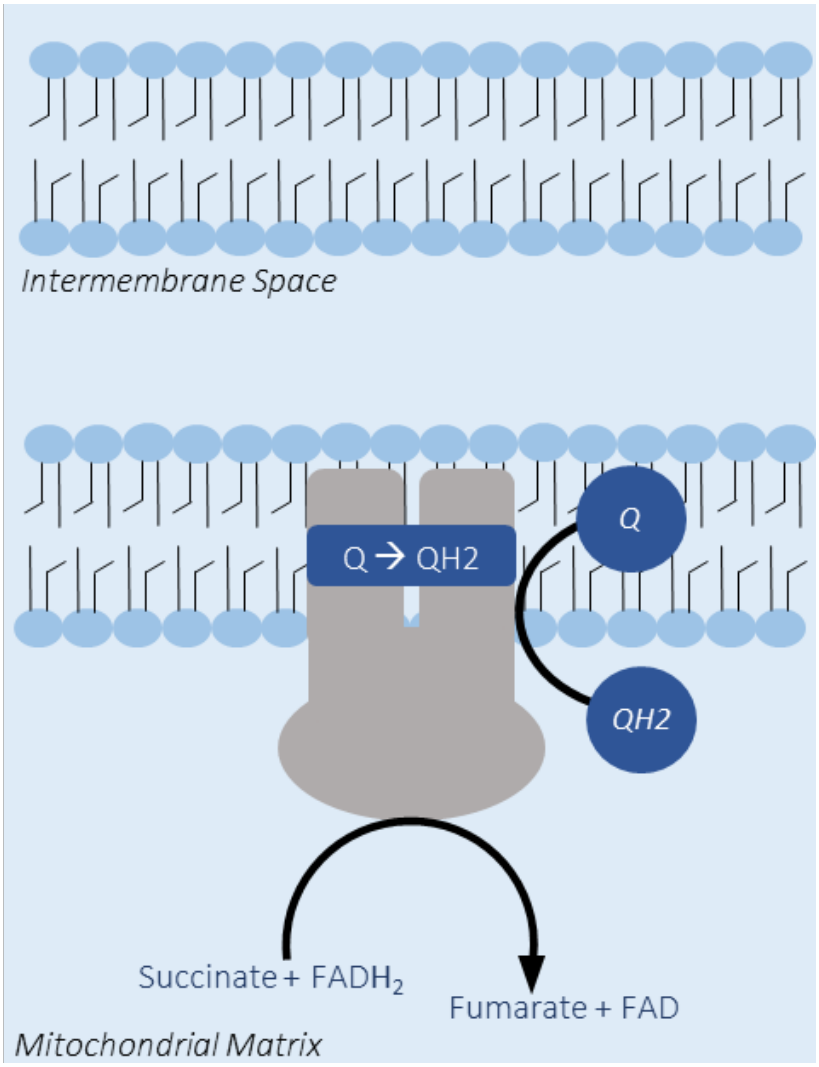

Figure 1.4. Complex II. The oxidation of succinate to fumarate causes the reduction reactions of FAD to $FADH_2$ which transfers electrons to the quinone pool via 3 Fe-S clusters (Figure adapted from Kühlbrandt 2015, Stefely and Pagliarini, 2017).

1.2.2.6 The OXPHOS system – Complex III (Ubiquinol Cytochrome c reductase)

Complex III holds 11 subunits, 10 nuclear and 1 mtDNA (cytochrome b) (Xia *et al.,* 1997). The single mtDNA encoded subunit, Cytochrome b, catalyses electrons transfer from ubihydroquinone (QH_2) to Cytochrome c through the Q cycle which utilises QH_2 (Mitchell, 1976). Each QH_2 entails movement of two protons (to the IMS) and two electrons to cytochrome c (via the Rieske Fe-S cluster through cytochrome c1) and cytochrome b respectively. In the latter reactions, electrons are transferred through two haem b (protoheme) groups: low (bL) and high (bH), affinity prior to the binding ubiquinone and being reduced to semiquinone (Kim *et al.,* 2012) (Figure 1.5).

$2[QH_2] + Q + 2[\text{Cyt c}]\ ox + 2[H^+]\ matrix \rightarrow 2\ [Q] + QH_2 + 2[\text{Cyt c}]\ red + 4[H^+]\ cytoplasm$

Equation 1.6. Complex III reaction (Berg et al., 2012b)

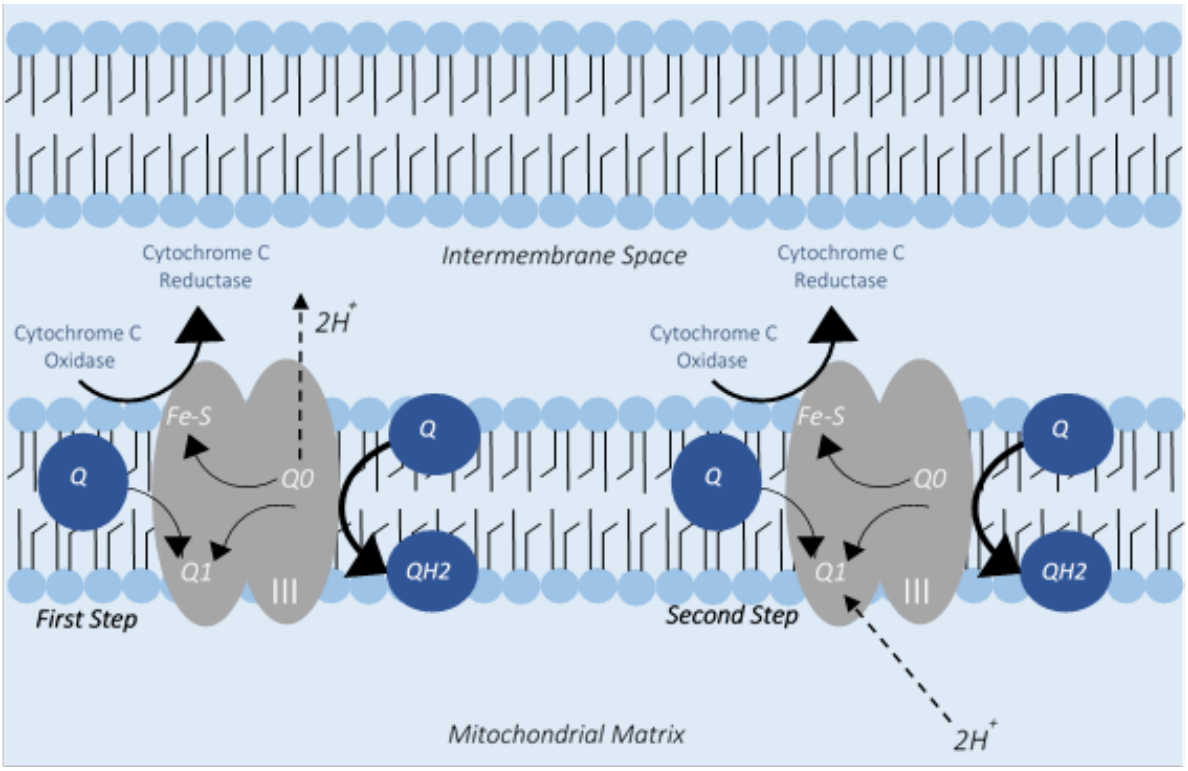

Figure 1.5. Complex III. Electrons are transferred from the reduced ubiquinone pool to cytochrome c via the Q cycle. The shuttling of electrons is coupled with the translocation of protons from the matrix to the intermembrane space, where a net movement of 4 H^+ occurs. (Figure adapted from Kühlbrandt 2015, Stefely and Pagliarini, 2017).

1.2.2.7 The OXPHOS system – Complex IV (Cytochrome c oxidase)

In the final OXPHOS step, electrons are transferred to complex IV. Of the 13 subunits in this complex, 3 subunits (COX I, II, III) are encoded by the mitochondrial genome. The substrate for complex IV is Cytochrome c which transfers electrons between complexes III and IV. Cytochrome c donates electrons to the binuclear protein prosthetic group Cu_A, then to haem a and finally to the oxygen binding site haem a3-Cu8, generating H_2O. Electron transfer is coupled with the translocation of 4 protons to the IMS (Tsukihara *et al.,* 1996) (Figure 1.6).

$$4[\text{Cyt c}]\ \text{red} + 8[\text{H+}]\ \text{matrix} + O_2 \rightarrow 4[\text{Cyt c}]\ \text{ox} + 2H_2O + 4[\text{H+}]\ \text{cytoplasm}$$

Equation 1.7 Complex IV reaction (Berg et al., 2012b)

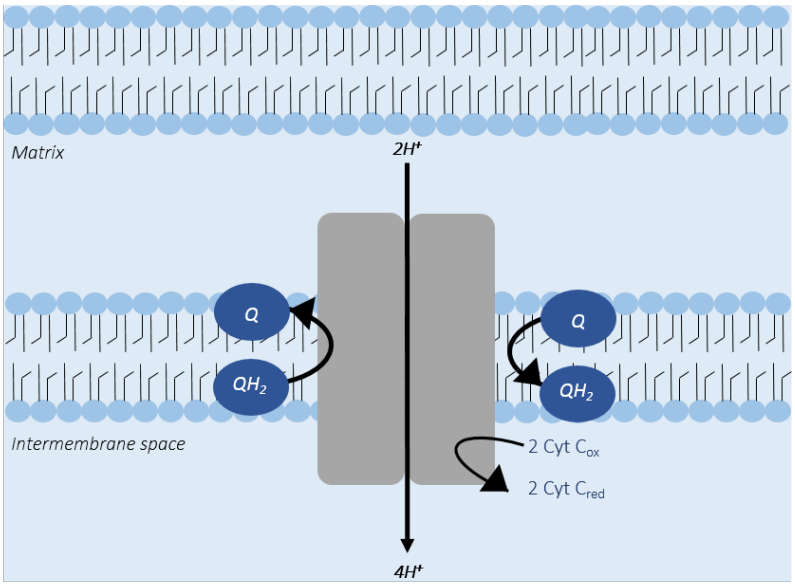

Figure 1.6. Complex IV. Electrons from cytochrome c are transferred which allows the binding of molecular oxygen and hydrogen atoms to form water. The shuttling of electrons is also coupled to the translocation of 4 H^+ from the matrix to the intermembrane space. (Figure adapted from Kühlbrandt 2015, Stefely and Pagliarini, 2017).

1.2.2.8 The OXPHOS system – Complex V (ATP synthase)

Complex V is the last mitochondrial complex where ATP synthase reactions convert ADP to ATP. Complex V is formed from 15 -18 subunits (2 mtDNA and ~ 13 nDNA encoded) and is approximately 600kDa in size (Stock *et al.,* 2000).

The F_1 region of this complex is water soluble and is made of three α and β subunits as well as the catalytically active δ and ε s polypeptide chains (Figure 1.7a). F_1 protrudes into the mitochondrial matrix and associates with subunit c ring structure on the F_0 region situated on the IMM through a stalk structure (Figure 1.7b) (Chaban *et al.,* 2014).

In addition to the c-ring like subunit, F_0 also contains the 2 mitochondrially encoded subunits: a (*ATP6*) and A6L *(ATP8)* alongside the e, f and g subunits. Within the central stalk segment the remaining oligomycin sensitivity-conferring protein (OSCP), b, d and F6 subunits can be found (Wittig and Schagger, 2008). The movement of protons across the membrane occurs through a proton motive force resultant of the proton gradient. This transfer is linked to F_0 c-ring rotation as well as the γ, δ and ε subunits. The trimeric F_1 α and β subunits do not rotate and therefore conduct ATP synthesis through a conformational change (Gresser and Boyer, 1982). A single 360° rotation transfers 8 protons, generating 5 ATP molecules (Watt *et al.,* 2010) (Figure 1.7).

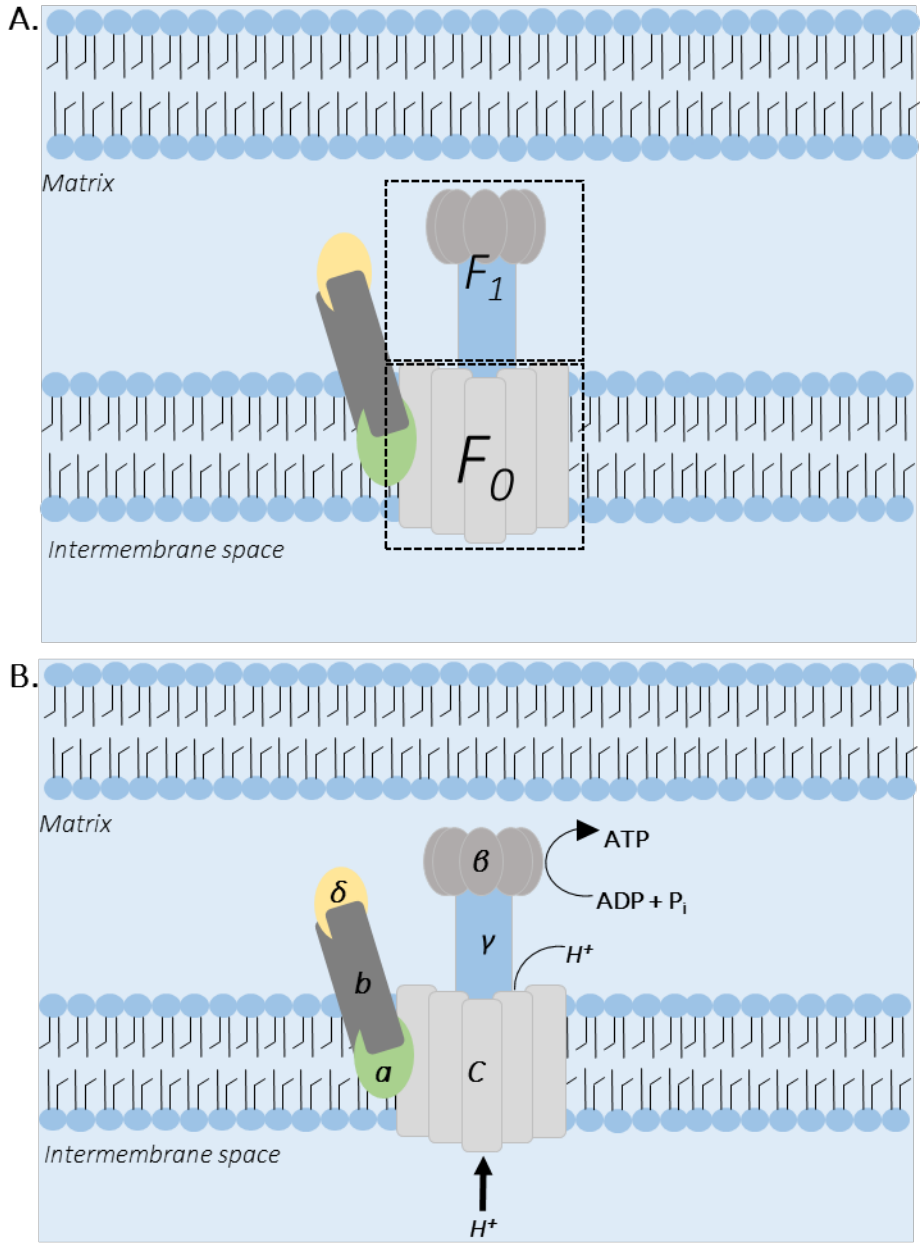

Figure 1.7. Complex V. ATP synthase catalyses the final step in ATP synthesis via the electrochemical gradient which stimulates the rotation of the F_0 rotary ring, which instigates ADP phosphorylation forming ATP. **A)** The F_0 unit in the IMM and F_1 unit projects into the mitochondrial matrix. **B)** F_0 consists of a c-ring and subunits a, b, d, F6, OSCP, as well as subunits e, f, g and A6. Subunits a and A6L are the only mitochondrially encoded subunits. The F_1 unit consists β and α chains that create a hexameric α3β3 ring structure which catalyses ATP synthesis, the δ and γ polypeptides form the central stalk of complex V, joining both regions together. A proton motive force is produced as a result of the proton gradient, where the flow of protons through the c-ring is coupled with the rotation of the c-ring (F0) and γ, δ and ε subunit. This rotation causes the β subunits to undergo a conformational change, whilst being bound to ADP and Pi thus causing the phosphorylation of ADP and releasing ATP (Chaban *et al.,* 2014). (Figure adapted from Stefely and Pagliarini, 2017).

1.2.2.9 Synthesis of new mitochondria

Mitochondrial biogenesis is the process by which pre-existing mitochondria undergo growth and subsequent division (Shiota *et al.,* 2015) giving arise to newly synthesised mitochondria. Through this process, mitochondrial mass increases where up to 1,000 proteins are transported into the mitochondria via the TOM complex (Chacinska *et al.,* 2009). Found initially within brown adipose tissues, peroxisome proliferator-activated receptor gamma coactivator 1-alpha (PGC-1α) was identified to partake in adipogenesis (Puigserver *et al.,* 1998). PGC-1α, has been shown as a vital regulator of mitochondrial biogenesis in brown adipose and skeletal tissue (Lehman *et al.,* 2000).

Very little is actually known about mitochondrial biogenesis in neurons. However, there remains a large level of similarities between the regulatory network that execute this process within neurons. Mitochondria exhibit a longer half-life in neurons in comparison to other post-mitotic somatic cells, where their renewal is vital for functional neuronal development (Gross *et al.,* 1969, Korr *et al.,* 1998, Miwa *et al.,* 2008, O'Toole *et al.,* 2008). Mitochondrial biogenesis occurs as a result of collaboration between both the nuclear and mitochondrial genome. This function can cause mitochondrial biogenesis to occur within the soma. Thought to only occur within the soma, mitochondrial biogenesis has also recently been identified distally within axons, heavily aided by microtubular motors (Uittenbogaard and Chiaramello, 2014).

1.3 OTHER MITOCHONDRIAL FUNCTIONS

1.3.1 Iron sulphur cluster biogenesis

Fe-S cluster biogenesis has been largely explored in Yeast*, Saccharomyces cerevisae*. Mitochondrial iron-sulphur cluster (ISC) assembly is conserved and inherited from mitochondrial bacterial ancestors (Johnson *et al.,* 2005, Bandyopadhyay *et al.,* 2008, Py and Barras 2010). Over the last decade, experiments conducted in cell culture have strengthened evidence for this inheritance within a eukaryotic model (Sheftel *et al.,* 2010, Rouault 2012).

ISC assembly consists of 3 main steps involving 17 mitochondrial components (Muhlenhoff *et al.,* 2003). Firstly, a [2Fe-2S] cluster is created on the Isu1 scaffolding protein that associates with the sulphur donor: cysteine desulfurase (Nfs1) (Stehling and Lill, 2013). In this step, Fe-S cluster formation utilises frataxin, ferredoxin and ferredoxin reductases, housed in the ETC. Following this, the Fe-S cluster dissociates from Isu1 and binds Hsp70 (Heat shock) proteins, which then binds Fe-S cluster transfer proteins. Finally, Fe-S cluster is directed towards particular mitochondrial apoproteins, causing Fe-S cluster polypeptide chains (Stehling and Lill, 2013).

1.3.2 Mitochondrial Calcium handling

Ca^{2+} buffering within the cell is regulated by modulating the movement of Ca^{2+} into and out of the mitochondria. Mitochondrial Ca^{2+} ($_{m}Ca^{2+}$) influx is regulated by the mitochondrial Ca^{2+} uniporter (MCU) in the IMM (Baughman *et al.,* 2011, De Stefani *et al.,* 2011), while $_{m}Ca^{2+}$ efflux release is via an ion exchange with Na^{+} (Palty *et al.,* 2010). Regulating this movement is crucial to mitochondrial function. Chapter 6 will delve further into mitochondrial calcium handing.

1.3.3 Apoptosis

Mitochondria mediated programmed cell death can be triggered due to the perturbed cristae architecture and the opening of the mitochondrial permeability transition pore (mPTP) (Rizzuto *et al.,* 2012). Moreover, in response to cellular stress, the intrinsic and extrinsic apoptotic pathways have been identified and described.

The intrinsic pathway, (the mitochondrial pathway) entails mitochondrial damage occurring through the apoptosis complex, cytochrome *c*, and the extrinsic pathway (the alternative pathway), which is activated outside the cell through ligation reactions of death receptors (Wang and Youle 2016). Both pathways can induce ROS production, calcium overload (Brookes *et al.,* 2004), ATP deficiency (Lieberthal *et al.,* 1998) or loss of mitochondrial membrane potential (Zhang *et al.,* 2009).

1.3.4 Reactive Oxygen Species

Reactive oxygen species (ROS) can damage both protein and DNA (Cui *et al.,* 2012). The close proximity of mitochondrial proteins and mtDNA to the respiratory chain, a major generator of ROS, can render mitochondria vulnerable to oxidative damage (Turrens, 2003). Reactive oxygen species (ROS) include the superoxide anion radical (O_2^{2-}), hydroxyl radical (•OH) and hydrogen peroxide (H_2O_2). The superoxide anion, is mainly generated by mitochondrial complexes I and III of the ETC, is highly reactive and can cross the IMM, where it can be reduced to H_2O_2 (Stefanatos and Sanz, 2017). Superoxide is created as a consequence of electron leak from the respiratory chain that provokes electron acceptance directly by molecular oxygen (Turrens, 2003). The enzyme superoxide dismutase, which resides within the cell, can convert superoxide into H_2O_2 and although rather stable, H_2O_2 still remains highly toxic, until it can be broken down to water and oxygen by catalase (Sheng, 2014).

1.4 THE MITOCHONDRIAL GENOME

The mammalian mitochondrial genome is described as being negatively coiled: the DNA helix under winds anti clockwise when the two DNA strands combine. The mitochondrial genome is double stranded and spans 16.6 kilo bases (kb) (Figure 1.8).

MtDNA comprises two strands, heavy (H strand) and light (L-strand), containing guanine and cytosine abundant base pairs respectively (Anderson *et al.,* 1981, Taanman, 1999). MtDNA contains 37 genes, 13 of which are involved in the coding of OXPHOS proteins, with the remainder encoding for the small and large ribosomal units and tRNAs. The mitochondrial genome contains no introns, unlike the nuclear genome (Ojala *et al.,* 1981), but does contain a non-coding region (NCR), referred to as the displacement loop (D-loop), which spans 1kb (positions 16024-576) of the entire structure. It is at this location that heavy strand replication (O_H) occurs (Anderson *et al.,* 1981) (See Section 1.4.1).

Many copies of mtDNA can be found within one mitochondrion, where a cell can hold hundreds of copies of mitochondria (cell energy dependant). In post mortem brain tissue, mtDNA copy number increases with age where levels of mtDNA copy number were found to range from 10,000 to 70,000, in the cerebral, frontal cortex and substantia nigra neurons (Dolle *et al.,* 2016)

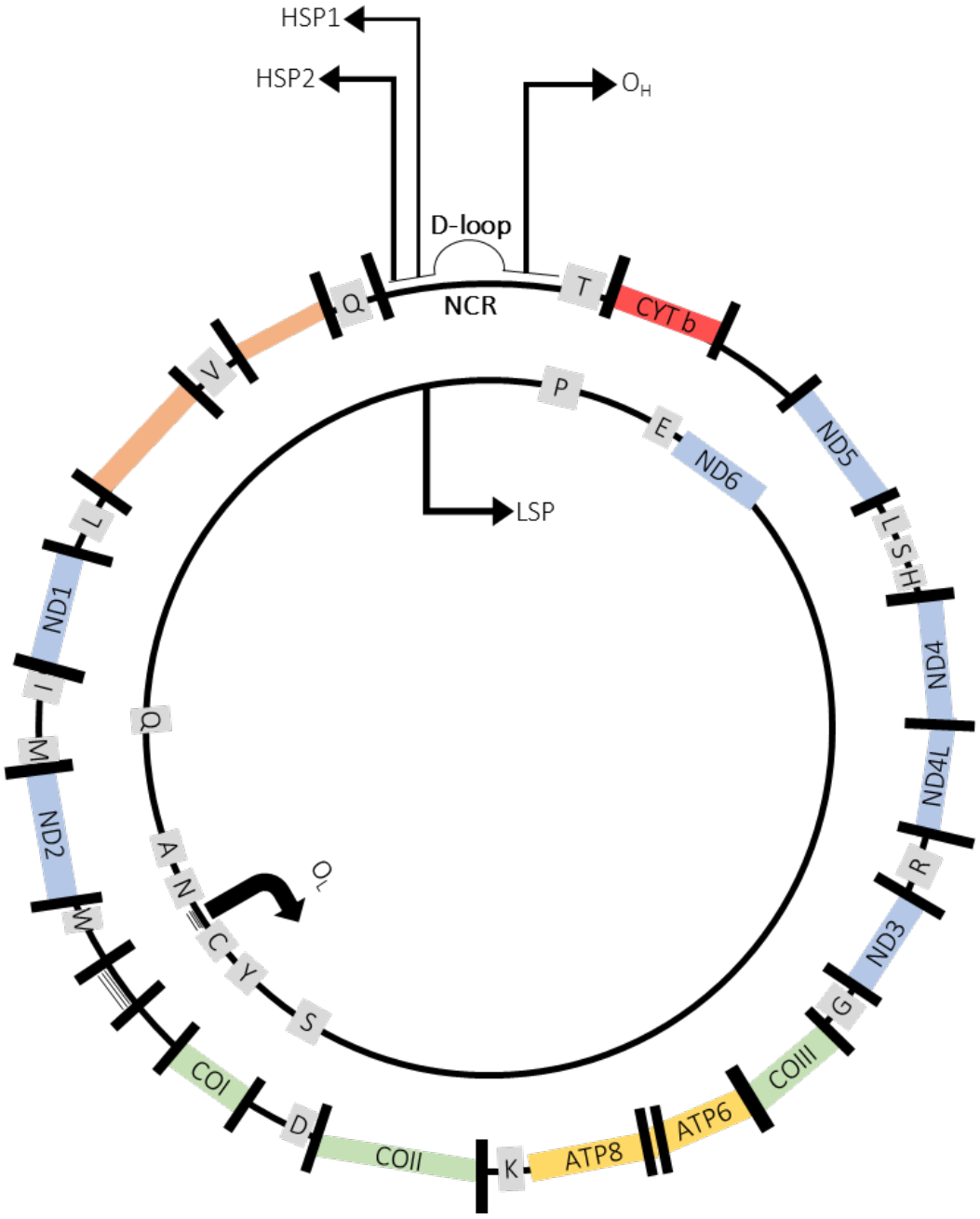

Figure 1.8. The mitochondrial genome. Proteins encoding mitochondrial complex I (blue), complex III (red), complex IV (green) and complex V (yellow) are highlighted. The ribosomal RNA genes and tRNAs are indicated as orange and grey respectively. Origins of replication, the heavy strand (O_H) and the light strand (O_L) (light strand) are highlighted with black arrows. Within the displacement-loop (D-loop) structure, the non-coding region (NCR) can be found, in addition to the heavy strand promotor (HSP), light strand promotor (LSP) and the O_H. (Figure adapted from Nicholls and Minczuk, 2014).

1.4.1 The replication of mitochondrial DNA

Mitochondrial replication begins at the H-strand (O_H) of the D-loop, and is dependent on the following proteins: polymerase gamma ([POLG], which manages mtDNA replication), Twinkle ([TWNK] an mtDNA helicase), mitochondrial single strand binding protein (mtSSB) ligase and POLRMT, an RNA polymerase (Wanrooij and Falkenberg, 201).

Proposed models of mtDNA replication consists of two commonly studied mechanisms, the asynchronous (Figure 1.9a) or the synchronous (Figure 1.9b) model. The Asynchronous (or strand displacement: SDM) model of replication proposes that replication is initiated at O_H, where following on from two thirds of heavy strand replication, the O_L (the origin of light strand replication) is exposed and light strand replication is initiated. Following on from this, heavy strand replication proceeds in a clockwise direction and light strand replication in a counter-clockwise direction. Light strand replication lags behind the heavy strand, coining the terms lagging and leading strand. Once replication is complete, the mtDNA is circularised, becoming supercoiled, and lastly, the D-loop is replicated and serves as a template for its own replication (Clayton, 1982).

The synchronous model (Coupled leading-lagging strand) of replication initially proposed by Robberson *et al.,* (1972), and further developed by Holt *et al.,* (2000) indicates that heavy strand replication is initiated at the O_H, and light strand replication occurs simultaneously through short oligonucleotide Okazaki fragments (Holt *et al.,* 2000). In the 2000s, Holt *et al.,* identified double stranded replication intermediates that were found to house long stretches of RNA and DNA hybrids (Holt *et al.,* 2000). This instigated RNA formation via the lagging strand which follows the Ribonucleotides are Incorporated ThroughOut the Lagging Strand (RITOLS) model (Holt and Reyes, 2012) (Figure 1.9c). This model hypothesises that the leading H strand carries out replication via O_H, however lagging strand replication occurs as short RNA segments which hybridise with the leading strand and then mature into DNA. This model comprises of similarities between that of the strand displacement model where both reactions are initiated at the O_H in unidirectional manner (Figure 1.9).

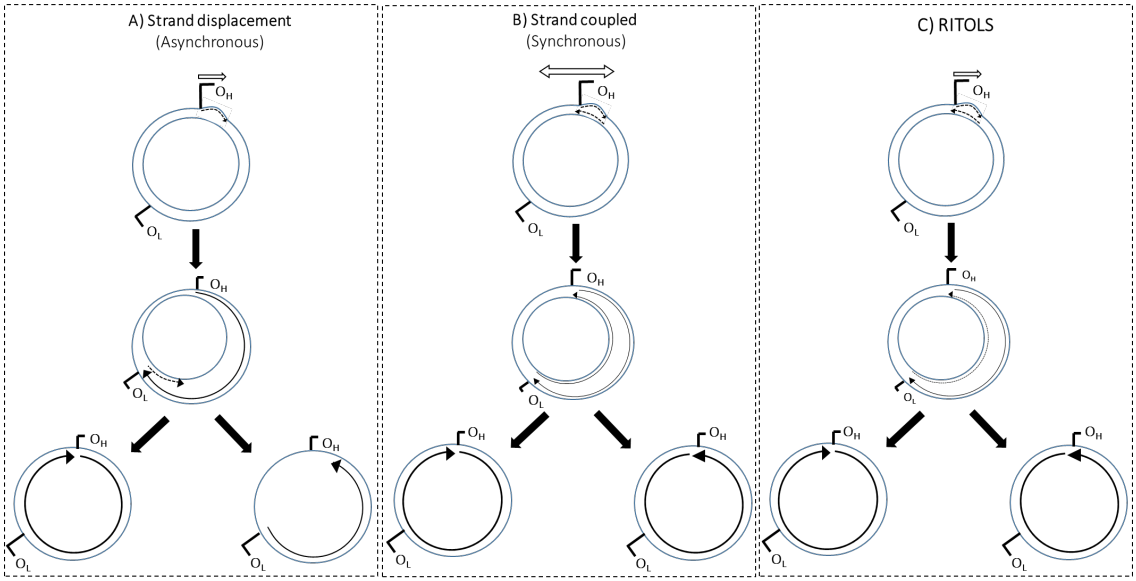

Figure 1.9. Mitochondrial DNA replication. Three methods of mtDNA replication have been suggested. **A)** The strand displacement or asynchronous model where replication is initiated at two separate locations **B)** The strand coupled or the synchronous model describes that replication begins simultaneously for both strands at the same region, where the L lagging strand is replicated using okazaki fragments and finally **C)** The RITOLS model is an extension of the strand coupled theory but suggests that the lagging strand is protected by an RNA intermediate species which then undergo DNA hybridisation (Figure adapted from McKinney & Oliveira, 2013).

1.4.2 The transcription of mitochondrial DNA

Mitochondrial transcription is bi-directional and the proteins that control these reactions are totally nuclear encoded. This process begins at the HSP1 and HSP2 sites of the D-loop structure of mtDNA and the light strand promoter (LSP), which is the origin of L-strand transcription (Chang and Clayton, 1984) which creates polycistronic mRNA.

Mitochondrial RNA polymerase (POLMRT) undertakes mitochondrial transcription, alongside, transcriptional factor A (TFAM) and transcription factor B2 (TFB2M) (Falkenberg *et al.,* 2002). POLRMT and TFAM attaches to the promotor forming an initiation complex, following which POLRMT binds and dissolves the promoter prohibiting DNA interaction (Morozov *et al.,* 2014). TFB2M is then recruited creating the pre-initiation complex, where mitochondrial transcribing elongation factor (TEFM) attaches the POLRMT and by doing so, initiates transcription (Minczuk *et al.,* 2011)

Transcription initiated at HSP1, then undergoes terminations which is managed by mitochondrial termination factor (mTERF), thought to play a role in the recycling of the initiation complex, and transcript termination at the LSP site (Martin *et al.,* 2005).

1.4.3 The translation of mitochondria DNA

The proteins necessary for OXPHOS are encoded for by the mitochondrial genome, where mitochondrial ribosomes (mitoribosomes) conduct translation of the required genes (Lightowlers *et al.,* 2014).

Mitoribosomes encode *12s* and *16s rRNA* proteins that are measured in Svedberg units (s) as a measure of their sedimentation rate. The 55s mitoribosome sedimentation coefficient, comprises a large subunit (LSU), 39s and a small subunit (SSU), 28s, much smaller in comparison to cytoplasmic ribosomes. The 39s and 28s subunits partake in peptidyl-transferase and translation initiation reactions respectively, and also house the 28s and 12s rRNA subunits (Smits *et al.,* 2010) (Figure 1.10).

Mitochondrially encoded mRNA transcripts are processed at tRNA sites before translation begins and are completed with the mitochondrial poly (A) polymerase (mtPAP) regulating a poly-A tail addition reaction (Ojala *et al.,* 1981). Mitochondrial translation can be segregated into three steps, initiation, elongation and termination.

The first, initiation step recruits mt-mRNA to the smaller mitochondrial (28s) ribosomal subunit (mt-SSU) disrupting association with the large subunit (mt-LSU), consequently removing initiation factor: mtIF3 from mt-SSU. Formylated methionine (fMet), then promotes translation via the fMet- tRNAMet complex where the remaining unformylated variant is used to conduct elongation. Following this, the fMet- tRNAMet are enlisted to the mt-SSU P-site by mtIF2, where GTP hydrolysis reactions release mtIF2 allowing mt-LSU to re-attach to this complex (Smits *et al.,* 2010, Mai *et al.,* 2016).

Aminoacylated mt-tRNA mediates mtDNA transcription-elongation reaction which is regulated by the mitochondrial elongation factor Tu (mt-EFTu) and GTP hydrolysis (Valente *et al.,* 2007). Mt-EFTu is then released from the complex where peptide bonds are generated at the peptidyl transferase centre (PTC) of the mt-LSU. Following this, mitochondrial elongation factor 1 (mtEFG1) instigates a conformational change, moving the mRNA three codons from the A (Aminoacyl) to the E (Exit)-site. The resultant polypeptide is relocated into the matrix to undergo folding (Smits *et al.,* 2010, Mai *et al.,* 2017).

The concluding step of the mitochondrial translational triad is termination and is stimulated by A-site mitoribosomal stop codon. Stop codons associate with mitochondrial release factor 1a (mt-RF1a), which hydrolyses the P-site-tRNA and terminal amino acid ester bond. This reaction causes the detachment of the P-site polypeptide from the ribosomal complex and following this the vacant ribosomal complex undergoes mitochondrial release factor 1 (mt-RRF1) and mitochondrial elongation factor G2 (mt-EFG2) mediated recycling. Mt-SSU and LSU dissociate and mtIF3 re-binds mt-SSU to restart transcription-initiation (Nicholls *et al.,* 2013).

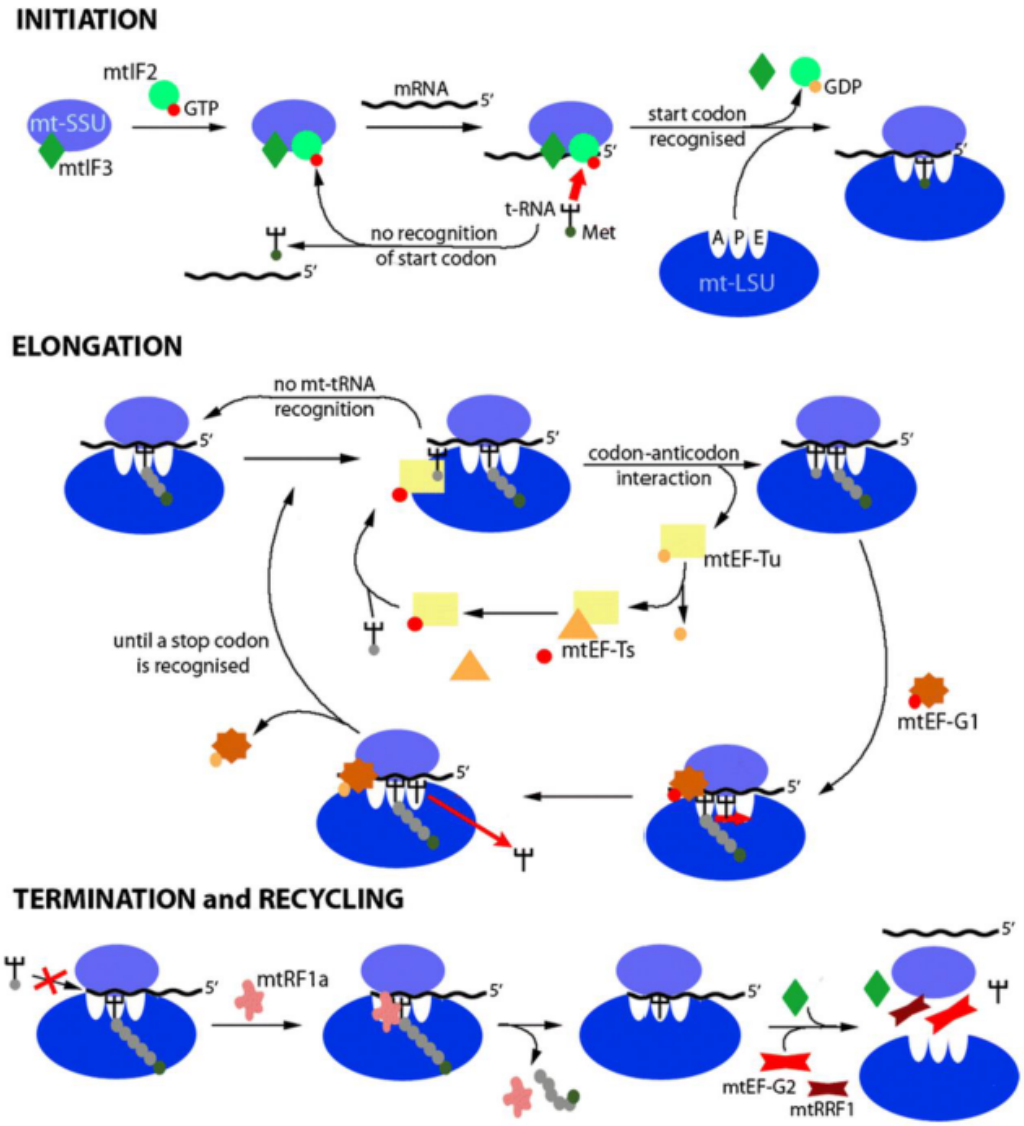

Figure 1.10. Mitochondrial translation. MtDNA translation is categorised into 3 main stages, initiation, elongation and termination. (Figure taken with permission from Mai *et al.,* 2016).

1.4.4 Mitochondrial Repair

As the mitochondrial genome is situated near the ETC it is highly susceptible to mtDNA damage as direct consequence of ROS production. MtDNA repair systems must therefore exist to counteract these damages, namely short patch base excision repair (SP BER). In this case, mtDNA repair is conducted by DNA glycosylases that identify the incorrect base and rectify this by hydrolysing the sugar phosphate backbone of the DNA molecule (Zinovkina, 2017). Mammalian glycosylases identified include UNG1, UNG2 and MUTYH where MUTYH partakes in the removal of the incorrect base on the secondary DNA strand. These mitochondrial targeted glycosylases then interact with AP endonucleases, in a mechanism which inserts the correct base at the single strand 3'-OH (hydroxyl group) end via DNA polymerase involvement. Following this the strand is ligated via DNA ligase III. In cases where the DNA polymerase interactions fail, long patch (LP) base excision repair (LPBER) occurs where several bases are inserted as opposed to one (Kroeger *et al.,* 2003).

1.4.5 Mitochondrial heteroplasmy and the threshold effect

Individual cells can hold more than one copy of mtDNA. Homoplasmy refers the situation by which all mtDNA copies within a cell are identical, whereas heteroplasmy suggests that within one cell, some mitochondria may harbour a mutation, and some may not (Taylor and Turnbull, 2005). MtDNA mutations become harmful to the cell once a particular mutation threshold is exceeded. This threshold effect indicates that around 60-80% of mutated mtDNA (though this can vary for different mtDNA mutations and within different tissues) must occur to cause OXPHOS dysfunction. Chapter 5 will discuss this further.

1.4.6 Clonal expansion

The process by which mtDNA deletions increase to high levels are referred to as clonal expansion. So far there exists three theories that explain this phenomenon.

Proposed in 1992, the first theory is termed the 'survival of the smallest' describes that deleted mtDNA molecules replicate at a faster rate due to their smaller size. mtDNA molecules then undergo more frequent replication which may cause an accumulation of deleted mtDNA molecules (Wallace *et al.,* 1992). Evidence against this scenario has shown that mtDNA point mutations specifically, (regardless of their genome size) still accumulate to levels that are as high as the mtDNA deletions (Taylor *et al.,* 2003).

Following this the 'survival of the slowest' theory was suggested by DeGrey (1997). This hypothesis suggests that mtDNA deletion can perturb the OXPHOS system thus generating large amounts of reactive oxygen species (ROS). Through this method, increased mtDNA deletions occur which cannot undergo lysosomal degradation and consequently allowing the continuous replication of mutated mtDNA (DeGrey, 1997)

The third is the 'random genetic drift' theory, arising in the early 2000s, indicates that mtDNA molecules replications containing deletions are completely random and their clonal expansion occurs via no selective advantage (Elson *et al.,* 2001)

1.5 MITOCHONDRIAL DYNAMICS

Mitochondrial movement and their morphological dynamics were first sighted in 1914 via light microscopy studies (Lewis and Lewis, 1914) where over the last 30 years, live imaging dyes been utilised to track of mitochondrial movement (Johnson *et al.,* 1981, Bereiter-Hahn and Voth, 1994, Rizzuto *et al.,* 1996). These experiments demonstrated that mitochondria are constantly undergoing mitochondrial fission and fusion. The balance between these two processes determines mitochondrial shape and is a key contributor in determining organelle distribution, bioenergetics and mitophagy (Bliek *et al.,* 2013).

1.5.1 Mitochondrial fission

Mitochondria can divide through a process known as mitochondrial fission, where the organelle is split into two, or in some cases more than two structures (Scott and Youle, 2016).

Regulated by dynamin related protein-1: (DRP1), a protein member of the dynamin family of large GTPases, Drp1 is localised to the OMM through adaptor proteins, such as Fis1 (Hoppins *et al.,* 2007). Fis1 is recruited to the OMM where it interacts with Drp1, creating a 'collar' which surrounds the mitochondrion (Youle and Bliek, 2012). The tightening of this structure then causes constriction and the consequent division of the OMM, leading to mitochondrial fission.

Moreover, mitochondrial dynamics (MiD) proteins 49 and 51, and Mff have been identified as Drp1 recruiters to mammalian mitochondria (Elgass *et al.,* 2012, Youle and Bliek, 2012). Though OMM fission is a well described process, the factors mediating IMM mitochondrial fission remain unclear (Scott and Youle, 2016). (Figure 1.11a).

1.5.2 Mitochondrial fusion

Mitochondrial fusing is believed to combat mitochondrial stress and dysfunction through the fusing activity of damaged mitochondrial components with a healthier mitochondrion (Youle and Bliek, 2012). Similarly, to mitochondrial fission, mitochondrial fusion of the OMM is also dynamin GTPase dependant. Mitochondrial fusion is regulated by mitofusin (Mfn) 1 and 2 proteins in mammals residing on the OMM (Hales and Fuller., 1997, Chen *et al.,* 2003), and once mitochondria join these tethered proteins, mitochondrial fusion occurs. In regard to mitochondrial fusion of the IMM, more investigation is required, however some reports have showed Opa1 (Optic atrophy 1) involvement via its IMS and/or IMM location (Wong *et al.,* 2000, Olichon *et al.,* 2002) (Figure 1.11b).

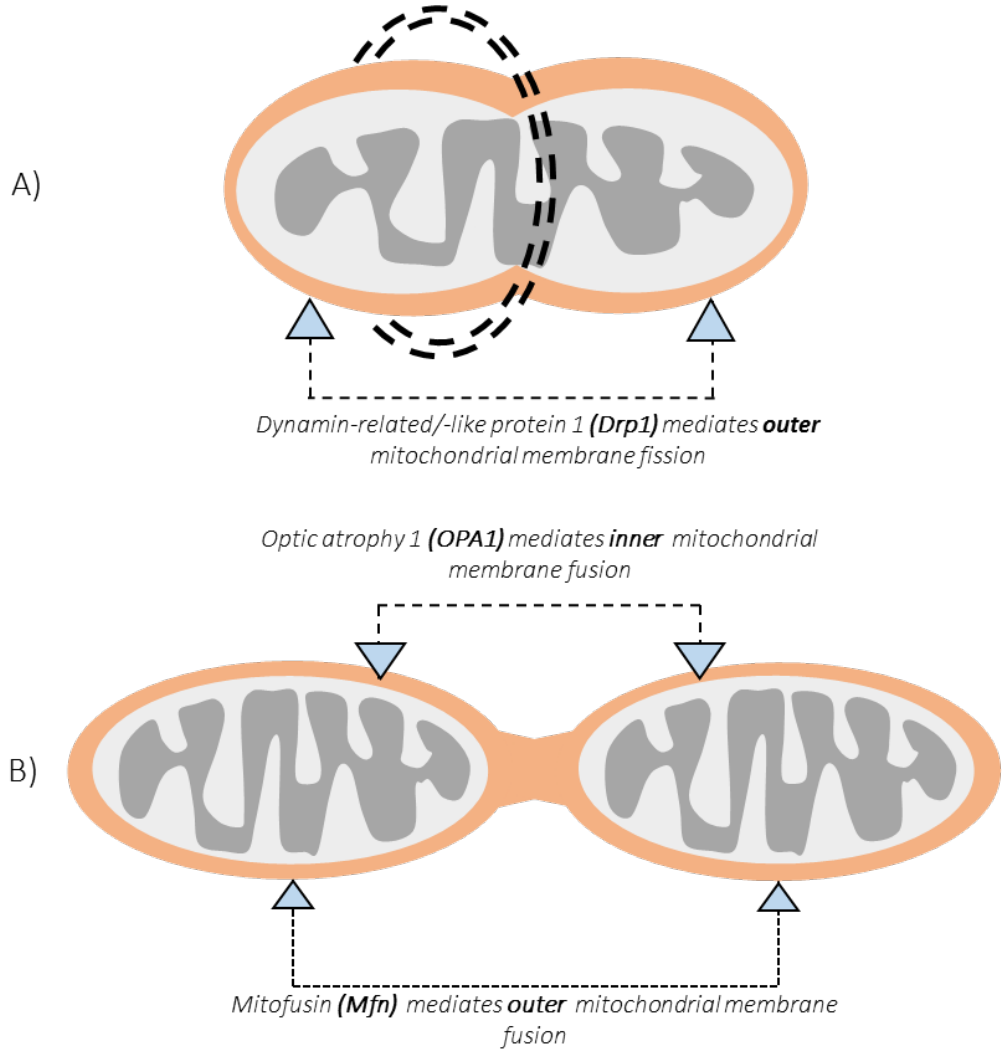

Figure 1.11. Mitochondrial fission and fusion in mammalian cells. A) Drp1 is located in the cytosol, where it shuttles back and forth to the OMM during fission events. Drp1 forms a collar that encircles the mitochondrion, the tightening of this collar leads to the splitting of the OMM, inducing mitochondrial fission. **B)** Mfn proteins are found on the OMM, which promote the joining of two mitochondria at the early stages of fusion. OPA1 localised in the IMM, regulates IMM fusion.

1.5.3 Neuronal mitochondrial transport

Mitochondrial distribution is highly regulated by mitochondrial transport to balance the energy needs of several cell types, especially within neurons. The pre and post synaptic terminals, axonal branches and the nodes of Ranvier, contain more mitochondria than other neuronal regions (Bogan and Cabot, 1991, Fabricus *et al.,* 1993, Morris and Hollenback, 1993, Mutsaers and Carroll, 1998, Ruther and Hollenbeck, 2003, Li *et al.,* 2004, Zhang *et al*., 2010). Chapter 3 will discuss ATP provision within neurons further.

Time lapse studies have shown that neuronal mitochondria undertake bidirectional transport along neuronal processes, and their movement is dynamic and sporadic: showing varied directionality, pausing and docking/halting (Morris and Hollenback, 1993, Hollenbeck and Saxton, 2005, Miller and Sheetz, 2006, Misgeld *et al*., 2007, Kang *et al*., 2008). Furthermore, dysfunctional mitochondria supposedly return for degradation by the autophagy-lysosomal system (Sheng and Cai, 2012). Given this situation, it can be suggested neurons may contain a system which regulates mitochondrial movement from the soma to energy demanding regions of the neuron.

These patterns of mitochondrial movement convey how varied this organelle's motility can be where within *in vivo* experiments, mitochondrial movement is either stationery or motile. Motile mitochondrial can pause and then continue onwards without alterations in their directionality whilst stationary mitochondria remain anchored (docking/halted) (Faits *et al.,* 2016, Lewis *et al.,* 2016, Smit-Rigter *et al.,* 2016). Alterations in mitochondrial trafficking are due to mitochondrial attachment to anterograde and retrograde motor proteins. The halting of mitochondria occurs via various docking and anchoring systems to microtubules. It has been shown that mitochondria attach to these motor proteins directly to allow mitochondrial movement and directionality (Sheng and Cai, 2012).

Mitochondrial movement over long distances i.e. from soma to distal axon/ dendrites, depends upon neuronal polarity and microtubule organisation. Microtubules are created from the polymerisation of alpha- and beta-tubulin and are arranged in a polarised manner with their minus and plus ends (Hirokawa and Tanaka, 2010). Axonal microtubules are arranged so that the minus ends are targeted towards the soma and plus ends directed distally.

Kinesin superfamily (KIFs) and cytoplasmic dynein are the two main microtubule-based motor proteins that have been identified. KIF motors move towards the microtubule plus-end

whereas cytoplasmic dynein motors mediate microtubule minus-end directed transport. Both motor proteins promote long distance transport of mitochondria (Martin *et al.,* 1999, Hirokawa and Tanaka, 2010). In axons, the minus end directed cytoplasmic dynein regulates retrograde movement towards the soma whilst the plus end kinesin motors allow anterograde transport to distal axonal regions and synaptic terminals (Martin *et al.,* 1999, Hirokawa *et al.,* 2010).

1.5.3.1 Anterograde mitochondrial motors

Partaking in anterograde mitochondrial transport, KIFs are composed of 3 major groups that are dependent on the position of the motor domain within the molecule: the N-terminal motor domain KIFs (N-KIFs), the middle motor domain KIFs (M-KIFs), and the C-terminal motor domain KIFs (C-KIFs) (Seog *et al.,* 2004). KIFs comprise two functional domains: a motor domain that reversibly binds to the cytoskeleton, and the rest of the molecule (the tail) that interacts with cargo directly (Figure 1.13a). Around 45 different KIF motor genes exist and are classified into 14 families (Aizawa *et al.,* 1992, Lawrence *et al.,* 2004).

Research indicates that the members of the kinesin-1 family are termed as KIF5 and play a role in anterograde transport of neuronal mitochondria (Reviewed in: Tanaka *et al.,* 1998, Gorska-Andrzejak *et al.,* 2003, Pilling *et al.,* 2006). Each KIF5 heavy chain contains an amino-terminal motor domain, while their carboxy terminal regulates kinesin light chain association and/or direct interactions with mitochondrial adaptor proteins and hence mitochondria (Pilling *et al.,* 2006, Hirokawa *et al.,* 2010, MacAskill and Kittler, 2010).

Mammals have three KIF5 motor isoforms, KIF5A, KIF5B and KIF5C, where only KIF5A and KIF5B are expressed within neurons (Kanai *et al.,* 2000). Murine *Kif5b* mutations have been shown to instigate the clustering of mitochondria near the nucleus in undifferentiated extra-embryonic cells, however in wild type conditions mitochondria are transported peripherally (Tanaka *et al.,* 1998).Mutations in the KIF5 homologue in *Drosophila melanogaster* have been shown to cause impaired mitochondrial transport in larval motor axons (Pilling *et al.,* 2006). The overexpression of the KIF5 cargo binding domain in hippocampal neurons, disrupts KIF5 and microtubule adaptor protein association, dysregulating anterograde mitochondrial transport (Cai *et al.,* 2005). Though mutations of *Khc* in *D.melanogaster* reduces anterograde mitochondrial movement in motor neurons, it was not entirely depleted (Pilling *et al.,* 2006).

Together these studies detail the role of anterograde kinesin motors indicating how these motors regulate mitochondrial transport in neurons and also appear to manage the correct distribution of neuronal mitochondria.

1.5.3.2 Motor adaptors

Milton is a motor adaptor protein characterised in *D.melanogaster.* Milton is associated with KIF5 during mitochondrial transport and connects in an indirect manner to mitochondria via interactions with mitochondrial Rho (Miro), a RHO family GTPase on the OMM (Stowers *et al.,* 2002, Fransson *et al.,* 2003, Frederick *et al.,* 2004, Fransson *et al.,* 2006) (Figure 1.12).

Miro contains two EF hands, Ca^{2+} binding motifs and two GTPase domains that form connections with Milton, KIF5 and then mitochondria. Milton directly binds the C-terminal domain of KHC (Glater *et al.,* 2006), where KIF5 is recruited to the mitochondrial surface by Milton and Miro adaptors, via the kinesin light chain.

Recently, Milton orthologues (TRAK1 and TRAK2) and MIRO orthologues (MIRO1 and MIRO2) have been identified in mammals. TRAK1 and TRAK2 have been shown to interact with KIF5 (Brickley *et al.,* 2005, Smith *et al.,* 2006). TRAK can also bind the first GTPase domain of MIRO1 and MIRO2 (Fransson *et al.,* 2006).

In hippocampal neurons, MIRO functions as a vital mitochondrial acceptor site for TRAK2. This creates the MIRO1-TRAK2 complex and has shown to be a key regulator of mitochondrial transport (MacAskill *et al.,* 2009). TRAK1 knockdown experiments in hippocampal neurons result in a dysfunctional respiratory capacity in axons, further eliciting that endogenous TRAK expression mediates mitochondrial movement (Brickley *et al.,* 2011).

These studies demonstrate that together the KIF5, Milton and Miro triad encompass the anterograde mitochondrial transport system.

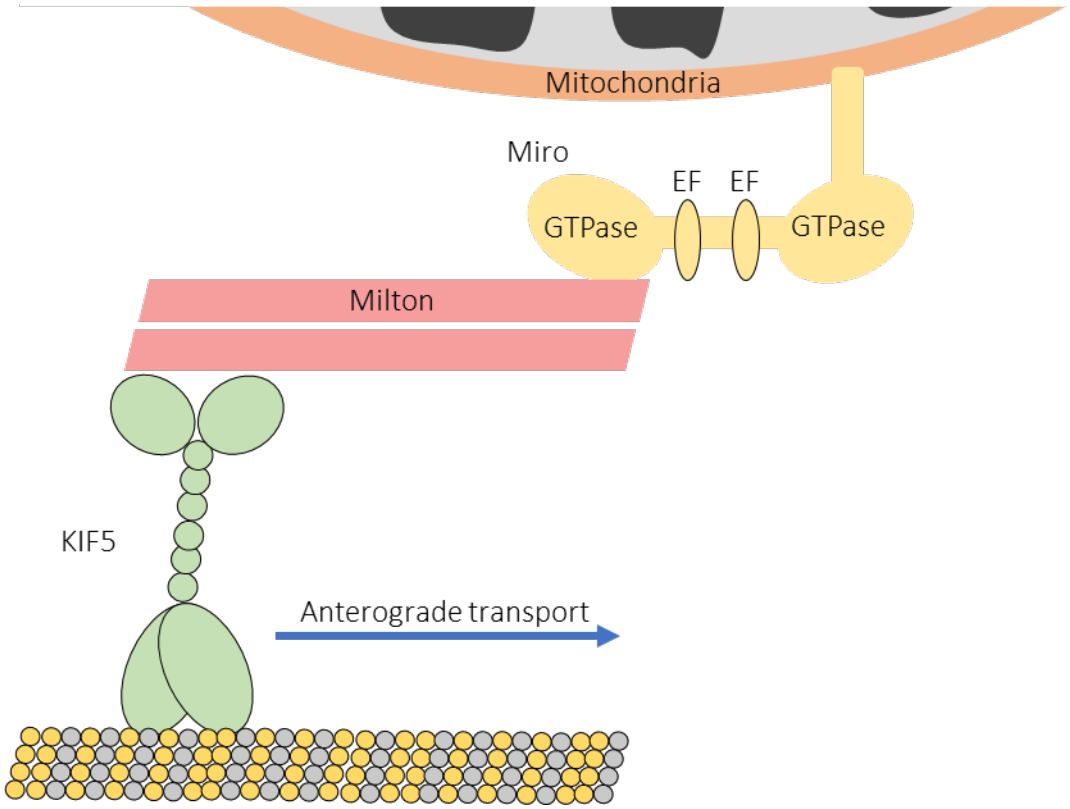

Figure 1.12. The Miro-Milton kinesin complex. The structural of Miro (Rho1/2) comprises of two GTPase domains loosely related small GTPases of the *ras* superfamily, separated by two Ca^{2+}-binding EF hands. The carboxyl terminus of the Miro contains a *trans*-membrane domain that can anchor Miro in the OMM. Milton can bind both Miros and kinesin heavy chain (KIF5), facilitating mitochondrial movement in the anterograde direction. (Figure adapted from Schwarz, 2013)

1.5.3.3 Retrograde transport motors

Cytoplasmic dynein regulates retrograde movement of mitochondria within axons to the cell body. Structurally dynein comprises two heavy chains, which binds cargo and is a polypeptide dependant reaction. Cytoplasmic dynein associates with a protein complex known as dynactin, which is a large 11-subunit complex which binds to cytoplasmic dynein and to microtubules, regulating its interactions with cargo (King and Schroer, 2000).

Only two dynein heavy chains have been identified, cytoplasmic dynein heavy chain 1 (Dync1h1) and 2 (Dync2h1) (Tanaka *et al.,* 1995, Pfister *et al.,* 2006). Furthermore, dynein motors also house, several dynein intermediate chains (DIC), dynein light intermediate chains (DLIC) and dynein light chains (DLC) (Sheng and Cai, 2012) (Figure 1.13b).

It has been suggested that dynein forms contacts with proteins on the mitochondrial membrane via their light chains. TCTEX1, a dynein light chain protein is believed to attach to the mitochondrial OMM protein, VDAC1 (Schwarzer *et al.,* 2002).

In context of the mitochondrial transport system, the loss of MIRO was shown to impair kinesin and dynein axonal transport (Russo *et al.,* 2009). Though the direct association of MIRO with dynein motors has not been shown, it appears that MIRO may not only be an adaptor for KIF5 but also for dynein mediated retrograde transport. Whether dynein associates with the mitochondrial membrane directly or indirectly however still remain unanswered.

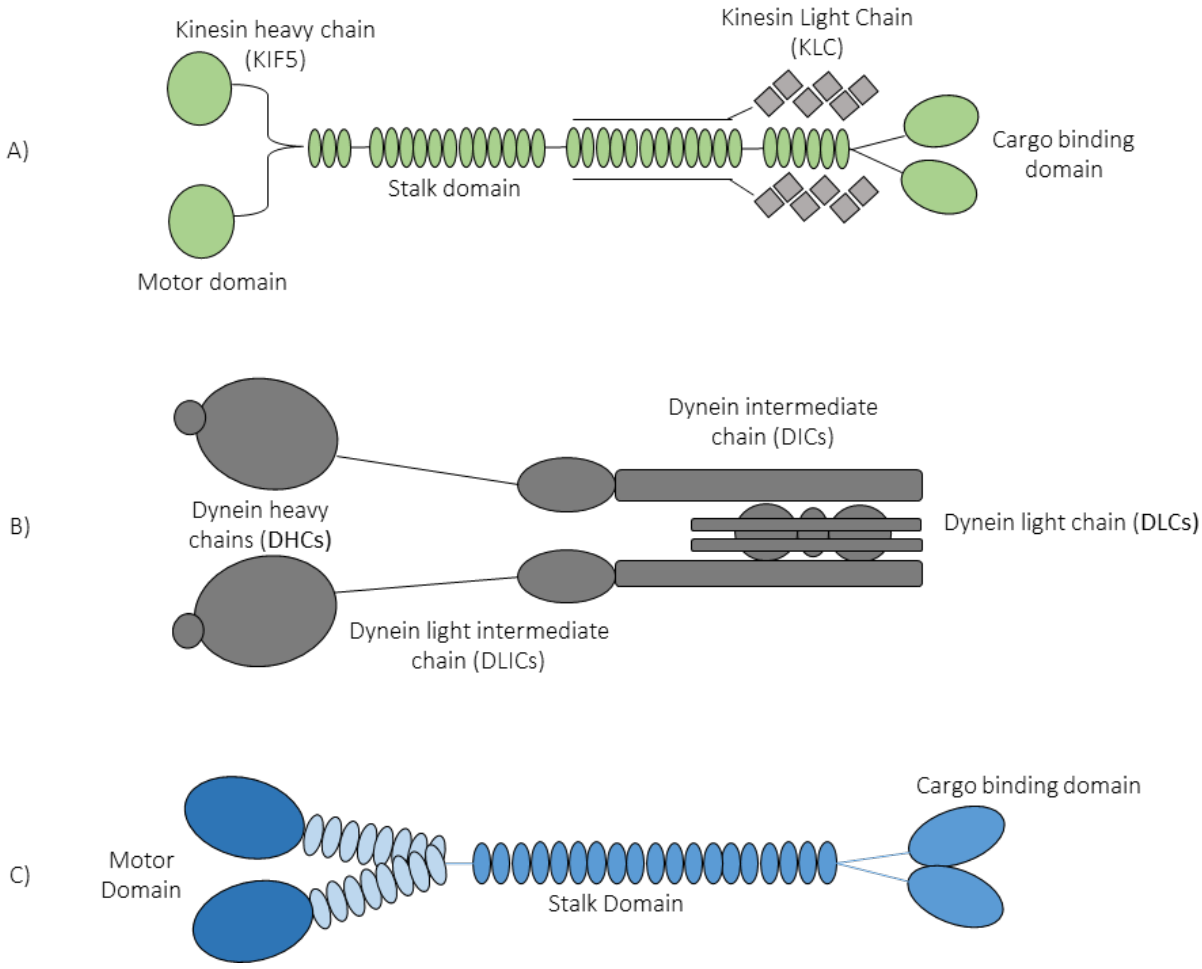

Figure. 1.13. The structure of motor proteins that mediate mitochondrial transport. Motor protein structure plays a large role in the way it associates with the microtubule and actin filaments. **A)** Kinesins are made of four chains: two heavy (KHCs) and two light (KLCs). Main kinesin motor functions are mediated by its heavy chains that are attached to the coiled regions of the stalk segment of the protein. These heavy chains comprise an amino-terminal motor domain, which partakes in ATPase activity and as a result interact with the microtubule. Additionally, the role of the carboxy-terminal is to regulate light chain interactions and to consequently bind adaptor proteins.
B) Unlike kinesin, dynein only contains two dynein heavy chains (DHCs). The remainder of the protein comprises numerous dynein intermediate chains (DICs), dynein light intermediate chains (DLICs) and dynein light chains (DLCs). Similarly, to kinesins, dynein motor activity is also regulated by its heavy chain component which manages the protein's interactions with cargoes via polypeptide interactions. **C)** The energy required for myosin motor activity across actin filaments is ATP dependant and so far, 18 types of myosin motor proteins have been identified (Figure adapted from Sheng and Cai, 2012)

1.5.3.4 Bidirectional mitochondrial transport

Bidirectional mitochondrial transport occurs when both both anterograde and retrograde motors are associated with an individual mitochondrion simultaneously.

Dynein has been shown to localise with bi-directionally moving mitochondria (Hirokawa *et al.,* 1990), whereby interrupting kinesin motors does not instigate dynein motor mediated retrograde (Saotome *et al.,* 2008, Wang and Schwarz, 2009). This suggests that kinesin and dynein motor proteins may coordinate bidirectional transport, rather than opposing one another (Ligon *et al.,* 2004, Welte, 2004) (Figure 1.15a).

D.melanogaster mutants that lack the dynactin complex showed disrupted anterograde and retrograde movement, indicative that dynactin may coordinate the activity of the opposing motors (Haghnia *et al.,* 2007). Likewise, Pilling *et al.,* 2006 demonstrated that kinesin-1 inhibition reduces anterograde and retrograde mitochondrial movement and is required for dynein–driven retrograde transport. This observation was accompanied by organelle-filled axonal swellings, perhaps reflecting autophagocytosis of senescent mitochondria accumulated in axons as a consequence of retrograde transport failure. It was suggested that this may be a protective process aimed to suppress cell death signals and neurodegeneration (Pilling *et al.,* 2006).

How mitochondrial directionality mediates mitochondrial transport is unclear. Further investigation is required to understand if mitochondrial movement occurs via a 'tug of war' mechanism between the motor proteins and how alterations of one motor may affect the other motor tipping the balance of anterograde and retrograde transport.

1.5.3.5 Short range myosin motors

Shorter range mitochondrial movement is observed within nerve terminals predominantly comprised of actin filaments mediated by myosin motors. Mitochondrial trafficking regulated by myosin motors have not been observed in axon terminals. However, myosin XIX is targeted to mitochondria via its tail domain, where it may play a role in mitochondrial transport in neuronal processes and synaptic terminals (Naisbitt *et al.,* 2000). Myosin V has also been shown to form a motor complex with dynein light chains, where this motor complex may regulate short and long-distance mitochondrial movements (Naisbitt *et al.,* 2000) (Figure 1.13c).

Mitochondrial motility is enhanced by actin (Morris and Hollenbeck, 1995) and is essential for axonal mitochondrial docking (Chada and Hollenbeck, 2004). Myosin V supposedly competes with dynein for organelle binding, displacing them from microtubule tracks to actin filaments during retrograde movement and myosin V depletion increases bidirectional mitochondrial velocity (Sheng and Cai, 2012)

What may be occurring is that myosin actually favours actin-based mitochondrial docking to transport mitochondria away from their microtubule tracks. These mitochondrial transport regulatory systems may illustrate various types of neuronal mitochondrial movement though how myosin motors achieve these regulations requires further research (Figure 1.14).

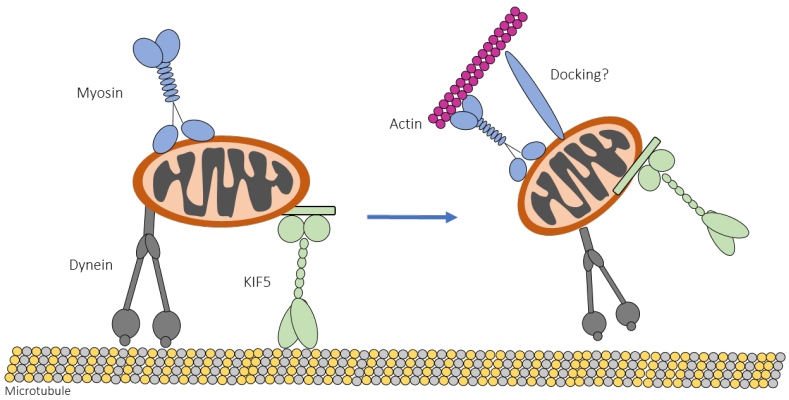

Figure 1.14. Myosin and actin mediated mitochondrial trafficking. The transition from long to short–range microtubule based mitochondrial trafficking is myosin driven, leading to subsequent actin-based movement, following which actin based docking may occur through unidentified docking and anchoring proteins (Figure adapted from Sheng and Cai, 2012)

1.5.3.6 Microtubule based mitochondrial docking

Maintaining a reliant mitochondrial docking system is necessary to keep the required numbers of stationary mitochondria in regions that rely heavily on energy production and an efficient Ca^{2+} buffering capacity. For that reason, stationary mitochondria are required to provide a localised source of ATP and are crucial in maintaining Na^{+}/K^{+} ATPase activity, fast spike propagation and synaptic transmission (Billups, 2002). Immobilised mitochondria are either dissociated from transport motors or anchored to the cytoskeleton.

Syntaphillin, has been recently described as neuron specific 'static anchor' for axonal mitochondria via its its C-terminal domain (Kang *et al.,* 2008). Syntaphillin *(Snph)* deletion in a murine model augmented the percentage of mobile axonal mitochondria in comparison to wild type neurons (Sheng and Cai, 2012). Co-localisation studies have shown that syntaphilin interacts with TOM20 on the OMM of the mitochondria, though the specifics of this interaction remain unknown (Caino *et al.,* 2016). Syntaphillin overexpression completely abolishes axonal mitochondrial transport.

The syntaphilin mechanism of action constitutes anchoring mitochondria to microtubules via its direct association with kinesin-1 (Hirokawa *et al.,* 1982, Linden *et al.,* 1989, Price *et al.,* 1991, Jung *et al.,* 1993). Recently, it has become of great interest to understand the role of syntaphilin as a molecular target for delving into the mechanistics of what differentiates stationary and motile neuronal mitochondria. It was observed that as mitochondrial motility becomes limited, the length of time that mitochondria spend at presynaptic boutons increases (Takihara *et al.,* 2015, Lewis *et al.,* 2016, Smit-Rigter *et al.,* 2016). Furthermore, this reduction of motility was accompanied by an increase in syntaphilin expression with ageing (Zhou *et al.,* 2016) (Figure 1.15D and E)

1.5.3.7 The role of Ca^{2+} in the regulation of the KHC, Miro and Milton complex

Neuronal microtubule based mitochondrial arrest occurs at elevated Ca^{2+} levels (Rintoul *et al.,* 2003, Yi *et al.,* 2004, Hollenbeck and Saxton, 2005, Chang *et al.,* 2006, Szabadkai *et al.,* 2006). During increased cytosolic Ca^{2+} levels there may be an inefficient ATP supply which can interrupt Ca^{2+} transfer across the plasma membrane. This may also affect dysfunctional mitochondrial buffering capacity through impaired ETC activity. Therefore, the halting of mitochondrial movement in the presence of increased Ca^{2+} appears to increase stationery mitochondria, which may be useful in regions that require large supplies of ATP when energy resources are limited (Figure 1.15C).

It has previously been shown that the level of mitochondrial Ca^{2+} inversely correlates with the speed of mitochondrial motility, with no indication as to whether this affects directionality of mitochondrial movement (Chang *et al.,* 2011). Conversely, Miro EF hand mutation studies revealed a failure to arrest mitochondrial motility during elevated cytoplasmic Ca^{2+} levels (MacAskill *et al.,* 2009, Wang and Schwarz, 2009). It appears that instead of dissociating kinesin-1 from the mitochondria, Ca^{2+} binding allows Miro to interact directly with the motor domain of kinesin-1, preventing motor and microtubule interactions, altering kinesin-1 from an active state (bound to Miro only via Milton), to an inactive state (direct binding to Miro). This was found to inhibit its interaction with microtubules (Wang and Schwarz, 2009).

Chang *et al.,* 2011 discovered that mutations within the EF hand domain of miro1 decreased Ca^{2+} influx into the mitochondria. Thus, it can be suggested that blocking mitochondrial Ca^{2+} influx via miro1 EF-hand mutants, can trigger a lapse in mitochondrial motility within neurons (Chang *et al.,* 2011). These studies shed some light on how mitochondrial movement can be regulated by intra-cellular Ca^{2+} levels (Niescier *et al.,* 2018). Intra-mitochondrial Ca^{2+} may also be a key player in mitochondrial transport whereby Ca^{2+} thresholds may be set to inhibit mitochondrial movement.

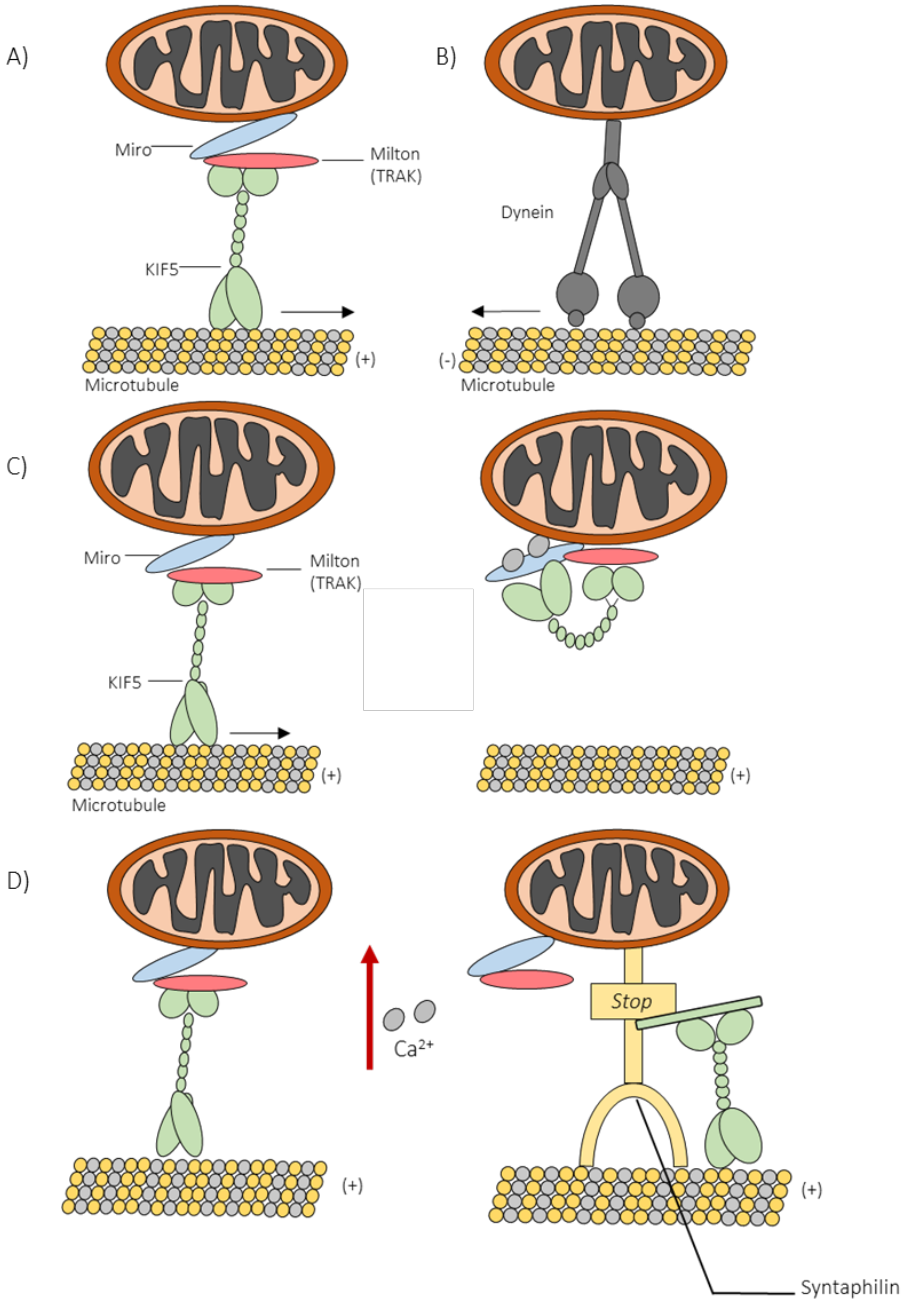

Figure 1.15. The regulation of mitochondrial transport. **A)** The Miro–Milton (or Miro–Trak) motor adaptor complex, mediates KIF5 anterograde mitochondrial transport. **B)** Retrograde mitochondrial transport mediated by dynein motors. **C)** Ca^{2+} regulation of Miro-driven mitochondrial transport occurs as Miro contains Ca^{2+} binding EF-hand motifs. The C-terminal cargo binding domain of KIF5 motors bind the Miro–Trak adaptor complex, where, Ca^{2+} binding to Miro's EF-hands causes a separation of the motor domain with microtubules, preventing mitochondrial transport via inhibition of any motor and microtubule contact (Wang and Schwarz, 2009). **D-E)** Mitochondrial docking and its arrest occurs through a syntaphilin-mediated model. A Miro-Ca^{2+} sensing pathway triggers the binding switch of KIF5 motors from the Miro–Trak adaptor complex to anchoring protein syntaphilin, which immobilises axonal mitochondria via inhibiting motor ATPase activity. This model is termed the 'engine switch off and brake' model where syntaphilin turns off the KIF5 motor by sensing increased Ca^{2+} levels, which function as the stop sign, anchoring mitochondria to the microtubule. (Figure adapted from Sheng and Cai, 2012)

1.6 MITOPHAGY

1.6.1 Autophagy

Autophagy is the process by which intracytosolic components such as proteins and/or organelles are delivered to lysosomes in the soma to be degraded. Autophagic substrates are engulfed inside an autophagosome, a double membrane vesicle which contains degradation molecules. These fuse with the lysosome, a small single membrane organelle that contains within its matrix degradation enzymes (Martinez-Vincent, 2015).

This process maintains neuronal survival and eliminates damaged components. Basal autophagy is essential for neuronal viability where faulty autophagic mechanisms can cause the accumulation of protein aggregates and/or damaged organelles, all contributors of neuronal death (Hara *et al.,* 2006, Komatsu *et al.,* 2006). During basal autophagy the constant turnover of intracellular components provides the necessary cellular metabolites under compromised conditions. Furthermore, induced autophagy occurs when the cell experiences stress signals and exists to maintain vital amino acids through the elimination of damaged material. This process can be provoked mitochondrial damage (Kim *et al.,* 2007, Singh *et al.,* 2009).

1.6.2 Mitophagy

Mitophagy is mitochondria specific autophagy. First observed in mammalian cells, this process is responsible for increased mitochondrial sequestration in lysosomes (De Duve and Wattiaux, 1966). Kim and colleagues, created the term 'mitophagy' to define the process of the engulfment of mitochondria into vesicles that are coated with the autophagosome marker MAP1 light chain 3 (LC3), in a process that occurred within 5 minutes (Kim *et al.,* 2007). LC3 is a ubiquitin-like protein that covalently attaches to phosphatidylethanolamine during autophagosome biogenesis, allowing its integration into the membrane (Nakatogawa *et al.,* 2007) promoting cargo recruitment (Noda *et al.,* 2010).

1.6.3 Mitophagy - Mitochondrial mediated receptors

OMM proteins including: B-cell lymphoma 2 19 kDa interacting protein 3 (BNIP3), Nix, Bcl-2-like protein 13 (Bcl2-L-13) and FUN14 domain containing 1 (FUND1) have been identified as regulators of mitophagy. They share a similar protein structure: an LC3-interacting region (LIR) motif which enables their involvement of the mitochondrion with LC3.

BNIP3 and Nix (members of the Bcl-2 family of proteins) are pro-apoptotic proteins (Zhang and Ney, 2009). Mitophagic Nix activity can remove mitochondria from the erythrocyte (Schweers *et al.,* 2007, Sandoval *et al.,* 2008). It is believed that BNIP3 and NIX function is controlled via hypoxia-inducible factor-1 (HIF-1) activity, a transcriptional factor which enhances BNIP3 and NIX expression under low oxygen conditions (Zhu et al., 2013). FUND1 dependant mitophagy is also triggered under these conditions (Wu *et al.,* 2016).

Primary sightings of mitophagy were identified in yeast, which suggested Atg32 as a mitophagy receptor. Mammalian studies have since then identified Bcl2-L-13 as its homologue. Not only can Bcl2-L-13 conduct mitophagy but can also alter mitochondrial morphology, via creating mitochondrial fragmentation (Murakawa *et al.,* 2015).

1.6.4 Mitophagy – Non - mitochondrial mediated receptors

Mitochondria are recognised by two domains present in these receptors: the ubiquitin binding domain (UBD) that binds to polyubiquitinated OMM proteins on the mitochondrial surface, and the LIR motif that binds LC3-II present on the autophagosome structure (Wild *et al.,* 2014). In this mechanism, two main proteins, Phosphatase and tensin homologue-induced putative kinase 1 (PINK1) and a E3 ubiquitin ligase (Parkin) are involved. PINK1/Parkin-mediated mitophagy has largely contributed to the understanding of mitophagy in mammalian cells in response to mitochondrial depolarisation (Martinez-Vicente, 2017).

Basally, PINK1 is recruited to the mitochondria from the cytosol. Within the cytosol, TOM and TIM complexes regulate PINK1 transport, relocating it from the OMM to the IMM. Here, PINK1 undergoes cleavage which is regulated by mitochondrial processing peptidase (MPP) and presenilin-associated rhomboid-like protease (PARL). The cleaved PINK1 is cytosolically exported for degradation purposes managed by the proteasome system (UPS) (Deas *et al.,* 2011, Yamano and Youle, 2013). Following its export to the mitochondrial surface, PINK1

initiates mitophagy by identifying mitochondrial dysfunction i.e. a depolarised membrane potential. PINK1 detects mitochondrial dysfunction and signals Parkin to ubiquinate PINK1-phosphorylated residues (p-S65-Ub) upon the surface of a damaged mitochondrion (Fiesel & Springer, 2015) thus triggering mitophagy. Parkin ubiquitinates these proteins on the mitochondrial surface which are then phosphorylated by PINK1, creating a PINK1/Parkin mediated positive feedback loop (Pickrell and Youle, 2015) (Figure 1.16).

In the absence of Parkin, it has been shown that five different autophagy receptors (p62, neighbour of BRCA1 gene [NBR1], Optineurin [OPTN], NDP52 and TAX1BP1) are all able to recognise polyubiquitinated signals in PINK1/parkin mediated mitophagy. p62, has been shown as one of the main markers of autophagy and is widely used as a marker of autophagic flux together with LC3-II (Klionsky *et al.,* 2016). However, a recent study which manipulated various knockouts of all five receptors, deduced that only OPTN and NPD52 were the primary receptors for PINK1/parkin-mediated mitophagy (Lazarou *et al.,* 2015). Proposing that though p62 and NBR1 partake in mitophagy, they are not essential (Narendra *et al.,* 2010).

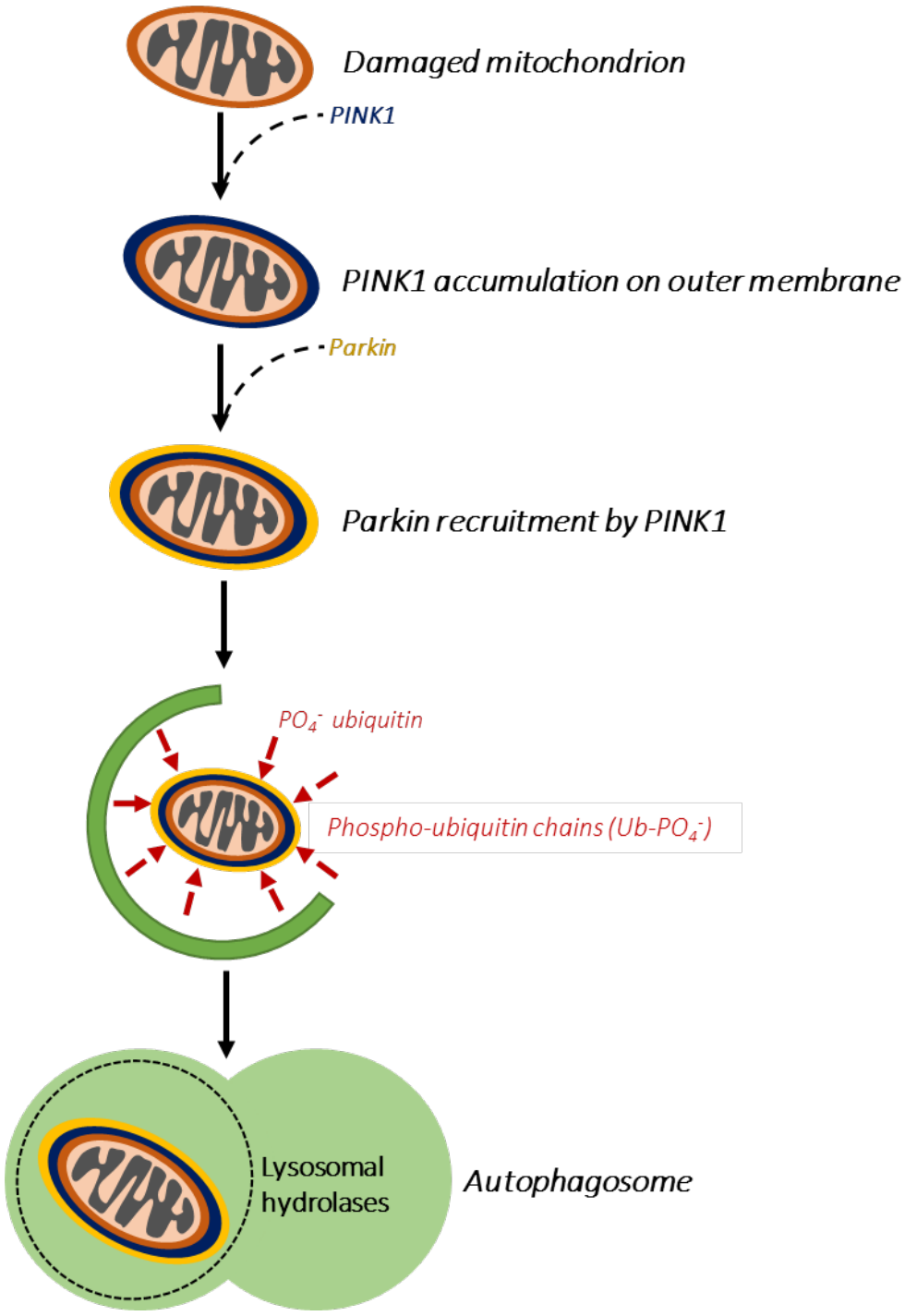

Figure 1.16. PINK1/Parkin mitophagy. Mitochondria increase PINK1 expression on their OMM when depolarised. This increased PINK1 expression allows phosphorylation reactions to occur to both ubiquitin and Parkin, which promotes Parkin activity. Parkin ubiquitinates substrates on the OMM, which then promotes the recruitment of autophagosomes that are transported to the cell body for lysosomal degradation.

1.6.5 Neuronal mitophagy

Neurons, as post-mitotic cells exhibit increased vulnerability to mitochondrial impairment. Most studies that discuss PINK1/Parkin-dependent mitophagy have been carried out in non-neuronal cell models and although they provide valuable insight do not mimic physiological nor neuronal mitophagic conditions (Grenier *et al.,* 2013).

In neuronal mitophagy, the translocation of endogenous Parkin to mitochondria upon depolarisation is a controversial concept, as most groups cannot detect this (Sterky *et al.,* 2011, Rakovic *et al.,* 2013). Neurons rely upon OXPHOS for ATP production (in comparison to glycolysis dependant non neuronal cells) therefore differences in mitochondrial bioenergetics between cell lines and neurons may justify their inability to recruit parkin (Van Laar *et al.,* 2011).

Mitochondrial turnover is essential for neuronal survival. Neuronal mitophagy can be quantified by measuring mitochondrial mass in the presence of lysosomal inhibitors. Studies have shown that when lysosomal degradation is blocked, a loss of mitochondrial membrane potential can function as a signal which is detected under basal or induced (CCCP treatment) (Mauro-Lizcano *et al.,* 2015). Low levels of Parkin in neurons can induce mitophagy upon strong depolarisation in a PINK1-dependent manner, though the rate of mitochondrial clearance still remains slow, due to an exclusion of Parkin amplification (Chu *et al.,* 2013)

Therefore, studies distinguish between either mitochondrial degradation under basal conditions or under increased mitochondrial depolarisation. The well described PINK1/parkin dependent pathway might be activated in response to severe mitochondrial damage, however occurring sparingly due to the low levels of endogenous parkin within neurons. (Mauro-Lizcano *et al.,* 2015) (Figure 1.17)

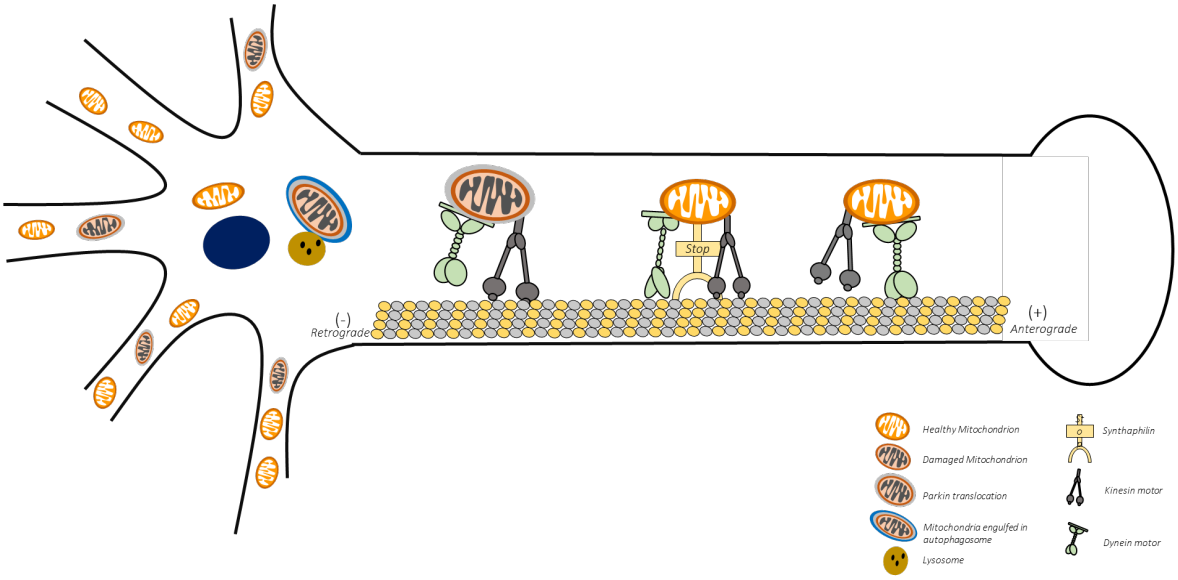

Figure 1.17. Axonal mitochondrial transport and mitophagy. Within axons, microtubule plus ends (+) are orientated toward axon terminals, where kinesin motors regulate anterograde mitochondrial transport and minus ends (-) are directed towards the soma, where dynein motors regulate retrograde mitochondrial movement. Motile mitochondria can be recruited into stationary pools via dynamic anchoring interactions between syntaphiln and the microtubules, ensuring that neuronal mitochondria are distributed along axons and at synapses, where constant energy supply is vital. Damaged mitochondria (harbouring a low mitochondrial membrane potential), associate with Parkin on the mitochondria and are then transported to the soma for lysosomal degradation through mitophagy. Inversely, healthy mitochondria are transported away from the some (Adapted from Sheng, 2014)

1.7 SELECTIVE NEURONAL VULNERABILITY IN NEURODEGENERATION

Within neurodegeneration the main unanswered question remains why particular neurons are more susceptible to vulnerability than others, and what determines which neuronal populations degenerate at later stages of disease. The mechanisms that surround selective neuronal vulnerability, include molecular and cellular factors that determine how and when particular neurons succumb to or resist an age-related disease (Morris *et al.,* 1998)

Dopaminergic (DAergic) neurons in the substantia nigra (SNc) are damaged in PD and are long projection neurons with extending axons (Smith *et al.,* 1987). These neurons are easily rendered dysfunctional during ageing as they require a large level of ATP for survival. In Parkinson's disease (PD), dopamine (DA) adds to the demise of the neurons through oxidative stress in presynaptic terminals and synapses (Cookson, 2005); the most vulnerable regions of the neuron (Mattson and Magnus, 2006).

1.8 PARKINSON'S DISEASE AND THE BASAL GANGLIA CIRCUITRY

1.8.1 Parkinson's disease

Parkinson's disease (PD) is an age-related neurodegenerative disorder affecting more than 1% of the population aged over 60 years of age (Dawson & Dawson, 2003). Identified in the 1800s, James Parkinson described this disease as 'shaking palsy' (Bartels & Leenders, 2009) as this CNS disorder was shown to affect motor activity. PD patients with long-term neurodegeneration demonstrated typical Parkinson symptoms which included motor impairments, muscle rigidity and impaired posture and balance (Dawson & Dawson, 2002).

Neuropathologically, PD is characterised by the loss of DAergic neurons from the SNc that project to the striatum , causative of the characteristic PD motor symptoms (Fahn and Sulzr, 2004, Sulzer and Surmeier, 2013). Most cases of PD are sporadic (idiopathic), but 15% of cases are inherited (familial) (Bartels & Leenders, 2009). Inherited genetic factors, chemical agents (pesticides), genetic mutations, dysfunctional mitochondrial trafficking and mitophagy and ROS have all been suggested as contributors to PD pathogenesis (Nguyen *et al.,* 2011).

Whilst PD aetiology is multifactorial (some of which will be discussed below) it has been shown that α-synuclein (SNCA) protein aggregates termed Lewy bodies (LBs) are a central component in disease pathogenesis. Mechanisms surrounding SNCA related PD toxicity are still being investigated where the involvement of mitochondria have been suggested to be contributors to this damage. Chapter 4 will further discuss the effects of SNCA and mitochondrial dysfunction.

1.8.2 Autonomous pace-making

DAergic neurons within the SNc of the nigrostriatal pathway are autonomous pacemakers, generating 2–4 Hz action potentials (APs) without synaptic inputs (Guzman *et al.,* 2009). This pace making activity relies on a mechanism involving calcium influx via L-type Ca^{2+} channels Cav1.3 pore-forming subunit. This allows high concentrations of intracellular Ca^{2+} that cannot be immediately removed from cells and are instead sequestered (Surmeier et al., 2017). Ca^{2+} storage in the endoplasmic reticulum (ER) and mitochondria increases the neuron's metabolic rate, resulting in the production of free radicals and ROS, which are thought to accelerate ageing. This can lead to significantly higher rates of neuronal loss in SNpc compared to other areas of the brain with advancing age (Guzman *et al.,* 2010).

Studies that were conducted in cultured primary mesencephalic DAergic neurons have demonstrated that the opening of L-type Ca^{2+} channels can cause an increase in mitochondrial oxidative damage in dendrites (Pacelli *et al.,* 2015). SNCA aggregate formation can further impair this within the perinuclear and dendritic regions (Caraveo *et al.,* 2014). This Ca^{2+} dyshomeostasis most likely explains the reason why DAergic neurons in the SNpc are so susceptible to damage in comparison to other neuronal areas.

The ventral tegmental area (VTA) neurons, though effected to some extent in PD, are relatively spared in comparison to DAergic neurons (Sulzer and Surmeier, 2013) expressing lower levels of the L-type calcium channel Cav1.3 (Surmeier *et al.,* 2017). This lower expression occurs as VTA neurons do not manifest Ca^{2+} oscillations and utilise HCN/Na^{+} channels for pace making activity (Neuhoff *et al.,* 2002). Therefore, cytoplasmic DA levels are increased in SNc neurons compared to VTA dopaminergic neurons. The constant maintenance of this pace making activity (regardless of posing a high risk of cellular damage and stress) serves an essential

purpose in preserving the steady striatal extracellular dopamine concentration necessary for network activity.

1.8.3 Dopamine

Dopamine (DA) undergoes oxidation forming DA quinones and free radicals. A reaction which is catalysed by tyrosinase (Munoz *et al.,* 2012). Monoamine oxidases (MAO) and catechol O-methyl transferase (COMT) are also involved in DA metabolism, where MAO-A and MAO-B are situated on the OMM, degrading any excess cytosolic DA through oxidative deamination (Jenner and Langston, 2011). DA levels are modulated through MAO-A oxidative reactions (Riederer *et al.,* 1987), however, with ageing and PD, the concentration of MAO-B within glial cells increases, taking over the main share of DA metabolism (Saura *et al.,* 1997, Youdim *et al.,* 2006, Fowler *et al.,* 1997). DA is taken up by astrocytes via Na-dependent mechanisms for metabolism (Kimelberg and Katz 1986). The products of MAO-B mediated DA metabolism are 3,4-dihydroxyphenyl-acetaldehyde (DOPAL), an ammonium molecule and H_2O_2. H_2O_2 is membrane permeable and enters DAergic neurons within close proximity, which may then partake in the Fenton reaction, where H_2O_2 reacts with Fe^{2+} to generate hydroxyl radicals (Nagatsu and Sawada, 2006). Elevated MAO-B expression has been associated with enhanced enzyme activity within astrocytes of adult mice showing selective, progressive loss of DAergic neurons (Mallajosyula *et al.,* 2008).

DA oxidation generates DA quinones, a highly reactive aminochrome, which promotes superoxide generation in addition to its reduction to NADPH. Furthermore, DA reuptake into nigrostriatal terminals following synaptic release requires a DAergic transporter (DAT), thus any alterations in these reactions can affect the concentration of cytoplasmic free DA that is prone to oxidation (Hastings, 1995, Graham, 1978).

1.8.4 Organisation of the basal ganglia

The basal ganglia are a set of subcortical nuclei that are involved in regulating processes such as motor, cognitive and mnemonic functions. The ventral region of the basal ganglia consists of the ventral striatum and the nucleus accumbens which are associated with limbic functions. The dorsal region of the basal ganglia consists of the striatum (STR) (also known as the caudate putamen), the globus pallidus (GP), the entopeduncular nucleus (EP), the subthalamic nucleus (STN) and the substantia nigra (SN) (Bolam *et al.,* 2000). The SN is divided into 2 regions, i) the

dorsal pars compacta (SNc) where DA nigrostriatal neurons are located and ii) the ventral pars reticula (SNr).

Input to the basal ganglia comes from the cortex, where almost the whole cortical mantle projects to the basal ganglia. The corticostriatal projection conveys information to the striatum and other regions of the basal ganglia, forming the basal ganglia circuitry (Albin *et al.,* 1989, DeLong, 1990, Smith *et al.,* 1998). Corticostriatal projections are processed within the striatum, in addition to other inputs from the amygdala and hippocampus that innervate the striatum, and once processed are transmitted to the output nuclei of the basal ganglia, the EP and SNr. The flow of cortical information through the basal ganglia occurs via 2 routes, the direct and indirect pathways (Albin *et al.,* 1989, DeLong, 1990).

1.8.5 The direct pathway and indirect pathway

The striatonigral/direct pathway consists of information that is transmitted directly from the striatum to the output nuclei (Hersch *et al.,* 1995, Bolam *et al.,* 2000).

At resting state, output nuclei of the basal ganglia are inhibitive with a reduction in inhibition observed during basal ganglia associated behaviour. Neurons that project from the striatum are GABAergic and inactive at resting state. The basal ganglia output neurons are also GABAergic but have a high discharge rate which inhibits basal ganglia targets. This system is activated by the firing of corticostriatal glutamatergic neurons, causing striatal neurons to discharge which inhibits the basal output nuclei, the EP and SNr (Bolam *et al.,* 2000).

D_1 and D_2 receptors come from a superfamily of G protein-couple receptors which respond to inputs from the SN to the striatum. Functionally, these receptors stimulate and inhibit adenylyl cyclase (AC) (Kebabian and Calne, 1979, Jackson and Westlind-Danielsson, 1994, Missale *et al.,* 1998). In the striatum, these receptors are separated into two types of medium spiny neurons: the striatonigral/direct and the striatopallidal/indirect pathway neurons (Hersch *et al.,* 1995, Surmeier *et al.,* 1996). The latter of which will be discussed further below.

D_1 receptors in the direct pathway partake in AC/PKA signalling. PKA activation promotes PKA phosphorylation of the substrate dopamine to cause to alterations in neuronal functions (Greengard *et al.,* 1999, Hyman and Malenka, 2001). DA receptors co-express the peptide substance P and dynorphin, and provide a direct inhibitory effect on GPi/SNr neurons. Inhibition of the output neurons causes release from inhibition of neurons in the targets of the

basal ganglia and therefore is linked to basal ganglia behaviour (Bolam *et al.,* 2000) (Figure 1.19).

Striatal neurons in the indirect pathway transmit corticostriatal information in an indirect manner to the output nuclei via synaptic connections in the GP and STN (Shink *et al.,* 1996).

1.8.6 The role of the indirect pathway in motor symptoms of Parkinson's disease

The striatum comprises both projection and interneurons (Bolam & Bennett, 1995, Kawaguchi *et al.,* 1995, Kawaguchi, 1997), where the major projection neurons are medium size densely spiny neurons, accounting for the majority of the total population of the striatal neurons (Kemp & Powell, 1971a). These neurons use GABA as their main neurotransmitter. Several feedback pathways exist with the basal ganglia circuitry, where the major feed-forward reaction is involved the DA neuronal projection from the SNc to the striatum.

Input from DA terminals that arrive from the SNc (that degenerate in PD), create synaptic contacts with the necks of the dendritic spines of these spiny projection neurons (Bouyer *et al.,* 1984, Freund *et al.,* 1984, Smith *et al.,* 1994, Hanley & Bolam, 1997). The head of the spines that receive the DA input, then form synapses via creating contacts with the nigrostriatal neurons (Freund *et al.,* 1984). This anatomy facilitates DA released from the nigrostriatal terminals, which will act on DA receptors that are within the post synaptic membrane (Yung *et al.,* 1995) in order to regulate the excitatory input at the head of the spine.

Cholinergic and GABAergic inputs are also observed in contact with the necks of the spines, displaying a similar anatomy (Bolam *et al.,* 1985, Izzo & Bolam, 1988, Pickel & Chan, 1990). The striatopallidal/indirect pathway utilises D_2 receptors and the peptide enkephalin (ENK). Activation of the indirect pathway arises from increased firing of output neurons, and therefore, the increased inhibition of basal ganglia targets, where the indirect pathway functions to dismiss basal ganglia associated movement or to subdue unwanted movement (Mink & Thach, 1993) (Figure 1.18).

Nigrostriatal DAergic neurons form highly branched networks within their striatal targets, Matsuda *et al.,* 2009, where a single DAergic neuron can innervate up to 5.7% of the striatum, whilst adjacent DAergic inputs also demonstrate a large degree of overlapping targets. It was calculated that a single post-synaptic medium spiny neuron, could be influenced by up to 194

DAergic inputs, thus clinical signs of PD only develop after up to 70% of neurons are lost (Matusyda et al., 2009) (Figure 1.18).

The reduced activation of DA receptors, caused by a dopamine (DA) deficiency, results in reduced inhibition of neurons of the indirect pathway and decreased excitation of neurons of the direct pathway. Reduced inhibition from the indirect pathway leads to over-inhibition of the GPe, disinhibition of the STN and increased excitation of GPi/SNr neurons, whereas decreased activation from the direct pathway causes a reduction in its inhibitory influence on the GPi/SNr. The net result is therefore, an excessive activation of basal ganglia output neurons accompanied by excessive inhibition of motor systems, leading to the characteristic parkinsonian motor features. Following DAergic lesions, expression of D2 receptor and preproenkephalin mRNA increases in striatal neurons of the indirect pathway, whereas expression of mRNA encoding the D1 receptor, substance P and dynorphin decreases in neurons of the direct pathway (Albin *et al.,* 1989, DeLong, 1990).

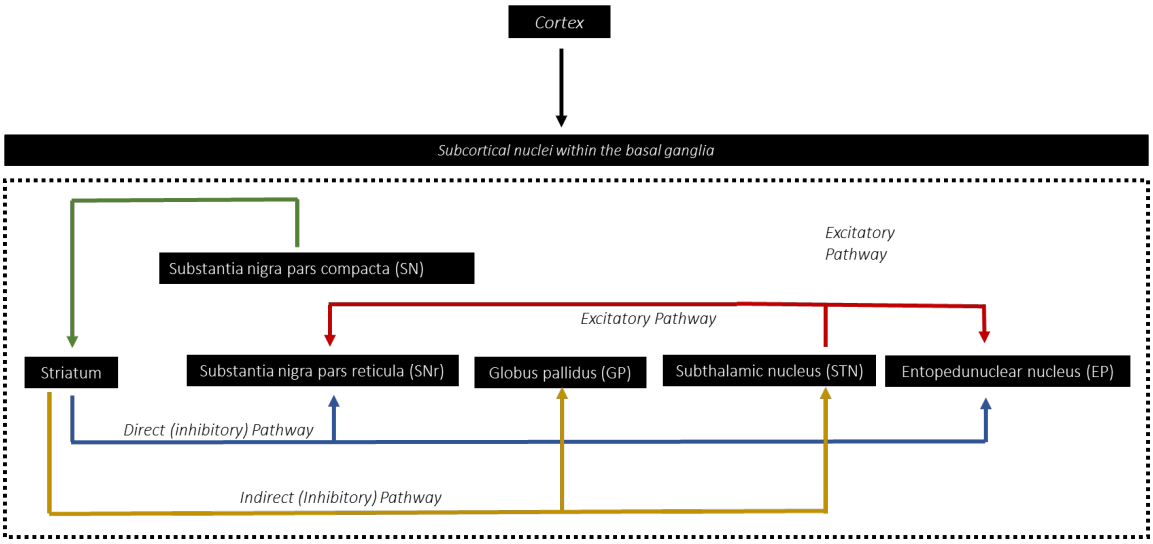

Figure 1.18. The direct and indirect pathway. Cortical information that reaches the striatum is conveyed to the basal ganglia output structures (SNr}, EP, and the SNpr, via 2 pathways. The first pathway: the direct pathway comprises of inhibitory projections from the striatum to the SNr and EP (blue line). This direct pathway houses D1 receptors that provide a direct inhibitory effect on GPi and SNr neurons. The second: The indirect pathway, which holds the D2 receptors and houses inhibitory projections from the striatum to the GP. From the GP another inhibitory projection is observed from the GP to the STN (yellow line). Excitatory projections are then found from the STN to the output nuclei, the SNr and EP. DAergic neurons of the SNc generate a massive feedback projection to the striatum (green line) which consequently modulates the flow of cortical information within the basal ganglia system.

1.9 MITOCHONDRIAL INVOLVEMENT IN PARKINSON'S DISEASE

There is evidence of increased oxidative stress in PD, though it remains unclear whether ROS accumulation is a primary event or consequential due to the influence of other cellular dysfunctions. Increasing evidence has suggested mitochondrial dysregulation as a key player in PD pathogenesis (Mattson and Magnus, 2006).

The first suggestion of a mitochondrial role in PD pathogenesis came from the discovery of the opiate 1-methyl-4-phenyl-1, 2, 3, 6-tetrahydrodropyridine (MPTP) which was accidently infused by drug addicted young individuals, triggering Parkinsonism. Biologically, MPTP undergoes oxidation becoming 1-methyl-4-phenylpyridinuim (MPP^+) in glial cells which is a dopaminergic transporter (DAT) substrate. It is taken up into DAergic neurons, and can selectively inhibit complex I of the ETC which is observed in SN and skeletal muscle of PD patients (Bindoff *et al.,* 1989, Schapira *et al.,* 1990, Haas *et al.,* 1995, Schapira 2007, Langston *et al.,* 1983, Burns *et al.,* 1985, Mattson and Magnus, 2006). A complex I defect can initiate cell degeneration in PD through ATP synthesis reduction, generating a bioenergetic defect. Catalytic subunits isolated complex I from the frontal cortex of PD patients display damage due to oxidative stress, which has been associated with disruption of Complex I assembly (Keeney *et al.,* 2006). Complex I deficiency has also been observed in the platelets and skeletal muscle of PD patients (Krige *et al.,* 1992, Bindoff *et al.,* 1991, Parker *et al.,* 1989). Mitochondrial dysfunction in PD has shown to manifest within several biological pathways some of which are described further below.

1.9.1. PINK1 and Parkin function in Parkinson's disease

Parkin (or PARK 2) mutations are the most common cause of autosomal recessive early onset PD (Corti *et al.,* 2011, Martin *et al.,* 2011, Kitada *et al.,* 1998). *Parkin* encodes a 465-amino acid E3 ubiquitin ligase which ubiquitinates different lysine linkages (Lutz *et al.,* 2009, Akepati *et al.,* 2008, Narendra *et al.,* 2010). Over a 100 pathogenic parkin mutations have been reported, disrupting its E3 ligase activity via altering protein stability and thus causing DAergic cell death (Corti *et al.,* 2011, Martin *et al.,* 2011, Houlden and Singleton, 2012). Post-mortem PD brain sections and mouse models have suggested that parkin is inactivated by post-translational modifications, including the oxidation, nitrosylation, and phosphorylation by c-

Abl, a stress-activated non-receptor tyrosine kinase (TH) triggered in sporadic PD brains and in animal models of PD. What promotes parkin activation remains undiscovered though its translocation to the mitochondria or association with its substrate, E2 conjugating enzyme may be causative factors (Imai *et al.,* 2002, Byrd and Weissman, 2013).

The PINK1 (or PARK6) gene was first associated with PD through studies within consanguineous families that presented with early-onset PD (Valente *et al.,* 2004, Corti *et al.,* 2011). PINK1 mutations have been identified as the second most common cause of PD. PINK1 encodes a mitochondrial targeted serine/threonine kinase, where the loss of this kinase function is associated with PD development. Mitochondrial-localised PINK1 is located on the OMM, with its C terminus and kinase domain facing the cytosol (Zhou *et al.,* 2008) indicating that disease relevant PINK1 substrates can be found in the cytosol and/or on the OMM.

The loss of PINK1 or Parkin genes in *Drosophila* has shown evidence of mitochondrial aggregation and cellular degeneration in DAergic neurons, muscle and sperm, causing motor impairment and decreased fertility (Yang *et al.,* 2006, Clark *et al.,* 2006, Park *et al.,* 2006). PINK1 knockout flies exhibited approximately 70 % reduction in ATP levels in comparison to control flies as well as demonstrating a smaller mitochondrial morphology (Clark *et al.,* 2006, Yang *et al.,* 2006). Parkin overexpression studies have shown rescue of the phenotypes caused by PINK1 deficiency, though not the other way around (Yang *et al.,* 2006, Clark *et al.,* 2006, Park *et al.,* 2006). It appears that Parkin activity is independent of PINK1.

Phenotypes that arose as a consequence of PINK1 and Parkin mutations were rescued by increased Drp1 activity, and reduced Mitofusin (Mfn) or OPA1 activity (Yang *et al.,* 2008, Deng *et al.,* 2008, Poole *et al.,* 2008). Promoting mitochondrial fission was found to suppress flight muscle and DAer neurons in Pink1 mutant flies. It was suggested that Fis1 may act in-between Pink1 and Drp1 in controlling mitochondrial fission, suggesting a role for Pink1 within the mitochondrial fission/fusion paradigm (Yang *et al.,* 2008). Knocking down the muscle-specific Mfn fly homologue (Marf) also caused large mitochondrial fragmentation, with altered cristae morphology, where the pink1/parkin pathway was found to trigger mitochondrial fission and supressing mitochondrial fusion by down regulating Mfn and up regulating Drp1 (Deng *et al.,* 2008).

In rat hippocampal neurons, PINK1 or Parkin overexpression, increased mitochondrial number, being smaller in size as well as a reduction in mitochondrial number within neuronal processes, all in all describing the possibility that the mitochondrial fission/fusion balanced sways towards more fission (Yu *et al.,* 2011). PINK1 knockdown showed evidence of an elongated mitochondrial structure, tipping this balance towards mitochondrial fusion. In the same study, cultured rat midbrain DAergic neurons were transfected with lentiviral vectors expressing PINK1 shRNA, PINK1-WT or Parkin-WT constructs, where PINK1-WT/ Parkin-WT expression caused fragmentation of the mitochondria within these neurons (Yu *et al.,* 2008). A study by Yang *et al.,* 2008, showed that mitochondrial aggregates were formed in PINK1 mutant flies within DAergic neuronal clusters and overexpression of Drp1, inhibited this aggregate formation. This abnormal mitochondrial morphology and dynamics have also been observed in cultured mammalian neurons can suggest that PINK1 and Parkin may have conserved roles in the regulation of neuronal mitochondrial dynamics.

In terms of a mammalian model, the knockout of mammalian PINK1 and Parkin has not managed to reproduce the motor deficits that are associated with PD (McWilliams and Muqit, 2017, Gispert *et al.,* 2009, Kitada *et al.,* 2007, Palacino *et al.,* 2004). However, mitochondria from knockouts display mild defects in respiration and sensitivity to oxidative stress (Gispert *et al.,* 2009, Palacino *et al.,* 2004, Gautier *et al.,* 2008, Mortiboys *et al.,* 2008). Parkin-deficient mice that were crossed with the $Polg^{D257A}$ 'mutator' mice, showed that these mice accumulated mitochondrial DNA mutations as a consequence of their defective mitochondrial proofreading system, where lone Parkin-deficiency did not any PD pathology and double-mutants displayed age-dependent DAergic neuron loss and motor dysfunction (Pickrell *et al.,* 2015). This finding elicits the contribution of endogenous Parkin to maintain DAergic neuronal integrity *in vivo*. A PINK1 knockout rat model, recently displayed locomotor dysfunction and age-related DAergic neuronal loss, where, Parkin KO rats did not exhibit any significant PD pathology, perhaps due a to loss in ligase activity (McWilliams and Muqit, 2017)

Recently, pivotal evidence has been provided by Fiesel and Springe, which reveals age-dependent phospho-ubiquitin accumulation in post-mortem brains, and its absence in SNpc regions from a patient with a compound heterozygous PARK6 mutation (Fiesel *et al.,* 2015). Furthermore, the investigation of this observation within iPSC derived DAergic neurons from PINK1/Parkin-patients displayed similar findings to that of the study above, where in addition

neurons demonstrated altered mitochondrial morphology as well as a-synuclein accumulation (Chung *et al.,* 2016).

1.9.2 Impaired mitochondrial fission and fusion in Parkinson's disease

In fibroblasts, it was shown that rotenone may also play a role in regulating mitochondrial transport. It was found that rotenone treatment triggered mitochondrial swelling which consequently reduced mitochondrial motility (Pham *et al.,* 2004) and similar findings were observed in differentiated DAergic SH-SY5Y cells (Borland *et al.,* 2008). Disrupting mitochondrial fission via DRP1 may cause synaptic loss and DA neuronal cell death (Berthet *et al.,* 2014). Two heterozygous missense mutations in the mitochondrial fusion protein OPA1 (p.G488R, p.A495V) have shown to affect conserved amino acid positions in the guanosine triphosphate domain, found in two Italian families. The patients exhibited symptoms of PD and dementia. Fibroblasts of these patients showed lower OPA1 protein expression, normal mRNA expression, impaired bioenergetics, mitochondrial fragmentation and increased autophagy (Van Laar and Berman, 2010). Mitochondrial morphology studies that have been conducted in brain tissue from the SNc of PD patients is limited, and although post -mortem tissues is available, the ultrastructural details in these models are not well preserved.

1.9.3 Impaired mitophagy in Parkinson's disease

The disruption of the mitochondrial membrane potential by CCCP in mammalian cultured cells (Valente *et al.,* 2004, Beilina *et al.,* 2005, Clark *et al.,* 2006, Zhou *et al.,* 2008, Jin *et al.,* 2010, Becker *et al.,* 2012) or *Drosophila* showed that Parkin translocates to mitochondria with low membrane potential, instigating LC3-mediated autophagy, as a method to eliminate the damaged mitochondria (Park *et al.,* 2006). After Parkin translocation, mitochondrial accumulation of Lys63-linked poly-ubiquitin and Lys48-linkages (Fischer *et al.,* 2012, Yang *et al.,* 2006), recruited ubiquitin, p62 (Deng *et al.,* 2008, Poole *et al.,* 2008, Becker *et al.,* 2012) and deacetylase HDAC6 (Fischer *et al.,* 2012) to the OMM. Lys63-linked poly-ubiquitination may contribute to proteasomal degradation of mitochondrial proteins (Yang *et al.,* 2008) and HDAC6- and/or p62-mediated sequestration of mitochondria (Yang *et al.,* 2006, Fischer *et al.,* 2012). Depolarised mitochondria are then engulfed by autophagosomes, followed by lysosomal degradation (Park *et al.,* 2006).

The translocation of Parkin from the cytosol to the mitochondria, requires intact PINK1 with kinase activity (Beilina *et al.,* 2005). Then through the ubiquitin proteasome pathway, Parkin ubiquitinates and degrades several proteins localised at the mitochondrial OMM, including Mfn (Yu *et al.,* 2011, Akepati *et al.,* 2008, Ziviani *et al.,* 2010), Drp1 (Tondera *et al.,* 2009), VDAC1 (Becker *et al.,* 2012, Ziviani *et al.,* 2010) and Bcl-2 (Youle and Strasser, 2008). *In vivo,* the loss of PINK1/Parkin enhances perturbed mitochondrial fusion, which was reversed as soon as Mfn expression was reduced. It may be the case that mitophagy promotes Mfn degradation, triggering the clustering of these mitochondria near the nucleus, which inhibits mitochondrial fusion of damaged mitochondria with healthy ones, compromising damaged mitochondrial motility (Deng *et al.,* 2008, Yu *et al.,* 2011). *In vivo Drosophila* studies have demonstrated that PINK1 mediated phosphorylation of Miro can protect against DA neuron damage (Rakovic *et al.,* 2013).

These studies suggest that PINK1 and Parkin play important roles in the neuronal mitochondrial quality control system and not only mitophagy. PINK1/parkin act together to detect mitochondrial depolarisation and to label damaged mitochondria, simultaneously regulating various aspects of the mitochondrial quality control system, such as mitochondrial fragmentation, the arrest of mitochondrial motility, and the degradation of damaged mitochondria by mitophagy. As mitochondrial impairment renders neurons vulnerable to cell death, alterations of mitochondrial homeostasis may be a key contributor to PD pathogenesis. In mouse models, damage to the mitochondria might not be sufficient to affect neuronal viability, or other processes might compensate for the PINK1/parkin loss. In humans, however, the occurrence of mutations in these genes might be enough to trigger PD.

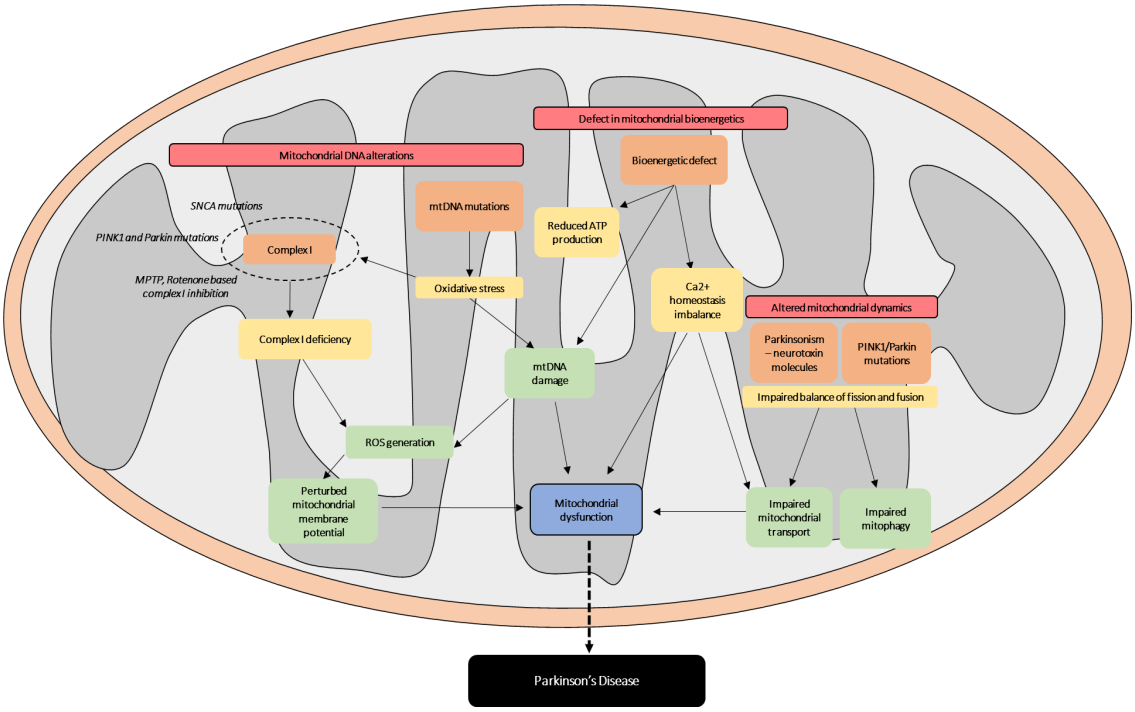

Figure 1.19. Mitochondrial dysfunction leading to Parkinson's disease. Summary figure highlighting how altered mitochondrial genetics, bioenergetics, dynamics, respiration and cell death pathways are triggered by impaired mitochondrial function in PD (Figure adapted from Bose and Beal, 2016)

1.10 AIMS OF THIS THESIS

The overarching aim of this project was to investigate mitochondrial trafficking within dopaminergic neurons in Parkinson's disease, using both iPSC and mouse models. Specifically delving into how mitochondrial dysfunction and alpha-synuclein pathology impacts mitochondrial trafficking within these neurons. This study consisted of four aims:

1. **Optimise an *ex vivo* method to image mitochondrial transport within dopaminergic neurons of the nigrostriatal pathway.** Nigrostriatal slices were taken from Dendra2/DATCre^{IRES} mice, containing mito-Dendra2 fluorescence within DAergic neurons. Nigrostriatal slice viability was maintained under an artificial cerebrospinal fluid (ACSF) perfusion system where videos of nigrostriatal axonal mitochondria were collected by confocal microscopy.

2. **Study the effect of ageing and human wild type alpha synuclein (SNCA) on mitochondrial transport within dopaminergic neurons of the nigrostriatal pathway.** The technique optimised from the previous aim was employed in this study to observe mitochondrial trafficking within aged and alpha synuclein Dendra2/DATCre^{IRES} mice. This study aimed to understand alterations in mitochondrial movement in an ageing and PD model. The first cohort comprised aged mice for 6 (young) and 12 (old) months, to represent young and old populations, and the second cohort comprised human wild type SNCA mice (6 – 10 months of age) to observe the impact of important PD pathologies i.e. aggregating synuclein on mitochondrial transport in brain slices. Videos of nigrostriatal axonal mitochondrial movement were collected by confocal microscopy and analysed via kymographs.

3. **Differentiate two iPSc cell lines harbouring two levels of a single, large scale mtDNA deletion into dopaminergic neurons.** This study confirmed the mitochondrial defect within iPSCs harbouring a single, large scale mtDNA deletion via observing mitochondrial protein complex expression and alterations in mitochondrial membrane potential through TMRM staining. It was also attempted to generate a homogeneous dopaminergic neuronal population harbouring an mtDNA deletions, via the addition of dopaminergic growth supplements from previously established protocols.

4. **Observe the role Ca^{2+} plays in regulating mitochondrial trafficking, by investigating the effects of $_{m}Ca^{2+}$ efflux on mitochondrial trafficking within these iPSC derived neurons.** This study first compared modifications in mitochondrial trafficking in iPSC derived neurons from mitochondrial disease patients harbouring a large scale mtDNA deletion. Mitochondrial movement in a heterogeneous population of neurons differentiated from iPSCs harbouring a large scale mtDNA deletion were then investigated. The role of Ca^{2+} in mitochondrial transport was explored by observing how mitochondrial Ca^{2+} ($_{m}Ca^{2+}$) extrusion into the cytoplasm within neurons harbouring an mtDNA deletion can affect mitochondrial motility. This study comprised of live cell TMRM and Fluo-4-AM Ca^{2+} imaging in cultured neurons.

CHAPTER TWO

Methods & Materials

2.1 CELL CULTURE

2.1.1 Generation of neurons from human iPS cells.

Human fibroblasts were converted into induced neuronal (iN) cells and via the use of a single transcription factor, Ngn2 were converted into functional iN cells. Human induced pluripotent stem cells (iPSCs) were generated from patient fibroblasts with a single, large-scale mtDNA deletion, spanning 6kb base pairs (m.7777- 13794), which removes the following genes, COXII, ATPase 6 and 8, COXIII, ND3, ND4L, ND4, ND5 a part of ND6 and several tRNAs. The deletion cell line was sent to Novartis for programming into iNGN2 stem cells (Protocol followed Zhang *et al.,* 2013). Once reprogrammed, iPSCs were sent to the Wellcome Centre for Mitochondrial Research, and were maintained and grown (seeding density of $5x10^5$) in 6cm matrigel (Corning) coated dishes. IPSCs were maintained in Nutristem media (Biological Industries) containing 0.1mg/ml G418, which allows the antibiotic selection of iPSCs containing the ngn2 DNA construct and 10µM Rock inhibitor (Y-2763) (ROCKi) (Millipore).

2.1.2 Preparation of matrigel

Thawed cells were plated onto a 6cm matrigel dish. Diluted into X-Vivo^{TM} 10 (Lonza) in a 1:5 ratio. Matrigel dishes were pre-made and stored at 4°C until use. All iPSCs and proliferating cells were maintained in matrigel dishes until differentiation.

2.1.3 Defrosting iPSCs

IPSCS were suspended in cryotubes in Cryostore serum free freezing media (Stem Cell Technologies) containing 10% dimethyl sulfoxide (DMSO) and stored in liquid nitrogen. 1 x 10^6 cells were frozen down per mL of cryostore freezing media. Thawed iPSCs were transferred into new Nutristem media and centrifuged at 1200 RPM for 5 minutes to remove DMSO. The supernatant was then discarded and the pellet was re-suspended in Nutristem media containing 0.1mg/ml G418 and 10µM ROCKi and maintained at 37°C to allow cellular attachment to the Matrigel coated plates.

2.1.4 Passaging iPSCs

Confluent cells (70% coverage) were passaged after approximately 48 hours. Cells were lightly washed with Dulbecco's Phosphate Buffered Saline (DPBS) and the harvesting of iPSCs was carried out by the addition of trypsin, which is used to dissociate cells attached to the matrigel.

Cells were stored at 37°C for 5 minutes during trypsin treatment. The trypsin was then neutralised by the addition of Nutristem through protease inhibition activity and centrifuged at 1200 RPM for 5 minutes. The supernatant was then discarded, the pellet retained and re-suspended in fresh Nutristem media. Cell count was performed by taking 20µl of the cells and mixing with 20µl Trypan blue (Gibco) solution, an indicator of intact cell membranes and thus cell viability. Live cell counts were carried on the Nexcelom cell counter. iPSCs were re-plated into a new matrigel coated dish at a density of 5 x 10^5cells/cm^2 in NutriStem containing 10µM Rock inhibitor and 0.1mg/ml G418 antibiotic. Cells were kept at 37°C. After 24 hours ROCKi was removed and iPSCs were maintained at 37°C.

2.1.5 Generating neuronal progenitor cells (NPCs)

IPSCs were passaged via the same protocol as above, however 2x10^6 cells were seeded per matrigel dish for proliferation (Table 2.1 for proliferation reagents). 1µg/ml doxycycline was added to the proliferation media, instead of G418, to induce ngn2 gene expression in NPCs, alongside 10µM ROCKi. Cells containing proliferation media, doxycycline and ROCKi were kept at 37°C for 48 hours. After 48 hours ROCKi was removed and NPCs were maintained in proliferation media containing only 1µg/ml doxycycline at 37°C.

2.1.6 Preparing coverslips

13 and 22mm glass cover slips (for 24 well and 6 well plates respectively) were etched in 1M hydrochloric acid overnight whilst shaking, prior to the differentiation of NPCs, which was followed by a thorough wash in distilled water and overnight baking. Coverslips were dried and sent for autoclaving. Coverslips were etched and baked in order to allow the efficient attachment of neurons.

2.1.7 Coating coverslips

Etched coverslips were placed in 6 and 24 well plates for immunofluorescence studies. coverslips were coated with 0.1mg/ml Poly D Lysine (PDL), a synthetic, positively charged amino acid chain, used as a coating substrate to enhance cell attachment and adhesion to plastic and glass surfaces. Well plates were incubated with PDL for 30 minutes at room temperature. This was followed by 2x DPBS washes, and the addition of 5 µg/ml Laminin, an extracellular matrix protein. Laminin allows increased cellular adhesion, migration, proliferation, and

differentiation. The laminin was left on the well plates until use for experiments. NPCs were mounted onto coverslips for differentiation.

2.1.8 Passaging neuronal progenitor cells (NPCs) into neuronal differentiation

Neuronal progenitor cells were then passaged, as mentioned above and plated into PDL-laminin coated plates (Table 2.1 for differentiation reagents). For the purpose of live cell imaging, 2.5 x 10^5 cells were seeded into glass bottom (Ibidi) dishes containing differentiation media. For immunofluorescent assays, 3 x 10^5 cells were seeded onto PDL-laminin glass coverslips into their respective plates. A half media change was carried out every other day for 7 days, during the neuronal differentiation process. After day 7 the differentiation media was completely removed and the cells were prepped for their individual experiments.

2.1.9 Freezing down cells

1 x 10^6 passaged iPSCs were centrifuged and re-suspended in freezing media and aliquoted into cryotubes (Thermo Fisher Scientific). Cryotubes were then placed into a freezing container, Nalgene Mr Frosty™ (Thermo Fisher Scientific) at - 80°C, containing isopropyl alcohol which permits the gradual cooling of the cells at -1°C per minute, allowing optimum cell preservation. After 24 hours in the Mr Frosty™, cells were then moved into liquid nitrogen storage.

Table 2.1. NGN2 differentiation reagents

Reagent	Concentration/Volume	Supplier	Function
Passaging cells			
Trypan Blue	20µl	Gibco	Used to observe cell viability during cell count
TrypLE Express (Trypsin)	1ml	Gibco	Harvests iPSCs attached to matrigel
Rho-associated kinase(ROCK) inhibitor	10µM	Sigma-Aldrich	Enhances survival of dissociated iPSc after passaging by inhibiting apoptosis
Dulbecco's Phosphate Buffered Saline (DPBS)	6ml	Gibco	Wash out matrigel dish
Matrigel-matrix	3ml in 6cm dish	Corning	Allows attaching of cells to dish
X-VIVO 10 Chemically defined, Serum free Hematopoietic Cell Medium	1:5 ratio	Lonza	Media used to dilute matrigel
Nutristem hPSC XF Medium	100ml	Biological Industries	Media used to maintain iPSCs
Sodium Pyruvate	1mM	Gibco	
Penicillin/streptomycin (pen/strep)	1%	Gibco	Antibiotic
Uridine	1ml	Sigma-Aldrich	
G418 antibiotic	0.1mg/ml	Sigma-Aldrich	Selective for iPSCs containing DNA construct
ROCK inhibitor	10µM	Sigma-Aldrich	ROCK inhibitor
Proliferation Media			
B27 supplement	2%	Gibco	Growth and survival of cell
N2 supplement	1%	Gibco	Growth and survival of cell
Human Epidermal Growth Factor (hEGF)	10ng/ml	Gibco	Promotes cell survival
Human Fibroblast Growth Factor (hFGF)	10ng/ml	Gibco	Promotes cell survival
Penicillin/streptomycin (pen/strep)	1%	Gibco	Antibiotic
L-Glutamine	2mM	Gibco	

Dulbecco's Modified Eagle Medium DMEM/F12 media	100ml	Gibco	Media used to maintain neuronal progenitor cells
Doxycycline	1µg/ml	Sigma-Aldrich	Replaces role of G418 – induces differentiation by activation if INGN2 gene
Differentiation media			
B27 supplement	2%	Gibco	Growth and survival of cell
Neurobasal media	100ml	Gibco	Neurobasal media
N2 supplement	1%	Gibco	Growth and survival of cell
Brain Derived Neurotrophic factor (BDNF)	10ng/ml	R & D systems	Survival and morphological differentiation of neurons
Glial-cell derived neurotropic factor (GDNF)	10ng/ml	R & D systems	Survival and morphological differentiation of neurons
Human Neurotrophin-3 (hNT3)	10ng/ml	(R&D) systems	Survival and morphological differentiation of neurons
Penicillin/streptomycin (Pen/strep)	1%	Gibco	Antibiotic
Freezing Media			
Cryostore serum free freezing media	1 x 10^6 cells/ml	Stem Cell Technologies	Preservation of iPSCs at low temperature
Coating plates for neuronal differentiation			
Laminin		Sigma-Aldrich	Allows neuronal attachment onto coverslips
Poly-D-Lysine (PDL)		Sigma-Aldrich	Allows neuronal attachment onto coverslips

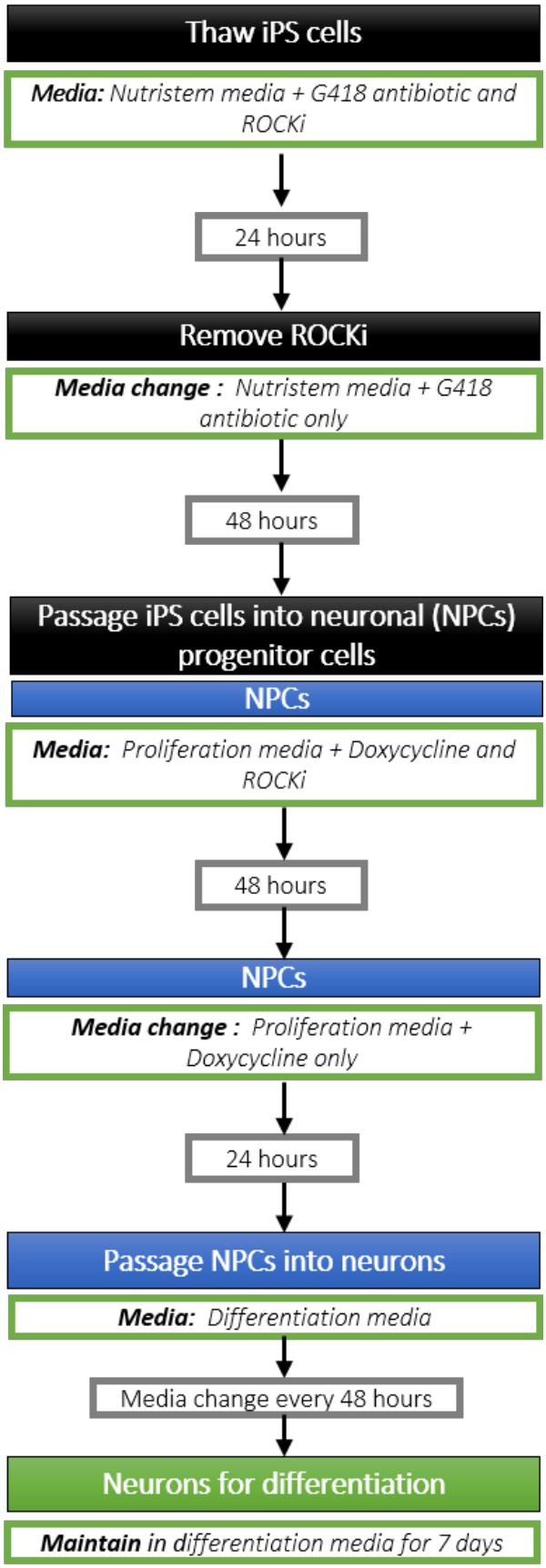

Figure 2.1. NGN2 Differentiation. Flow chart of INGN2 differentiation from IPSCs to neurons, with indicative media changes and which reagents are added to media, when conducting media changes

2.2 IMMUNOFLUORESCENT ASSAYS

2.2.1 Fixation of neurons

Differentiated neurons were washed with PBS, and coverslips were 2fixed in 4% paraformaldehyde and left to incubate for 10 minutes at room temperature. After incubation, cells were then washed 3x PBS and prepared for imaging.

2.2.2 Immunofluorescence on differentiated neurons

Fixed neurons were stored in PBS at 4°C until ready to use. When ready, PBS was removed and coverslips were left to incubate in 5% normal goat serum (NGS) (Sigma Aldrich) to minimalise background fluorescence for 30 minutes at room temperature. Cells were then incubated with primary antibodies diluted in 5% NGS, and incubated overnight at 4°C. The next day, coverslips were PBS washed 3 x over 5 minutes, and incubated for 30 minutes with relevant secondary antibodies (Thermofisher) made up in 5% NGS at a 1:200 dilution. Coverslips were then washed in 3x in PBS, and incubated with Hoescht for 10 minutes to stain for nuclei. Coverslips were washed once more and mounted using Prolong Gold (Invitrogen). All images were obtained on the Nikon (Inverted Confocal) A1r at 20x magnification, using DAPI, TRITC, FITC and Cy5 filters.

2.3 GENOTYPING EXPERIMENTAL MICE

2.3.1 DNA extraction

The Qiagen DNeasy Blood and Tissue kit was used to extract DNA from ear notches collected from four week old pups for use in slicing experiments. DNA was extracted as per the manufacturer's instructions as follows, Notched ear samples were placed in 1.5ml centrifuge tubes, followed by the addition of 180µl buffer ATL, 20µl proteinase K per notch. Each sample was vortexed and incubated at 56°C overnight until completely lysed. After lysis, 200µl buffer AL was added to centrifuge tubes, vortexed and incubated at 56 °C for another 10 minutes. The mixture was then pipetted into a mini spin column placed in 2ml collection tube. Tubes were then spun down at 8,000 RPM for 1 minute. Flow through and collection tube were discarded. The spin column was then placed into a new 2ml collection tube, to which 500µl buffer AW1 was added. Tubes were centrifuged at 8000 RPM for 1 minute, and the flow through and collection tube was discarded. The spin column was replaced into a new 2ml collection tube, to which 500µl buffer AW2 was added, which were centrifuged at 14,000 RPM for 3 minutes. Flow through and collection tube was discarded. The spin column was transferred to a new 1.5ml centrifuge tube and DNA was elute by adding 200µl buffer AE to the centre of the spin column and incubated at room temperature for 1 minute. The DNA was then eluted by centrifugation at 8000 rpm for 1 minute.

2.3.2 Cre primers

The following primers were used: Cre common [oIMR6625] 5'TGGCTGTTGGTGTAAAGTGG3', Cre Wild type reverse [oIMR6626] 5'GGACAGGGACATGGTTGACT3', Cre Mutant reverse [oIMR8292] 5'CCAAAAGACGGCAATATGGT3'. The Cre wild type PCR product yields a band at 264bp and the Cre mutant at 152bp.

2.3.3 Dendra primers

Dendra2 common [13840] 5'CCAAAGTCGCTCTGAGTTGTTATC3', Dendra2 Wild type reverse [oIMR13841] 5'GAGCGGGAGAAATGGATATG3', Dendra2 Mutant reverse [oIMR7320] 5'TCAATGGGCGGGGGTCGTT3'. The Dendra wild type pcr product is 604bp whilst the Dendra2 mutant yields a band at ~376bp.

2.3.4 PDGF-hα- synuclein primers

The following primers were used to identify pups which expressed the human α-synuclein gene: PDGF-hα-synuclein forward 5'CCAGACGGGTGTGACAGCAGT3' and PDGF-hα-synuclein reverse 5'CCAAGGTTGTTAACTTGTTTATTGCAGC3'. The PDGF-hα-synuclein pcr product yields a band at 350 bp.

Dendra, Cre and PDGF-hα-synuclein primers were all obtained from Eurofins.

2.3.5 Polymerase chain reaction (PCR) reactions for genotype indentification of Cre and Dendra mice

25 µl PCR mastermix (GoTaq Flexi Kit) was made up for each sample which included: [2 mM $MgCl_2$, 9.3 µl dH_20, 1x PCR buffer, 0.2 mM deoxynucleotide (dNTPs) solution, 1 µM Cre Forward, Cre Wild type reverse, Cre Mutant reverse primers, 0.2 µl GoTaq Polymerase and 2 µl of DNA sample. The same protocol was repeated for Dendra PCR, however mastermix contained 10.3 µl dh_20, alongside, 0.5 mM Dendra Forward and Dendra mutant reverse primers.

DNA products were amplified by Veriti 96 well plate thermo cycler PCR machine (Applied BioSystems). Thermal cycle was programmed for 2 minutes at 95°C (1 cycle) as initial denaturation, followed by 30 cycles of 30 sec at 95°C for denaturation, 30 sec at 62°C annealing, 1 minute at 72°C for extension, and a final extension at 72 °C for 10 min. PCR products were observed via gel electrophoresis, 1.5% agarose gels were run at 100V for 60 minutes in a in 1 x TAE buffer with 1:10,000 SYBR Safe DNA stain. Norgen PCR ranger 1kb molecular weight marker was used. The BioRad ChemiDoc™ system and Image Lab software were then used for visualising the gel and image analysis respectively.

2.3.6 PCR reactions for PDGF-hα- synuclein mice

DNA extraction was completed as mentioned above, alongside the same PCR mastermix (GoTaq Flexi Kit). 50 µl PCR mastermix (GoTaq Flexi Kit) was made up for each sample which included: [2 mM $MgCl_2$, 22µL dh_20, 1x PCR buffer, 0.2 mM deoxynucleotide (dNTPs) solution and 100ng/ µl PDGF-Hα- synuclein forward primer, PDGF-Hα- synuclein reverse primer, 0.2 µl GoTaq Polymerase and 1.5 µl of DNA sample].

DNA products were amplified by Veriti 96 well plate thermo cycler (Applied BioSystems) PCR machine. The thermal cycle was programmed for 3 minutes at 94°C (1 cycle) as initial denaturation, followed by 5 cycles of 30 sec at 94°C for denaturation, 30 sec at 49°C as annealing, and 72°C for extension. This was followed by the 25 cycles of 30 seconds at 92°C for denaturation, 30 seconds at 49°C as annealing, and 72°C seconds for extension. PCR reaction was concluded by a final extension at 72°C for 5 minutes. PCR products were observed via gel electrophoresis as above.

2.3.7 *PhAM*^{floxed} mouse line

The mouse model chosen for this study was the *PhAM*^{floxed} line, developed by Pham *et al.,* 2012. This mouse line comprises of a mitochondrial localised version of the photo-convertible fluorescent protein Dendra2 (mito-Dendra2) targeted ubiquitously to the *Rosa26* locus, alongside upstream *loxP*-flanked termination signal. The mitochondrial targeting sequence of subunit VIII of cytochrome c oxidase (COX8) was fused to the N-terminus of Dendra2 driving the expression of Cre in *PhAM*^{floxed} cells resulting in mito-Dendra2 fluorescence.

The *PhAM*^{floxed} line mice were subsequently crossed with Cre mice under a dopaminergic transporter (DAT^{IRES}*cre*) obtained from The Jackson Laboratory, in order to observe mito-Dendra2 only within DA neurons of the mouse brain (See chapter 3, section 3.1.5 for further details)

CHAPTER THREE

Optimising an *ex vivo* technique to image mitochondrial trafficking within the nigrostriatal pathway

3.1 INTRODUCTION

3.1.1 Mitochondrial trafficking within neurons

3.1.1.1 ATP provision within neurons

Neurons can extend their axons and dendrites for up to a meter. Thus, the neuron poses a case for mitochondrial distribution where the need to supply energy to further cellular regions is vital as a consequence of their unique morphology (Hall *et al.,* 2012).

Patch clamp analysis revealed that electrical signalling within neurons dominates ATP consumption within mammalian brains (Alle *et al.,* 2009, Harris and Attwell, 2012, Harris *et al.,* 2012). OXPHOS, generates around 93% of ATP within neurons (Sokoloff, 1960), with the remaining 7% coming from glycolysis. Pre and postsynaptic mechanisms show that 55% of total ATP is used for action potential generation (APs), synaptic transmission and resting potential maintenance in neurons and glia (Attwell and Laughlin, 2001).

Within rat cerebral cortex (Attwell and Laughlin, 2001) and human cortex (Lennie, 2003), it was demonstrated that synaptic transmission is the largest consumer of ATP (Sengupta *et al.,* 2010, Harris and Attwell, 2012). ATP consumption by synaptic signalling mechanisms begins presynaptically, where ATP is consumed by 4 types of ATPase. The first is the sodium pump, which extrudes Na^+ ions, generates action potentials and powers Ca^{2+} removal by Na^+ /Ca^{2+} exchange, secondly, calcium-ATPase in the plasma membrane which lowers intracellular Ca^{2+} , thirdly, vacuolar H^+ -ATPase, which energises vesicle transmitter uptake, and finally motor proteins (kinesin, dynein, myosin) that aid mitochondrial and vesicle motility around the cell (Attwell and Laughlin, 2001).

With postsynaptic activities, ATP consumption is larger, expended mostly on pumping out ions that regulate synaptic currents, and a smaller designation to returning Ca^{2+} to intracellular stores and mitochondrial trafficking (Harris *et al.,* 2012). Increased transmission within glutamatergic synapses can increase intracellular neuronal Ca^{2+}, which can depolarise mitochondria and reduce their ATP production. In extreme cases this causes cytochrome *c* release and apoptosis initiation. Increasing evidence has shown that these events can contribute to the development of neurodegenerative disorders (Attwell and Laughlin, 2001).

Neuronal mitochondria travel long distances, regulated by kinesin and dynein motors (For further details see Chapter 1, section 1.5.3.1) (Harris *et al.,* 2012). *In vivo,* two classes of

mitochondrial movement are observed, reflecting two different pools of mitochondrial trafficking, the motile mitochondrial pool, which includes mitochondria that may temporarily pause but usually continue onwards without alterations in their directionality and the stationary pool, which remain anchored (Faits *et al.,* 2016, Lewis *et al.,* 2016, Smit-Rigter *et al.,* 2016, Misgeld and Schwarx, 2017). The movements of the motile pool are microtubule based and are either, anterograde ([+] along microtubules towards the periphery) or retrograde ([-] towards cell bodies) movements which are regulated by kinesin and dynein microtubular proteins respectively (Hollenbeck *et al.,* 2005, Chang *et al.,* 2006). Several studies have reported disturbances in mitochondrial trafficking in neurodegeneration (Millecamps and Julien, 2013).

3.1.2 Transgenic mouse models for Parkinson's disease

The development of transgenic animal models have enhanced understanding of PD through tissue-specific expression of genetic mutations within the following systems: vertebrates, human-IPSC derived neurons, *Drosophila melanogaster, Medake fish, and Caenorhabditis elegans* (Pallanck and Whitworth, 2007, Wong, 2007, Chesselet *et al.,* 2008, Lim and Ng, 2009). Furthermore, Lewy body (LB) pathology in PD, has enhanced the interest and consequently the generation of α-syn mouse models over the last twenty years (Discussed further in Chapter 4).

3.1.3 *In vivo* mitochondrial imaging

Live imaging of mitochondria has transformed our understanding of the dynamics of these organelles. In culture, axons are around a micrometre in diameter (Chang *et al.,* 2006). The mitochondria therefore move within an easily visualised plane and as long as the cell body of the axon can be identified, movements are easy to distinguish from plus-end and minus-end directed transport allowing the tracking of up to 100 µm or more (Chang *et al.,* 2006, Schwarz 2013). Smaller mitochondria are more frequent in their motion than longer mitochondria, where the relationships between the size of mitochondria and motility are still undergoing investigation (Misgeld *et al.,* 2007).

Determining the fraction of motile mitochondria has given variable results, with 10% – 40% of mitochondria moving and 60% – 90% recorded as stationary (Morris and Hollenbeck, 1993, Ligon and Steward 2000a, Misgeld *et al.,* 2007). Of the moving mitochondria, approximately half move anterogradely and half retrogradely (Schwarz, 2013). Researchers are now delving

into understanding whether the anterograde-moving population comprises healthy mitochondria and whether the retrograde moving mitochondria, represent older, damaged mitochondria with lower mitochondrial membrane potentials (determined with voltage-sensing dyes) and whether these mitochondria are targeted towards the soma to undergo lysosomal degradation (Schwarz, 2013).

Mitochondrial fission and fusion events (Chapter 1, section 1.5.1 and 1.5.2) are observed in axons and dendrites (Amiri and Hollenbeck, 2008), where even during brief moments of contact can involve fusion (also evident in non-neuronal cells) (Liu *et al.* 2009). Therefore, mitochondria that appear to be stationary, at least for the duration of what can be successfully imaged, may be refreshed *in situ* by exchanging proteins with the motile fraction. Consequently, due to these factors that go some way to explain the sporadic behaviour of mitochondria, developing a system by which *in vivo* mitochondrial trafficking can be captured in an accurate, representative, high-resolution manner, has provided to be one of the biggest challenges in understanding mitochondrial dynamics *in vivo* over the last 15 years.

Much of the research that is currently occurring only pinpoints a segment of an axon (< 150 μm) and mitochondrial motility within this region, where it can be argued that this observation is not an accurate representation of the organelle's movement. As stated previously, the typical protocol to visualise these organelles is to isolate neurons in culture and to stain with a mitochondrial tracker which relies on the membrane potential of the mitochondrion, allowing the visualisation of their distribution and dynamics (Johnson *et al.,* 1981, Bereiter-Hahn and Voth, 1994, Rizzuto *et al.,* 1996). Though the results of these studies have provided valuable insights into the behaviour of neuronal mitochondria, it is important to remember that cultured neurons have a different biological geometry to an *in vivo* model, and although such models are largely informative, still lack the normal biological milieu which represents disease.

Fortunately, over the past decade, the view of mitochondrial dynamics has expanded from *Drosophila* to murine models in order to understand variances of mitochondrial dynamics within neurons. Scientists have successfully attempted to image axonal mitochondrial transport in mammalian *in vivo* systems (Misgeld *et al.,* 2007a, Misgeld *et al.,* 2007b, Ohno *et al.,* 2011, Pluckinska *et al.,* 2012, Okashi and Okabe, 2013, Sajic *et al.,* 2013, Sorbata *et al.,* 2014, Jackson *et al.,* 2014, Takihara *et al.,* 2015, Faits *et al.,* 2016, Lewis *et al.,* 2016), observing mitochondrial dynamics through high resolution imaging, producing novel findings that have been pivotal in the understanding of mitochondrial movement in a 'live' setting (See Table 3.1).

3.1.4 Quantifying in vivo mitochondrial trafficking in neurons

The first *in vivo* study which observed neuronal mitochondrial movement was conducted by Misgeld *et al.,* 2007, who surgically exposed the sciatic nerve in two well-established mouse models. Neuronal promoters were used to control expression of fluorescence in the *thy1-mitoCFP* mito-mouse, which allows cyan fluorescent protein (CFP) expression under the control of the mouse thymus cell antigen 1, *Thy1*, promoter and the neuron-specific enolase (*nse)*-promoter model to express yellow fluorescent protein (YFP) in *nse-mitoYFP* mice. In these mouse models CFP and YFP are specifically localised to the mitochondria by a human cytochrome *c* oxidase subunit 8A (ubiquitous) construct, which targets signals fused to the N-terminus. The mitochondria labelled in this study were imaged via confocal and electron microscopy, where it was found that the mitochondria exhibited normal physiological structure. Mitochondrial membrane potential sensitive mitochondrial dyes, such as MitoFluor Red 589, MitoTracker Red CMXRos and Rhodamine 123 displayed the same distribution and intensity in mitoCFP-positive and control synapses indicative of physiologically normal mitochondria (Misgeld *et al.,* 2007).

In these Mito-Mouse lines, a broad spectrum of neuronal populations showed labelled mitochondria, including cortical and hippocampal projection neurons, spinal motor neurons, Purkinje cells, retinal ganglion cells and basal ganglia neurons. This *in vivo* study revealed that anterograde mitochondrial transport exceeded retrograde transport throughout the branching regions of mature motor axons. The difference between anterograde and retrograde transport suggests that some parts of the mitochondrion are degraded by the autophagy machinery along the axon or in the synapses (Misgeld *et al.,* 2007).

Sorbata *et al.,* (2014) then utilised the same paradigm of study as Misgeld *et al.,* to study how impaired axonal transport can contribute to axon degeneration in 6-12 week old mice. Multiple sclerosis (MS) is a common neuroinflammatory disease characterised by progressive axon degeneration. This experiment comprised of *in vivo* two-photon imaging to assess the transport of organelles and the stability of microtubule tracks in individual spinal axons. The mouse model of MS, comprised of acute experimental autoimmune encephalomyelitis (EAE), where inflammatory lesions develop within the spinal cord of the mouse. The tracking of single mitochondria revealed that the stop duration greatly increased in the inflamed spinal cord, suggesting a detachment of cargoes from tracks. This notion was further supported by the

increased density and content of mitochondria observed in experimental autoimmune encephalomyelitis (EAE) axons that suggest that moving mitochondria accumulate in the lesion area (Sorbata *et al.,* 2014).

Glaucoma is the most common neurodegenerative eye disease characterised by axonal degeneration and death of retinal ganglion cells (RGCs). The occurrence of glaucoma increases with ageing, as observed with neurodegenerative diseases of the CNS including, AD and PD. *In vivo* observation of mitochondrial motility in a glaucoma model conducted via minimally invasive multiphoton imaging of mouse RGC, demonstrated that mitochondria were highly dynamic in the mammalian CNS. Younger mice (4 months old) showed a reduction in motile mitochondria (percentage not stated) prior to cell death, without shortening of the mitochondria. Conversely, in older mice (23-25 months old), the duration and distance of mitochondrial trafficking were augmented, where it was suggested that a change in mitochondrial transport in ageing perhaps may underlie the age-related increase in glaucoma (Takihara *et al.,* 2015).

Most recently, a study in cortical neurons by Lewis *et al.,* observed mitochondrial trafficking in cortical neurons in P30/45 awake mice. Their study demonstrated that mitochondrial motility is greatly reduced during cortical axon maturation *in vitro* and that mitochondrial motility is very limited in adult cortical axons. It was also shown that axonal mitochondria remain immobilized over long time periods in mature neurons. This study demonstrated that mitochondrial motility is extremely low in mature cortical axons *in vitro* and *in vivo* using two-photon microscopy. These results suggested that mitochondrial immobilisation and presynaptic localisation are highly important hallmarks of mature CNS axons both *in vitro* and *in vivo* (Lewis *et al.,* 2016). Table 3.1 summarises these models, and the research that has pioneered our understanding of mitochondrial movement within *in vivo* models.

Table 3.1. Mitochondrial movement in vivo studies (Adapted from Lewis *et al.,* 2016)

Study	Model	System	Neurons imaged	Compartment	Age	Anaesthesia	% Stationary Mitochondria	Speed of mitochondria
Misgeld *et al.,* 2007	Mouse – in vivo	PNS	Sciatic nerve	Axon	?	Yes	~ 87% over 5 mins	-
Plucinska *et al.,* 2012	Zebrafish – in vivo	PNS	Rohon Beard	Axon	2-3 (Days post fertilisation) dpf	No	99% distal, 83% proximal over 10 mins	-
Sajic *et al.,* 2013	Mouse – in vivo	PNS	Saphenous nerve	Axon	8-12 weeks	Yes	-	0.3 µm/s
Sorbata *et al.,* 2014	Mouse – in vivo	PNS	Spinal Cord	Axon	6-12 weeks	Yes	93 +/- distal, 83% proximal over 10 mins	0 - 0.8 µm/s
Takihara *et al.,* 2015	Mouse – in vivo	CNS	Retinal Ganglion Cells	Axon	2-25 months	Yes	-	0.2 µm/s
Lewis *et al.,* 2016	Mouse – in vivo	CNS	Cortical L2/3	Axon	P30/45 awake	No	93+/- 4.5 % over 10-20 mins	-
Smit-Rigter *et al.,* 2016	Mouse – in vivo		Visual cortex	Axon	P70-80 days	Yes	99% stationary	-

3.1.5 Imaging mitochondria within SNpc neurons

This study designed a unique method to image mitochondrial movement within the SNpc DA neurons of the nigrostriatal pathway, as there is currently no available *in vivo* model which yields insight into understanding mitochondrial transport within SNpc neurons in PD.

The mouse model chosen for this study was the *PhAM*^{floxed} line, developed by Pham *et al.,* 2012. This mouse line comprises a mitochondrial localised version of the photo-convertible fluorescent protein Dendra2 (mito-Dendra2) which is targeted to the ubiquitously expressed *Rosa26* locus, along with an upstream *loxP*-flanked termination signal. The mitochondrial targeting sequence of subunit VIII of cytochrome c oxidase (COX8) was fused to the N-terminus of Dendra2 driving the expression of Cre in *PhAM*^{floxed} cells resulting in mito-Dendra2 fluorescence, without adverse effects on mitochondrial morphology. When crossed with Cre drivers, the *PhAM*^{floxed} line expresses mito-Dendra2 in specific cell types, allowing mitochondria to be tracked even in tissues that have high cell density. The *PhAM*^{floxed} line mice were subsequently crossed with Cre mice under a dopaminergic transporter (DAT^{IRES}*cre*) obtained from The Jackson Laboratory, in order to observe mito-Dendra2 only within DA neurons of the mouse brain.

This photo convertible model has been previously employed within rodent studies of the nervous system to investigate neuronal activity-dependent control of mitochondrial trafficking using mito-Dendra2 sagittal hippocampal brain slices (Stephen *et al.,* 2015). Further insight to the effect of calcium handling within neurons, have been elucidated with mito-Dendra2 primary hippocampal neurons, in an investigation into the role of mitochondrial calcium uniporter with Miro (Niescier *et al.,* 2018).

Several challenges were overcome to optimise a robust tool, which included difficulties such as establishing a perfusion system which maintained nigrostriatal slice viability and the accurate detection of axons within the nigrostriatal pathway. Offsetting these technical challenges, this study successfully managed to image part of the nigrostriatal pathway and obtain videos of mitochondrial motility. This technique was achieved via manipulations in microscopy, transgenic mice models in combination with specialised scientific approaches.

3.2 AIMS OF THIS STUDY

1. Optimise an *ex vivo* method to image mitochondrial movements within the dopaminergic (DA) neurons of the nigrostriatal pathway in a mito-Dendra2 tagged mouse model

2. Record mitochondrial trafficking within cell bodies, axons and synapses of the nigrostriatal pathway

3.3 METHODS & MATERIALS

3.3.1 Generating transgenic mice with photoactivatable mitochondria

3.3.1.1 Mouse model

Dendra2 is an enhanced version of a green to red photoswitchable fluorescent protein Dendra, derived from *octocoral Dendronephthya sp.* Dendra2 exhibits faster maturation and brighter fluorescence both before and after photoswitching when compared to Dendra *(*Gurskaya *et al.,* 2006). Dendra2 conducts irreversible photoconversion from a green to a red fluorescent form. Dendra2 exists in a monomeric state and is suitable for protein labelling, high contrast photoconversion with fluorescence at the red spectral region, has low phototoxic activation with 488nm laser (available on common confocal microscopes), high photostability of the photoconverted state, and efficient chromophore maturation at 37°C in mammalian cells. This combination of advantageous properties renders Dendra2 an ideal tool for the real-time tracking of organelle dynamics (Gurskaya *et al.,* 2006, Zhang *et al.,* 2007, Chudakov *et al.,* 2007).

Developed by Pham *et al.,* 2012, this transgenic mouse model was generated via homologous recombination in mouse embryonic stem (ES) cells. A neomycin expression cassette containing mito-Dendra2 (a version of Dendra2 targeted to the cytochrome oxidase subunit 8A (*COX8)* subunit in the mitochondrial matrix) was inserted into the ubiquitously expressed *Rosa26* locus. First identified in the 1990s, Rosa26 is the locus which permits constitutive, ubiquitous gene expression in mice (Friedrich and Soriano, 1991). The expression cassette included the CAG (cytomegalovirus/β-actin) enhancer-promoter, which has been reported to enhance expression several fold compared to the endogenous Rosa26 promoter (Chen *et al.,* 2011). Once the mice were generated from the correctly targeted ES cells, the neomycin selection

cassette was removed to generate the PhAM^{floxed} line. Mice were maintained as heterozygotes or homozygotes without apparent defects in viability or fertility (Pham *et al.,* 2012).

3.3.1.2 Identifying mitochondria within DA neurons

Mito-Dendra2 [PhAMfloxed, Gt(ROSA)26Sortm1(CAG-COX8A/Dendra2)Dcc/J), stock#18385] mice were crossed with a DAT-Cre [DAT^{IRES}cre, B6.SJL-Slc6a3tm1.1(cre)Bkmn/J, stock#006660] mouse line. Both mouse lines were obtained from The Jackson Laboratory. Cre mice contained a loxP-flanked (floxed) termination sequence upstream of mito-Dendra2. The genotyping for these mice were carried out as described in (Methods section). In this model, mito-Dendra2 expression relies on Cre mediated excision of the termination sequence, restricting ubiquitous mitochondrial expression. Cre expression was regulated by the dopaminergic (DAT) transporter protein, and therefore its expression was only observed within DA neurons. Mitochondria emitted bright green fluorescence at 405 nm emission which co-localized precisely with HSP-60, a marker of the mitochondrial matrix (Pham *et al.,* 2012).

3.3.2 Mouse dissection

The brains of experimental mice were collected on the day of experiment and all procedures were performed according to the requirements of the UK Animals Scientific Procedures Act (1986). Mouse brains were collected following Schedule 1 cervical dislocation.

3.3.3 Slicing preparation

3.3.3.1 Obtaining the nigrostriatal pathway

Once removed, the mouse brain was submerged in cold (4–5°C) sucrose solution [250 mM sucrose, 3 mM KCL, 1.25 mM NaH_2PO_4, 24 mM $NaHCO_3$, 2 mM $MgSO_4$, 2 mM $CaCl_2$, and 10 mM glucose (Sigma-Aldrich)]. In order to obtain an intact nigrostriatal pathway for imaging, the brain was vertically halved into two hemispheres. Each hemisphere was further sliced at a 45° angle and replaced into sucrose solution.

3.3.3.2 Slicing the mouse brain

The sliced brain was then mounted onto the vibratome, with the cut side facing downwards and midline facing upwards and were fully submerged in ice cold sucrose solution. Slices were cut at a thickness of 300 µm. Approximately 6 slices were obtained per animal and transferred into a large petri dish with sucrose solution. Slices were then transferred into a holding chamber containing artificial CSF (ACSF) [in mM: 126 NaCl, 3 KCL, 1.25 NaH_2PO_4 , 24 $NaHCO_3$, 1 $MgSO_4$, 1.2 $CaCl_2$, and 10 glucose] (Dheerender *et al.,* 2018). All salts were obtained from BDH chemicals (Poole, UK).

3.3.3.3 Incubating slices

The holding chamber was maintained at room temperature at the interface between ACSF and warm, moist carbogen gas (95% O_2/5% CO_2). Slices were allowed to equilibrate on the holding chamber for 30 minutes before being loaded with TMRM and MitoTracker Deep Red FM, to allow the simultaneous imaging of mitochondrial membrane potential within the striatum and photo-switched mitochondria within SNpc cell bodies respectively. The use of these two separate dyes allows us to overcome an overlap in dye fluorescence.

3.3.3.4 Preparation of DiD solution

1:33 dilution from a 10 mg/ml stock concentration of DiD (Life Technologies) was diluted into 1ml 1M potassium acetate. This was then sonicated on a mse soniprep 150 with ultrasonic disintegrator at 16 khz for 3 seconds. The solution was stored at – 20°C until use. Alexa fluorophore 647 hydrazide (Life Technologies) was used in addition to the DiD to optimise intracellular recordings.

3.3.3.5 NucRed Live probes

Nuclear staining was conducted on nigrostriatal slices in order to access viability of slices after 3 hours of imaging. This was conducted by adding of 2 drops/mL of NucRed® Live 647 ReadyProbes® Reagent (ThermoFischer) to the slices that were perfused with ACSF. NucRed was kept at room temperature.

3.3.4 Imaging mitochondria with the dopaminergic neurons of the nigrostriatal pathway

3.3.4.1 Perfusion system setup

In order to ensure that slices were kept 'alive' during inverted confocal imaging (Nikon A1r), a perfusion system was created. This system maintained a constant circulation of oxygenated ACSF through the slices, throughout the entire imaging session. ACSF was aspirated from the glass (Ibidi) bottom dish and circumvented through tubing connected to a vacuum pump. This vacuum pump stabilised the level of liquid circulating the system at all times. As slices were submerged in ACSF, this flow of liquid can cause movement of the whole slice, which can result in severe distortion during time lapse studies. To minimise this movement, slices were stabilised with a slice anchor (Warner Instruments) placed on top of the slices, to prevent the slice from floating within the ACSF solution. Once the slices were anchored to the bottom of the Ibidi dish, no movement was observed during the experiment. Slices were also maintained at 37°C and held in a glass (Ibidi) bottom dish in a temperature-controlled chamber. ACSF is saturated with O_2 and CO_2 at room temperature, which comes out of solution in the heated imaging chamber and can produce small bubbles during imaging. These bubbles can reduce image quality, damaging the slices. To prevent this, we kept the ACSF container inside the chamber saturating these gases at 37°C.

3.3.4.2 Imaging membrane potential within the striatum

Slices were loaded with 125nM Tetramethylrhodamine, methyl ester (TMRM), TMRM and left to incubate for 30 minutes prior to imaging, in order to allow dye uptake into the slice. A dye with a 561 nm emission wavelength was selected to limit overlap with the 488 nm emission of the mito-Dendra2.

3.3.4.3 Imaging mitochondrial membrane potential within cell bodies in the SNpc

Slices were loaded with 125nM MitoTracker Deep Red and left to incubate for 30 minutes prior to imaging, in order to allow dye uptake into the slice. As photo-switching was to be carried out within cell bodies (405 excitation and 561 emission), we could not incubate with TMRM, due to the overlap in fluorescence signals.

3.3.4.4 Imaging Mito-Dendra2 fluorescence

Mito-Dendra2 were imaged in the cell body, axons and striatum of the nigrostriatal pathway, using a 488nm laser. Mitochondrial movement was observed via videos captured at 5 frames/second for 10 minutes at x20 magnification.

3.3.5 CLARITY optimisation in ex vivo slices

CLARITY experiments were conducted to ensure the slicing methods were producing an intact nigrostriatal pathway. All CLARITY experiments were conducted on nigrostriatal slices by Dr Amy Reeve and Dr Jonathan Phillips. Protocol followed as it appears in Jonathan Phillips *et al.,* 2016

3.4 OPTIMISING SLICE IMAGING

Studying nigrostriatal mitochondrial dynamics in an *ex vivo* model posed the following challenges, i) identifying intact neurons (that are not axotomised by sectioning) to track mitochondria motility within the nigrostriatal pathway ii) slicing the mouse brain at the right angle to obtain intact neurons along the whole length of the nigrostriatal pathway and iii) ensuring slices are kept alive throughout the imaging process. This section provides details of the optimisation of this technique and how such issues were combatted.

3.4.1 Identification of intact DA neurons of the nigrostriatal pathway

In order to identify neurons within the nigrostriatal pathway it was suggested that a method to track neurons would be required. Literature indicated that long-chain dialkylcarbocyanines, such as (DiA and its analogues) were widely used tools to detect neuronal structures in living and fixed cells. It has been shown that DiI labelling does not affect neuronal viability, development, or any other basic physiological properties, where instances of DiI-labelled motor neurons were found to remain viable for up to four weeks in culture and up to one year *in vivo* (Kuffler, 1990). The dyes permit uniform tracking of neurons via lateral diffusion into the plasma membrane at a rate of about 0.2 – 0.6 mm per day in fixed specimens (Godement *et al.,* 1978, Gordon *et al.,* 1993). In living tissue, labelling is quicker (approximately 6 mm per day), due to active dye transport processes.

This study manipulated DiD (D307, D7757), an analogue of DiI with a 647 nm excitation and emission spectra, that did not interfere with the 488-emission fluorescence of the mito-Dendra2. This was carried out to characterise only the DAergic neurons within the nigrostriatal pathway. Three different approaches were explored to optimise the most efficient method of DiD uptake into neurons following the observations and results presented in other studies. These comprised of i) pressing a few DiD crystals directly onto the slice, ii) pipetting a dissolved DiD solution directly onto the slice and iii) microinjections of the DiD solution onto the slice. The following will describe how these experiments were undertaken and the limitations and advantages each method poses.

Initial optimisation studies of DiD uptake into neurons were carried out on hippocampal slices of rat brain without mito-Dendra2 fluorescence, as they were readily available (courtesy of Clare Tweedy, PhD student, Institute of Neuroscience). Sections were initially cut on a

vibratome at a 450µm thickness, which were then modified to a 300µm thickness, rendering the slices thinner, granting easy visualisation of DiD within the slices and also reducing the area for DiD penetration. Once in contact with the dye, slices were permitted to equilibrate in ACSF for 30 minutes before any recordings commenced.

3.4.1.1 Direct application of DiD crystals onto hippocampal slice

This technique pressed a few crystals of undissolved DiD onto the 450µm hippocampal brain slice. Studies have shown that dye crystals can be applied directly to intact or cut neurons for retrograde or anterograde labelling (Godement *et al.,* 1978, Gordon *et al.,* 1993, Thanos and Mey, 1995. In particular cases the direct application of crystals produces more consistent labelling than the injection of a dye solution (Thanos and Bonhoeffer, 1987). DiD crystals were applied to a micropipette tip for delivery onto the hippocampal site via a gelatin sponge (Thanos and Bonhoeffer, 1987), to hold the crystals in place during the time required for DiD transport along the neuronal pathway.

Z-stack analysis identified DiD penetration at 90µm into the slice, however the dye labelled all neurons and processes that it came into contact with. Pressing the crystals onto the slice inhibited precise identification of individual neurons, as the dye had localised to several cells and not just one cell on the tissue. The widespread labelling of many cells, as a consequence of the ad-hoc pressing of the crystals, demonstrated that the fluorescent signal on the slice was saturated within pressed region. This region of amplified fluorescence, impeded any detection of individual cell bodies within the neurons and so it was decided that though this method was working, in terms of DiD passing into and through the tissue, the crystals within the dye were causing a large visual hindrance and non-specific binding of neurons were sighted where transport into processes were also not observed (Figure 3.1A-B)

3.4.1.2 Microinjecting DiD solution onto hippocampal slice

Whole-cell patch clamp is commonly used to study electrophysiological properties of neurons in brain slices (Edwards *et al.,* 1989). Using electrodes filled with fluorescent dyes, the whole-cell configuration of patch clamp injects dye into neurons by diffusion through the pipette tip to neuron. This technique has the advantage that the labelling is rapid and that any neuron in the slice can be targeted and therefore visualised. When electrophysiological measurements are combined with imaging, a lower concentration of dyes are used and the whole-cell patch

clamp is maintained during an experiment (Yuste and Denk, 1995). The microinjection of a small volume of the concentrated DiD solution was an alternative to the direct application of the crystalline dye for neuronal tracing (Honig and Hume, 1986).

Applying this technique to our studies, DiD crystals were injected into neurons to observe DiD incorporation into the tissue. Extracellular recordings (1-300 Hz) were conducted with ACSF-filled glass microelectrodes (2-4 MΩ) connected to an extracellular amplifier (EXT-10-2F, npi electronic GmbH, Tamm, Germany) (Ehrrmann *et al.,* 2016). Microelectrodes were filled with DiD solution. Recordings were conducted within the CA3 sub-field of the hippocampus, and DiD contents within electrode were transferred into neurons within the hippocampus. This technique involves the rupturing of the cell membrane in order to inject the cell with DiD, which may have detrimental effects on the cellular content, and therefore possibly mitochondrial health and trafficking.

Whilst attempting to image these slices, it became apparent that DiD crystals were prohibitive in two aspects i) the large crystals within the DiD were not allowing the contents of the injection to be transferred to the neuron and ii) crystals within the DiD solution transferred to the neuron were proving a visual hindrance, as they formed large clusters on the slices inhibiting clear vision of where the dye had penetrated (Figure 3.1D)

Therefore, it was decided that the crystals had to be removed from the DiD solution, and once removed, a known concentration and volume of DiD must be incorporated into the brain slice in order to devise a reliable method that can be reproduced.

As the protocol illustrated by Honig and Hume, 1986 uses a 10 mg/mL (1.0 w/v) solution, the dye was further diluted down to a 2.5 mg/mL (0.25% w/v) to optimise dye penetration via microinjection. Prior to microinjection, the DiD was sonicated and centrifuged, in order to dissolve dye crystals blocking the pipette tip. Via replicating this method, the dye was prepared, and cells were injected intracellularly. Initial experiments were conducted in hippocampal sections at 2.5 and 10 mg/ml concentrations. Intracellular recordings were then taken from a single cell in the hippocampal cortex (CA1, CA2 region) by injecting DiD at a 2.5 and 10 mg/ml concentration. Here, it was observed that injecting the dye at 2.5 mg/ml was too low a concentration and was not taken up efficiently by neurons in the hippocampus. However, at a 10 mg/ml concentration, dye was taken up into slice with very little background signal, targeting only the neuron injected (Figure 3.1C).

There are many limitations to microinjections, where finding and patching onto a cell is time consuming and in some instances a neuron may not even be located during electrophysiology. Injecting the dye into a neuron was also a very intricate process whereby on a few occasions the injection had failed to incorporate the dye into the cell completely, as exchanging of the contents of the needle was inefficient, and vice versa where the DiD was not efficiently taken up by the injection. Using a 10 mg/ml solution showed some DiD penetration into the neuron, where perhaps a larger concentration of the dye incubated over a longer time period would be required in order for targeted fluorescence within the nigrostriatal pathway. However, the issue of a larger concentration causing a larger background fluorescence on the brain slice was identified, in addition to decreased cell viability as a consequence of the extended incubation time of the slice. Moreover, slices have to be kept alive when imaging, so confocal microscopy will be set in accordance to this, ensuring that slices are constantly pumped with artificial cerebrospinal fluid in order to prevent slice death.

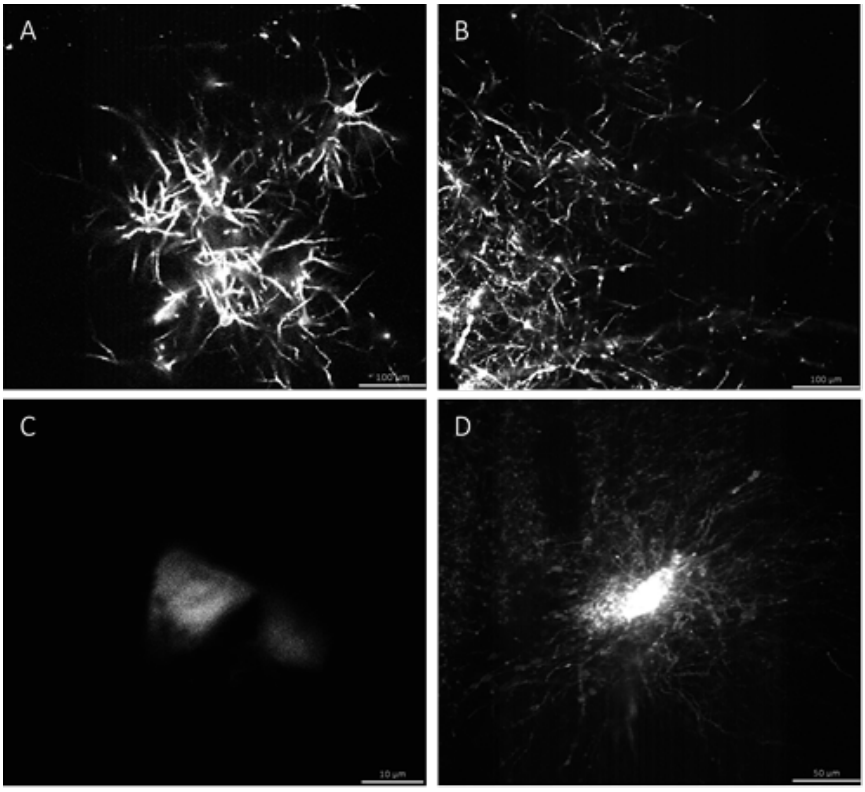

Figure 3.1. DiD incorporation on to brain slice. Various methods were used to incorporate DiD into neurons. **A, B)** Direct application of DiD onto the slice via gentle pressing of gelatine crystals and **C) U**se of microinjections filled with 2.5 mg/ml DiD **D)** Use of microinjections filled with 10.0 mg/ml onto slice. Images taken at x 20 magnification on Nikon A1r Invert confocal.

3.4.1.3 Pipetting DiD solution onto hippocampal slice

Direct pipetting of DiD onto the brain slice was carried out with two volumes, <0.5 and <1.0 µl of a 10 mg/ml stock. Slices were left to incubate for 60 minutes at room temperature to allow time for absorption, within the ACSF holding chamber. DiD was pipetted straight onto hippocampal slices, away from the targeted region to observe the degree of penetration over 60 minutes. DiD uptake was highly efficient within the slice, where emerging neuronal processes and pyramidal cell bodies were observed. It was decided that persisting with pipetting the dye onto the slice would be the most reliable option, as dye uptake was continuous, however more practise was required in terms of directing the dye and where it would be localised (Figure 3.2).

3.4.1.4 Using transgenic Mito-Dendra2 fluorescence to identify the nigrostriatal pathway

Optimisation of DiD insertion into cell bodies distinctly showed that though the DiD was penetrating the slice, this process took over two hours. In cases of culture studies, this would be a viable situation, however as brain slices will lose viability within 6 – 10 hours once isolated from the rodent, it was not practical to let slices incubate with DiD for 3-4 hours, to optimise dye uptake.

Although it was believed that having a neuronal tracer would be essential for the identification and tracking of single neurons, it became apparent that due to the organisation of the nigrostriatal pathway the engineered mito-Dendra2 fluorescence was sufficient to allow neuronal tracing. Therefore, the additional labelling of slices and neurons with DiD was not taken further. Efficient slicing of the pathway enabled visualisation of all structures of the pathway, and further eliminated incubating slices with a dye prior to imaging, and therefore minimalising the length of time the slice remained isolated from the brain. Therefore, future experiments were conducted in slices that were not stained with DiD, already expressing mito-Dendra2.

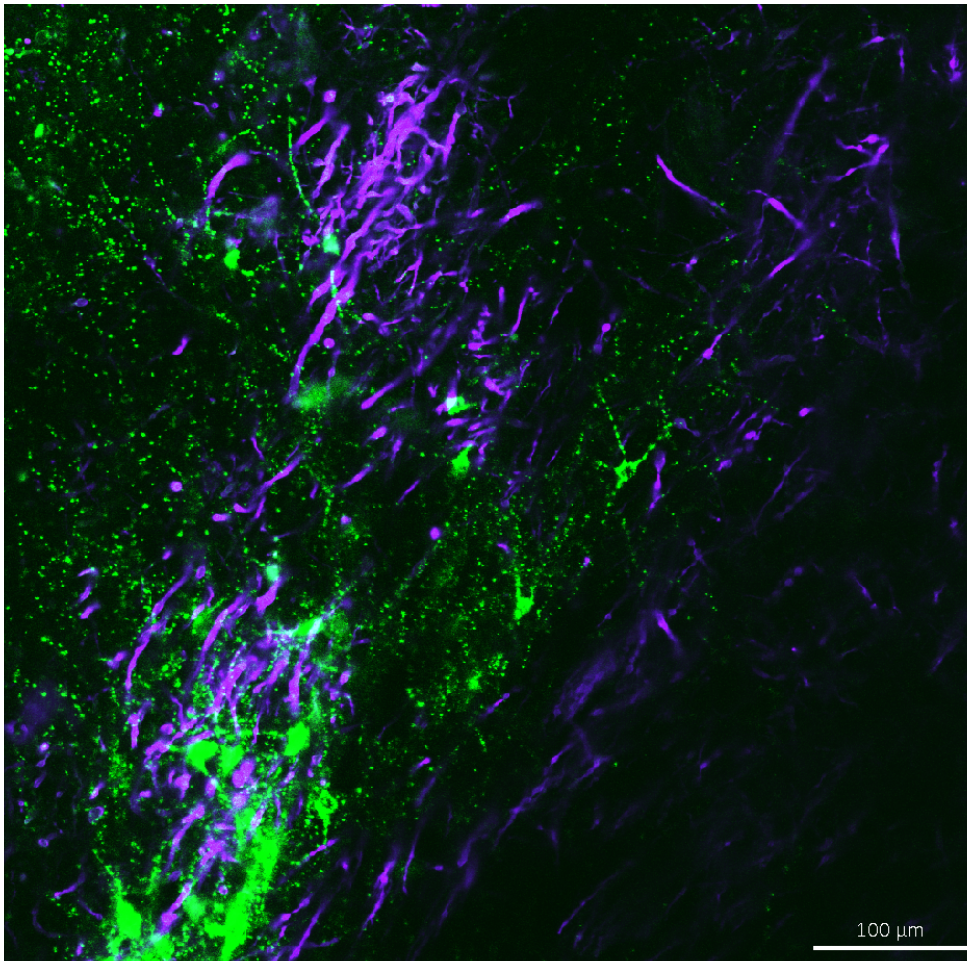

Figure 3.2. Pipetting DiD onto nigrostriatal slices. Pipetting the DiD onto the slice was found to be the most robust and efficient method that incorporate DiD into slices. 1.0 µl of a 10 mg/ml of DiD as directly applied to slices, where in addition to the mito-Dendra fluorescence at 488 nm, neuronal structures can be observed at 647 nm fluorescence, labelling axons of the nigrostriatal pathway.

3.4.2 Slicing to obtain the nigrostriatal pathway

Once the ability to trace individual neurons was confirmed, the next obstacle in the optimisation of these *ex vivo* experiments was the slicing of the mouse brain in the correct orientation to consistently obtain an intact nigrostriatal pathway.

3.4.2.1 Angled slicing to obtain the nigrostriatal pathway

Once a brain was harvested and divided into two hemispheres (Figure 3.3A), slicing the brain in an orthodox manner (horizontal, sagittal, coronal) would disrupt the desired neuronal processes, as projections of the nigrostriatal pathway do not lie in one plane. Thus, to combat this problem, the mouse brain would have to have a small section sliced removed from the cortex of each hemisphere in order to allow angled slicing to be performed.

To allow the intact pathway to be imaged, a segment was removed from the brain, by trialling three different angles: 40° 45° and 50° to appreciate which angle of slicing permitted an intact nigrostriatal pathway (Figure 3.3B). Angled sectioning of the brain was carried out by a metal block which contained slicing guides angled at 40° 45° and 50°(Figure 3.3B). Once a segment of the brain was removed, both hemispheres of the brain were sectioned at a 300 µm thickness on the vibratome (Figure 3.3C).

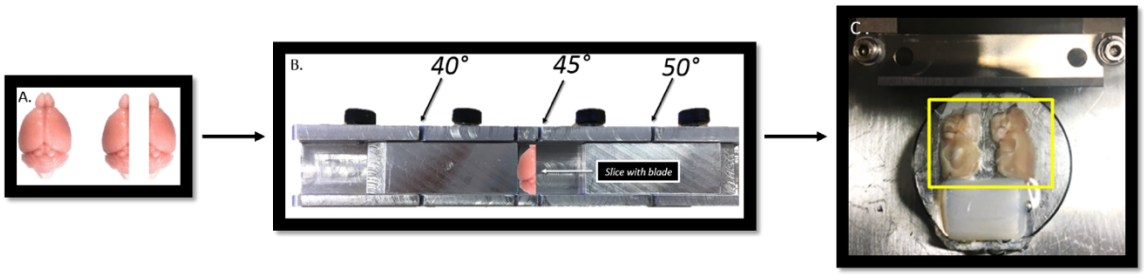

Figure 3.3. Live imaging setup. Imaging of the nigrostriatal sections were initiated with **A)** halving the Dendra2/CRE mouse brain into two hemispheres. **B)** Optimisation of the best angle for slicing was then carried out by slices the hemispheres at three different angles: 40, 45 and 50° with a blade that sat within the angled guides. **C)** Slices were mounted onto vibratome with cut side facing downwards and 300µm thick sections were obtained

Of the three angles, 45° showed to be a better provider of an intact nigrostriatal pathway. Imaging at 45° provided evidence of the mito-Dendra2 and facilitated the visualisation of the nigrostriatal pathway, where individual mitochondria within axons and axon terminals leading into the striatum could be identified. On repeating this angled slicing method, it was established that cutting the sections at 45° and 50°, reproducibly gave an intact nigrostriatal pathway, for each experiment. Surprisingly, this further confirmed that the addition of DiD to identify neurons was not required, as the mito-Dendra2 assisted identification of single neuronal processes, as mitochondria were distributed within defined structures through the pathway. This allowed their movements to be tracked easily from cell body to striatum. Experiments were thus continued by removing a segment of the brain at 45° and imaging according to mito-Dendra2.

Further CLARITY experiments conducted on wildtype mice that were angled at this section, demonstrated that at 45°, the nigrostriatal pathway was easily observed via tyrosine hydroxylase (TH) staining as an indicator of DAergic neurons. DA neurons were identified at large, projecting from the SNpc and towards the striatum. (Figure 3.4)

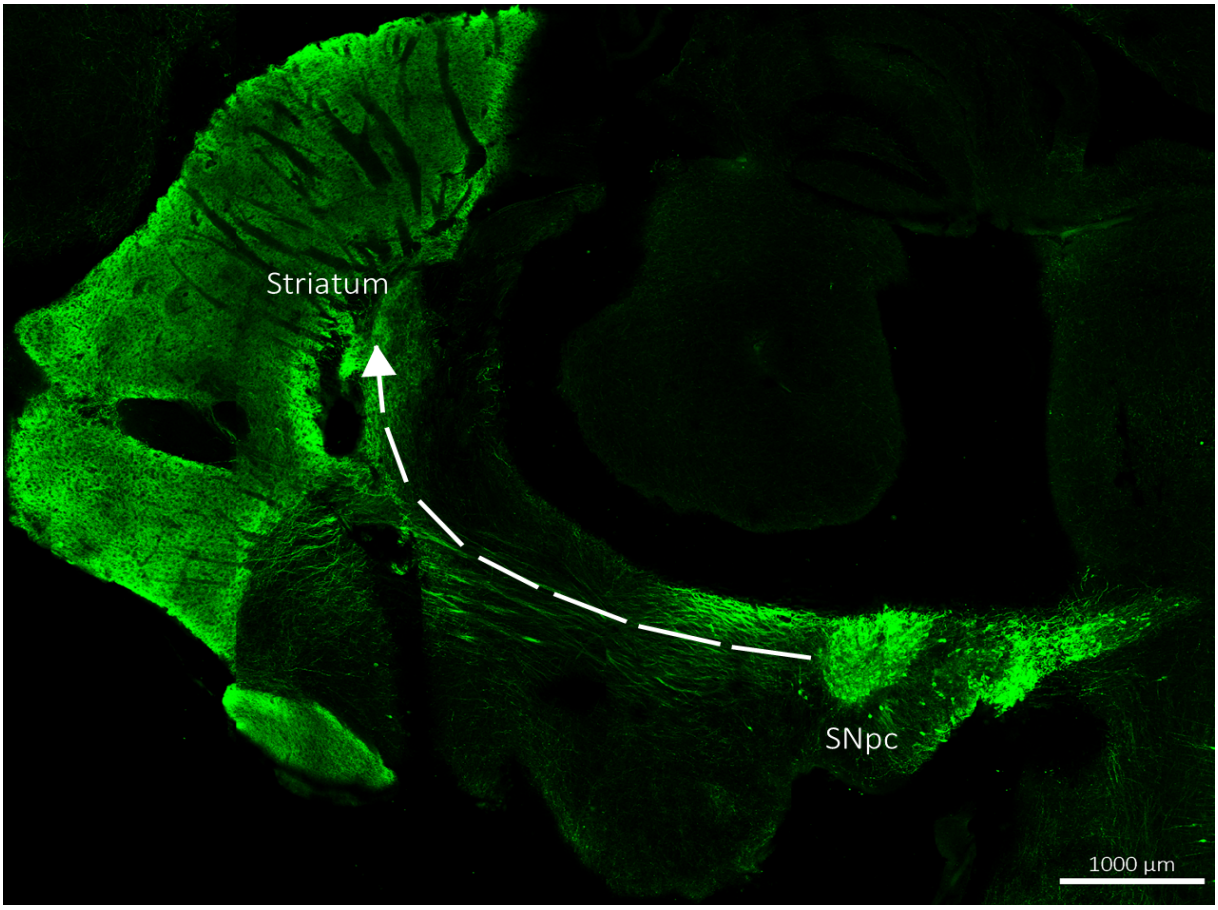

Figure 3.4. Nigrostriatal pathway stained with tyrosine hydroxylase via CLARITY. CLARITY assay on nigrostriatal pathway within wild type mouse showing, dopaminergic processes from the substantia nigra to the striatum by staining with tyrosine hydroxylase (TH)-positive neurons (green). Staining shows intact nigrostriatal projections from the cell bodies to the striatum. Scale bars, 1000 µm.

3.4.3 Imaging the nigrostriatal pathway in Dendra/Cre mice – Slice viability

The aim of this study was to image mitochondrial trafficking within 'live' DA neurons of the nigrostriatal pathway. The most crucial aspect of this study was to maintain living slices throughout the imaging process on the Nikon A1r. *In vivo* studies have monitored and analysed live mitochondrial trafficking for 10 -15 minutes (Misgeld *et al.,* 2007a, Misgeld *et al.,* 2007b, Pluckinska *et al.,* 2012, Sajic *et al.,* 2013, Sorbata *et al.,* 2014, Lewis *et al.,* 2016) and so this length of imaging was replicated in this model, where all experimental videos were of a 10 minute duration.

To counteract tissue death, it was key that a method of maintaining live cells for a long duration, whilst imaging on the confocal had to be created. Therefore, a perfusion system was created, where slices that were being imaged were always supplied with ACSF, imitating the environment in which they are retained in prior to imaging, in the holding chamber. In addition to the perfusing ACSF solution, a gas cylinder was also incorporated, which ensured that the ASCF was oxygenated. This system allowed imaging of the slices of up to 4 hours, without losing slice viability. Slices were maintained under the microscope in a glass (Ibidi) bottom dish throughout imaging, where a 1.0 mm slice anchor was positioned on top of slices to disable floating whilst imaging from below on an inverted confocal microscope.

Nigrostriatal slice viability was assessed by incubating slices with 2 drops/mL Nuc Red dye, which emits signal at 647 nm, indicating cell death. Images were taken of nigrostriatal slices at 60 and 120 minutes into imaging (Figure 3.5A-F), where cell death was observed around the circumference of the slice, where the edges of the sections appeared to begin to degrade during imaging. In relation to how this affects the nigrostriatal pathway, the striatum is located at the anterior end of the brain slice, in relation to the posteriorly located SNpc. In all cases of imaging the striatum was imaged first, simply due to its easy identification as a structure. Imaging within the striatal region of the section was conducted within the first 45 minutes, after which point, posteriorly located axons and cell bodies of the SNpc were imaged. By these means, the imaging usually lasted around 3 hours, by which the middle of the section was shown to decay (as identified by NucRed staining) (Figure 3.5G).

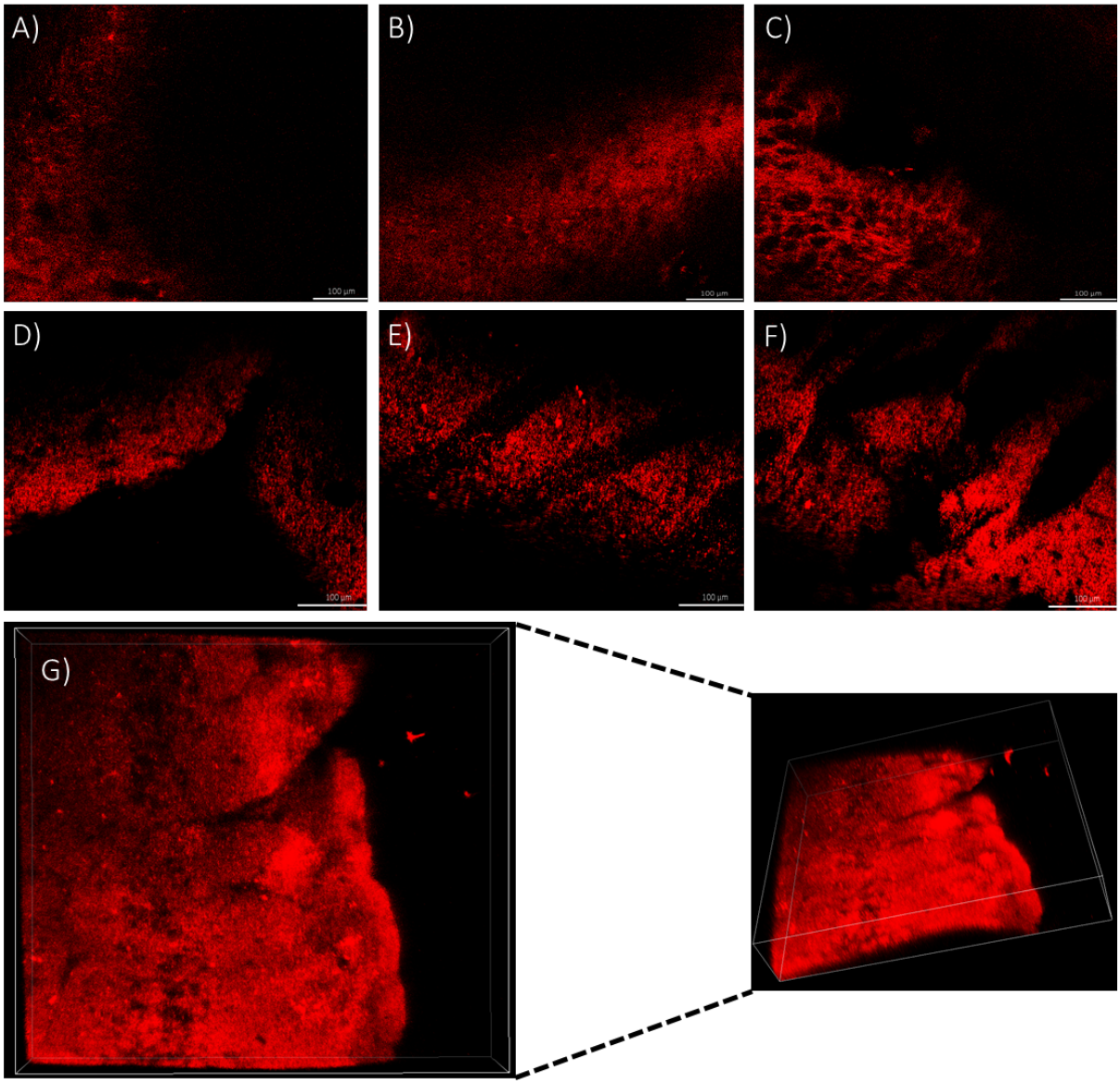

Figure 3.5. Assessing slice viability with NucRed staining. NucRed images were taken after **A-C)** 60 minutes into imaging and **D-F)** 120 minutes into imaging, where slice viability is reduced around the edge and the middle of the nigrostriatal slice respectively. **G)** Z-stack analyses of Nuc red staining shows that after 180 minutes of imaging, the slice is almost completely degraded, with NucRed penetration of 118.30µm within a 300µm section.

Furthermore, in order to attain as much data from each animal as possible, a minimum of 9 videos were recorded per slice. Therefore, the nigrostriatal pathway was divided into 3 parts, cell bodies in the SNpc, axons projecting toward the striatum and lastly the striatum, where the nigrostriatal pathway terminates. For each region, a minimum of 3 videos were obtained, generating 9 videos per slice.

Each mouse generated a minimum of 4 viable, intact slices that could be retained for imaging. However, it was not always the case that all four slices could be used, as this would mean they would be kept on the confocal for up to 6 hours after dissection, which undoubtedly may not provide an accurate representation of live mitochondrial trafficking. The first few hours of recording consisted of videoing the 3 regions throughout the nigrostriatal pathway within the cell bodies (Figure 3.6), axons (Figure 3.7), and striatum (Figure 3.8). A maximum of two nigrostriatal slices were imaged within each experiment, the remainder of which, if viable, were fixed for CLARITY experiments.

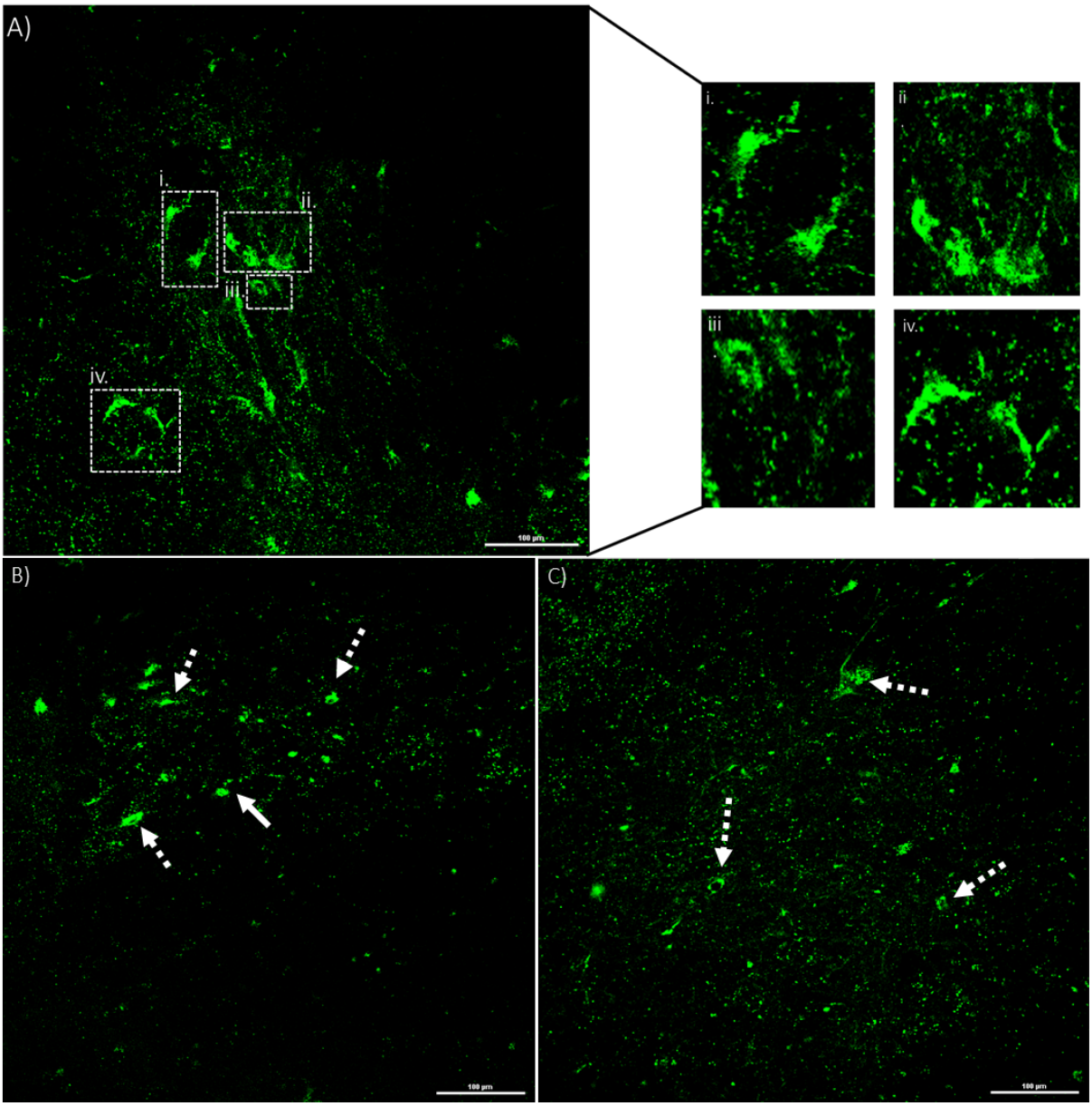

Figure 3.6. Cell bodies within the SNpc in Mito-Dendra2 labelled Dendra2/DATIRESCre mice. Confocal imaging was conducted on 300 µm thick slices of 7 month wild type HetDendra/HetCre mice. Mitochondria were labelled with mito-Dendra2 and under a DAT Cre promoter, which ensures DA neuronal fluorescence. Ai-iv) Shows mito-Dendra2 show evidence of SNc cell bodies and the respective axonal processes where individual mitochondria can be observed. A large quantity of cell bodies within the SNpc and their interconnected axonal pathways can be seen, where individual mitochondria can be observed within these intricate axonal pathways. B-C) Further show emerging cell bodies within the SNpc in the nigrostriatal pathway. Scale bars, 100µm. All videos were obtained at x20 magnification.

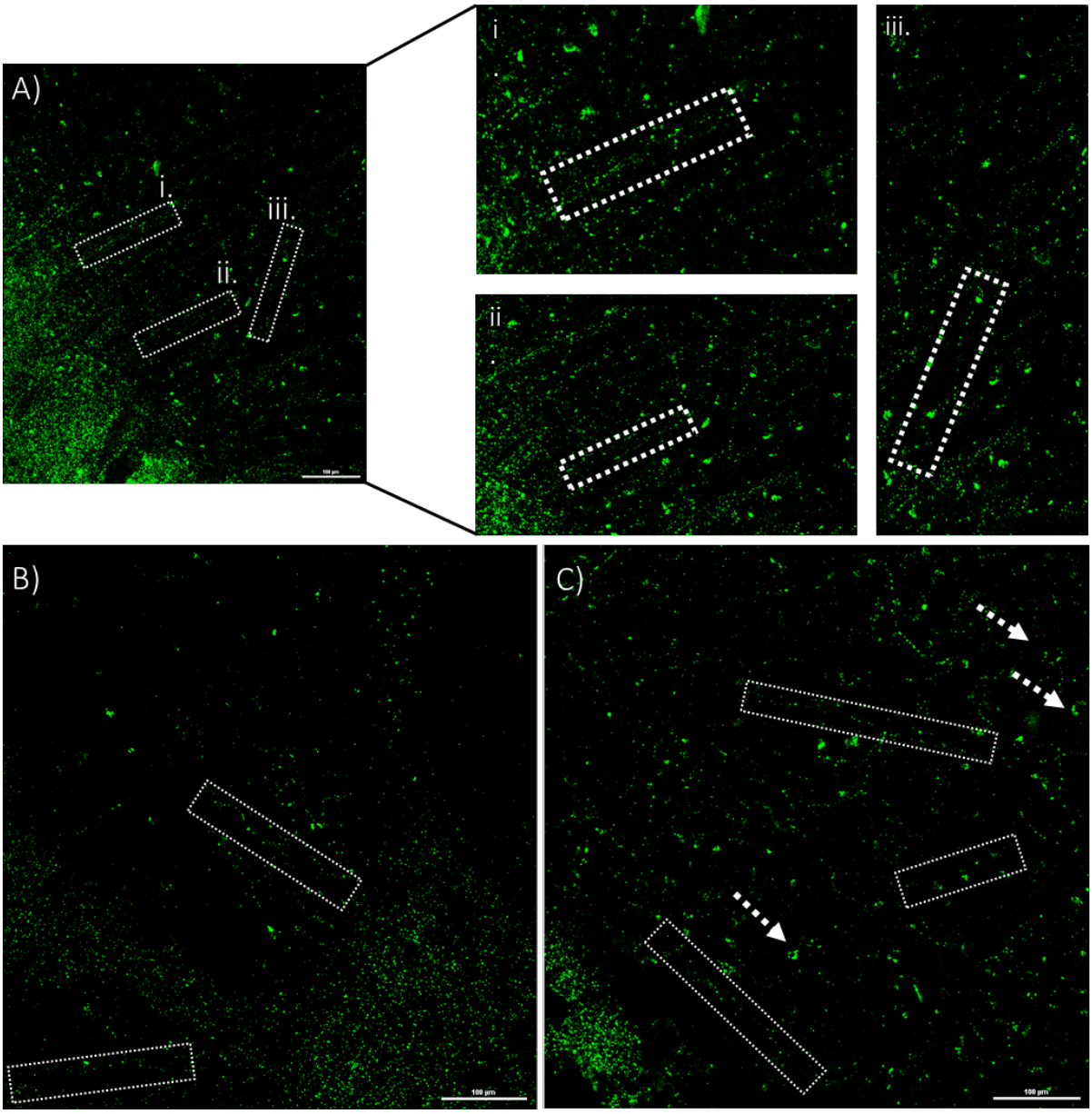

Figure 3.7. Nigrostriatal projections within in Dendra2/DATIRESCre mice. Confocal imaging was conducted on 350µm thick slices of 7 month wild type HetDendra/HetCre mice. A-B) Neurons form synapses at their axon terminals in the striatum where each neuron can synapse into more than one axonal terminal (white boxes), where mitochondrial tracks are less dispersed towards their axon terminals. Cell bodies (white arrows) are also observed. C) Axonal terminals, where individual mitochondria can be observed within these processes. Scale bars, 100µm. All videos were obtained at x 20 magnification.

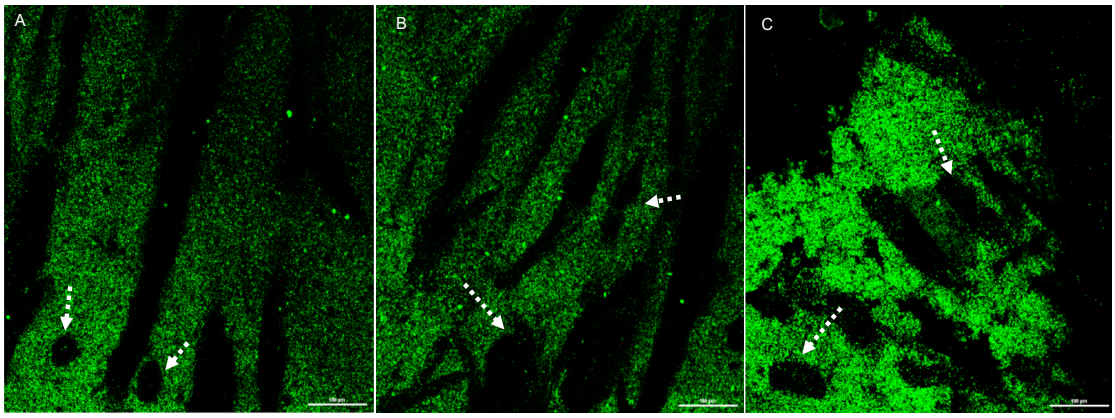

Figure 3.8. Identification of the striatum in the nigrostriatal pathway in Dendra2/DATIRESCre mice. Confocal imaging was conducted on 350 µm thick slices of 7 month wild type HetDendra/HetCre mice. **A-C)** Neurons form synapses at their axon terminals, where neurons can synapse into more than one axonal terminal. The identification of Wilson's pencils were used to identify the striatum within the nigrostriatal pathway (white arrows) in the slices, where mitochondria within the striatum are tightly compact and occur in large volumes. Scale bars, 100µm. All videos were obtained at 20x magnification.

3.5 ANALYSING MITOCHONDRIAL TRAFFICKING IN NEURONS

Many factors render the imaging and analysis of mitochondrial movement an intricate and complex task. Firstly, the deviations in mitochondrial morphology render mitochondria difficult to segment and identify as individual objects. Secondly, photo bleaching throughout imaging may enforce a compromise to occur between the frame rate and duration of tracking time (Yang *et al.,* 2010); (combatted in this study by maintaining a constant low laser power during experiments) and lastly, the efficient methods to track and quantify mitochondrial movement are yet to be established (Yang, 2012). Mitochondrial trafficking analyses described in this section used two softwares to image mitochondrial trafficking, IMARIS 9.2 (IMARIS 9.2, Bitplane AG, software available at http://bitplane.com) and FIJI, to generate kymographs.

Movement analysis was optimised for use in the following disease models:

i) Nigrostriatal brain slices, to observe mitochondrial dynamics in the cell bodies, axons and striatum of the nigrostriatal pathway
ii) iPSC cultured neurons to observe mitochondrial dynamics within cell bodies and axons

The recording of mitochondrial trafficking was conducted on the Nikon A1R Inverted Confocal, where all videos measured were 10 minutes and at a frame/second. This section will describe analysis optimisation in both models and justify our selection of the particular analyses. The final optimised method could then be applied to neurons in culture or *ex vivo* slices.

3.5.1 Observing mitochondrial dynamics - Cell bodies

These studies sought to measure the mitochondrial membrane potential via TMRM/MitoTracker Deep red staining within cell bodies of SNpc nigrostriatal slices (Figure 3.9A and 3.9B) and cultured neurons harbouring low and high heteroplasmy neurons (Figure 3.9C. See Chapter 6). Nigrostriatal slices were loaded with 5nm TMRM and 125nm Mito tracker dye, where cultured neurons were loaded with 5nm TMRM. During this analyses individual cell bodies were selected and measured within both cultured neurons and slices. In the cultured neurons, many cell bodies can be observed, whereas in nigrostriatal cell bodies were not found in similar numbers. In cultured neurons around 10 cell bodies were measured for each video taken per experiment and in slices, all the cell bodies that could be observed were analysed (around 5-6 per video). Individual ROIs (boxes) were created for each cell body; the size of which would vary dependant on cell body size; with the main objective being to avoid axons and/or projections from these cell bodies as intensity values of these mitochondria would be included in these measurements.

TMRM staining (Fig 3.9A) within the SNpc cell bodies was very punctate reflecting mitochondrial staining, here individual cell bodies were identified allowing the measurement of mitochondrial membrane potential via IMARIS. Having repeated TMRM staining in other nigrostriatal slices, it was found that punctate TMRM staining was not reproducible. Reasons for this being, i) the loading concentration of TMRM may have been too high or too low, ii) not enough time was given for TMRM dye uptake onto the slice, (more than 30 minutes for TMRM uptake is not advisable due to the risk of reducing slice viability), iii) the dye may have been largely concentrated within one region only and did not penetrate other regions and finally iv) when TMRM was loaded correctly onto the brain slice, this staining was not punctate. For these reasons stated it was decided to discontinue this analysis.

MitoTracker Deep Red staining (Figures 3.9B) revealed no individual cell bodies, were stained, rather the tissue that surrounded the SN, where no punctate staining that co-localises with the mito-Dendra2 were observed and therefore this staining was discontined. Altogether, it was decided that observing mitochondrial membrane potential within SNpc cell bodies required further optimisation.

Within cultured neurons (Figures 3.9C) TMRM was loaded prior to live imaging (See chapter 5 and 6 for details of the methods) where individual cell bodies can be observed (Fig 3.9Ci-iii). Videos were analysed on IMARIS, masking analyses were created around these punctate cell bodies and analysed for variations in mitochondrial membrane potential, between low and high heteroplasmy neurons.

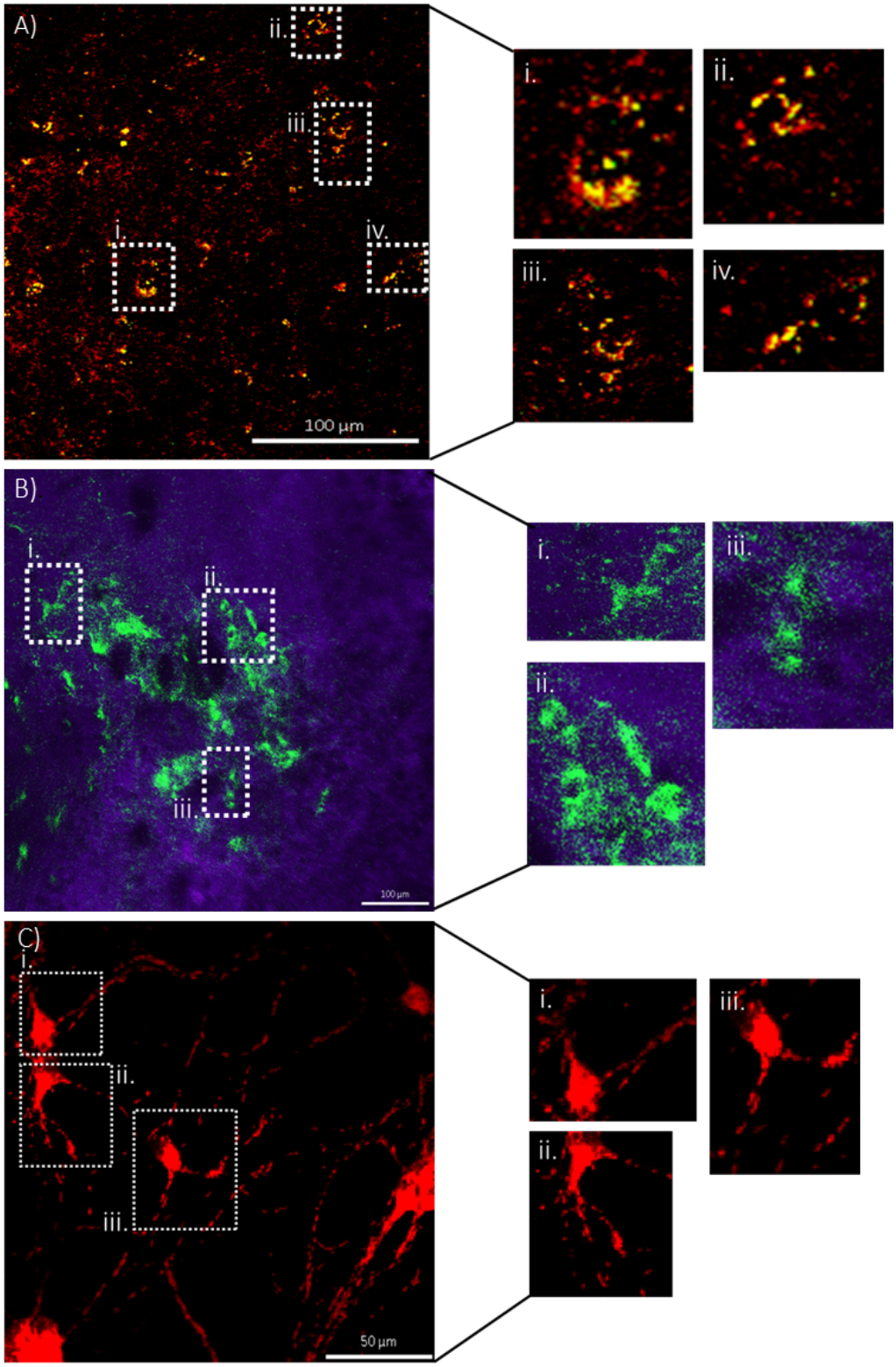

Figure 3.9. Assessing mitochondrial function via mitochondrial membrane potential. Mitochondrial function was assessed by loading cells with TMRM (A and C) and MitoTracker Deep Red (B). **A)** Staining of SNpc cell bodies (green) loaded with TMRM (red) in nigrostriatal slices. **B)** Staining of SNpc cell bodies (green) loaded with MitoTracker Deep Red (Purple) in nigrostriatal slices and **C)** TMRM (red) staining in axons and cell bodies on cultured neurons.

3.5.2 Observing mitochondrial dynamics - Axons

3.5.2.1 IMARIS time lapse imaging

IMARIS 9.2 allows the analysis of movements over time and can also generate information about surrounding stationary objects. It allows the tracking of mitochondrial motility throughout videos through trajectories of Brownian motion, encompassing the size of the voxels (individual mitochondria) and therefore producing data on a number of parameters that include track speed, duration, length as well as mitochondrial volume and TMRM intensity.

During optimisation of time-lapse imaging on IMARIS, selected mitochondrial parameters were measured throughout the recorded videos. The aim of IMARIS analysis, was to identify mitochondria within axons and how they vary in individual parameters in the presence of a respiratory chain defect (cultured neurons) or aging/PD pathology (Mouse model). IMARIS generated information for the parameters that were selected, and if mitochondria did not undergo fusion or fission , would have been an adequate method to analyse this data.

3.5.2.2 IMARIS time lapse parameters

During the initial surface analysis, within an ROI, each mitochondria within each axon would have its own track, where IMARIS would trace mitochondrial displacement from its origin and would also track mitochondrial directionality. From these tracks, the following mitochondrial properties were observed:

- *Track speed* (μms^{-1}) – This measured the instantaneous speed of individual mitochondria throughout the track, where data for each mitochondrion throughout each track is provided for each time point.
- *Track length* (µm) - This measures the total length of displacement within each Track, and is indicative of the direction of mitochondrial movement within a track over time.
- *Track Duration (s)* – The track duration measures the time each mitochondrion takes between the first and last time point within each track, and provides insight into how short and/or long the tracks are and how this changes throughout the video.
- *Mitochondrial membrane potential (Arb, U)* – Cultured Neurons - IMARIS analysis was used to measure the intensity of the TMRM (TRITC) channel. The 'Intensity mean' was generated as a data point for each mitochondrion at each time point, these values were then averaged. The intensity mean indicates the average intensity of each mitochondria within a surface.

Time lapse imaging analysis conducted on IMARIS in both models, indicated that IMARIS did not count for the fission and fusion properties of mitochondria throughout a video, as the surfaces created did not amend themselves throughout the imaging time in order to cater for these mitochondrial properties, but remained fixed throughout imaging, once set. Furthermore, if a mitochondrion was to exit the plane of view, this was not controlled for within IMARIS imaging, therefore, we did not continue to measure mitochondrial trafficking via the IMARIS software in either model.

3.5.3 Observing mitochondrial dynamics – Axonal kymographs

After having eliminated the tracking of mitochondria within axons using IMARIS, analyses moved onto using kymographs to analyse mitochondrial movement. The generation of kymographs from time lapse imaging has become the most common method to image mitochondrial transport (e.g., Miller and Sheetz, 2004, Hollenbeck and Saxton, 2005, Wang *et al.,* 2011).

In kymograph analyses, there are 4 types of mitochondrial movement classed as dynamic pause (DP), stationary (ST), anterograde (AR) and retrograde (RR) movement (Figure 3.10) (Chen *et al.,* 2016). Directionality and speed of mitochondrial trafficking were recorded for cultured neurons, and within the nigrostriatal slices, kymographs were generated for both axons and axon terminals.

Mitochondrial movement in the cultured neurons were observed to be stationery, anterograde and retrograde. Furthermore, they exhibited 'dynamic pause' movement and also anterograde and retrograde movement was found to occur in several speeds. In contrast, within the slices very little mitochondrial movement was observed, whereby movement was observed as a mitochondrion generating small shuffles adjacent to its original location.

Due to the dynamic and sporadic nature of mitochondria not all types of movemements were analysed in this project. Two thresholds were set: Speeds between 0 – 0.005 μm/s moving mitochondria were identified as stationary and speeds above 0.005 μm/s were classes moving.

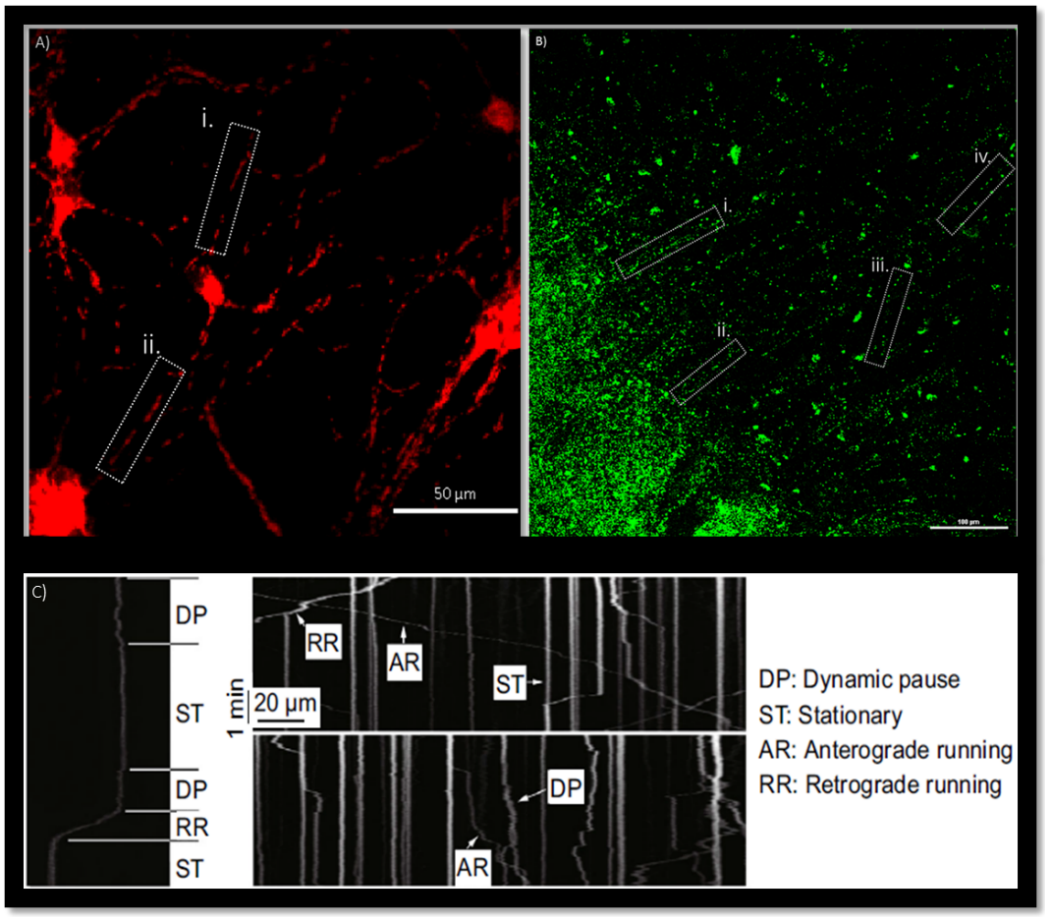

Figure 3.10. Kymograph analysis. A) Axons analysed in TMRM stained cultured neurons from human IPSCs harbouring large scale mtDNA deletion. **B)** Nigrostriatum with projecting axon terminals **(i and ii)** and axons **(iii and iv)** that will be analysed through kymograph analyses. **C)** Directionality of mitochondria movement is shown in the kymograph as dynamic pause (DP), stationary (ST), anterograde (AR) and retrograde (RR) movement (Chen *et al.,* 2016).

3.5.3.1 Generating kymographs

The kymograph plug in was downloaded and installed, which consists of all four "*.class" files, which were moved to the ImageJ Plugins folder. Axonal videos recorded on the confocal are created as '.Nd2' files that were opened in the IMAGEJ software for analysis.

Creating segments on IMAGEJ - Using the line function on IMAGEJ, equivocal lines were created (in order to combat subjectivity), outlining axons for measuring. The line function allows the altering of the thickness of the line, where this can be altered, by increasing or decreasing the thickness to include all mitochondria of interest within the axon and conversely, to exclude mitochondria that are not a part of the axon of interest (Figure 3.11A).

Creating kymographs - Once the ROI was selected, the 'Multiple kymograph' tool was selected on the plugin tab. This generated a kymograph, where white straight lines represent stationary mitochondria, while moving mitochondria were indicated by the diagonal direction of these lines indicating anterograde or retrograde direction. A diagonal upward movement represents retrograde movement and a diagonal downward movement indicates anterograde movement (Figure 3.11B-C).

Kymograph statistics - Individual mitochondria were selected and their serial numbers were recorded via ROI manager, where each ROI generated its own table of information. Mitochondria were analysed individually. The macros plugin allowed the analysis of selected ROIs, to extract their velocity data. Excel sheets were created for each mitochondrion, where velocity and distance travelled for each mitochondrion were calculated (Figure 3.11D-E).

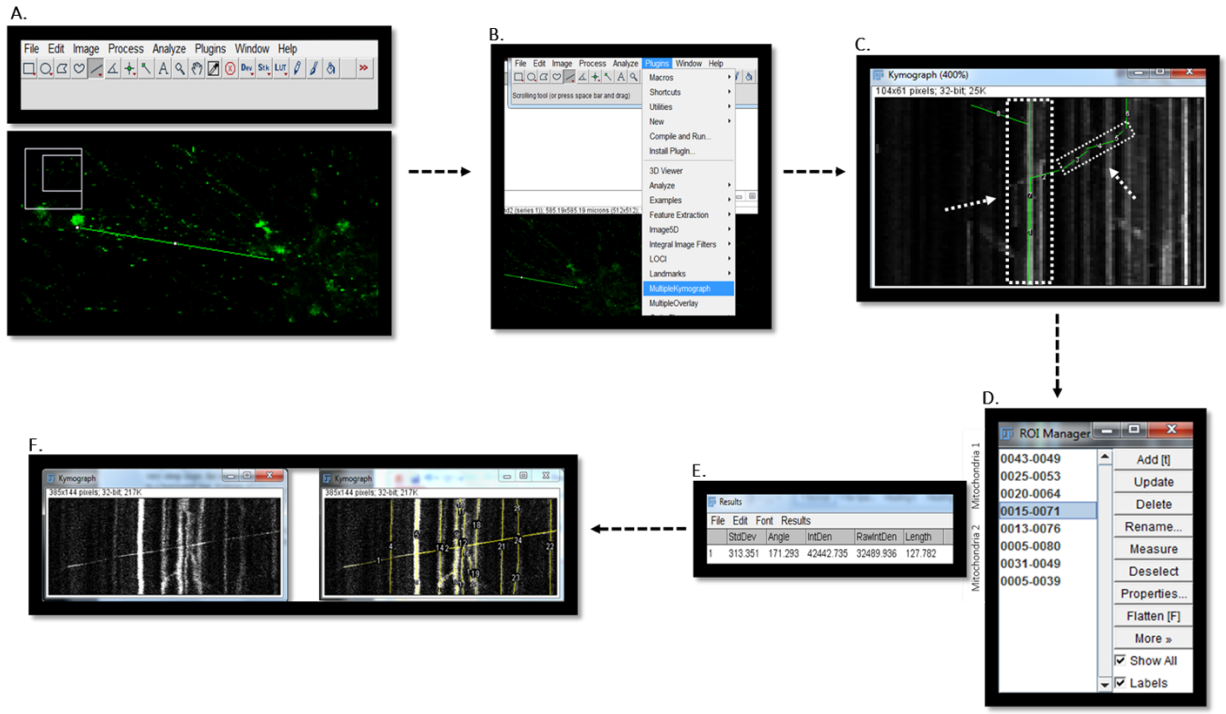

Figure 3.11. Kymograph generation. Figure shows steps taken to generate kymographs to analyse mitochondrial trafficking. **A)** Lines were drawn over axons to mark the length of the axon in which mitochondria are measured. **B)** The MultipleKymograph plugin was selected to generate a kymograph. **C)** Kymograph was generated where velocity and directionality of mitochondria within the selected axon could be observed. **D-E)** Selecting tracks within the kymograph, created more information about each mitochondria and its mode of direction by generating a statistics table. **F)** Exemplar kymograph with individually labelled mitochondria.

3.5.4 Observing mitochondrial dynamics – Striatum

Striatal analyses comprised of understanding two parameters of mitochondrial function, i) mitochondrial trafficking within the nigrostriatum and ii) membrane potential analyses via TMRM staining in order to understand membrane potential deviances within synapses of the nigrostriatal pathway. This section will describe 3 different methods housed within the IMARIS 9.2 software, which include surface, spots and masking analyses to carry out this analysis.

3.5.5 IMARIS surface analyses – Striatal mitochondrial movement

As kymographs help to understand the movement of an object within a linear projection, this method of analysis was not applicable to the neurobiological structure of the striatum, as the mitochondria found within this region are organised in a tight compact manner within nerve terminals and the striatum. Therefore, the following will describe the 'Surfaces' IMARIS protocol and how this was conducted in order to understand mitochondrial movement within the striatum. Surfaces were created over ROIs over (FITC) channel.

Segmentation – Prior to creating surfaces, the area of interest must first select within each video. This is achieved by using the 'segmenting function' that helps shape and analyse an arbitrarily shaped region of interest (ROI) within the video. Segmenting within the video, instead of analysing the video as a whole, limits the level of background that would be produced from neighbouring axons and permits more control of which objects within the neurons are being tracked. From these manually created segments, a surface object could be generated around the mitochondria.

Defining the ROI - The creation of surfaces on IMARIS to detect mitochondria within selected axons, is based on staining intensity. In addition, the user can input an expected size of the object to be tracked which detects a uniform size of mitochondrion throughout the tracking process. The manual tracking requires drawing around the area of interest with the use of the 'draw' tool within the creation wizard. A surface is created over the selected channel. Following this one could decide whether or not the smoothing tool was to be used. The smoothing tool determines how uniform your surface is and whether the rough surface generation is needed, via application of a Gaussian filter. However, the correct detection of these structures was crucial for analysis, therefore the smoothing tool was not used, as the smoothing tool supresses

noise of the segment homogeneously, which may cause mitochondrial fusing, disregarding smaller, individual mitochondrial.

Tracking surfaces over time - The surface creation wizard allows the option of tracking the surfaces over time. Time points could be individually selected through the scrolling bar, whereby the mitochondria that are being recorded can be tracked through each time point.

Creating surfaces - IMARIS will generate a surface encompassing the ROI, where the sensitivity of surface creation can be altered by adjusting the threshold. Thresholds within the image were adjusted, in order to avoid creating surfaces on unwanted background fluorescence. The threshold was adjusted to ensure the surfaces accurately detected positive signal and that the surfaces created were most representative of the fluorescent signal.

Background subtraction – The calculation of background subtraction is intensity based and is carried out by taking the smallest diameter of mitochondria measured and then creating a surface over this voxel. Once selected the creation wizard will attempt to identify the diameter of an object, by recommending an appropriate size of mitochondria and automatic recognition of the objects. However, in these experiments, mitochondrial shape was measured in the 'slice view' tab, where thresholds of mitochondrial shape were altered by checking the threshold level, in order to determine a mitochondrial diameter that allowed accurate tracking of all mitochondria within the video. This was further confirmed by manually playing the video and observing whether the surfaces created were representative of all mitochondrial shapes. Furthermore, surfaces can be removed if it seems that the track that is being created is incorrect or does not accurately track the mitochondria for the duration of the video. For our analyses, no surfaces were removed.

Adjusting voxels - Following on from this the voxels detected within the ROI were ordered and displayed as a histogram, depending on size of voxel. A three-dimensional environment is typically represented with the use of volumetric features (not to be mistaken with Z-stacks), such as voxels, that characterise the complex character of visibility obstacles. In this step, surfaces that were too small removed/did not encompass mitochondrial shape. This ensured that analysed surfaces did not include those which may have been created based on background signal.

Tracking algorithms and identifying distance – Finally a tracking algorithm is created for each surface. There are four algorithms that are available for motion analysis on IMARIS, these include, Brownian motion, autoregressive motion, autoregressive motion expert and connected components. Of these, the autoregressive motion was selected for my studies, as it is indicative of the random movement observed in biological processes. Once the algorithms were defined, the 'maximum distance' was established. This parameter defines the maximal connection distance between the surface and its predicted position over subsequent time points. The tracking algorithms were displayed as individual lines, where tracks could then be filtered on various parameters i.e. track duration, length and speed. However, all tracks were measured in this analysis. Following this final step of the analysis, all surfaces (mitochondria) and their respective tracks could be observed. This allowed the observation of the movement of all selected mitochondria throughout the entire video.

Statistics – Once tracks were determined, measurements were generated for each surface created throughout the videos as an excel spreadsheet. Results were tabulated for each parameter that was measured for each surface, which included data for track duration, length and speed, TMRM intensity (as a measure of mitochondrial membrane potential) and mitochondrial volume. Mitochondrial movements were measured in an average of 10 axons per video, from which intensity averages (as an indication of mitochondrial membrane potential) were compared between experimental cohorts via ANOVA testing with a post Dunnett's correction. However, a few limitations were observed during IMARIS analyses of the striatum and therefore this analyses was discontinued (Section 3.5.6)

3.5.6 Limitations of imaging mitochondria in the striatum

Segments of the striatum were used to track mitochondrial movement, where unfortunately, as mentioned previously, fission and fusion properties of the mitochondria were discounted. Furthermore, IMARIS surface tracking showed that actually not all mitochondria were being detected by the software, as the software excluded those objects that were too large or small. This then created a bias in the tracking of mitochondrial motility throughout the video, as the mitochondria that were recognised by IMARIS were only of a defined size.

The mitochondrial distribution within the striatum renders the analysis of this movement a practical challenge. This is due to the fact that mitochondria within the striatum are in large quantities which are organised in a tight, compact manner within the striatal fibres. Due to this structure, mitochondria within the striatum were mostly found to be stationery in motion and if they did move, only shifted slightly and did not displace much from their point of origin. Therefore, when tracking this movement, IMARIS generated several tracks (not representative of the true mitochondrial movement of each individual mitochondria), as a consequence of striatal mitochondria 'wobble-like' movement.

Therefore, it was decided to exclude this analytical approach from this study and instead generate TIFFS from each video, which were then analysed for mitochondrial membrane potential only, as still images. As sections were stained with TMRM (TRITC), the surface analysis was used again to select segments, and extract values that could be averaged, obtaining mitochondrial membrane potential values. For reasons to similar the TMRM staining within SNpc cell bodies, it was decided that the membrane potential of striatal mitochondria would not be measured, as further optimisation was required in this field in order to achieve a reproducible TMRM staining within brain slices (Figure 3.12).

Therefore, this study continued to observe mitochondrial membrane potential within the cell bodies of TMRM stained cultured neurons only via the masked surface analyses function of IMARIS. And kymographs will be generated for the analysis of mitochondrial movement in the axons of the cultured neurons and also within the nigrostriatal axons and axon terminals.

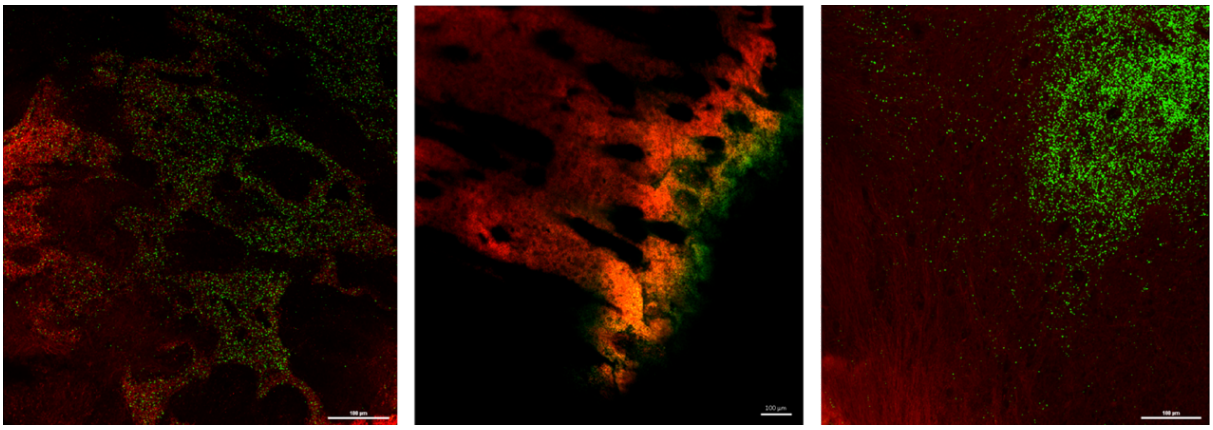

Figure 3.12. TMRM stained striatum. Figures left to right demonstrate variety in TMRM staining which cannot be compared for analysis purposes.

3.6 DISCUSSION

3.6.1 Summary of results

- Successfully sliced Dendra2/DATCre mouse brains at an angle to obtain an intact nigrostriatal pathway
- Established a perfusion system that could maintain nigrostriatal slice viability for up to 4 hours of confocal imaging
- Optimised a technique that allows the recording of mitochondrial movement within SNc axons of the nigrostriatal pathway
- Optimise method of analysis to quantify mitochondrial movement in axons

Acute live slices prepared from the brain have become a standard preparation commonly used to study electrophysiological properties of neurons in circuits (Alger *et al.,* 1984) and, more recently, imaging (Yuste, 2000b). Most of this work is carried out with slices from mouse nigrostriatum, where the relatively high degree of preservation of neuronal networks after slicing and the availability of a variety of easy experimental manipulations make acute slices an attractive experimental preparation. Generally, acute slices can be maintained in good condition for up to 6 – 12 hours (Buskila *et al.,* 2014) and all experiments conducted in this study have been in nigrostriatal slices that have been observed for less than 6 hours.

Observing mitochondrial motility within the nigrostriatal pathway is an intricate procedure. This study has developed a method by which mitochondria can be imaged within a mouse model that targets the nigrostriatal pathway, the largest neuroanatomical structure affected by Parkinson's disease. Manipulation of the Dendra2/DAT^{IRES}Cre mouse model has facilitated detecting mitochondria solely within the dopaminergic neurons of the mouse brain, a crucial feature in these experiments. Optimising this technique has allowed to obtain nigrostriatal slices in a reproducible manner, which allows the individual tracking of mitochondria throughout the nigrostriatal projections. Creating a perfusion system on a confocal microscope has now allowed the visualisation of cell bodies within the SNpc and their axonal projections towards the striatum, where axonal terminals can be successfully observed within the optimised 300μm angled nigrostriatal slices. This method demonstrates that it can be replicated between individual mice, highlighting its potential as a means to study mitochondrial trafficking within dopaminergic neurons of the mouse brain and how this is affected in Parkinson's disease.

3.6.2 Visualising DA neurons in the nigrostriatal pathway

In an attempt to identify dopaminergic neurons whilst imaging, slices were incubated with DiD a widely used lipophilic neuronal tracer. It was thought that in addition to observing mitochondrial transport, it was key to highlight intact axonal projections in which mitochondria were moving within. However, it was found that dye penetration required a large time period for incubation, which was not feasible as this meant compromising slice viability. Additionally, when trying to incorporate a dye within dopaminergic neurons via patch clamping techniques, it proved to be largely time consuming. This then compromised slice viability, displayed insufficient, non-uniform dye penetration along axons and was unreliable as the dye would not be incorporated into the neuron even after hours of incubation with it. These factors combined, lead to the decision to not utilise a neuronal dye within these slices, as the time consumption of this, was not representative of live mitochondrial trafficking, where any of these variables may have had adverse/bias effects on mitochondrial dynamics. Taken together, this study confirms that mito-Dendra2 fluorescence provides as a useful tool to identify and image mitochondrial movements within nigrostriatal axons.

This study focussed on establishing a method by which mitochondrial trafficking could be successfully observed in a mammalian model. This method allows significant input into understanding individual mitochondrial movement within the cell bodies, axons and terminals of the nigrostriatal projection. This study provides a novel tool that comprises of an *ex vivo* model that can potentially be manipulated to access the nigrostriatal pathway in all murine PD models. The development of the Dendra2/DAT^{IRES}Cre transgenic mice provides as a useful *in vivo* model to specifically study the role of neuronal mitochondria within nigrostriatal projections.

3.6.3 Observing mitochondrial membrane potential throughput the nigrostriatal pathway

Dysfunctional and aged mitochondria are directed in a retrograde direction for lysosomal degradation via mitophagy in the cell body and healthy mitochondria are directed anterogradely (Saxton and Hollenbeck, 2012). In order to explore this concept further, the cell body and striatum were stained with dyes that fluoresce upon detection of mitochondrial membrane potential.

Healthy mitochondrial membranes maintain a difference in electrical potential across their inner membrane, referred to as the membrane potential. Due to mito-Dendra2 fluorescence at 488nm, the striatum was incubated with Tetramethylrhodamine, methyl ester (TMRM), a 546nm (TRITC) cell-permeant dye, overcoming an overlap in signals. TMRM staining detects active mitochondria with intact membrane potentials, where healthy cells with functioning mitochondria display a bright signal and conversely, upon the loss of the mitochondrial membrane potential, TMRM accumulation ceases where the signal dims or disappears. However, within cell bodies of the SNpc, due to an overlap in the fluorescence brought about by the photo switching experiments in the TRITC channel, recording membrane potential in the SNpc was instead conducted by incubating the slices with MitoTracker Deep Red FM, harbouring an excitation and emission at 644 and 665nm respectively.

3.6.4 Microscopic challenges

All mitochondria were videoed over a period of 10 minutes on an inverted confocal microscope, where initial experiments were undertaken in slices that were 450µm thick slices. It was found that the slices were too thick, and due to the thickness of the sections, axonal projections could only be superficially viewed, where their projections were disrupted due to fluctuations of focusing on the microscope, caused by the ACSF. This obstructed visualising axonal projections and the tracking of mitochondria along the axon, though cell bodies and the striatum could easily be viewed at this thickness. In contrast, slicing the brain into thinner sections risked slice integrity since it may not have remained intact during the imaging process, which is a necessity to observe the direction of mitochondrial motility in this study, and also to retain an intact pathway. Therefore, it was decided that slices would be cut at 350µm, withstanding the possibility of the slice disassembling throughout imaging but also ensuring that mitochondria could be traced and recorded throughout axonal projections.

The usage of confocal microscopy in brain slices permits the high-resolution sub micrometre structural observation of neurons. It allows the accurate tracking of engineered fluorescent proteins within neuronal structures of the brain. Initial experiments in this study were conducted at x40 magnification, where it was found that a large proportion of the mitochondria were bleached after a 10-minute recording, whereby this was drastically decreased at x20 magnification.

3.7 CONCLUSION & FUTURE WORK

This study has designed an *ex vivo* approach to observe mitochondrial trafficking within brain slices, in order to decipher the directionality and parameters of mitochondrial trafficking with dopaminergic neurons of the nigrostriatal pathway. This system has allowed novel insight into directionality of mitochondrial motility within cell bodies of the SNpc and axons. The following chapter will use this technique to observe changes of mitochondrial transport between aged and SNCA mice.

Future work in this study will include:

- Optimising TMRM/MitoTracker staining on these slices in order to gain more information about differences in mitochondrial function with the cell bodies and the synapses
- Photo-switch individual mitochondrial populations within cell bodies of the SNpc and the striatum to observe fusion events within the nigrostriatal pathway (Figure 3.13).

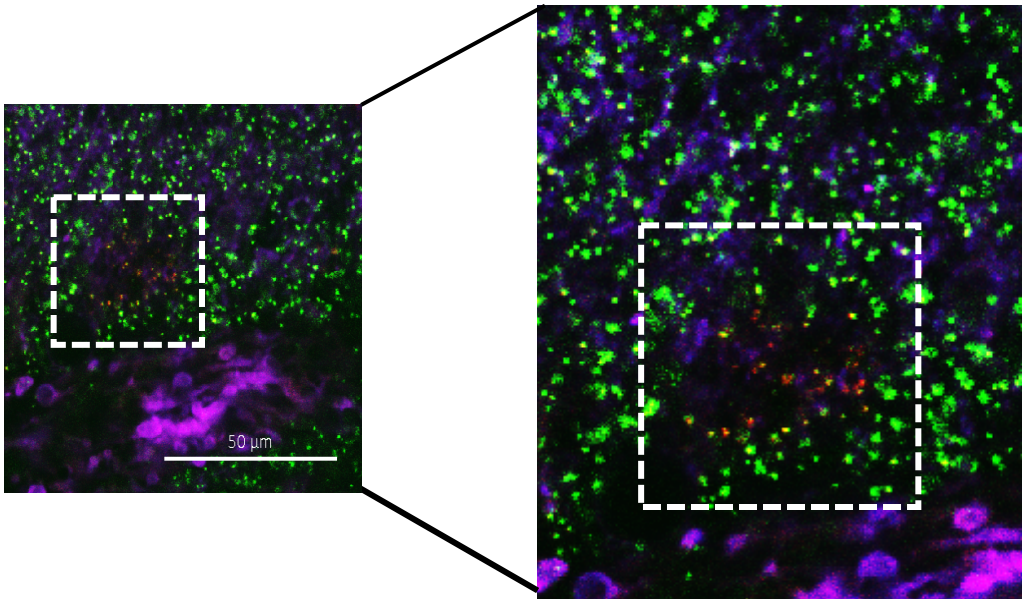

Figure 3.13 Photo-switching mitochondria within striatum. Photo conversion was achieved with **A)** A small population of around 10 mitochondria within the striatum. **B)** Mitochondria were photo converted with a 405 nm laser within the nigrostriatal pathway, causing their emission spectra to convert from a green 488 nm fluorescence to a red fluorescence at 546 nm. All videos were obtained at x20 magnification

CHAPTER FOUR

Ex vivo imaging of mitochondrial trafficking within dopaminergic neurons of the nigrostriatal pathway

4.1 INTRODUCTION

4.1.1 Ageing and mitochondrial trafficking

During ageing, mitochondrial biogenesis, dynamics and turnover by mitophagy are not efficiently maintained, contributing to cellular senescence (Seo *et al.,* 2010).

Dysfunctional mitochondrial dynamics are observed during neurodegeneration in Charcot-Marie-Tooth Neuropathy Type 2A (CMT2A) (Detmer and Chan, 2007), Alzheimer's disease (AD) (Zhu *et al.,* 2013), PD (Spillantini *et al.,* 1998, Kamp *et al.,* 2008) and Huntington's disease (HD) (Wang *et al.,* 2008). For example, β-amyloid (Aβ)-containing plaques trigger mitochondrial damage as well as alterations to mitochondrial structure which contributes to AD pathogenesis, while APP overexpression causes mitochondrial fragmentation, via alterations of mitochondrial fusion and fission proteins in neurons (Wang *et al.,* 2008).

4.1.2 Alpha – synuclein structure and function

The neuropathology of PD is characterised by the presence of Lewy bodies (LBs). These eosinophilic, cytoplasmic inclusions are predominantly composed of aggregated alpha–synuclein (α–syn) protein (Lewy, 1912, Spillantini *et al.,* 1998). SNCA (PARK1 [Chromosome 4q22]) encodes α-syn, and mutations within this gene have been associated with cases of familial PD (Polymeropoulos *et al.,* 1997 , Devoto and Falzone, 2017).

One percent of total neuronal protein is comprised of α–syn, which is densely enriched presynaptically (Iwai *et al.,* 1995). α–syn is widely distributed within neurons, located within the cytosol, nucleus, mitochondria and mitochondria associated membranes (MAMs) (Guardia-Laguarta *et al.,* 2014). α-syn is a 140 amino acid cytosolic protein consisting of three different domains, i) the N-terminal amphipathic domain, ii) the non-amyloidogenic component (NAC) hydrophobic mid-region, and iii) the acidic domain in the carboxyl tail. The N-terminal region consists of six imperfect KTKEGV repeats forming two α-helical structures when the protein interacts with lipids (Ulmer *et al.,* 2005). The middle hydrophobic region of α-syn confers the oligomerisation properties that drive LB formation in PD (Giasson *et al.,* 2001). The negative charges in the C-terminal acidic domain confer chaperone-like properties supporting this oligomerisation process (Li *et al.,* 2005) (Figure 4.1).

α-syn oligomerisation forms fibrils that spread from cell to cell, becoming the predominant driving factor that influences its pathogenic effect (Frost and Diamond, 2010,Winner *et al.,* 2011, Lashuel *et al.,* 2013).

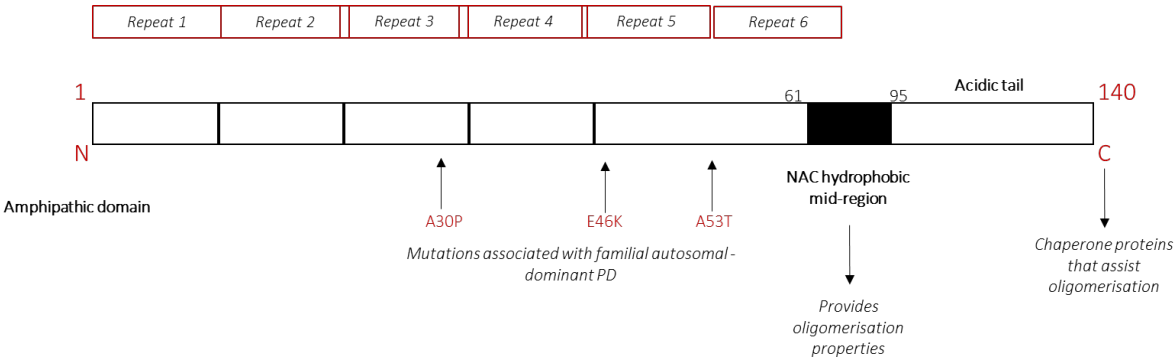

Figure 4.1. Alpha – synuclein structure. A–syn is 140 amino acid cytosolic protein harbouring 3 domains, the N-terminal amphipathic domain, which contains six imperfect repeats (KTKEGV) forming two α-helix structure on lipid interaction, the non-amyloidogenic component (NAC) hydrophobic mid-region, and the acidic domain in the carboxyl tail. The middle hydrophobic region of α-syn provides the oligomerisation properties driving Lewy body formation in PD, supported by the negative charges in the C-terminal acidic domain which hold chaperone-like properties supporting the oligomerisation process (Li *et al.,* 2005). (Figure adapted from Stefanis, 2012)

4.1.3 Alpha – synuclein mutations in Parkinson's disease

α-syn is prone to various post-translational modifications such as ubiquitination, truncation, oxidation, and phosphorylation (Oueslati *et al.,* 2010). Functionally, monomeric α-syn is soluble within the cytoplasm of presynaptic terminals. Here, it may be phosphorylated, causing its accumulation, and formation into insoluble oligomeric or fibrillary aggregates that cannot be processed by quality control pathways. These aggregates can be seen within neurites and/or cell bodies (Giasson *et al.,* 1999). Although the exact mechanism behind the conformational change in α-syn which leads to its accumulation into LBs in sporadic PD is currently unknown, mutations within the gene also change its structure, providing insight into a model for its aggregation and spread. SNCA mutations associated with familial PD often occur within the N-terminal region. Previously described mutations lead to α–syn aggregation and include those leading to the following amino acid changes: A30P, A53T, A53E, E46K, H50Q and G51D (Polymeropoulos *et al.,* 1997, Pasanen *et al.,* 2014).

One of the most common familial PD associated SNCA mutations is A53T, identified in 12 families of Greek, Korean and Swedish origin, which arises from a genomic G51D mutation (Polymeropoulos *et al.* 1997, Athanassiadou *et al.,* 1999, Spira *et al.,* 2001, Klein and Westenburger, 2012). The onset of PD in these patients ranges between 30–50 years, earlier than idiopathic PD which generally occurs over the age of 60 (Pozo Devoto *et al.,* 2017). The A53T mutation disrupts the alpha-helical conformation of the protein (Polymeropoulos *et al.,* 1997) (which aids beta-sheet formation) proceeding onwards to perturb tertiary protein structure.

The A30P α–syn variant was first observed within a German family and arises from a genomic G88C missense mutation (Kruger *et al.,* 1998). Though the A30P mutation is prone to causing self-aggregation at a slower rate than A53T mutated α-syn, it still aggregates faster than wild type human α-syn (Giasson *et al.,* 1999, Conway *et al.,* 2000). The E46K mutation has also been shown to give rise to early onset Parkinsonism (Krüger *et al.,* 2001, Zarranz *et al.,* 2004). SNCA multiplication, another gene variant, was initially identified as a SNCA triplication in a family with autosomal dominant PD. The average disease onset for this mutation was 34 years of age (Singleton *et al.,* 2003). SNCA triplication results in an early onset and more aggressive form of, whereby patients harbouring an α–syn triplication have earlier PD onset in comparison to patients with an α–syn duplication (Fuchs *et al., 2007*).

4.1.4 The effect of alpha- synuclein on mitochondrial bioenergetics

α-syn has been suggested to directly modulate mitochondrial complex I activity, with some researchers suggesting that wild-type, natively unfolded α-syn can be transported inside the mitochondrion, where it inhibits complex I activity (Liu *et al.,* 2009, Luth *et al.,* 2014), possibly through direct association with the protein complex (Devi *et al.,* 2008).

In mice overexpressing α-syn (harbouring the familial A53T mutation) in DAergic neurons, complex I was found to be inhibited (Chinta *et al., 2010*), further illustrating that α-syn has a physiological role in regulating complex I activity (Loeb *et al., 2010*).

Contrastingly, Banerjee and colleagues found that neither WT nor mutant α-syn has any effect on complex I activity (or other respiratory chain complexes), instead finding that WT and mutant forms of α-syn triggered a depolarisation of the mitochondrial membrane potential (Banerjee *et al.,* 2010). Reeve *et al.* (2015) supported these findings showing that α-syn reduces mitochondrial membrane potential, though interestingly not within cells already expressing a complex I deficit (Reeve *et al.,* 2015).

4.1.5 Alpha – synuclein favours curved membranes

The toxic effect of α-syn, particularly within the synapses of dopaminergic neurons, may be driven by its preferential interaction with curved membranes, i.e. those of synaptic vesicles and mitochondria.

α-syn is referred to as a "curvature sensing" protein (Drin *et al.,* 2010, Pranke *et al.,* 2011) as it becomes involved through electrostatic interactions with phospholipid bilayer head groups (Jensen *et al.,* 2011). The reason why α-syn favours curved membranes such as mitochondria, may be due to errors in the packing of protein binding sites of the phospholipid bilayer which results in anexposed hydrophobic acyl chain that forms a binding site (Pranke *et al.,* 2011). As the organisation of these is vital in maintaining membrane polarity, changes in this composition might enhance α-syn binding and thus its damaging effects (Snead and Eliezer, 2014).

4.1.6 The role of alpha – synuclein in mitochondrial trafficking

In vivo, in α-syn expressing zebrafish, it was shown that the movement of axonal mitochondria was reduced within α-syn expressing axons, and within the population of motile mitochondria, there were more retrograde than anterograde movements (O'Donnell *et al.,* 2014).

α-syn overexpression in human-derived neurons has been shown to lead to the development of dysfunctional anterograde and retrograde mitochondrial movements (Pozo Devoto *et al.,* 2017). It is thought that α-syn perturbs mitochondrial movement by interacting with kinesin-1 (Utton *et al.,* 2005) and interrupting mitochondrial associations with microtubules (Prots *et al.,* 2013). Aggregated WT α-syn in Lund Human Mesencephalic cells (LUHMES) was found to reduce kinesin-driven microtubule motility (Prots *et al.,* 2013). The number of active motors interacting with microtubules is regarded as the overall mechanism dominating how organellar transport is controlled (Leidel *et al., 2012*, Fu and Holzbaur, 2014, Lacovich *et al.,* 2017). Therefore, defects in mitochondrial function in PD may be triggered by excessive levels of α-syn or by its abnormal aggregation.

4.1.7 Transgenic alpha – synuclein mouse models

4.1.7.1 Knockout mouse models

The first α-syn knockout mice model showed evidence of reduced striatal DA levels alongside motor phenotypes. Reduced locomotor activity in new open-field surroundings were observed in α-syn null mice, alongside increased locomotor behaviour on amphetamine administration (enhances motor behaviour via increasing DA release), (Abeliovich *et al.,* 2000). Secondly, in individual knockout mice (generated in 2002), these mice were unaffected by both acute and chronic MPTP intoxication (complex I inhibitor), though primary neuronal cultures derived from the same mice displayed sensitivity to rotenone (Dauer *et al., 2002*). The authors concluded that this MPTP resistance may be due to reduced MPP^+ entry via DAT and/or increased storage of MPP^+ within vesicles. Similarly, a third knockout also model also showed some protection against MPTP-induced striatal DAergic loss (Schluter *et al., 2003*) when the α-syn locus was deleted in a subpopulation of C57Bl/6J mice (Specht and Schoepfer, 2001). Of these 3 models, only Abeliovich *et al., (*2000) monitored motor functions and have therefore limited the

understanding of phenotypic alterations in α-syn knockout models. Research by both the Dauer *et al.,* (2002) and Schluter *et al.,* (2003) labs indicate that though MPP^+ inhibits complex I, perhaps in the absence of α-syn, mitochondrial dysfunction in PD can be perhaps be rescued, if not stabilised.

4.1.7.2 Alpha – synuclein over expression mouse models

Mice overexpressing α-syn have been generated, using different promoters to drive transgene expression. All the mice, express WT or mutated forms of the human α-syn protein.

The first human α-syn overexpressing mouse model, expressed α-syn under the control of the platelet-derived growth factor– β (PDGF-β) promoter (Masliah *et al., 2000*). The PDGF-β promoter was chosen as it had been successfully used to drive human α-syn mRNA expression in the brain of several lines of transgenic mice (Games *et al., 1995*). In this experiment, mice were generated with varying levels of transgene, where mice from 'line D' displayed the highest levels of human α-synuclein mRNA and protein (Masliah *et al., 2000*).

The Line D transgenic mice displayed intraneuronal inclusions within synuclein dense regions in the deeper layers of the neocortex, CA3 region of the hippocampus, olfactory bulb and occasionally the SN (Masliah, 2000) (Figure 4.2). Furthermore, within the neurons of the line D mice (2 to 3 months of age) electron-dense deposits were identified associated with the rough ER, indicative of α-syn-ER localisation. TH-positive nerve terminals within the striatum were significantly reduced in line D mice though cell body degeneration was not observed in the SNc. The transgenic mice also had lower striatal TH levels and enzymatic activity suggesting that the accumulation of human α-syn may lead to injury of nerve terminals and synapses in the absence of overt neuronal loss (Masliah *et al., 2000*).

As the loss of DAergic neuronal input to the striatum is associated with PD–related motor impairments (see Chapter 1, section 1.8.6) rotarod tests were conducted at 12 months (Forster *et al., 1999*). Line D mice showed impaired motor performance compared to the low expression and control mice (Masliah *et al., 2000*).

Later, Hashimoto *et al.,* demonstrated a 25–50% reduction in striatal DA within mice of 12 months of age, indicating that functional defects in α-syn expressing mice may be age-dependant (Hashimoto *et al., 2003*). The PDGF transgenic mice also demonstrated α-syn expression within glial cells (Iwai *et al., 1995a,b*), where α-syn has been shown to accumulate in glial cells in dementia with Lewy bodies (DLB) (Takeda *et al.,* 2000, Piao *et al.,* 2000).

The second model generated, expressed A53T α-syn regulated by a murine Thy1 regulatory sequence. Early and dramatic decline of motor function was observed in mice < 3 weeks of age, where a harsher motor phenotype was observed in a male mouse that died at 5 weeks (van der Putten *et al., 2000*). Neuropathologically, α-syn and ubiquitin-positive inclusions were only identified, within the spinal cord during motor neuron degeneration (Sommer *et al., 2000*, van der Putten *et al., 2000*). The overall lack of nigral pathology could possibly be due to insufficient transgene expression within the nigrostriatal pathway.

Mouse lines expressing wild-type or A30P α-syn under the control of the Thy-1 promoter displayed A30P α-syn accumulation in the cerebellum, SNc, neocortex, and brainstem but no motor phenotype (Kahle *et al., 2000*). Mice expressing WT, A30P or A53T α-syn under the control of the rat TH promoter, presented high levels of expression in the SNc but did not display changes in the levels of striatal dopamine regardless of α-syn accumulation within DAergic neurons (Matsuoka *et al.,* 2001). Mice expressing wild-type or α-syn with a double A30P and A53T mutation under the rat TH promoter, demonstrated increased DAergic transporter (DAT) density and increased MPTP vulnerability (Richfield *et al.,* 2002). Reduced DA striatal levels were found in addition to decreased locomotor activity and coordination (Richfield *et al., 2002*). A summary of all available α–syn transgenic mice can be found in Table 4.1.

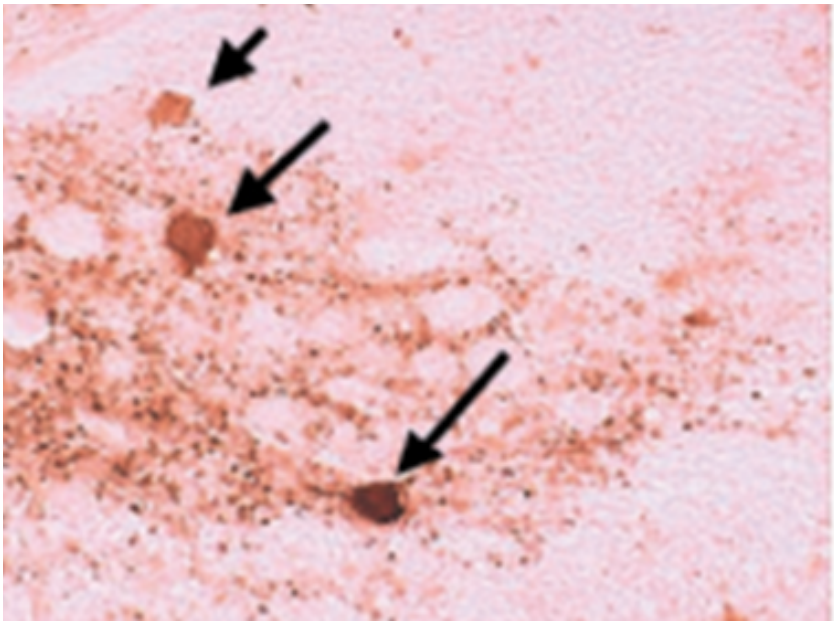

Figure 4.2. Alpha–synuclein neuropathology in human α-synuclein expressing transgenic mice. Human α-syn immunoreactivity (black arrows) observed in the cytoplasm of SNpc neurons in transgenic mice (Figure taken from Masliah *et al.,* 2000)

Table 4.1. Alpha synuclein transgenic mice (Adapted from Fernagut and Chesselet, 2004)

Reference	HUMAN A-SYN	PROMOTER	EXPRESSION LEVEL	NEUROPATHOLOGY	MOTOR PHENOTYPE
Masliah *et al.,* 2000	WT	PDGF-β	10-80% human control	-Reduced striatal TH levels -Reduced DA levels -Reduced TH fibres -PDGF-β expression in glial cells -Motor neuron degeneration	Middle (12 months) age onset Mild reduced rotarod
Van der Putten, 2000	A53T	Murine-thy-1	N/A	-Motor neuron degeneration -Inclusions telencephalon, brainstem, cerebellum, spinal cord, -Ubiquitin inclusions	Early onset, severe (rotarod) –(3-5 weeks)
Kahle *et al.,* 2000	WT, A30P	Murine-thy-1	two fold end α-syn striatum	-Inclusions substantia nigra, striatum, cortex, brainstem	None
Matsuoka *et al.,* 2001	WT, A30P, A53T	Rat TH	Striatum	-Ubiquitin unidentified	N/A
Richfield *et al.,* 2002	WT, A30P + A53T	Rat TH	30-50% of mouse α-syn	-Reduced DAT density -Reduced DA	Middle age onset Reduced locomotor activity and coordination none
Rockenstein *et al.,* 2002	WT, A30P	Murine-thy-1	10 fold human levels	N/A	N/A

4.1.8 Selecting an alpha-synuclein mouse model in which to observe mitochondrial trafficking

To allow the study of the effect of α-syn pathology on mitochondrial movement within the nigrostriatal pathway, it was imperative to select a model that accurately reflected PD associated α-syn pathology.

The above mouse models were all compared to understand which model would be best suited for this study. Of all the models, it was noted that the PDGF-β transgenic mice demonstrated higher, more widespread transgene expression. This is beneficial as transgene expression was reported within neuronal and glial cells in cortical and subcortical brain regions (Rockenstein *et al., 2002*) unlike the Thy-1 promoter. Human α-syn under the control of the PDGF-β promoter also showed α-syn accumulation in synapses of the neocortex, limbic system, and olfactory regions in addition to the generation of inclusion bodies within neurons in the deeper layers of the neocortex. Additionally, Masliah *et al., (*2000) showed that in Line D PDGF-β transgenic mice decreased TH striatal activity and DAergic loss were observed. Motor impairments were also observed at 12 months of age, altogether suggesting that this transgenic mouse model largely represented a PD phenotype and was therefore selected as model to use in this current study to generate human wild type α-syn expressing Dendra2/DATCre mice.

4.2 AIMS OF THIS STUDY

This study involved observing mitochondrial trafficking within i) a control group to observe the effects of ageing on mitochondrial trafficking and ii) and an α-syn expressing cohort,. Using the *ex vivo* slicing method described previously in Chapter 3, this study observed patterns of mitochondrial trafficking within nigrostriatal slices expressing mito-Dendra2. To interrogate these aspects this study fulfilled the following aims,

- To record mitochondrial trafficking in mito-Dendra2 within the DAergic neurons of the nigrostriatal pathway within aged and human α-syn expressing mice (Masliah *et al.,* 2000).
- To quantify directionality of mitochondrial movement through kymograph analyses within nigrostriatal axons of aged and human α-syn expressing mice.

4.3 METHOD & MATERIALS

4.3.1 Identifying mitochondria within dopaminergic neurons

4.3.1.1 Ageing studies

Mito-Dendra2 mice were crossed with a DAT-Cre mouse line obtained from The Jackson Laboratory. Cre expression, regulated by the dopaminergic (DAT) transporter ensured Dendra2 expression was only observed within DA neurons. In Mito-Dendra2 mice, mitochondria are labelled and emit bright green fluorescence at 488nm (Pham *et al.,* 2012). Mice were aged for experiments (Table 4.2).

4.3.1.2 Alpha-synuclein studies

The Mito-Dendra2/DATCre mice were then crossed with human wild type α-syn mice (provided by Dr. Chris Morris, Newcastle University) under the PDGF promoter (Masliah *et al., 2000*) and were aged for experiments (Table 4.2). The initial study design included the analysis of mitochondrial movement in young and aged SNCA mice, however this then had to be altered. Unfortunately, the ageing SNCA mice had to be prematurely culled as a precaution after Mouse Parvovirus was detected by a sentinel animal, within the animal house. Therefore, these mice could not be aged for an equivalent time period as those in the wild-type aged cohort.

4.3.2 Genotyping mice

Genotyping protocol of the Dendra, Cre and α-syn expressing mice is described in Chapter 2, section 2.3.

4.3.3 Mouse dissection

The brains of experimental mice were collected on the day of experiment and all procedures were performed according to the requirements of the UK Animals Scientific Procedures Act (1986). Mouse brains were collected following Schedule 1 cervical dislocation. This study aimed to understand mitochondrial trafficking within old vs young control animals and then in human α-syn over-expressing animals. Table 4.2 describes the genotypes of the mice used within this study. Power calculations were performed as part of the experimental design. To be able to detect a predicted 20-30% reduction in mitochondrial motility, a minimum of 4 animals per cohort were required for experiments. This calculation assumed a standard deviation of 20, with a power of 0.8 and significance level (alpha) of 0.05. Thus, in order to be able to compare mitochondrial movements with sufficient power to detect differences in the data an N=5 was used for each cohort in this study.

Table 4.2. Details of mice used in this experiment

SEX	GENOTYPE	D.O.B	EXPERIMENT	AGE OF MOUSE	STRAIN OF MOUSE
FEMALE	HetCre/HomDendra	24.08.15	Old control	21 months	All mice: C57BL/6 mice
FEMALE	HomCre/HetDendra	06.08.15		21 months	
FEMALE	HetCre/HomDendra	07.11.15		19 months	
FEMALE	HetCre/HomDendra	06.11.15		19 months	
FEMALE	HetCre/HomDendra	06.11.15		19 months	
FEMALE	HomCre/HomDendra	21.09.16	Young (ageing) control	10 months	
MALE	HomCre/Hom Dendra	21.09.16		10 months	
FEMALE	HetCre/HetDend	04.11.16		8 months	
FEMALE	HetCre/HomDend	04.11.16		8 months	
MALE	HetCre/HetDend	04.11.16		8 months	
FEMALE	HomCre/HetDendra/SNCA	04.11.16	Alpha synuclein	10 months	
FEMALE	HomCre/HetDend/ SNCA	04.11.16		10 months	
MALE	HomDendra/HetCre/ SNCA	02.02.17		9 months	
MALE	HomCre/Hom Dendra/ SNCA	02.02.17		9 months	
FEMALE	HetDendra/HetCre/ SNCA	06.03.17		9 months	
FEMALE	HetDendra/ HetCre/ SNCA	14.09.17		7 months	
MALE	HetCre/HetDendra/ SNCA	18.10.17		6 months	
MALE	HetCre/HetDendra/ SNCA	18.10.17		6 months	
MALE	HetCre/HetDendra/ SNCA	18.10.17		6 months	
MALE	HetCre/HetDendra/ SNCA	18.10.17		6 months	

4.3.4 *Ex vivo* imaging of the nigrostriatal pathway

Chapter 3 describes the protocol which was followed for the imaging of the nigrostriatal pathway in this study. The methodology is summarised below.

Once removed, the mouse brain was submerged in cold (4–5°C) sucrose solution, then sliced to obtain to obtain the nigrostriatal pathway and mounted onto the vibratome to generate 300µm thick sections. Slices were then transferred into holding chamber containing artificial cerebrospinal fluid (ACSF), maintained at room temperature between ACSF and warm, moist carbogen gas (95% O_2/5% CO_2). Slices were allowed to equilibrate on the holding chamber for 30 minutes. An ACSF perfusion system was created on the Inverted confocal system throughout the entire imaging session. Nigrostriatal slice movement within ACSF solution was stabilised with a slice anchor (Warner Instruments) and maintained at 37°C. All videos were taken at 1 frame/second for 10 minutes.

4.3.5 Imaging mitochondria in the nigrostriatal pathway

Mito-Dendra2 positive fluorescent mitochondria were imaged in the axons of the nigrostriatal pathway, using a 488 nm laser. Mitochondrial movements were observed via videos captured at 1 frames/second for 10 minutes at x20 magnification. Around 3-10 axons were analysed per video.

4.3.6 Nigrostriatal axonal kymographs

Kymograph analyses was conducted to analyse mitochondrial movement within nigrostriatal axons, methods for which are described in Chapter 3. For this thesis mitochondrial movements was classified into 'stationary' and 'moving'.

4.3.7 Justification of statistical analyses of *ex vivo* mitochondrial movement

A mixed-effect regression model was undertaken by Dr Alasdair Blain (Wellcome Centre for Mitochondrial Research) to model the effect of ageing/α–syn on mitochondrial speed and distance whilst accounting for any variation between mice by including them as a random effect within the model. The data was decided to be plotted as logged values for visual aid only, due to the range in mitochondrial movement. Given the outliers found in the data, logging values would distort the normal data plots. All data is presented as box and whisker plots that show the distribution of mitochondrial speed and distance values for moving mitochondria for all individual mice, in control and α–syn mice. Raw values for both parameters were logged after defining a moving mitochondrion

as travelling above 0.005 μm/s and further than 0.01 μm/s. Calculating a linear regression for these experiments does not account for variation between the mice in each group. Therefore, a mixed-effect model was applied to understand significant differences between mice groups. Table 4.3 is an exemplar mixed model effects statistical table which assays mitochondrial movement in all mice versus α–syn mice.

	AIC	BIC	logLik		
	12816.97	12840.55	-6404.487		
	Value	Standard error	DF	t-value	P-Value
Intercept	2.1440779	0.3711952	2672	5.776146	0e+00
Alpha synuclein	-0.4059548	0.1052442	2672	-3.857266	1e-04

Number of Observations: **2683**

Number of Groups: **10**

Akaike Information Criterion (AIC) (yellow highlight) is used to compare model performance with a lower AIC value for the mixed-effect model (from 13023 for a linear regression model to 12817 for the mixed model) indicating an improved model fit.

The *Bayesian information criterion* (BIC) allows model selection between more than two models. During model selection, the goodness of fit will indicate how well it fits a given set of data. For this, the BIC value is calculated for each model where the lower the BIC value, the better the fit. During the process of fitting these models, AIC and BIC are utilised to ensure that 'overfitting' (a model containing more parameters that what the data can justify) does not occur via a penalty term for the number of parameters in the model. This BIC value must be greater than the AIC value.

The maximum likelihood function allows the estimation of how within a statistical model the observed data is most likely to occur. This is easier to conduct via the negative of the natural logarithm of the likelihood function, *Loglik.* Here, maximising the likelihood is converted to finding the minimised negative log-likelihood value, where smaller values of the negative log-likelihood signify a better fit. Lastly, the degrees of freedom (DF) indicate that when fitting a model's DF, it caters for data that is overfit.

4.4 RESULTS

4.4.1 Generating kymographs in nigrostriatal slices

To observe the movements of Mito-Dendra2 labelled mitochondria, time lapse imaging was conducted at (1 frame/second) on DAergic neurons of the nigrostriatal pathway within *ex vivo* brain slices. Since this is the first time that mitochondrial movements have been recorded within nigrostriatal slices, it was important to ensure that the videos taken generated representative kymographs when analysed. To further ensure that kymograph analysis accurately measured mitochondrial movements within the experimental setup steps were taken to ensure that false 'movements' from background pixels or slice drift were removed.

Kymographs were generated for the duration of each of the 10-minute videos, thus providing a measure of speed for each individual mitochondrion, within single nigrostriatal axons (Figure 4.3). Figure 4.3B and 4.3C show representative kymographs generated from a nigrostriatal slice. While the kymographs were able to track the movements of individual mitochondria, no large movements in either direction were observed, instead it was found that the mitochondria exhibited an 'arrested' movement state (remaining stationary throughout live imaging) (Chen *et al.,* 2016).

To ensure that background was not being detected in these videos, and that accurate tracking of mitochondria within axons was achieved, areas without the mito-Dendra2 fluorescence were also measured to be sure that nonspecific kymographs based on 'background noise' pixels, were not created (Figure 4.3D). As slices within the glass bottom dish are retained in ACSF, drifting may occur throughout the video, whereby the slice may drift away from the region of its origin (though this is minimised by the use of the slice anchor), therefore kymographs were also generated for these videos. Kymographs based on these videos were then used to ensure that experimental data was only collected from videos with no drift. From this analysis, videos that exhibited nigrostriatal drifting were excluded due to incorrect kymograph generation (Figure 4.3E).

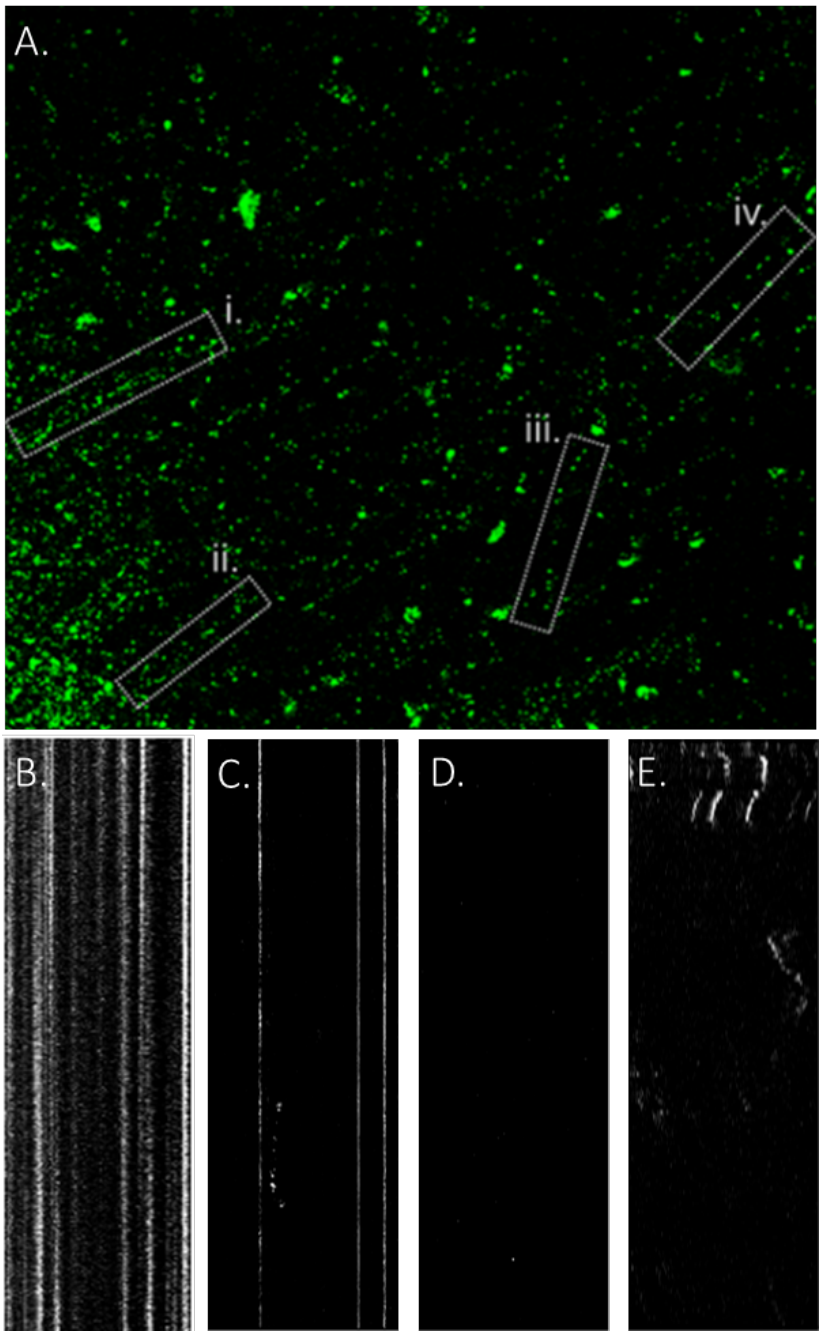

Figure 4.3. Kymograph creation within nigrostriatal slices. The kymographs were measured within videos which were obtained at 1 frame/second over 10 minutes. **A)** Videos generated from highlighted regions (white boxes i-iv) in videos. **B-C)** Kymographs demonstrate mostly stationary mitochondria within nigrostriatal axons. **D)** No kymograph is generated within a region of the video that does not contain mito-Dendra2 fluorescence. **E)** Kymograph generated from video that demonstrates nigrostriatal slice drifting which were excluded from these experiments.

4.4.2 Effect of ageing on mitochondrial movement with nigrostriatal slices

The primary risk factor for PD is advancing age (Collier *et al.,* 2012). The impairment of mitochondrial movement in neurons with advancing age might impact not only neuronal function but also survival. Thus, in order to understand the effect of ageing on mitochondrial motility, mitochondrial movements within the nigrostriatal pathway were recorded and analysed and compared between young (8-10 months) and old (19-21 months) wild-type mice (Table 4.2) (Figure 4.4).

Using kymograph analysis, the movements of 2120 mitochondria from 10 mice were characterised, where most mitochondrial movements within dopaminergic neurons of *ex vivo* slices occurred at speeds between 0 – 0.005µm/s. Based on previous experiments (Misgeld *et al.,* 2007, Ohno *et al.,* 2011, Takihara *et al.,* 2015), mitochondria with speeds below 0.005µm/s were defined as 'stationary', while any which moved with a speed greater than this were described as 'moving' (Figure 4.5).

In young mice, 14.82% of the total mitochondrial population were classed as moving and exhibited a mean speed of 0.008 µm/s (mean of moving mitochondria only), while in old mice 23.15% of nigrostriatal mitochondria were defined as moving with mean speed of 0.042 µm/s. The average speed of moving mitochondria did not significantly differ between young and old mice (p=0.15). Furthermore, the mean distance travelled of moving mitochondria in young mice was 1.906 µm, (with a standard deviation of 2.109) versus 1.901 µm (standard deviation 3.232) in old mice, with no significant changes were detected between young and old nigrostriatal slices by mixed effect statistical modelling (Figure 4.4 and 4.5).

The range of mitochondrial speed for the aged wild type mice ranged from 0 - 0.251 µm/s. indicative of large variation of mitochondrial speed within the moving mitochondrial population, which could be due to i) young cohort mice 1, 3 and 5 demonstrating higher speeds or ii(old cohort - old mouse number 5, which shows increased speed compared to the remaining 4 mice. Large intra-animal variability was observed within this experiment and was expected due to the nature of *ex vivo* experiments (See Chapter 3), this variability was taken into consideration for all statistical modelling.

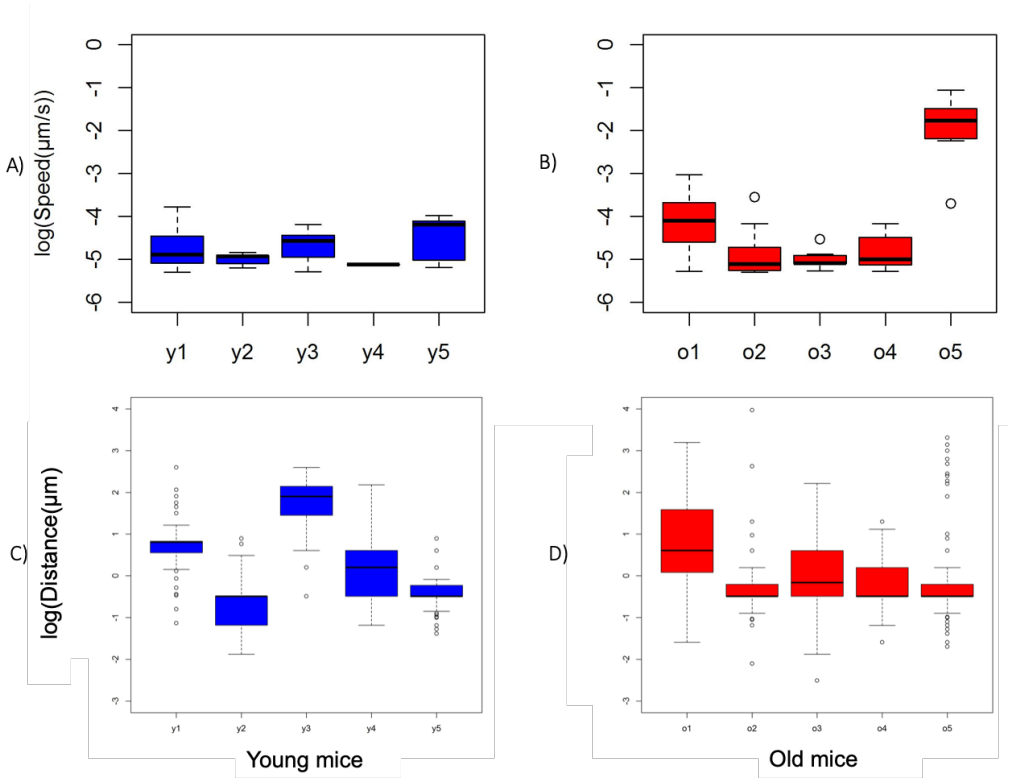

Figure 4.4. Box and whisker distribution plot of the speed and distance travelled of mitochondria in young vs old mice. Values are logged to aid visualisation. **A)** Speed of moving mitochondrial movement for young mice. 14.82% of these mitochondria were classed as moving and exhibited a mean speed of 0.008 µm/s. **B)** Speed of moving mitochondrial movement for old mice. 23.15% of these mitochondria were classed as moving and exhibit a mean speed of 0.042 µm/s. **C)** Mean distance travelled of moving mitochondria in young mice = 1.906 µm, SD 2.109 versus. **D)** Mean distance travelled of moving mitochondria in old mice = 1.90 µm, SD 3.232. Mixed effect statistics model shows no significant changes in the mitochondrial speed or distance travelled between young and old nigrostriatal slices.

A)

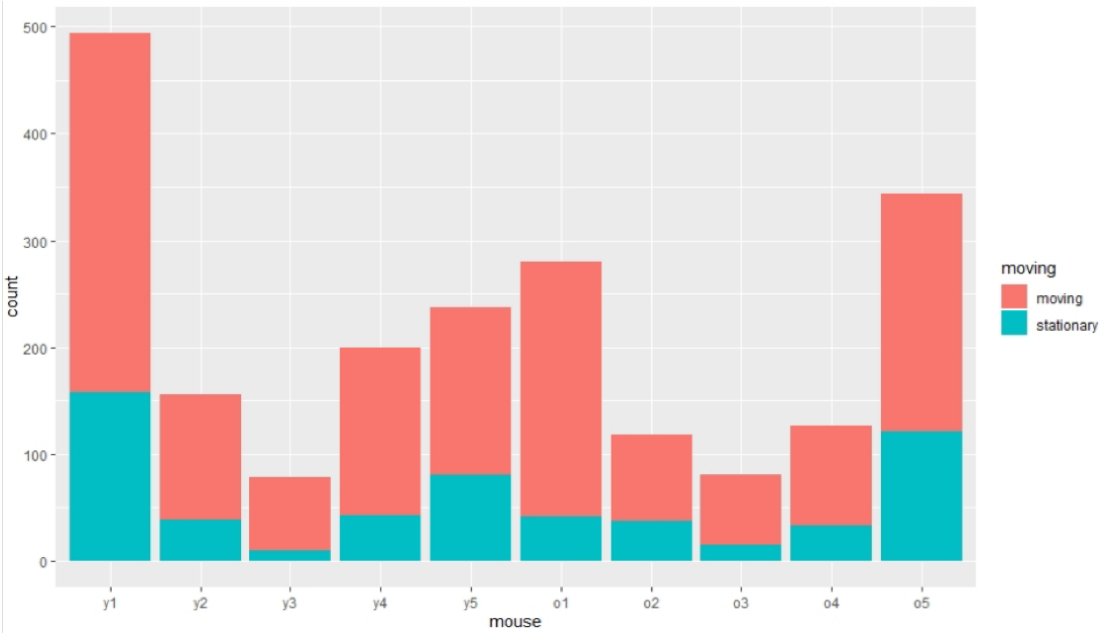

B)

Speed of mitochondrial movement (Ageing study)

Mouse	N	Moving	Mean	Stationary
Young 1	494	142	0.0095	352
Young 2	157	11	0.0069	146
Young 3	78	12	0.01	66
Young 4	201	1	0.006	200
Young 5	237	7	0.012	230
Old 1	278	146	0.018	132
Old 2	118	20	0.0084	98
Old 3	81	11	0.0068	70
Old 4	127	30	0.0083	97
Old 5	343	12	0.17	331

Figure 4.5. Proportion of mitochondrial movements in young vs old mice. A) Statistics table for each mouse (2-3 slices) used in this study comparing: number of mitochondria (N) observed within each experiment, number of moving mitochondria of the total mitochondria and their mean speed, and lastly the number of stationary mitochondria. **B)** Proportion of mitochondria that are moving versus stationary within individual young and old aged mice.

4.4.3 Effect of alpha-synuclein on mitochondrial movement with nigrostriatal slices

The characteristic pathological hallmark of PD is the presence of Lewy bodies (Spillantini *et al.,* 1998). Previous research has suggested that α–syn may interact with mitochondria and disrupt their movements (Prots et al., 2013). Thus, having characterised mitochondrial movement in aged nigrostriatal slices it was important to explore the effects of PD pathology on mitochondrial movement within these slices.

Following the ageing study, mitochondrial movements were characterised in nigrostriatal *ex vivo* brain slices from α–syn over-expressing animals (aged 6-10 months). The speed of 2117 individual mitochondria were measured in ten experimental animals, again the observation was made that the majority of mitochondria were stationary (88.6%), with only 11.40% of the total mitochondrial population classified as moving (4.6).

A)

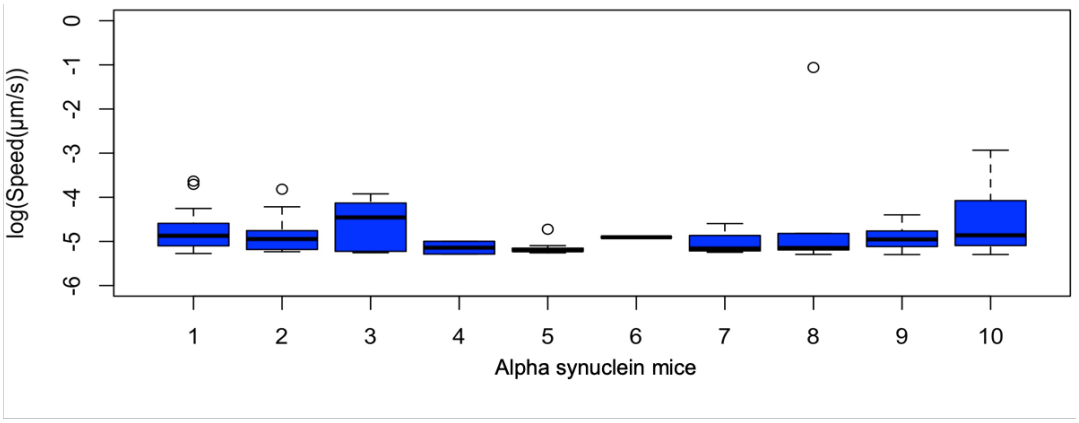

B)

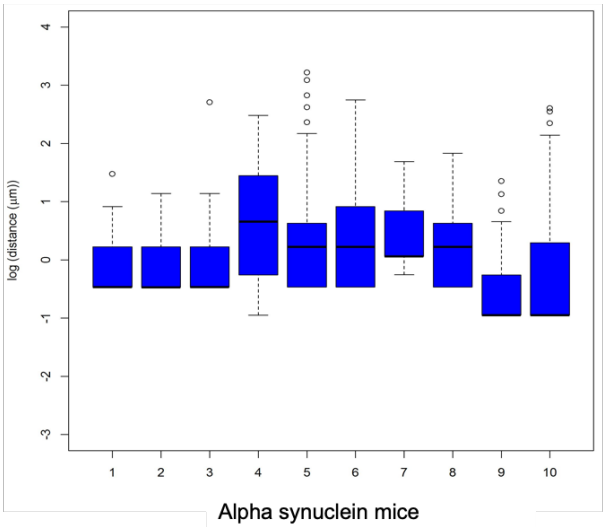

C)

Mouse	N	Moving	Mean Speed	Stationary
1	184	57	0.0089	127
2	142	28	0.008	114
3	144	8	0.011	136
4	196	2	0.0059	194
5	176	9	0.0059	167
6	300	1	0.0074	299
7	182	4	0.0067	178
8	261	5	0.074	256
9	279	75	0.0074	204
10	250	52	0.013	198

D)

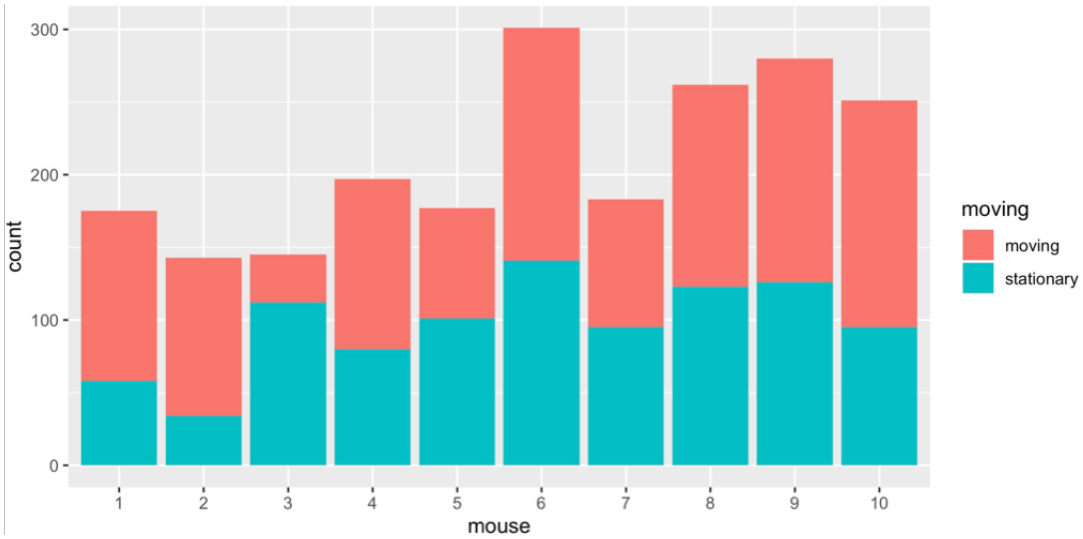

Figure 4.6. Box and whisker distribution plot of the speed and distance of mitochondrial movement in alpha synuclein mice. Values are logged to aid visualisation **A)** Speed of moving mitochondria for α–syn mice. 11.40% of these mitochondria were classed as moving and exhibited a mean speed of 0.015 µm/s. **B)** Mean distance travelled of moving mitochondria of α–syn mice = 1.593, SD 2.041. Mixed effect statistics model shows no significant changes in the mitochondrial speed or distance travelled within α–syn mice. **C)** Statistics table for each mouse used in this study comparing: number of mitochondria (N) observed within each experiment, number of moving mitochondria of the total mitochondria and their mean speed, and lastly the number of stationary mitochondria **C)** Proportion of mitochondria that are moving versus stationary within individual α–syn mice.

4.4.4 The effects of ageing and PD pathology on mitochondrial movement

Having characterised mitochondrial movements in both cohorts of mice, the final aim of this study was to understand how mitochondrial movement was affected by the involvement of two PD risk factors i) ageing and ii) alpha synuclein.

Having compared the effect of ageing on wild type mice and having characterised mitochondrial movements in α–syn mice, it was important to compare both groups of mice to understand how these important PD related changes impact mitochondrial movement.

4.4.4.1 Mitochondrial distance travelled

When the distance travelled by mitochondria was compared between all wild-type (young and old), and α–syn expressing mice, no significant changes were observed. Though it appears that the expression of human α–syn compromises the distance covered by mitochondria when compared to only the aged mice (reducing mitochondrial movements by approximately 0.5 μm), though these changes were not significant (Figure 4.7).

4.4.4.2 Mitochondrial speed

When the speed of moving mitochondria was compared, it was found that the number of moving mitochondria was higher in young mice 14.82% versus age-matched α–syn mice (11.40%). Moving mitochondria were observed in both groups of mice although the mean speed in young wild-type mice was lower (0.008 μm/s) than in age-matched α–syn mice (0.015 μm/s), however neither of these changes were significant (Figure 4.8).

When comparing the number of moving mitochondria in old wild-type mice (23.15%) versus α–syn mice (11.40%). Fewer mitochondria were found to be motile in α–syn mice and those which did move displayed a decreased mean speed (0.015 μm/s) compared to the aged wild-type mice. Although these differences were significant ($p<0.0001$: mixed effects model testing), these mice were not age-matched and therefore experiments must be repeated with aged-matched α–syn mice to draw firm conclusions (Figure 4.8).

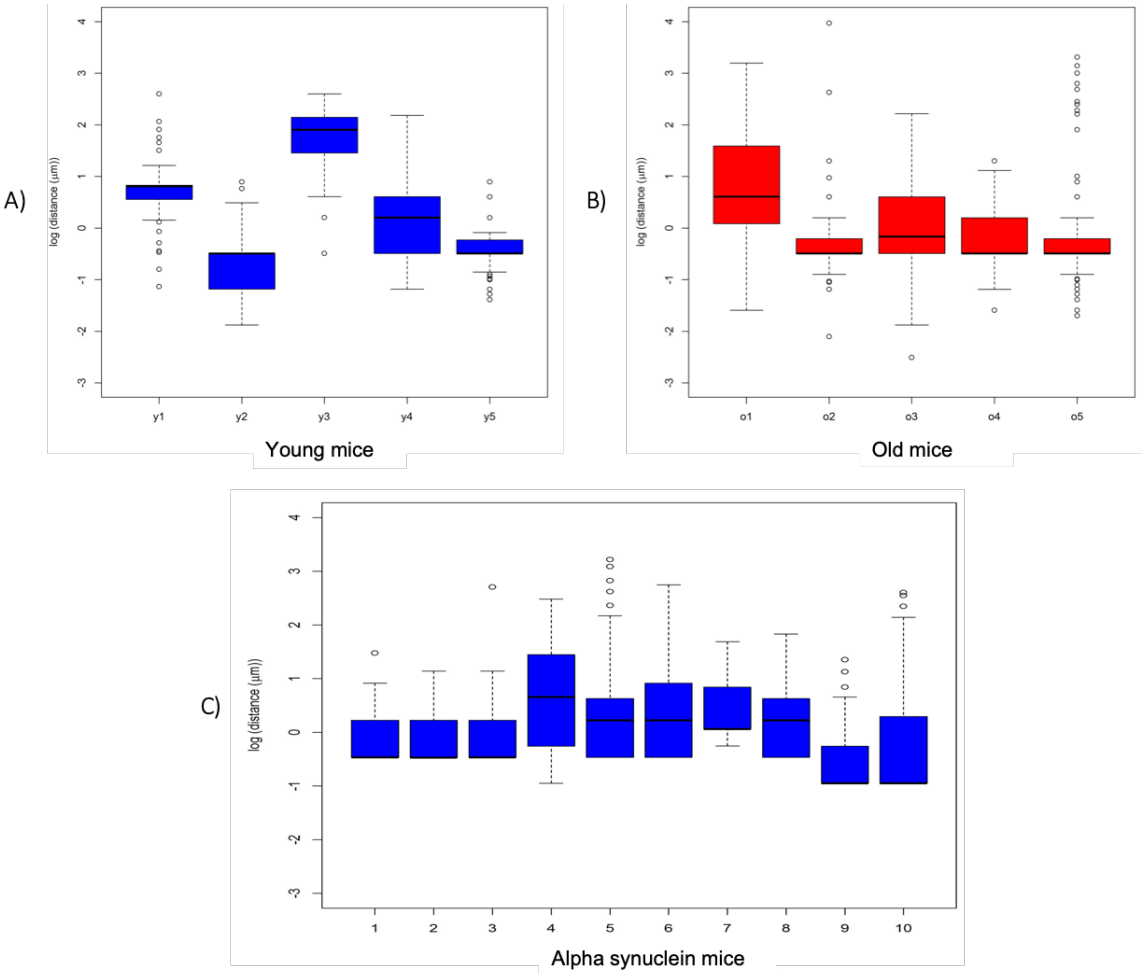

D) Mixed model statistics for mitochondrial distance travelled in aged versus alpha synuclein mice

	AIC	BIC	LogLik		
	5960.921	5984.496	-2976.46		
	Value	Standard error	DF	T-value	P-value
Intercept	0.15896852	0.1807722	2663	0.8793856	0.3793
Alpha synuclein mice	-0.09034038	0.2558644	18	-0.3530791	0.7281
Number of observations	2683				
Number of groups	20				

Figure 4.7. Box and whisker distribution plot of the distance travelled of mitochondria in aged and alpha synuclein mice. Values are logged to aid visualisation. **A)** Mean distance travelled of moving mitochondria in young mice = 1.906 μm, SD 2.109 versus **B)** Mean distance travelled of moving mitochondria in old mice = 1.90 μm, SD 3.232. No significant changes were observed between how far mitochondria move in young and old mice. Mean distance travelled for all aged mice = 2.137 μm, SD 3.162 **C)** Mean distance travelled of moving mitochondria of α–syn mice = 1.593, SD 2.041. **D)** Mixed model table shows intercept that represents the aged mice and indicates that mitochondria in α–syn mice move less (-0.09) than in aged mice, though these changes were not significant.

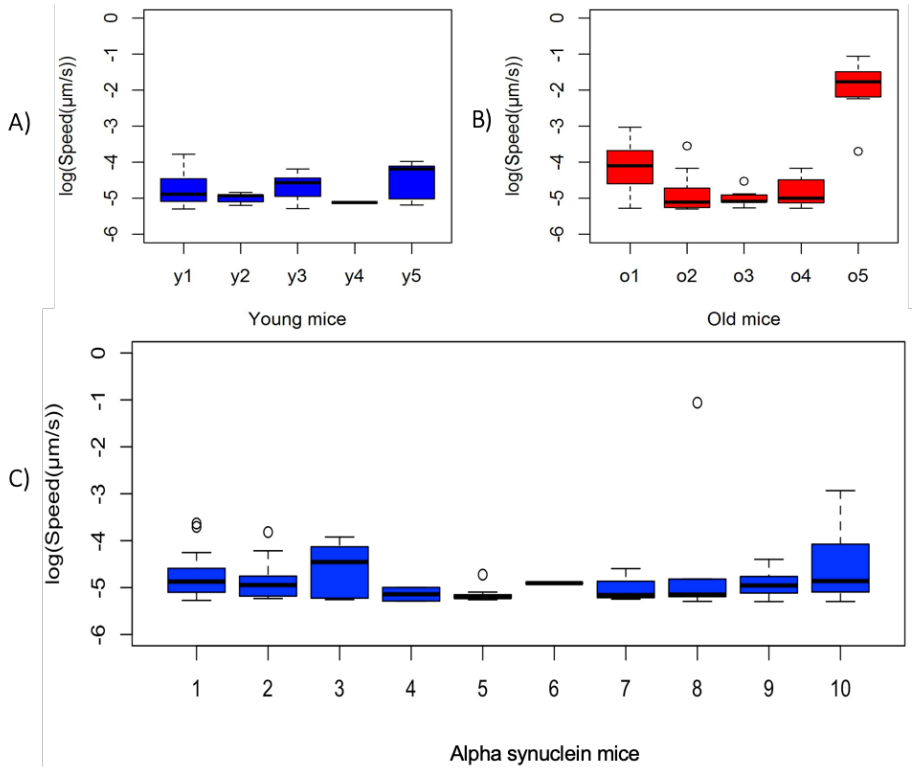

D) Mixed model statistics for speed of mitochondrial movement in aged versus alpha synuclein mice

	AIC	BIC	LogLik		
	12816.97	12840.55	-6404.487		
	Value	Standard error	DF	T-value	P-value
Intercept	2.1440779	0.3711952	2672	5.776146	0e+00
Alpha synuclein mice	-0.4059548	0.1052442	2672	-3.857266	1e-04
Number of observations	2683				
Number of groups	20				

Figure 4.8. Box and whisker distribution plot of the speed of mitochondrial movement in aged and alpha synuclein mice. Values are logged to aid visualisation. **A)** Speed of moving mitochondrial movement for young mice. 14.82% of these mitochondria were classed as moving and exhibited a mean speed of 0.008µm/s. **B)** Speed of moving mitochondrial movement for old mice. 23.15% of these mitochondria were classed as moving and exhibit a mean speed of 0.042 µm/s. **C)** Speed of moving mitochondria for α–syn mice. 11.40% of these mitochondria were classed as moving and exhibited a mean speed of 0.015 µm/s. A mixed effect statistic model was carried out to show significant changes in the speed of moving mitochondria in old aged mice versus α–syn mice ($p<0.0001$). **D)** The model intercept represents the aged mice. The results of the mixed-effect model suggest that α–syn mice move significantly less (-0.41) than aged mice.

4.5 DISCUSSION

4.5.1 Summary of results

- Considerable variation exists in mitochondrial movements between individual mice
- No differences were observed in mitochondrial movements in young versus old aged mice within nigrostriatal axons
- Mitochondria within mice overexpressing human wild-type alpha-synuclein are not significantly different to age matched wild-type mice (young) in terms of their movements.
- Young alpha-synuclein mice are significantly different from old wild-type mice, highlighting the need for further studies with appropriately aged alpha-synuclein mice.

4.5.2 Variability in mitochondrial movement observed between mice in this study

It must be understand that due to the nature of ex vivo experiments and also the pattern of mitochondrial movement; large variability in movement is observed both within mice and between mice. Instances of the latter were observed in the movement of mitochondria in young and old mice. For example, within the ageing experiment in the young cohort, the mitochondrial speeds of mouse 1 and 3 were very different in comparison to mice 2,4 and 5. Similarly, in the old cohort, old mouse 5 demonstrated different results in comparison to the remaining 4 mice, suggesting variability in mitochondrial movement between the mice. These differences will have an effect on the results of this chapter.

4.5.3 Understanding mitochondrial motility in *ex vivo* nigrostriatal axons

Various previous studies have provided insight into the movement of mitochondria within DAergic neurons (PI *et al.,* 2014, Fang *et al.,* 2016, Dukes *et al.,* 2017), however this is the first study to provide information regarding mitochondrial trafficking within mammalian DAergic neurons within nigrostriatal slices. Individual DAergic nigrostriatal axons were imaged to observe and quantify mitochondrial movements and how these altered with ageing and in a PD model. Results from these experiments demonstrated that within both young and old mice, most mitochondria were stationary within nigrostriatal axons.

Several studies have observed live mitochondrial movement in the peripheral and central nervous system (CNS). These studies have documented only the details of the percentage of stationary mitochondria, where investigation into other attributes such as mitochondrial speed and distance have only been briefly described (Table 4.3). Only one *in vivo* study has analysed mitochondrial movements in the CNS, and described 93% of mitochondria as being stationary within cortical neurons of mice (Lewis *et al.,* 2016), the speed and distance travelled of these mitochondria were not documented. A further three studies that were conducted in CNS rat and mouse explants showed that 60-100% of mitochondria remained stationary within hippocampal and retinal ganglion cells respectively (Jackson et al., 2014, Faits *et al.* ,2016). The mean speed of moving mitochondria was 0.132 ± 0.067µm/s (n = 66 mitochondria) and the Jackson *et al.,* (2014) study showed that over 15 minutes the average mitochondria speed was 0.15µm/s, with a maximum distance travelled of 5µm. Mitochondria are known to be held at discrete sites within neurons to provide localised ATP for a number of processes and protein interactions, this is particularly important for synaptic transmission and maintenance of ionic gradients within the axon. Thus, it makes sense that the majority of the mitochondrial population within these neurons would be stationary (Morris and Hollenbeck, 1993, Miller and Sheetz, 2004, Hollenbeck and Saxton, 2006). (Also see Table 4.4 for references for *in vivo* mitochondrial movement in mouse models).

Several factors affect mitochondrial localisation within neurons, some of which include the size of the neurons, neuronal metabolic activity and ageing. Interestingly, the size of stationary sites and the speed of mitochondrial transport are significantly increased following demyelination of axons (Kiryu-Seo *et al.,* 2010), which may play an important role within the poorly myelinated DA neurons of the nigrostriatal pathway (Braak *et al.,* 2004). Extended neuronal processes in the periphery present a challenge, in terms of mitochondrial distribution to the required sites, particularly since an inability to preserve mitochondrial dynamics within neurons can have detrimental effects on neuronal function and physiology (Schon and Przedborski, 2011). In this case, it is vital for neurons to sustain mitochondrial networks that are reliable and are capable of providing ATP to distant synapses, whilst adapting to changes in energy demand.

The study described here, attempted to provide information into how mitochondria move within CNS DAergic neurons via *ex vivo* imaging. This experiment was the first in which imaging within 'live' murine nigrostriatal DAergic neurons had been attempted, to investigate

mitochondrial dynamics in PD. This experiment revealed that in young, old and α–syn mice (aged 6-21 months) around 76 -100% of mitochondria remain stationary, with the mean speed of this movement ranging between 0.008 – 0.042 μm/s, though this speed is lower than what is described in the literature for over 10 minutes of imaging. The variations between these results and previously published data, may depend on several aspects of the experiment, including the length of the axon measured, number of frames taken during the video and the length of the video. Frame rate have shown to vary across *in vivo* studies i.e in the Faits and Jackson study the frame rate ranges from 0.6 to 6 frames per second. This study carried out imaging for 10 minutes and obtained videos mostly at 1 frame per second. In any slice study variability is bound to occur due the nature of the slice and maintaining its viability throughout imaging. Though differences in movement parameters were observed, together this data suggests that that neuronal mitochondria remain mostly stationary *in vivo*, which supports current literature observations (Jackson *et al.,* 2014, Faits *et al. ,*2016, Lewis *et al.,* 2016).

Mitochondria that appeared to be stationary in this study (at least for the duration of what can be successfully imaged), were thought to perhaps be refreshed *in situ* by exchanging proteins with the motile fraction. Mitochondrial fission and fusion events (Chapter 1, section 1.5.1 and 1.5.2) are often observed in axons and dendrites allowing the exchange of materials between mitochondria (Amiri and Hollenbeck, 2008), where even brief moments of contact can involve fusion and the exchange of proteins in each compartment of the mitochondrion, which is also evident in non-neuronal cells (Liu et al. 2009). Consequently, due to these factors that go some way to explain the sporadic behaviour of mitochondria, developing a system by which *in vivo* mitochondrial trafficking can be captured in an accurate, representative, high-resolution manner, has provided to be one of the biggest challenges in understanding mitochondrial dynamics *in vivo* over the last 15 years.

Table 4.3. *In vivo* imaging of neuronal mitochondria in mouse models (Adapted from Lewis *et al.,* 2018)

Authors	PNS/CNS	Neurons	Age	Anesthesia	Length of imaging (minutes)	% Stationary mitochondria
Misgeld et al., 2007	PNS	Sciatic Nerve	N/A	Yes	5	~ 87%
Misgeld et al., 2007 (Mouse explant)	PNS	Sciatic Nerve	N/A	N/A	5	87 ± 1%
Sajic et al., 2013	PNS	Saphenous nerve	8-12 weeks	Yes	N/A	N/A
Sorbata et al., 2014	PNS	Spinal cord	6-12 weeks	Yes	5-15	93 ± 6%
Takihara et al., 2015	CNS	Retinal ganglion cells	2-25 months	Yes	N/A	N/A
Lewis et al., 2018	CNS	Cortical L2/3	P30/45	No	10—20	93 ± 4.5%
This study	CNS	Nigrostriatal dopaminergic neurons	6-21 months	No	10	Over 76%

4.5.4 Ageing does not impact mitochondrial movements within dopaminergic neurons of wild-type mice

Though more mitochondrial movement was observed in old mice nigrostriatal axons compared to young mice, no significant changes were observed in their mitochondrial speed and distance (Figures 4.6 and 4.8).

There are a few possibilities for this occurrence that could be down experimental setup. This experiment observed mitochondrial movement in young and old mice, whereby firstly, the ages of these mice were not all exactly the same i.e. not all mice were from a specific age and instead were taken from a range of ages young mice (8-10 months) and old mice (19-21 months). Secondly, these mice were all of mixed genders i.e young mice used were both male and female and old mice used were all female. Though not investigated the above two factors might affect mitochondrial movement. Thirdly, perhaps the sample size of N=5 was not enough to gauge an accurate indication to mitochondrial movement defects with ageing and lastly , maybe the mice were in fact healthy and therefore did not display any specific ageing phenotypes, (alterations in mtDNA, motor impairment etc) though these were not measured, to instigate any alterations in mitochondrial movement.

Biologically, it may be that there exists is a compensatory method allowing efficient mitochondrial transport to occur during ageing. Mitochondrial dysfunction occurs within human nigrostriatal neurons with normal ageing. Defective OXPHOS arises as a consequence

of this, which may increase ROS production (Zhang *et al.,* 2010, Suramaniam and Chesselet , 2014). Oxidative stress has been previously shown to cause decreased mitochondrial transport both *in vitro* and *in vivo* following paraquat treatment (Liao *et al.,* 2017). Perhaps in this study, oxidative stress can lead to or be a consequence of mitochondrial dysfunction. It may be that a mechanism exists by which ageing mitochondrial transport defects are regulated within nigrostriatal axons.

Direct fibroblast-to-induced neuron (iN) converted cells have been recently manipulated as an ageing model (Kim *et al.,* 2019). This model has demonstrated that iNs from older donors show evidence of reduced OXPHOS gene expression, reduced mitochondrial density, increased mitochondrial fragmentation and reduced mitochondrial coverage (Kim *et al.,* 2019). Thus, it is important that future investigations of mitochondrial function and morphology within the aged and alpha synuclein mice should focus on whether mitochondrial volume and size affects how far mitochondria move. For example, by calculating the mitochondrial sphericity and branching via aspect ratio and form factor analyses, it will add valuable insight into whether it is the small or larger mitochondria that are being moved and whether harbouring an oxidative defect impacts these movements and their mitochondrial distribution.

4.5.5 Alpha-synuclein reduces mitochondrial movement in nigrostriatal axons

This study revealed that between the aged-matched mice number of moving mitochondria was higher, at a lower mean speed in young wild type mice when compared to the age-matched α–syn mice, though these changes were not significant.

Following this, the effects of ageing and α–syn on mitochondrial movement were analysed. This study demonstrated a significant decrease in mitochondrial speed between aged wild-type and α–syn overexpressing mice ($p<0.0001$), with a corresponding decrease in the proportion of moving mitochondria within α–syn mice when compared to aged wild-type mice cohort. However, to validate these findings, experiments will need to be repeated with aged-matched α–syn mice to confirm this.

A recently, well explored hypothesis is that α–syn mediates changes in mitochondrial transport. The mitochondrial transport machinery comprising the Miro/Milton/KHC motor adaptor complex is an intricate system shared amongst animal cells (Schwarz, 2013). Recently, several

roles for α–syn in this pathway have also been identified. Utton *et al., (*2005) revealed through co-immunoprecipitation studies that α–syn interacts with kinesin-1 (Utton *et al.,* 2005). Also, when α-syn oligomerises it has been shown to interrupt kinesin-1 motor interactions with microtubules (Prots *et al., 2013*). As motor association with microtubules regulates mitochondrial movement (Lacovich *et al., 2017*), in the presence of α-syn oligomers, microtubule velocity was decreases across kinesin-coated surfaces (Prots *et al., 2013*). Therefore, if α–syn is overexpressed it may cause the dissociation of the kinesins from their microtubules decreasing their trafficking properties and thus reducing mitochondrial movement parameters (Figure 4.9).

Furthermore, Parkinson's disease-linked α-syn variants have shown to induce tubulin aggregation as opposed to microtubule polymerisation, indicating that α–syn may be a novel, foldable, microtubule-dynamase, affecting the organisation of the microtubule network and thus inhabiting microtubule based mitochondrial transport (Cartelli *et al., 2016*).

Maybe these findings suggest mitochondrial transport defects in PD occur with α–syn pathology, but to consolidate these results i) experiments must be repeated in aged-matched α–syn overexpressing animals and ii) SNCA levels need to be measured in these mice both basally and when over expressing to observe whether wild type SNCA does actually effect mitochondrial movement.

4.5.6 Statistical analyses and graphical representation

Over the course of this study, several statistical tests and various graphical manipulations were conducted to ensure that data was being presented in the most accurate manner. During this optimisation several methods were used to firstly quantify mitochondrial movement, which were followed by the data being shown as various graphs. As thresholds for the speed and distance of moving and stationary mitochondria were set , it was observed that these data values displayed a very large spread. To ensure that visually this could be depicted in the most representative manner, the values were logged and displayed as box and whisker plots . As this was a suitable method to demonstrate the results, having perhaps a frequency histogram for these speed and distance values of aged versus SNCA mice might have also been a useful way to compare movement data across the cohorts. This way, the frequency of mitochondria moving at a particular speed/distance could have been directly observed between both cohorts.

Furthermore, this study measured the speed of mitochondrial movement as opposed to their velocity. The advantage of measuring velocities over speed are that velocity measures the speed with a direction , unlike speed measurements. It will therefore be important to include the velocities values so that a measurement of mitochondrial movement and speed can be taken simultaneously

Statistical comparisons were undertaken between old versus young, and old versus young SNCA mice. However, for future work it may be more beneficial to compare all control mice (n=10) versus the old (n=5) and young (n=5) SNCA mice. This is because the ages of the control mice match the both ages of the SNCA cohort mice and therefore can be statistically compared.

4.6 LIMITATIONS OF THE MODEL

- α-syn overexpression has recently been shown to bind curved membraned structures as well as to lead to dysfunctional mitochondrial movements (Prots *et al.,* 2013, Pozo Devoto *et al.,* 2017). This study wanted to observe whether α-syn alone can affect mitochondrial transport, before delving into whether α-syn mutations could further cause mitochondrial movement alterations. For these reasons, this study selected the human wild type SNCA PDGF-β transgenic mouse model as the original paper indicated widespread transgene expression including neuronal and glial cells in cortical and subcortical brain regions (Rockenstein et al., 2002), α-syn accumulation in synapses/ as inclusion bodies within neurons in the deeper layers of the neocortex and in relation to dopaminergic neurons and decreased TH striatal activity. Also, motor impairments were also observed at 12 months of age, suggesting that this transgenic mouse could potentially duplicate a PD model rendering this wild type SNCA overexpressor mouse model a useful paradigm.
- Unfortunately, this study did not observe the motor impairments reported at 12 months of ages, (Masliah *et al.,* (2000) and therefore could not associate α-syn pathology with motor impairments found within PD.
- Furthermore, this study did not measure SNCA levels within experimental mice, which is a crucial limiting factor to understand whether mice expressed alpha synuclein. However, as the original study shows evidence of human α-syn immunoreactivity within the cytoplasm of SNpc neurons, we continued with this model, to observe whether

these α-syn inclusions affect mitochondrial movement, Quantification of SNCA levels will be carried out in the future works of this study.

- The initial project plan included understanding mitochondrial movement in young vs old SNCA mice. This study was later eliminated due to the unmatched ages of the mice for these experiments as a consequence of the mice being culled as a precaution after testing positive for Mouse Parvovirus, detected by a sentinel mouse
- All mice (both SNCA and control) were of the same mouse strain; C57BL/6. Being from similar genetic backgrounds, this strain may have had a role on influencing results observed in this study

4.7 CONCLUSIONS & FUTURE WORK

This study explored the effects of ageing and PD pathology within nigrostriatal slices. It was found that in aged mice mitochondrial movement is faster in comparison to young mice, and in aged SNCA mice mitochondria motility is faster when compared to younger mice. Interestingly, it was found that in mice overexpressing human wild type α–syn, mitochondrial movement was significantly reduced in comparison to old aged mice, however this was not an aged-matched finding and therefore must be repeated to confirm this outcome. This indicates that SNCA pathology perturbs mitochondrial movement perhaps more so than ageing.

Future work in this study will include:

- Analysing mitochondrial morphology within aged and SNCA mice, to understand whether α-syn effects their structure and therefore the speed and distance of mitochondrial movement
- Carry out TMRM staining to observe whether α-syn pathology affects mitochondrial health within DAergic neurons, and whether this alters mitochondrial directionality in PD
- Quantify α-syn expression within the SNpc in SNCA mice via immunofluorescence to observer whether the levels of α-syn affects mitochondrial motility in DAergic neurons

CHAPTER FIVE

Characterisation of NGN2 neurons harbouring a single, large scale mtDNA deletion

5.1 INTRODUCTION

5.1.1 Mitochondrial mutations

Large-scale mtDNA deletions contribute significantly to mitochondrial diseases, ageing and neurodegeneration. Pathogenic mtDNA deletions were first discovered in 1988 (Holt *et al.,* 1988, Wallace *et al.,* 1988). Since this discovery, hundreds of mtDNA mutations have been identified in association with mitochondrial disease (http://www.mitomap.org), causing defects within the brain and skeletal muscle (Chan, 2006). Different mtDNA deletions/duplications have been reported in the development of mitochondrial diseases, including Kearns–Sayre syndrome (Zeviani *et al.,* 1988, Shoffner *et al.,* 1989, Moraes *et al.,* 1989), myopathies (Manfredi *et al.,* 1997, Wong *et al.,* 2003), progressive external ophthalmoplegia (Moraes *et al.,* 1989, Wong *et al.,* 2003) and diabetes (Ballinger *et al.,* 1992). Around 20% of patients suffering from mitochondrial disease harbour a single large-scale mtDNA deletion causative of respiratory deficiency in the mentioned post-mitotic tissues (Tawil and Griggs, 2002, Oldfors *et al.,* 2006, Whittaker et al., 2015). Most reported mtDNA deletions occur within the major arc of mtDNA (Oldfors *et al.,* 2006), though research in aged muscle tissue has identified deletions also within the minor arc (Rygiel *et al.,* 2016). Large-scale mtDNA deletions are heteroplasmic and are prone to clonal expansion (Rygiel *et al.,* 2016).

5.1.2 MtDNA deletions in SNpc neurons

Several studies have correlated high mtDNA deletion load within individual SNpc neurons with COX deficiency (Bender *et al.,* 2006, Kraytsberg *et al.,* 2006, Reeve *et al.,* 2008 and Dolle *et al.,* 2016). Furthermore, research has shown an age-related increase in COX-deficient cells in the human brain (Cottrell *et al.,* 2001). Bender *et al.,* (2006) showed that COX-deficiency was observed within the SNpc of individuals with PD and aged individuals (Kraytsberg *et al.,* 2006, Bender *et al.,* 2006). Further investigation into mtDNA defects within individual SNpc neurons leading to COX deficiency described the absence of pathogenic mtDNA point mutations within these neurons, where the level of mtDNA deletion was increased in aged controls and individuals with PD (Reeve *et al.,* 2008). A real-time PCR assay developed by He *et al.,* (2002), calculated a deletion level between 55–60% for these neurons. SNpc neurons with normal COX activity from individuals with PD or controls were shown to harbour very high levels of deleted

mtDNA, 52% in individuals with PD and 43% in aged controls. The level of mtDNA deletion showed a significant correlation with age. Furthermore, the level of mtDNA deletion was significantly greater in the COX-deficient neurons than in neurons with normal COX activity, confirming that COX deficiency is observed with high levels of deleted mtDNA (Bender *et al.,* 2006).

Most recently, Dolle *et al.,* investigated mtDNA deletions, alongside copy-number alterations in single SNpc neurons. This study showed that mtDNA copy number increases with age in these neurons, consequently maintaining the level of wild-type mtDNA despite deletion accumulation. These findings indicate that ageing SNpc neurons upregulate mtDNA copy number. This proposes a neuroprotective mechanism within these neurons, which allows neurons to maintain wild-type mtDNA molecules, regardless of age-dependent accumulation of deletions. However, this upregulation was not observed in individuals with PD, resulting in the depletion of the wild-type mtDNA population (Dolle *et al.,* 2016).

5.1.3 Generating dopaminergic neurons from IPSCs

IPSCs can be directly differentiated into midbrain DAergic neurons providing as a useful PD model, where pathological studies can be conducted in live neurons (Xiao *et al.,* 2016). Until recently, several protocols have attempted to generate these DAergic neurons from pluripotent stem cells, which were unsuccessful until researchers began to delve into the biology of floor plate tissue. The floor plate of the midbrain is crucial in the development of the nervous system within vertebrates, giving rise to nigral DAergic neurons. Here, the ventral neural tube degenerates in the spinal cord and hindbrain, whilst survives in the midbrain, thus generating midbrain DAergic neurons (Ono *et al.,* 2007).

Human floor plate cells differentiated from human embryonic stem cells (hESCs) into engraftable midbrain DAergic neurons requires the activation of the sonic hedgehog (SHH) pathway (Fasano *et al.,* 2010). With the addition of GSK3b inhibitor, CHIR99021 (CHIR), and the further activation of the WNT signalling pathway, midbrain floor plates were created (Kriks *et al.,* 2011) and differentiated into midbrain DAergic neurons. These neurons cultured *in vitro*, were found to express SNpc markers, such as GIRK2, and exhibit *in vivo* electrophysiological properties observed in SNpc neurons, such as slow spiking (Kriks *et al.,* 2011). On grafting midbrain DAergic progenitors into 6-hydroxy-dopamine (6-OHDA) lesioned mice and rats,

viable and functional neurons were identified, where the DA deficiency was rescued in these animals (Kriks *et al.,* 2011). Adjusting and optimising the various growth factors supplemented to facilitate midbrain DAergic neuron development is critical to producing the desired neuronal cell type. Consequently, these protocols have been optimised with either one or two cell lines, however the transference of this protocol to other cell lines, would require further optimisation and in some cases may not be reproducible (Boulting *et al.,* 2011, Devine *et al.,* 2011). This can be controlled for by quantifying neuronal subtypes in differentiated neurons (Dolt *et al.,* 2017).

5.1.4 Single transcription factor induced functional neurons

The generation of neurons from IPSCs proves a powerful tool to understand neurodegenerative mechanisms, although two major limitations have been identified. The first limitation describes functional characteristic differences between pluripotent cell lines (Osafune *et al.,* 2008, Hu *et al.,* 2009, Bock *et al.,* 2011), where neurons derived from the same protocol from two different cell lines can display different properties (Wu *et al.,* 2007). IPSC lines can also exhibit changes over time in culture (Mekhoubad *et al.,* 2012). The second limitation comes down to the time-consuming protocols, as some differentiation protocols can continue for over a month, therefore causing a prolonged time to conduct studies (Johnson *et al.,* 2007).

Zhang *et al.,* 2013 demonstrated that neurogenin-2 (NGN2) overexpression can rapidly convert IPSCs into neuronal cells. The forced NGN2 expression converted IPSCs into neuron-like cells, in less than one week, which exhibited mature neuronal morphology in less than two weeks, quicker than any other available method for generating neurons from human IPSCs. Furthermore, almost 100% of surviving IPSCs were converted into neurons, indicating that forced expression of a single transcription factor, NGN2 can successfully induce neuronal differentiation with high yield. This robust method renders itself highly efficient in comparison to the Kriks protocol which comprises of the use of four transcription factors for neuronal conversion, under the SMAD (similar to the products of the drosophila MAD genes and the c. elegans SMA genes) inhibition protocol, which spans a 30 day time period (Kriks *et al.,* 2011). Moreover, neuronal NGN2 cells can form synapses (Zhang *et al.,* 2013) and could be used successfully to observe neuronal plasticity, conduct Ca^{2+} imaging, as well as be manipulated to represent human genetic disorders.

5.1.5 IPSCs harbouring a large scale mtDNA deletion

Recently, Russell *et al.,* (2018) delved into the methodology of clonal expansion utilising reprogrammed single, large scale mtDNA deletion NGN2-IPSCs. The study described below utilised two reprogrammed iPSC lines from Patient 'A', a female child with Pearson's syndrome caused by a ~6.0 kb single, large-scale mtDNA deletion spanning m.7777- 13794 removing the following genes, COXII, ATPase 6 and 8, COXIII, ND3, ND4L, ND4, ND5, part of ND6 and several tRNAs (MT-TK, MT-TG, MT-TR, MT-TH, MT-TS2, MT-TL2). Reprogramming of fibroblasts from patient A was conducted using a sendai virus (a single stranded cytoplasmic RNA vector [Tokusumi *et al.,* 2002]) and Cyto-Tune-iPS reprogramming kit, yielding 2 clones with of < 10% and 40% mtDNA deletion respectively (Russell *et al.,* 2018).

The long-term culture of these IPSCs showed a consistent increase in mtDNA deletion levels over time, where mtDNA heteroplasmy (60%) correlated with an increased respiratory deficiency (Russell *et al.,* 2018). In this current study, mitochondrial respiratory complex protein expression as well as mitochondrial function was assessed between two cell lines harbouring varying levels of mtDNA deletion to confirm the presence of a mitochondrial defect.

5.2 AIMS OF THIS STUDY

1. Confirm presence of the mitochondrial defect reported by Russell *et al.* in cells used for this project through mitochondrial protein complex expression and alterations in mitochondrial membrane potential by TMRM staining

2. Differentiate iPSC lines harbouring two levels of large scale mtDNA deletion into dopaminergic neurons and quantify the efficiency of this differentiation and whether this may serve as a useful model of mitochondrial dysfunction in PD

5.3 METHODS & MATERIALS

Generation of iPSCs from patient fibroblasts harbouring a large scale mtDNA deletion, as well their differentiation into neurons are described in detail within (Methods and Materials, section 2.1).

5.3.1 Characterisation of mitochondrial function in low and high heteroplasmy IPSc

5.3.1.1 Cell lysis for western blot

IPSCs were washed with PBS before being scraped off with cell scrapers, followed by centrifugation at 350g at 4°C for 10 minutes in ice cold PBS to pellet the cells. The supernatant was removed again and the pellet was re-suspended in cell lysis buffer (Table 5.1A), which was followed by a 30 second vortex and subsequent 10 min incubation on ice. Lysed cells were then centrifuged at 560g at 4°C for 2 minutes, where the supernatant containing cell proteins was retained eliminating the cytoskeleton of the cell, snap frozen on dry ice, and stored at -80°C until use. Two technical repeats were conducted for western blot experiments.

5.3.1.2 Bradford assay

Bovine serum albumin (BSA) was used to prepare a standard curve by diluting a gradient of volumes (0, 2, 5, 10, 15 and 20µl) of 1µg/µl BSA into 800µL H_20. Following this, 1µL of unknown sample was also added to 800µl H20, alongside 200µl Bradford reagent. Proteins combine with the Coomassie blue under the acidic conditions, triggering a brown to blue colour change, due a shift in absorption maximum from 465 to 595 nm, allowing measurement of amino acid residues such as arginine, lysine and histidine (Bradford, 1976). Unknown sample protein concentrations were determined from values generated from the standard curve. The standard curve and samples were placed into an optical bottom plate and wavelengths were observed on SpectraMax M3 plate reader. Varying concentrations of BSA, created a standard curve, with concentration were plotted on the x-axis and absorbance plotted on the y-axis. The equation of the line was re-arranged to calculate the absorbance and therefore concentration of the unknown samples.

5.3.1.3 Sample preparation and gel electrophoresis

20µg of low and high heteroplasmy IPSC protein lysates were loaded and separated via gel electrophoresis. Lysates were prepared with sample buffer (Table 5.1A) and 10% dithiothreitol (DTT) in 200µL PCR tubes. Proteins were denatured by heating samples at 37°C for 30 minutes (to observe Complex IV) in order for the efficient transfer of proteins through the gel matrix. This was followed by centrifugation at 14,000 RPM for 10 minutes. The Spectra™ multicolour broad range protein ladder (ThermoFisher) and protein samples were loaded into 12% Mini-PROTEAN TGX (Bio-Radx precast gels (Table 5.1B) and run for 60 minutes at 120 Volts in Tris-glycine running buffer.

5.3.1.4 Protein transfer

After 60 minutes, the gel was moved and placed in between two ion reservoir stacks and the blotting membrane of the Trans-Blot Turbo Transfer system Transfer Pack. This membrane sandwich was then placed into a cassette and inserted into the Trans-Blot Turbo Transfer system (Bio-Rad). This turbo transfer system allowed rapid and efficient transfer at <25V for 3 minutes at 2.5 A.

5.3.1.5 Detecting mitochondrial protein expression via immunoblotting

The membrane was transferred into blocking buffer (Table 5.1A) and placed on a roller for 60 minutes at room temperature to eliminate non-specific antibody binding. Primary antibodies (Table 5.1C) were also diluted in blocking buffer and placed on a membrane and incubated overnight at 4°C on a rotator. This membrane underwent 3x 10 minute TBST washes, which was followed by secondary antibody incubation for 60 minutes at room temperature.

5.3.1.6 Membrane development

After secondary antibody incubation, the membrane was washed 3x in TBST for 10 minutes. Image development was carried out through the Amersham™ ECL™ prime reagent kit, which comprises of luminol and peroxide solutions These solutions are utilised by the horseradish peroxidase enzyme conjugated on the secondary antibody and which catalyses these reagents to produce detectable light. The membrane was incubated in a 1:1 ratio of both solutions for 5 minutes, followed by ChemiDoc system imaging and densitometry analysis (Image Lab) respectively.

Table 5.1 Western blot reagents

A.

Reagents	Concentration	Supplier	Use
Tris-HCL	100 mM	Roche	Western blot cell Lysis buffer
EDTA	500 µM		
NaCl	15 mM		
Triton X-100	1%		
IGEPAL (NP-40)	1%		
Mini-protease inhibitor	1 tablet		
DH_20	7.19 mL		
NaCl	16 g	Sigma	Tris-buffered saline with Tween-20 (TBST) (pH 7.6)
Trizma Base	4.8 g		
Tween-20	1 mL		
DH_20	2000 mL		
Glycerol	4 mL	Sigma	2x Laemmli sample buffer (without DTT)
SDS	20 %		
Bromophenol blue	0.02 g		
DH_20	2 mL		
Glycine	144 g	Sigma	5X Tris-glycine running buffer (pH 8.8)
Trizma Base	30 g		
SDS	10 g		
DH_20	2000 mL		
MOPS	104.6 g	Sigma	NuPAGE 20X MOPS running buffer (pH 7.7)
Trizma Base	60.6 g		
SDS	10 g		
EDTA	3 g		
DH_20	500 mL		
Powdered milk	5 g	Marvel	Blocking buffer
TBST	100 mL		

B.

Reagents	Supplier	Use
Bradford reagent	Bio-Rad	Bradford assay
Bovine serum albumin	Thermo Fisher Scientific	
Spectra TM Multicolor Broad range protein ladder	Thermo Fisher Scientific	Gel electrophoresis
4-20% Mini-Protean TGX Precast Protein Gel, 10 well, 50 µL	Bio-Rad	
12% Mini-PROTEAN TGX Precast Protein gel, 10 well, 30 µL	Bio-Rad	
Tran-Blot Turbo Mini PVDF Transfer pack	Bio-Rad	Semi dry transfer
Non-fat powdered milk	Marvel	Blocking step
Amersham™ ECL™ prime Western blotting detection reagent	GE Healthcare	Developing blot

C.

Western blot antibodies Primary Antibody	Dilution	Host/Type	Manufacturer	Molecular Weight (kDa)
NDUFB8 (Complex I)	1:1,000	Mouse Monoclonal	Abcam	22
NDUFA9 (Complex I)	1:1,000	Mouse Monoclonal	Abcam	17
SDHA (Complex II)	1:2,000	Mouse Monoclonal	Abcam	70
MTCO1 (Complex IV)	1:1,000	Mouse Monoclonal	Abcam	40
Alpha tubulin	1:10,000	Mouse Monoclonal	Abcam	50
Secondary Antibody				
Rabbit Polyclonal Anti-mouse horse radish peroxidase	1:1,000	Rabbit Polyclonal	Dako Agilent	

5.3.2 Quantifying mtDNA deletion in neurons

5.3.2.1 Freezing cells for PCR

A pellet of $1x10^5$ cells/mL were frozen at -80 °C until ready for DNA extraction.

5.3.2.2 DNA extraction and single cell lysis

DNA extraction from $1x10^5$ cells/mL IPSCs was conducted using single cell lysis buffer [50 mM Tris HCl (pH 8.5), 0.1% Tween 20, 0.2mg/ml proteinase K (ThermoFisher). Cells were incubated in buffer at 2 hours at 56°C, followed by a 10 minute 95°C Proteinase K denaturing step, to prevent proteinase K interfering with the Taqman mastermix during the PCR reaction.

5.3.2.3 Real Time PCR primers

The real time PCR protocol was followed as described by Rygiel *et al.,* 2015. PCR primers for these reactions and fluorogenic probes for these regions were designed by (He *et al.,* 2002). The following primers were synthesised: ***ND1*** - forward primer (L3485-3504), ND1 reverse primer (H3532-355), ND1 probe (L3506-3529) and MT-ND1 VIC-5′-CCATCACCCTCTACATCACCGCCC-3′-MGB (np 3506-3529). ***ND4*** - forward primer (L12087-12109), ND4 reverse primer (H12140-12170), ND4 probe (L12111-12138) and MT-ND4 FAM-5′-CCGACATCATTACCGGGTTTTCCTCTTG-3′-MGB (np 12111-12138) (Table 5.2).

5.3.2.4 Real Time PCR assay

Taqman chemistry was used to perform real-time PCR. All PCR amplification was carried out in 20µL reactions, 5µL of the standard curve and DNA samples and 15µL PCR master mix. All samples were run in triplicate in a Veriti 96 well (Applied BioSystems) PCR plate. Each plate contained serial 1:10 dilutions of a 7D1-B2M plasmid construct containing ND1 and ND4 genes in dH_2O to generate a standard curve (Rygiel *et al.,* 2015). Plates were sealed, and vortexed to mix all the reagents with the DNA samples and spun down. mtDNA deletion levels were quantified in low and high heteroplasmy IPSCs on a StepOne Plus (Applied Biosystems) real-time PCR machine, protocol as follows, 50°C for 2 minutes, 95°C for 10 minutes, 40 cycles of 95°C for 15 seconds, 60°C for 1 minute.

5.3.2.5 Real Time PCR analysis

MtDNA deletion levels were analysed where the trend line of the standard curve was assessed for efficiency of the PCR reaction and determining the level of each probe indicative of the presence of the gene. The gradient of the standard curve for every reaction needed to fall within the range of -3.25 to -3.45, with -3.33 being the optimal value. MTND1 is preserved in both WT and mutant mtDNA in this cell line, therefore acted as reference for mtDNA as, ND4 is deleted. The ratios of MT-ND1/D-Loop, MT-ND4/D-Loop and MT-ND4/MT-ND1 were calculated using standard curves.

For the cell line harbouring a higher mtDNA deletion a range of 40-48% mtDNA deletion was observed and for the second, lower cell line mtDNA deletion was observed as <10%. Any sample with measured heteroplasmy of 0–10% was classed as <1Ct. During experiments, the level of specific mtDNA deletion for both cells lines are highlighted.

Table 5.2. Real time PCR reagents for one reaction

Reagents	Base pairs	Volume (µl)	Final concentration	Manufacturer
Taqman Universal PCR master mix	-	10	1x	Applied Biosystems
MTND1 forward primer	L3485-3504	0.6	10 µM	Eurofins MWG
MTND1 reverse primer	H3532-355	0.6	10 µM	Eurofins MWG
MTND4 forward primer	L12087-12109	0.6	10 µM	Eurofins MWG
MTND4 reverse primer	H12140-1217	0.6	10 µM	Eurofins MWG
MTND1 probe VIC	L3506-3529	0.4	5 µM	Life Technologies
MTND4 probe FAM	L12111-12138	0.4	5 µM	Life Technologies
dH_20	-	1.8	-	-
Sample DNA	-	5	-	-

5.3.3 Neuronal imaging

5.3.3.1 Fixing cells, immunofluorescence and live imaging experiments

Conducted as highlighted in (Methods and Materials, section 2.3). Primary and secondary antibodies used in experiments are highlighted in (Table 5.3).

Table 5.3. Immunofluorescence primary and secondary antibodies

Primary Antibodies	Dilution	Detection	Type	Manufacturer
Tyrosine Hydroxylase (TH)	1:200	DAergic neurons	Rabbit/IgG1	Sigma
γ-aminobutyric acid (GABA)	1:1000	Inhibitory (GABA) neurons	Rabbit	Sigma
Vglut	1:500	Glutamatergic neurons	IgG2a	Synaptic systems
MTCO1 (COX IV)	1:200	Mitochondrial mass marker	IgG2a	Abcam
β-tubulin	1:500	All immature neurons	Rabbit	Sigma
Microtubule associated Protein (MAP2)	1:200	Neuronal marker	Rabbit	Abcam
Hoechst	1:500	Nuclear marker		Sigma
Secondary Antibodies				
Alexa Fluor 405 nm	1:200	Secondary Antibody marker		ThermoFisher
Alexa Fluor 546 nm				
Alexa Fluor 647 nm				
Alexa Fluor 750 nm				

5.4 RESULTS

5.4.1 Immunoblotting showing a reduction in mitochondrial protein expression in IPSCs harbouring a large-scale mtDNA deletion

Russell *et al.,* (2018) reported a reduction in mitochondrial oxygen comsumption rate (OCR) within IPSCs harbouring a higher level of mtDNA deletion. This study aimed to quantify mitochondrial protein complex expression within these two lines to confirm alterations in the mitochondrial oxidative capacity within IPSCs used for experiments and their differentiated neuronal phenotype in the presence of a large-scale mtDNA deletion.

The mtDNA deletion in this line spans 6kb (m.7777- 13794) of the mitochondrial genome. Therefore, mitochondrial protein expression was assessed to detect alterations between the two IPSC lines. Lysates were obtained from low and high heteroplasmy IPSCs, followed by western blot to observe protein levels of mitochondrial complex subunits. The following mitochondrial complex subunits were analysed: Complex I (NDUFB8), complex II (SDHA), complex IV (MTCO1) and complex V (ATP50) (Figure 5.1) (N=2). These results demonstrated that IPSCs containing 42% heteroplasmy (mtDNA deletion) displayed a decrease in Complex I and IV protein expression level, in comparison to IPScs with <10% lower heteroplasmy (Figure 5.1).

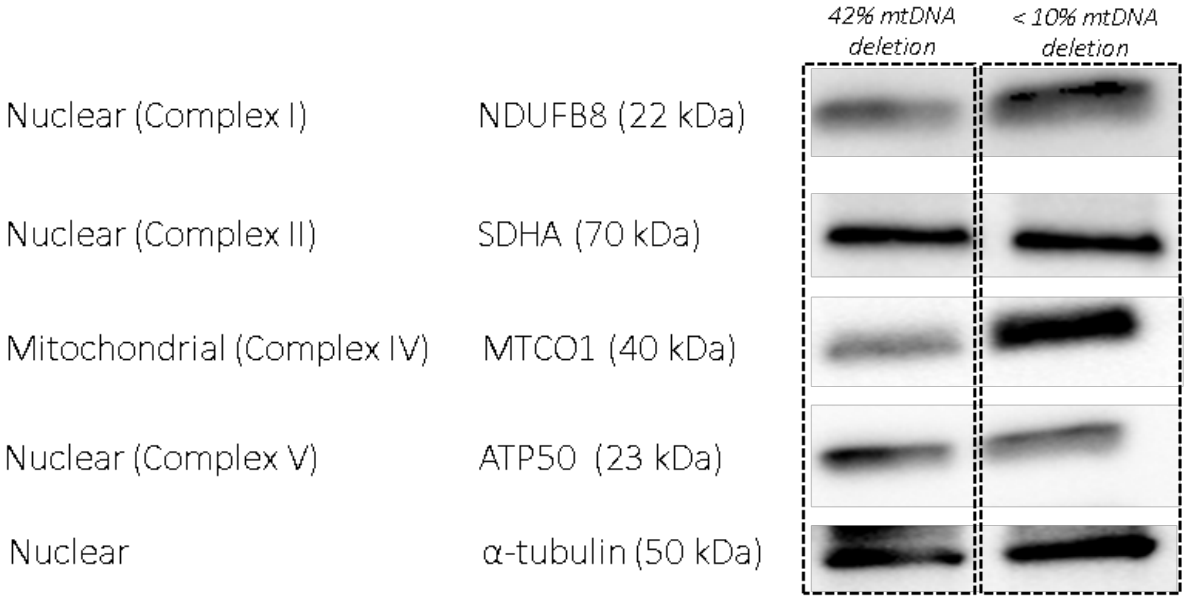

Figure 5.1. Respiratory chain protein expression in iPSCs. Western blot analyses of Complex I, II, IV and V of the respiratory chain via staining with NDUFB8, SDHA, MTCO1, and ATP50 antibodies. The downregulation of Complex 1 (NDUFB8) and Complex IV (MTCO1) can be observed within iPSC harbouring large scale mtDNA deletion (A.2 ~42% mtDNA deletion). All quantification was normalised to alpha-tubulin loading control. Decrease in protein level of Complex I and Complex IV (N=2).

5.4.2 Mitochondrial membrane potential analyses in large scale mtDNA deletion IPSCs vs neurons

The development of membrane potential reliant fluorescent stains has become a robust method to assess ΔΨm. TMRM, a fluorescent lipophilic cationic dye is efficient for this purpose (Tehrani *et al.,* 2018).

To observe alterations in mitochondrial membrane potential between both cell lines, and to confirm whether a decrease in these values were observed in these cell lines, Russell *et al.,* (2018) quantified the level of mitochondrial membrane potential within the IPSCs and neurons (Figure 5.2A and B). These findings demonstrated that TMRM fluorescence was slightly higher within IPSCs with ~53% mtDNA deletion level, ~10% mtDNA deletion level cell line although these changes were not significant.

This current study repeated the TMRM intensity analysis within IPSCs and differentiated neurons (8 days maturation) of these cell lines. It was also found that TMRM fluorescence within NGN2 derived neurons expressing a decreased TMRM fluorescence in observed within patients harbouring ~53% mtDNA deletion compared to cell line with lower mtDNA deletion (grey bar) (not significant, $p<0.05$) (Figure 5.2D). When repeated in this current study TMRM intensity was decreased in the axons of high heteroplasmy cell lines with 42% mtDNA deletion (not significant) (Figure 5.2E) and a significant decrease in TMRM intensity within cell bodies of neurons harbouring a 42% mtDNA deletion was observed in comparison to the low mtDNA deletion cell line (**=$p<0.0083$) (Figure 5.2F).

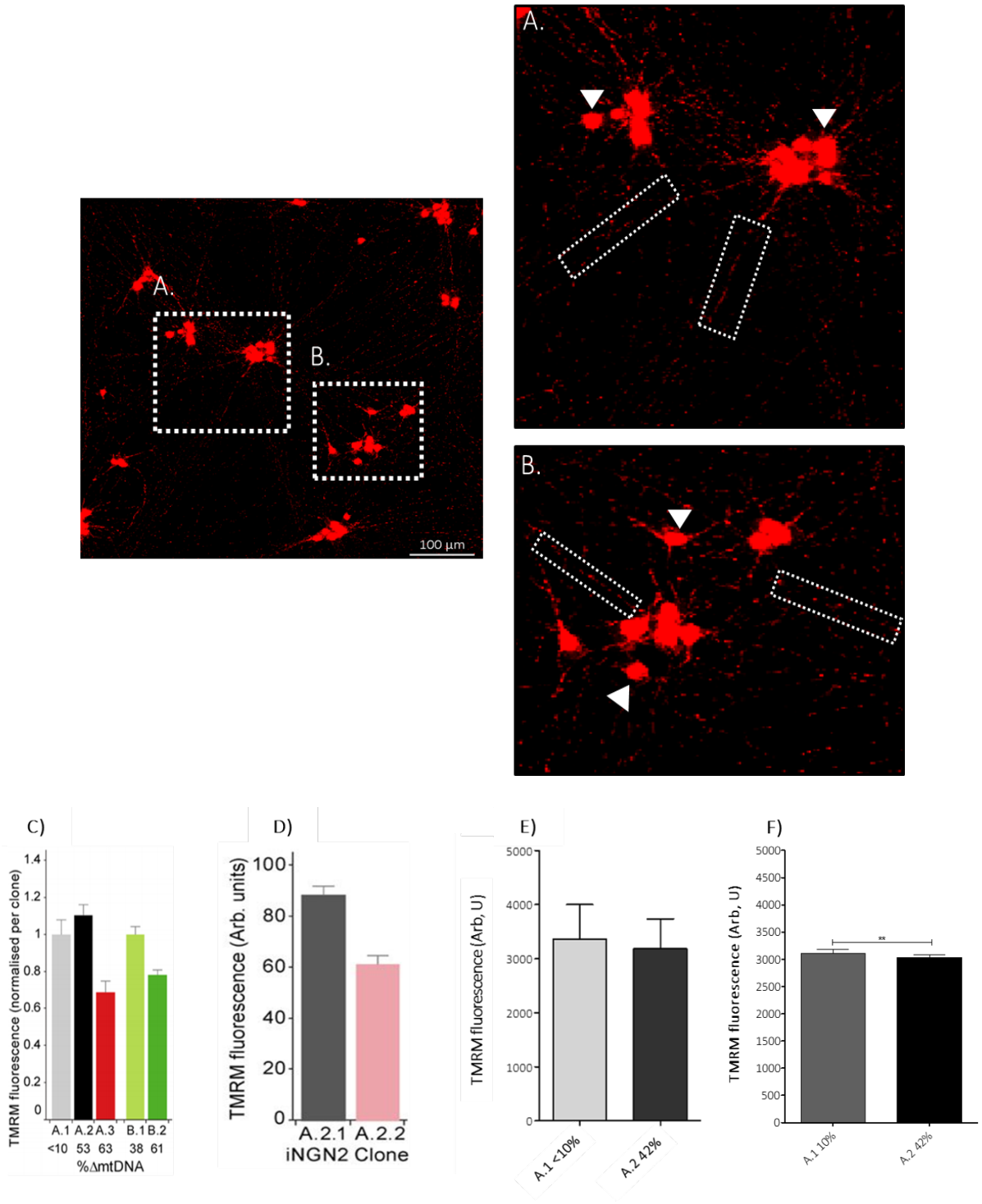

Figure 5.2. Mitochondrial membrane potential analysis in large scale deletion IPSC and neurons. A-B) TMRM intensity values taken from mitochondria within NGN2 axons (white boxes) and cell bodies (white triangles) in this study. **C)** IPSC TMRM fluorescence, demonstrates increased TMRM fluorescence in patient line harbouring increased (black bar) (53%) mtDNA deletion, followed by a large reduction in this intensity in patient line harbouring 63% heteroplasmy (Red bar) (not significant) (Russell *et al.,* 2018, included with permission). **D)** TMRM fluorescence within NGN2 derived neurons expressing a decreased TMRM fluorescence in observed within patients harbouring ~53% mtDNA deletion (pink bar), compared to cell line with lower mtDNA deletion (grey bar) (not significant) (Included with permission from Russell *et al.,* 2018). **E)** Current study – TMRM intensity was decreased in axons of high heteroplasmy cell lines with 42% mtDNA deletion (not significant) (N=230 axons [low heteroplasmy neurons] and N=250 [high heteroplasmy neurons]). **F)** Significant decrease in TMRM intensity in cell bodies of neurons harbouring a 42% mtDNA deletion was observed in comparison to the low mtDNA deletion cell line (N=226 cell bodies [low heteroplasmy] and N=228 cell bodies [high heteroplasmy]). Statistical differences identified through Mann Whitney U test (N=3) (**=p<0.0083, SEM error bars).

5.4.3 The differentiation of NGN2 stem cells into dopaminergic neurons – Challenges and Protocols

Following the protocol described by Russell *et al.,* 2018, IPSCs were successfully differentiated into a heterogeneous population of neurons harbouring two levels of a large scale mtDNA deletion: (<10%) and (<40%) mtDNA deletion respectively, since the aim of this thesis was to understand mitochondrial trafficking within PD. As the NGN2 neurons are a heterogeneous population of varying neuronal subtypes, efforts to drive differentiation of a DAergic-only neuronal subtype from these lines were attempted. Indeed, formation of midbrain DAergic neurons involves the addition of different growth factors and supplements at various stages of neuronal growth and differentiation (Table 5.4). Different growth factors and supplements were added throughout NGN2 neuronal development in accordance to the Kriks protocol (Kriks *et al.,* 2011), to support DAergic neuronal differentiation (Figure 5.3).

The 3 main factors added to *proliferation media* were sonic hedgehog (SHH), Purmorphamine and ChIR99021 (CHIR). SHH is a morphogen which promotes DAergic neuron formation along the dorsoventral axis. Purmorphamine acts as a SHH agonist and therefore enhances DAergic neuron formation. The addition of CHIR, allows the reprogramming of embryonic stem cells via WNT-signalling (Table 5.4). Growth factors were taken from Kriks *et al.,* (2011) protocol. Finally, doxycycline was added to the proliferation media with and without factors to drive NGN2 expression (Figure 5.3).

Table 5.4. Supplements used in NGN2 dopaminergic proliferation (PM) and differentiation media (DM)

Supplements	Final Concentration	Functions
Sonic hedgehog (shh)	100ng/ml	Signals for DAergic neuron formation along dorsoventral axis (PM)
Purmorphamine	2µM	SHH agonist (PM)
Chir - 99021 (CHIR)	3µM	It allows reprogramming of ES cells. It has also shown to activate WNT-signalling and induce formation of floor and roof plate (PM)
N-[N-(3,5-difluorophenacetyl)-L-alanyl]-S-phenylglycine t-butyl ester (DAPT)	10µM	γ-secretase inhibitor, inhibits notch signalling which increases DAergic neurons (DM)
Ascorbic acid	0.2mM	Cell survival (DM)
Brain derived neurotrophic factor (BDNF)	20nM	Survival and morphological differentiation of neurons (DM)
Fibroblast Growth factor 8 (FGF8)	100ng/ml	Survival of DAergic neurons, also involved in signalling via dorsoventral axis (DM)
Glial cell line derived neurotrophic factor (GDNF)	20ng/ml	Survival and morphological differentiation of neurons (DM)
Dibutyryl c-AMP	0.5mM	Enhances neuronal maturation (DM)

The factors added to the *differentiation media* included, BDNF, GDNF, FGF8, DAPT, L-Ascorbic acid and (db)–cAMP (Table 5.4). FGF8 promotes the survival of DAergic neurons and also further signals along the dorsoventral axis in the brain. DAPT inhibits NOTCH signalling, which in turn increases DAergic neuron formation (Yamauch *et al.,* 2009). L-Ascorbic acid further promotes cell survival. BDNF, GDNF and cAMP factors were all added to enhance neuronal maturation (Xia & Lee, 2016) (Figure 5.3).

Tyrosine hydroxylase (TH) catalyses the conversion of L-tyrosine to L-3,4-dihydroxyphenylalanine (L-DOPA), using molecular oxygen (O_2) (Daubner *et al.,* 2012). As L-DOPA is a precursor for DA, TH was selected as a marker for DAergic neurons. Once NGN2 neurons had reached 7 days of maturation, differentiated neurons were fixed stained with MAP2 (Microtubule associated protein 2) to identify neuronal processes, and Hoechst to stain nuclei, followed by subsequent imaging.

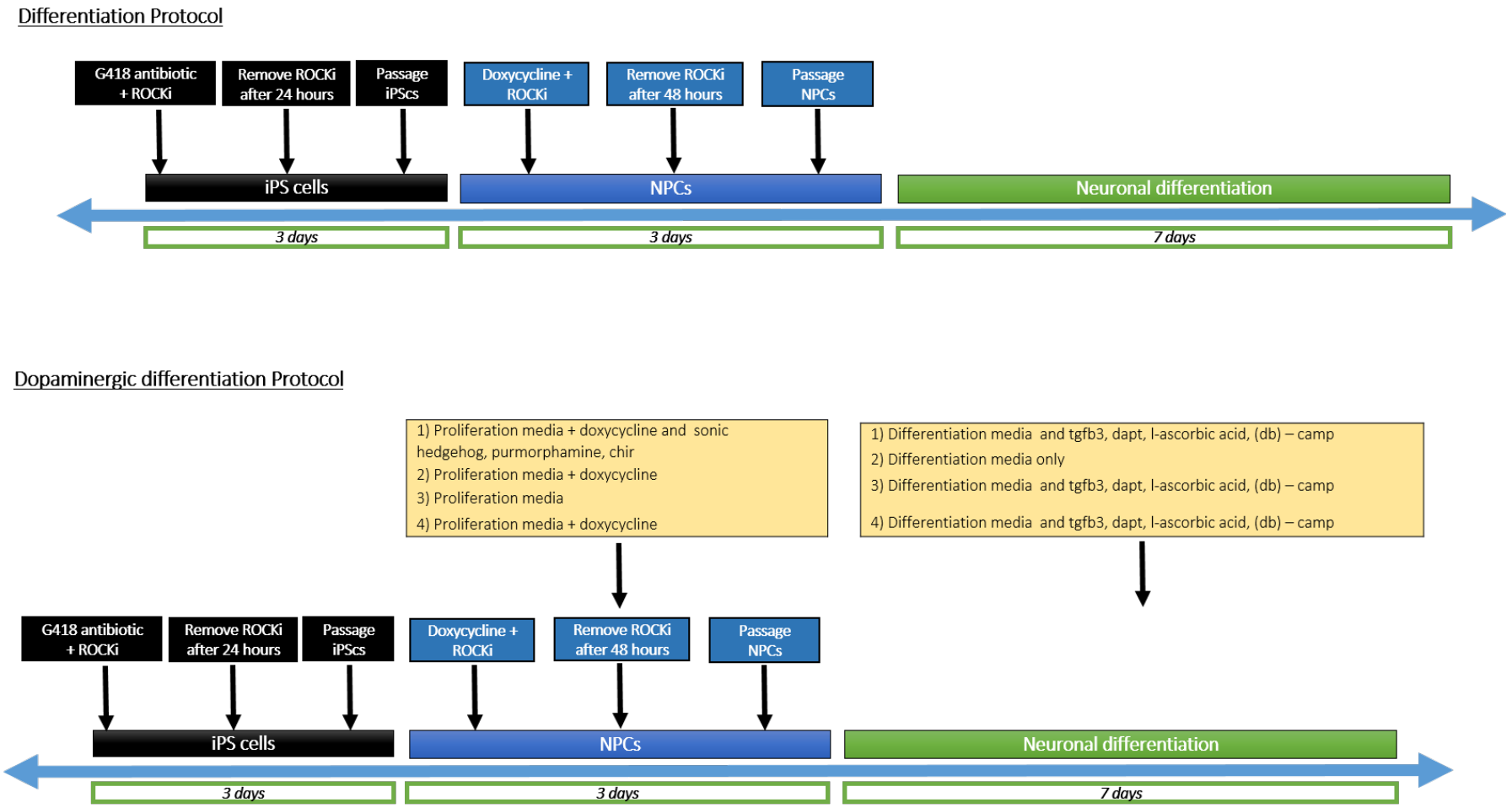

Figure 5.3. Conditions for DA neuron differentiation. Supplements added to proliferation and differentiation media, when differentiating neurons into DA neurons (Protocol adapted from Kriks *et al.,* 2011)

Neurons were grown under 4 different conditions (Figure 5.3) and differentiated for 8 days to generate neurons.

Condition number 1, followed the standard INGN2 differentiation protocol with the addition of supplements (that have been reported by Kriks *et al.,* 2011) to enhance DA neuron formation. Condition number 2 followed the standard protocol by Russell *et al.,* 2018, without the addition of any factors. Condition 3 entailed a protocol that does *not* involve the addition of doxycycline during proliferation and all growth supplements during differentiation. Condition 4 comprises the same protocol as condition 3 *with* the addition of doxycycline.

TH staining was used to observe whether DAergic neurons were being generated by these various protocols. They showed that DAergic neurons were only formed under conditions 1 and 2 (Figure 5.4). Furthermore, as experiments proceeded with culturing neurons under conditions 1 and 2, it was found that the addition of DAergic supplements (as observed in Condition 1) were not reproducible, due to increased neuronal death (data not shown) (N=3 biological repeats).

On the first day of neuronal progenitor cell (NPCs) culture, DAergic growth factors, SHH, Purmorphamine and CHIR were added and maintained over the 72 hour NPC culture. Within the dish, NPCs are seeded to be densely packed, in order to inhibit their spontaneous differentiation and enhance proliferation. The addition of these factors was found to perturb NPC growth, disrupt their distribution and alter cell morphology. This resulted in low yield of surviving and viable NPCs primed for differentiation. Growth condition 2 (Russell *et al.,* 2018) was therefore selected due to the presence of DAergic neurons after differentiation, but also due to efficiency of the neuronal differentiation compared with other conditions.

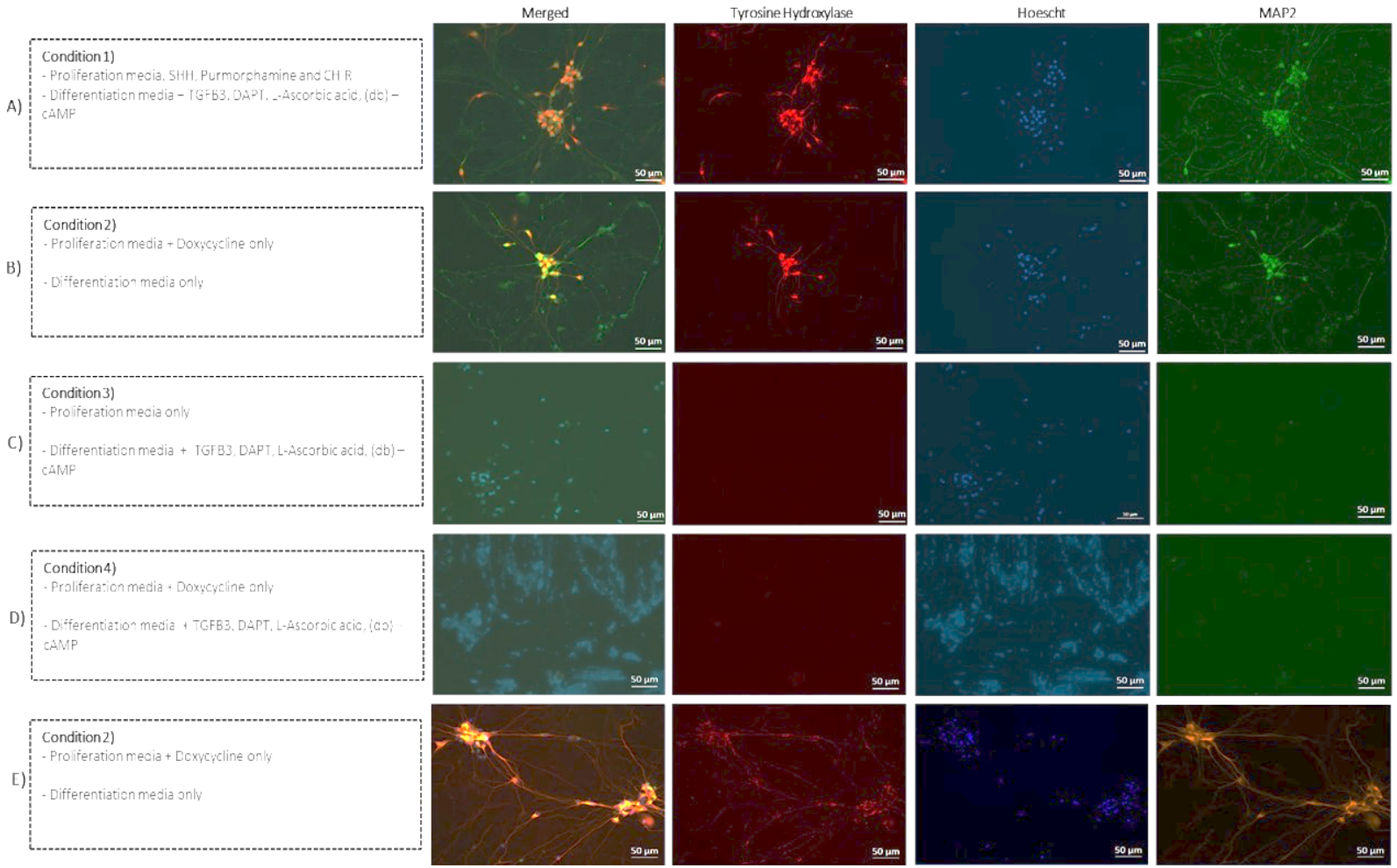

Figure 5.4. Low and high heteroplasmy DA neuron differentiation. A-B) DAergic neurons are observed in growth conditions 1 and 2 due to bright TH staining (red) and MAP2 (green) staining **C)** Condition 3 - indicate no TH-positive or MAP2 staining suggesting no neurons are formed **D)** Condition 4 shows no generation of neurons, due to cell death. **E)** Repeat differentiation using condition 2 of high heteroplasmy neurons exhibit TH-positive neurons indicative of DAergic subtypes Images taken at x 20 magnification.

Furthermore, to ascertain the proportion of DAergic neurons in this NGN2 heterogeneous neuronal population TH-positive neurons were counted. TH-positive neurons within this neuronal population were compared against MAP2 and Hoescht staining. Analysis revealed that low (<10%) and high (43.7%) heteroplasmy neurons showed 66.78% TH-positive and 78.02% MAP2-positive staining and 70.27% TH-positive and 96.06% MAP2 expression respectively (staining normalised to nuclear staining) (Figure 5.5).

It may be that the remaining percentage of cells that were undetected within this analysis could be glial or undifferentiated cells, not stained for in this experiment. This result indicates that neurons harbouring a higher level of mtDNA deletion, generated more neurons in comparison to the lower heteroplasmy line, as well as exhibiting increased TH expression indicative of DAergic neurons.

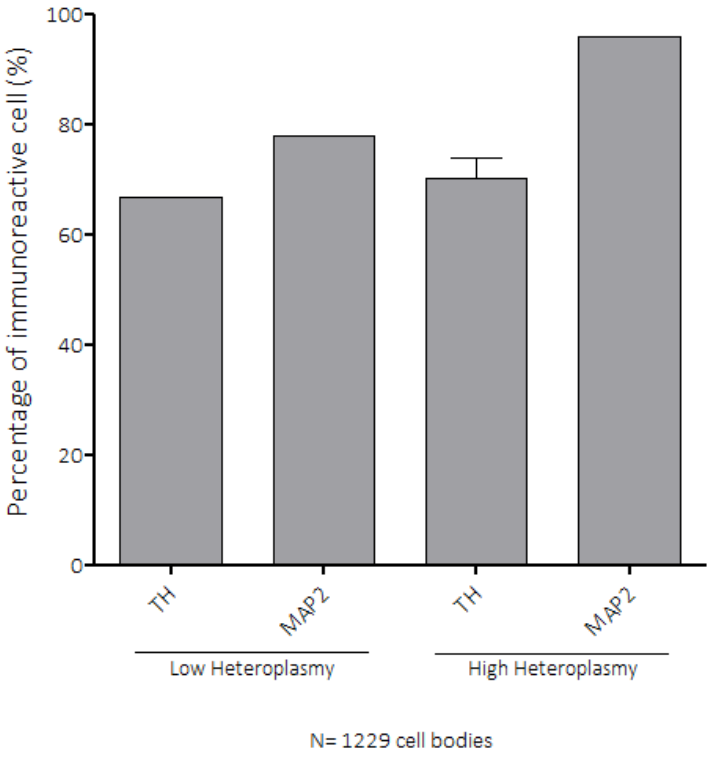

Figure 5.5. TH-MAP2 expression in heteroplasmy neurons. Low heteroplasmy neurons harbour a <10 % mtDNA deletion. Quantification of TH and MAP2 neurons indicate that in low heteroplasmy neurons 96.06% of neurons are MAP2 positive, of which 70.27% of these are TH positive. High heteroplasmy neurons harbour a <43.7 % mtDNA deletion, of which 66.78% are MAP2 positive and 78.02% of these are TH positive. (N=2). Error bars represent Mean +/- SEM. Images were again taken at x20 magnification.

5.4.4 Quantifying the expression of neuronal markers in iNGN2 derived neurons

Following this quantification, immunofluorescence was conducted on these neurons to compare the levels of other neuronal subtypes within the generated population. In addition to quantifying DAergic (TH antibody staining) expression, GABAergic (Gamma-aminobutyric acid) (GABA antibody staining) and glutamatergic (VGLUT1 antibody staining) positive neurons were also counted to understand other neuronal subtype expression within a heterogeneous neuronal population.

Quantification of 2145 cell bodies (low heteroplasmy neuronal cohort) were analysed for the neurotransmitter triad: TH, GABA, and VGLUT1 staining which demonstrated that 96% of neurons expressed TH, 88% were GLUT positive and 82% were GABAergic positive (Figure 5.6). Although a fully homogenous DAergic neuronal population could not be generated from these experiments, it is evident from that over 90% of NGN2 neurons express TH, alongside other neuronal markers.

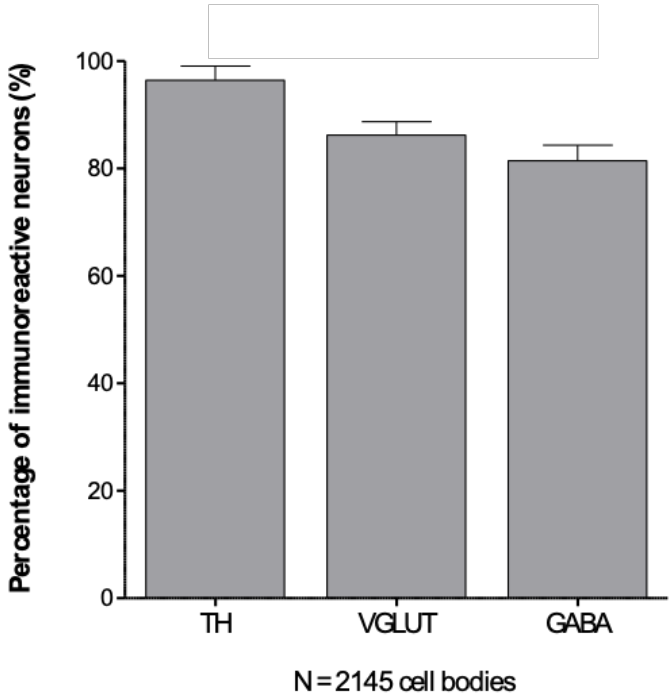

Figure 5.6. Quantification of neuronal differentiation. Tyrosine hydroxylase, glutamatergic and GABAergic quantification of low heteroplasmy NGN2 neurons. Co-localisation analysis measured as a percentage against total number of nuclei. Increased TH expression in NGN2 neurons (96%), followed by glutamatergic expression (88%) and GABAergic expression at (82%). Two technical repeats were conducted, where error bars represent Mean +/- SEM. (N = 2). Images were again taken at x20 magnification.

As a large amount of overlap in staining was observed, the co-localisation of these antibodies within these neurons was quantified. This study counted the co-localisation of TH-GABA-GLUT, TH-GABA, TH-GLUT and GABA-GLUT staining within 499 low heteroplasmy neuronal cell bodies.

Results revealed that the co-localisation of TH with these neurotransmitters within a heterogeneous neuronal population demonstrated large variability. The highest antibody co-localisation within these neurons were observed in the TH-GABA-GLUT cohort (Figure 5.8), showing that 76.5% of cell bodies expressed TH-GABA-GLUT staining, followed by co-localisation of TH-GABA (Figure 5.9) in 13.22% of neurons. TH-GLUT and GABA-GLUT co-localisation was found to be 0.6 % and 2.8% respectively (Figure 5.7 and 5.8). All counts were carried out as a percentage of the total number of nuclei.

Therefore, once neuronal subtypes were quantified, a heterogeneous population of neurons was used in all future experiments. From here onwards, the differentiation protocol described by Russell *et al.,* (2018) (Condition 2) was used to generated neurons harbouring a large scale mtDNA deletion to image mitochondrial trafficking (See Chapter 6).

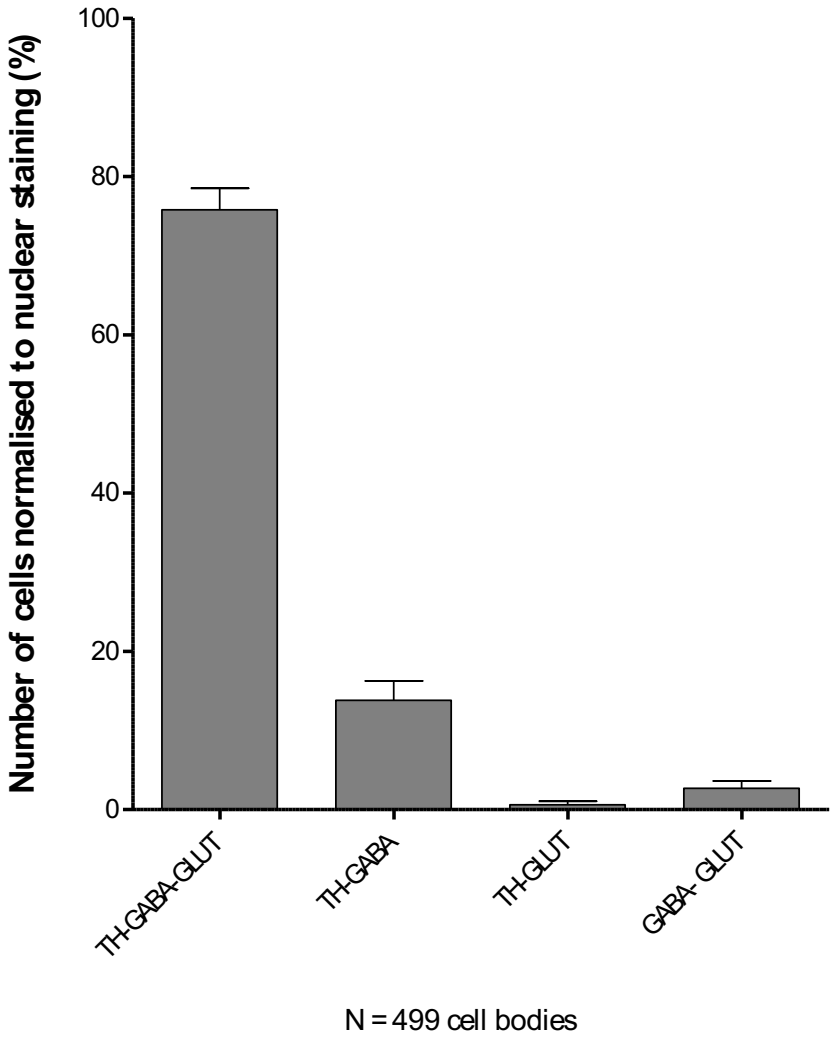

Figure 5.7. TH—GABA-GLUT co-localisation analyses. TH-GABA-GLUT co-localisation is 76.5%, followed by TH-GABA colocalisation at 13.22% of neurons. TH-GLUT and GABA-GLUT colocalisation is 0.6 % and 2.8% respectively. Analysis was conducted in low heteroplasmy cell bodie

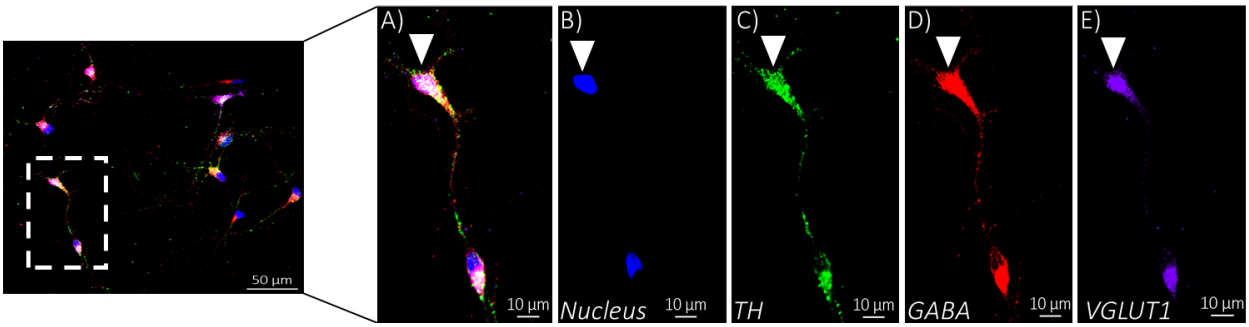

Figure 5.8. Quadruple neuronal staining of low heteroplasmy neurons. Co-localisation of TH, Glutamatergic and GABAergic neurons. White arrow heads indicate colocalised staining of TH-GABA-VGLUT1 cell bodies. Images taken at x 20 magnification.

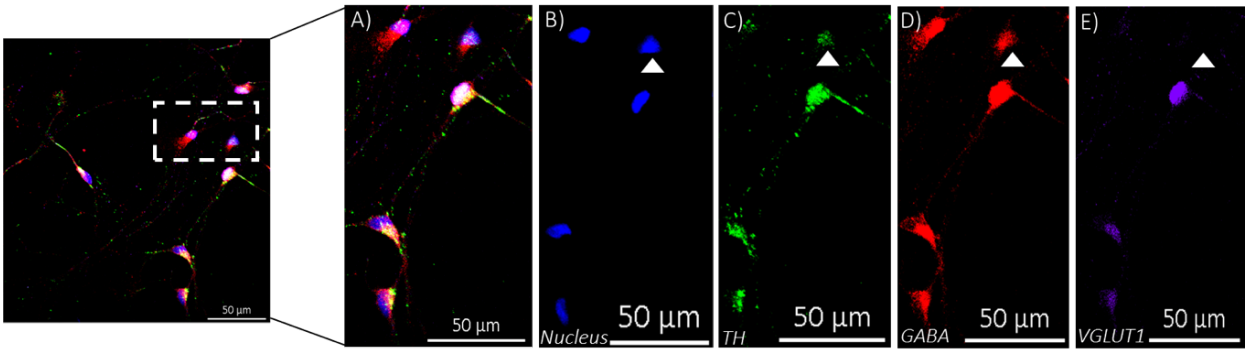

Figure 5.9. TH-GABA localisation in low heteroplasmy neurons. Co-localisation of TH and GABAergic neurons. White arrow heads indicate colocalised staining of TH and GABA positive staining. Images taken at x 20 magnification.

5.5 DISCUSSION

5.5.1 Summary of results

- Western blot analysis demonstrated that IPSCs harbouring a large scale mtDNA deletion exhibit a moderate decrease in mitochondrial complex I and IV protein expression, compared with isogenic control
- Cell bodies of neurons harbouring a large scale mtDNA deletion exhibit a small but significant decrease in TMRM intensity indicative of perturbed mitochondrial membrane potential in comparison to the low mtDNA deletion cell lines
- Differentiated neurons derived from both cell lines showed a heterogeneous neuronal population containing TH-expressing neurons indicative of DAergic neurons

5.5.2 Large scale mtDNA deletion IPSCs exhibit a mitochondrial dysfunctional phenotype at protein level

This study manipulated an induced pluripotent stem cell model harbouring a large scale mtDNA deletion (spanning 6017 base pairs from m.7777-13794). Deletions are the most common mtDNA mutation type observed in SNpc neurons, affected in PD. In order to confirm the presence of a respiratory chain deficiency within the cell lines (required for future experiments [See Chapter 7]) both deletion and control IPSCs were analysed for OXPHOS protein expression by western blot.

COX deficiency observed in the SNpc is caused specifically by mtDNA deletions reaching up to 50% heteroplasmy (Bender *et al.,* 2006, Kraytsberg *et al.,* 2006, Reeve *et al.,* 2009, Taylor *et al.,* 2003). For this reason, an mtDNA deletion cell line was used in this study as opposed to inducing mitochondrial damage via a complex inhibitor i.e. Rotenone or MPTP, in order to maintain physiological relevance. This cell line provides as a unique paradigm to observe PD and advancing age, since these individuals harbour mtDNA deletions, commonly observed within PD patients. This model provides insight into how mitochondrial trafficking is affected by the mitochondrial DNA alterations present within SN neurons.

The mtDNA deletion described in the high heteroplasmy cell line in the current study (~42%), removes subunits of complex I and complex IV. Therefore, a decrease was observed in expression of complexes I and IV (indicated by a reduction of NDUFB8 and MTCO1 levels

respectively). Furthermore, having already reported a decrease in oxygen consumption rate (OCR) following FCCP treatment, within the high heteroplasmy cell line compared to the low heteroplasmy cell line, Russell *et al.,* 2018 characterised this cell line as having reduced capacity to utilise oxidative respiration. This supported the findings in this study that a significant decrease in TMRM intensity was observed within high mtDNA deletion cell bodies compared to the lower mtDNA deletion cell line. This might indicate that dysfunctional mitochondria harbouring a lower membrane potential might remain within the cell body perhaps awaiting lysosomal degradation.

5.5.3 Using IPSCs with mitochondrial dysfunction as a Parkinson's disease model

Whilst the generation of DAergic IPSCs from PD patient lines provides as a powerful tool to understand PD pathology, the traditional protocol to generate these midbrain DAergic neurons, requires a long differentiation time period i.e. via the Krik's protocol (Kriks *et al.,* 2011). This is because it is important to create the correct biological milieu for these DA neurons via the addition of DAergic growth factors.

Mitochondrial dysfunction in PD can be driven by mtDNA deletions and therefore the utilisation of this NGN2 line containing a mitochondrial DNA deletion is hugely beneficial. Even the generation of a heterogeneous neuronal population would still provide valuable insight into the effect of these mitochondrial DNA mutations on mitochondrial transport, to support the *ex vivo* studies performed in this thesis.

Several studies have utilised PD-patient IPSCs, some of which now successfully demonstrate disease-specific phenotypes in differentiated neurons (Nguyne *et al.,* 2011, Siebler *et al.,* 2011, Cooper *et al.,* 2012, Jiang *et al.,* 2012, Sanchez-Danes *et al.,* 2012). This study therefore attempted to generate DAergic IPSC-derived NGN2 neurons from mitochondrial disease patients harbouring a large scale mtDNA deletion (Kraytsberg *et al.,* 2006, Bender *et al.,* 2006). Initial experiments were performed to differentiate neurons into a homogeneous DA population. It was found that though DAergic neurons were produced, though a homogeneous TH neuronal positive population could not be generated.

Directed neuronal growth towards a DAergic subtype were conducted using morphogens such as sonic hedgehog (SHH) and fibroblast growth factor-8a (FGF8a) (Cooper *et al.,* 2010), with further neuronal maturation achieved through the addition of ascorbic acid, BDNF, GDNF and cAMP (Schneider *et al.,* 2007,Chambers *et al.,* 2009, Cooper *et al.,* 2010). The selection of which growth factors were added when, was determined through examination of the timings from the Kriks protocol (Kriks *et al.,* 2011). This lead to SHH, CHIR and Purmorphamine being added during neuronal proliferation and L-ascorbic acid, FGF8, and cAMP were then added to promote DAergic neuronal differentiation from NPCs to neurons. Studies have shown that increased CHIR expression can create hindbrain neurons, and contrastingly, little CHIR can cause neurons to undergo a rostral-directed differentiation (Kirkeby *et al.,* 2012). The concentration of supplements used within the Kriks *et al.,* (2011) and Hartfield *et al.,* (2014) protocols were replicated in this study, although a homogeneous DAergic neuronal population was not achieved.

Unfortunately, this study could not generate a homogenous DAergic population, with the addition of these factors, most likely dependant on the NGN2 differentiation protocol, which generates neurons within 8 days from NPCs. Perhaps, as many studies report that a longer time period is required (to actually successfully culture these neurons), not enough time was allowed to generate DAergic neurons (in this study only 8 days of neuronal growth) and therefore only created adverse effects on the cells. Rock inhibitor prevents apoptosis and, in this study, even in the presence of ROCKi, NPCs did not survive, as the DA supplements caused large amounts of cell death (Figure 5.4).

As the focus of this project was to observe the impact of mtDNA deletions in mitochondrial trafficking in PD, it was decided that the heterogeneous population of neurons would be utilised in experiments, containing a largely TH-positive population harbouring a large scale mtDNA deletion.

5.5.4 NGN2 neuronal subtype quantification

The proneural gene neurogenin 2 (NGN2), is a transcription factor crucial for neuronal differentiation (Fode *et al.,* 1998), but also for the generation of neuronal subtype-specification within the CNS (Ma *et al.,* 1999, Scardigli *et al.,* 2001). Within the ventral midbrain (VM) region,

NGN2 expression is crucial to mesencephalic DAergic neuron generation, showing that NGN2 plays a role in DAergic neuron development (Thompson *et al.,* 2006). Knockout *NGN2* mice have demonstrated a reduction in DA neuron number in the developing ventral midbrain in comparison to wild type postnatal mice, which suggests that, in the VM, NGN2 is involved in specific mesencephalic DAergic neuronal differentiation. As over 90% of the NGN2 neuronal population in this study stained positive for TH, it may be possible that NGN2 actually facilitates DAergic neuronal development in this cell line, without the addition of DAergic supplements (Andersson *et al.,* 2005).

Immunofluorescent analysis of these large scale mtDNA deletion neurons revealed the co-localised staining of TH, GABA and Glutamatergic neurons. This is interesting, in regard to our understanding of the nigrostriatal pathway, where DAergic and GABAergic neurons have been known to partake in the nigrostriatal pathway (Gonzalez-Hernandez *et al.,* 2001). Further investigation into this pathway has demonstrated that a nonDAergic pathway exists within the substantia nigra reticula which utilises GABA (Fibiger *et al.,* 1972, Hattori *et al.,* 1991, Rodríguez & González-Hernández, 1999). Experiments revealed that rat nigrotectal neurons co-express TH and GAD (involved in GABA synthesis, Campbell *et al.,* 1991) (GonzaÂlez-HernaÂndez *et al.,* 2001). Therefore, taken together, a particular proportion of DAergic nigrostriatal neurons express GABA and if differentiated NGN2 neurons favour developing mesencephalic neuronal subtypes, it can be hypothesised that the overlap in immunostaining could be predicted, as the neurophysiology of the nigrostriatal pathway comprises of this co-localisation.

Whilst TH and GABA have been found to co-localise in these studies, the co-expression of VGLUT1 and GABA was also observed. Abundant co-expression of VGLUT1 and GABA has been observed in cortical and hippocampal glutamatergic synapses (Kao *et al.,* 2004, Fattorini *et al.,* 2009, Zander *et al.,* 2010), where electrophysiological experiments hypothesise that GABA is co-released from glutamatergic hippocampal mossy fibre terminals (MFTs) during postnatal development (Walker *et al.,* 2001, Gutiérrez 2003). GABA functions as an inhibitory neurotransmitter and the GABAergic signalling machinery arises earlier than glutamatergic transmission, GABA synthesis occurs from glutamate via glutamate decarboxylase (GAD). During GABA synthesis, glutamate (an excitatory neurotransmitter) is converted into GABA (an inhibitory neurotransmitter) (Petroff, 2002, Schousboe, 2007). Therefore, the co-localisation of GABA and VGLUT1 observed in this experiment may reflect the presence of immature

excitatory glutamatergic neurons that are still undergoing the conversion into GABAergic neurons. Thus, it can be concluded that the large overlap in TH-GLUT-GABA co-localisation observed in this study may either be a combination of two factors i) NGN2 preference towards mesencephalic neuronal derivation and immature GABAergic neurons and/or ii) a heterogenous immature neuronal population which are still undergoing neuronal maturation and stain positive for all markers.

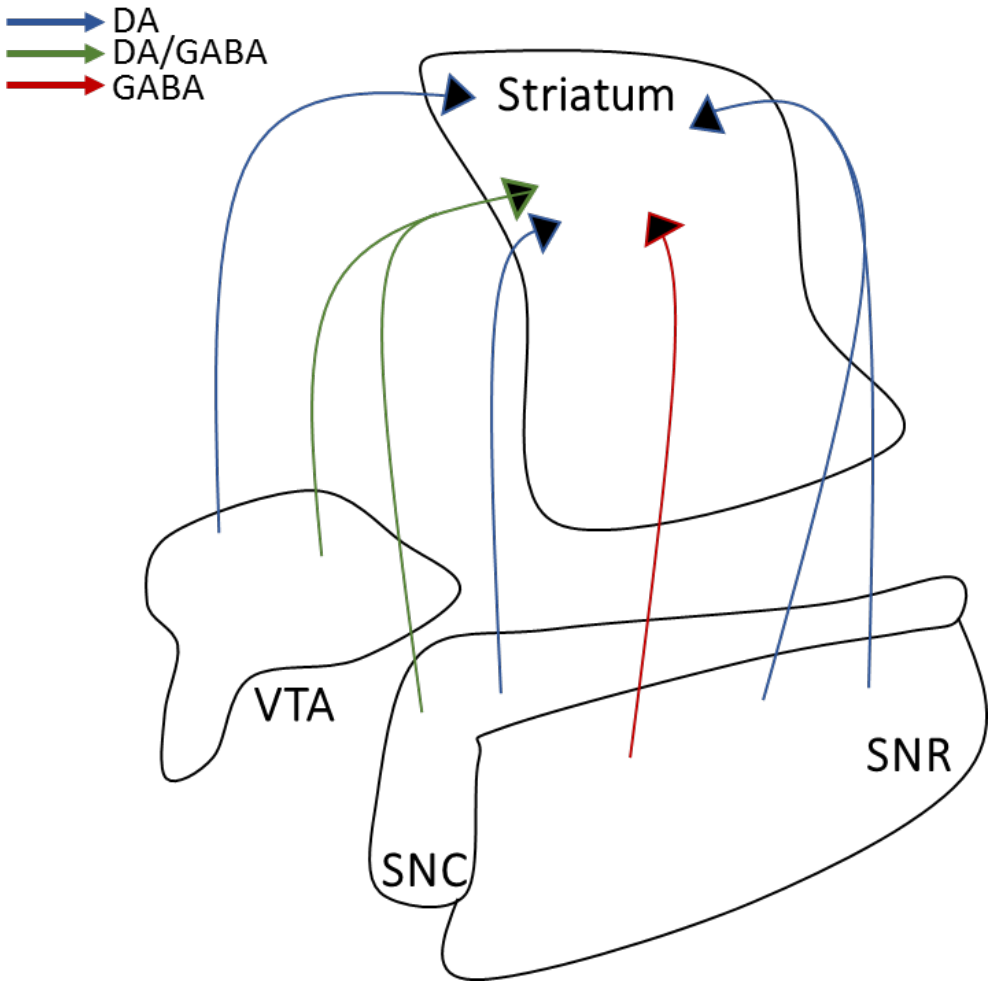

Figure 5.10. Mesostriatal projections. There are supposedly three mesostriatal pathways. The first DAergic pathway originates from DAergic midbrain nuclei (blue), the second GABAergic pathway (red) is derived from GAD67 positive neurons in the substantia nigra pars reticula (SNR) and finally the DAergic/GABAergic pathway (green) which arises from DAergic neurons (GAD65 mRNA positive) in the substantia nigra pars compacta (SNC) and the ventral tegmental area (VTA). (Figure adapted from GonzaÂlez-HernaÂndez *et al.,* 2001)

5.6 LIMITATIONS OF THIS STUDY

- Concentrations of the growth factors added to promote DAergic neuronal growth were taken from the Kriks *et al.,* protocol. It may have been that incorrect supplement concentrations were being administered to the NGN2 neurons, and therefore may have perturbed NPC differentiation. However, as this aim of this project was to observe mitochondrial movement in an IPSC model harbouring a mitochondrial defect, the following study continued to observe mitochondrial trafficking in a heterogeneous population of neurons, as NGN2 supports DAergic neurons.
- The overlap in the co-localisation of these neurotransmitters, firstly rendered the generation of a homogenous DAergic population a practically challenging task. Therefore, it was decided that both heteroplasmy cell lines would be differentiated into a heterogeneous neuronal population for all future experiments.
- Furthermore, this study did not measure mtDNA deletion levels after IPSC differentiation. Therefore, it remains undetermined whether the neuron still maintained an mtDNA deletion after differentiation, which may significantly affect the interpretation of the experimental results.

5.7 CONCLUSIONS & FUTURE WORK

These studies confirm decreased mitochondrial complex I and complex IV activity in the high heteroplasmy IPSCs in comparison to low heteroplasmy IPSCs. This model provides as a useful tool that provides insight to PD patients, since large scale mtDNA deletions are seen in affected neurons.

Future work in this study will include:

- Lentiviral transfection of a DA specific-GFP tag (under control of either the tyrosine hydroxylase or Dopamine transporter promoter) into NGN2 IPSCs to highlight dopamine expressing neurons within a heterogeneous population of neurons during live cell imaging. This tool will highlight DAergic neurons to be observed individually and therefore allow the analysis of mitochondrial movement within a solely DAergic neuronal population harbouring an mtDNA deletion, rendering it as a highly specific PD model.

CHAPTER SIX

Observing mitochondrial trafficking in neurons with a large scale mtDNA deletion

6.1 INTRODUCTION

6.1.1 ER- mitochondria Ca^{2+} signalling

The endoplasmic reticulum (ER) uses ATP-dependent transporters to take up Ca^{2+} from the cytoplasm into the ER lumen. As these Ca^{2+} stores are filled, cytosolic Ca^{2+} triggers the opening of ER Ca^{2+} channels letting Ca^{2+} ions flow back into the cytoplasm. Located near the mitochondria, this channel opening creates an increase in local Ca^{2+} concentration that drives Ca^{2+} influx into the mitochondrial matrix via MCUs (Szabadkai and Duchen, 2008). The high Ca^{2+} fluctuations that occur near the mitochondrion causes increased Ca^{2+} buffering activity, which leads to an inhibitory effect on Ca^{2+} release/influx channels and acts as a physiological regulator (Berridge, 2002, Pozzan and Rudolf, 2009).

Resting neuronal cellular Ca^{2+} concentration is around 1mM, at which most intracellular Ca^{2+} is bound to cytosolic proteins and/or retained by the ER (Figure 6.1). Free cytosolic Ca^{2+} is approximately 100nM, which upon stimulation can increase to 1µm (Meldolei and Pozzan, 1998). Within resting neurons, the total and free mitochondrial calcium ($_mCa^{2+}$) levels are low: 0.1mM and 100nM (Pozzo-miller *et al.,* 1997, Babcock and Hille, 1998). Within neuronal mitochondria, this leads to an increase of $_mCa^{2+}$ (100 – 500µM), as a direct consequence of increase cytosolic free Ca^{2+} (Cheng and Reynolds, 1998, Stork and YV, 2006).

The IP_3R (inositol 1,4,5-trisphosphate receptor) mediates interactions between the ER Ca^{2+} channel and the OMM; VDAC1 (Szabadkai 2006, Gomez-Suaga *et al.,* 2018). The close proximity of these two organelles at contact sites allows the formation of areas that meet the low affinity threshold of $_mCa^{2+}$ uptake mechanisms. Mitochondrial associated membranes (MAMs) assist with this Ca^{2+} handling as they are enriched with protein chaperones (Votyakova and Reynolds, 2001) such as calnexin and calreticulin which interact with IP_3Rs and SERCA2 (Sarco/endoplasmic reticulum ER-Ca^{2+} transport ATPases) to regulate Ca^{2+} signalling (Hayashi *et al,* 2009).

At the submicromolar level, the opening of the mitochondrial calcium uniporter (MCU) causes $_mCa^{2+}$ levels to increase to 0.2–3µM, if surrounding calcium levels are elevated. This triggers Ca^{2+} dependent enzymes such as (pyruvate-, α-ketoglutarate-, and isocitrate-dehydrogenases)

of the TCA cycle to generate more $NADH^{+}/NADPH^{+}$ (Bezprozvanny, 2009, Gibson *et al.,* 2010). Increased $_{m}Ca^{2+}$ also activates mitochondrial metabolism i.e. ATP supply for cellular processes (Halestrap, 2009). Mitochondria are highly sensitive to extracellular Ca^{2+}, with $_{m}Ca^{2+}$ levels determined by (i) Ca^{2+} influx through the mitochondrial calcium uniporter (MCU) which is driven by Δψm and (ii) Ca^{2+} efflux through the Na+/Ca^{2+} transporter (NCX) (Palty *et al.,* 2010). When extracellular Ca^{2+} is increased, exceeding the micromolar threshold, the matrix Ca^{2+} buffering activity ensures that $_{m}Ca^{2+}$ efflux remains constant, to efficiently control cellular Ca^{2+} signals (Szabadkai and Duchen, 2008).

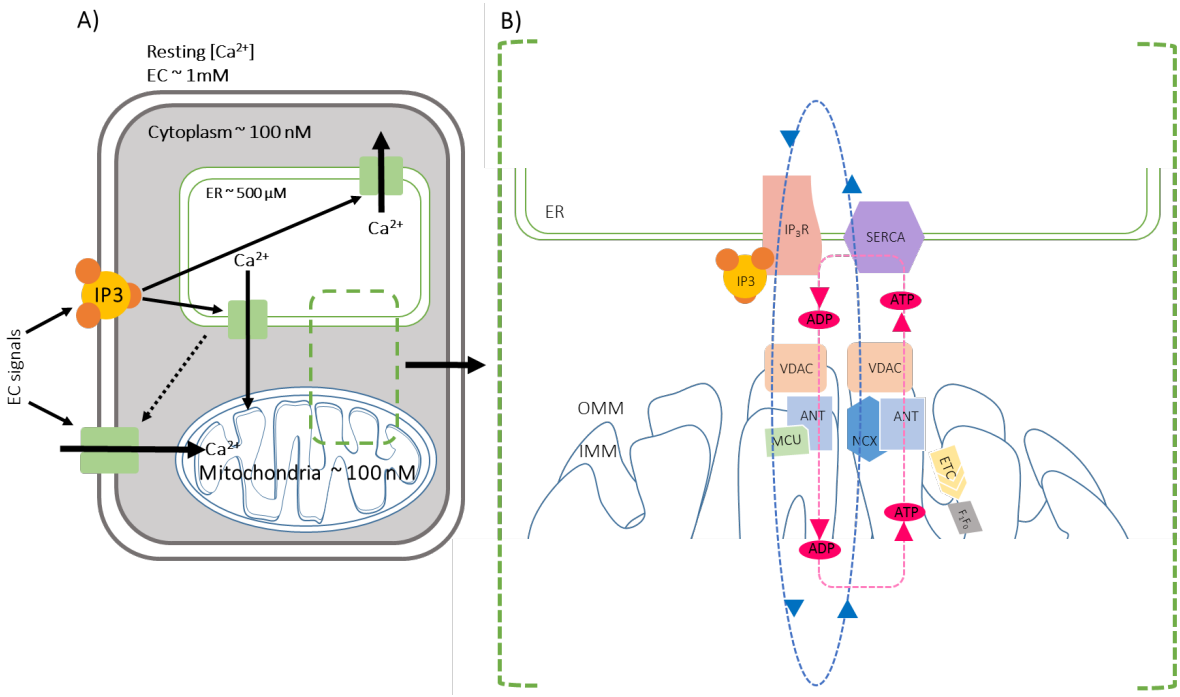

Figure 6.1. ER-Mitochondrial Ca2+ handling. A) Model of ER-mitochondria Ca^{2+} handling. The ER represents the large Ca^{2+} store, where basal level Ca^{2+} is approximately 10^{4} times higher than that within the cytoplasm and mitochondria (Szabadkai and Duchen,2008). Stimuli activate the formation of the IP_3 receptor (IP_3R), which leads to Ca^{2+} release from the ER. This in turn triggers a [Ca^{2+}] increase in the cytosol and [Ca^{2+}] reduction in the ER. **B)** Ca^{2+} and ADP/ATP micro domains are formed at the ER-mitochondrial contact regions that permit the direct control of ER Ca^{2+} content and direct Ca^{2+} channelling into the mitochondria. Ca^{2+} release from the ER occurs through the IP_3R, which supplies Ca^{2+} to mitochondria through the OMM voltage-dependent anion channel (VDAC) and the IMM Ca^{2+} uniporter (MCU). Limited mitochondrial Ca^{2+} loads upregulate mitochondrial ATP production [by supplying reducing equivalents to the electron transport chain (ETC and F_1F_0 ATPase), which is transported to the inner mitochondrial space by the concerted activity of the ATP/ADP translocase (ANT) and VDAC. The re-accumulation of Ca^{2+} into the ER lumen through the sarco-endoplasmic Ca^{2+} ATPase (SERCA) is directly controlled by the ATP supplied by mitochondria (Adapted from Szabadkai and Duchen,2008)

6.1.2 ER and mitochondrial involvement in PD

ER–mitochondria linked cellular processes are altered in PD, with such alterations including Ca^{2+} dysregulation, defects in axonal transport, and mitochondrial dysfunction (Winklhofer and Haass, 2010, Moreira *et al.,* 2010, Cozzolino and Carri, 2012, Surmeier *et al.,* 2017). Surmeier *et al.,* (2017) proposed that the autonomous pace making activity in SNpc DA neurons, (which maintains dopamine concentrations within the striatum) is sustained by specific voltage dependent L-type Cav1.3 channels, allowing Ca^{2+} influx that enhances cytosolic Ca^{2+} concentrations in these cells (Poupolo *et al.,* 2007, Guzman *et al.,* 2010).

Lewy body associated α-syn, localises to MAMS, and the presence of Lewy bodies is accompanied by signs of ER stress (Ryu *et al.,* 2002) (Figure 6.2). This interaction has been further supported by studies that showed within wild-type α-syn overexpressing cells, the co-localisation of ER and outer mitochondrial membrane protein; protein tyrosine phosphatase-interacting protein 51 (PTPIP51) (Cali *et al.,* 2012, Gómez-Suaga *et al.,* 2018).

Furthermore, overexpression of these mitochondrial markers lead to a loss of ER–mitochondria contacts. It was suggested that this overexpression interrupted mitochondria-ER Ca^{2+} exchange as well as ATP generation (Paillusson *et al.,* 2017), which may cause alerted organellar dynamics and perhaps even cell death. It has been shown that α-syn overexpression can alter Ca^{2+} homeostasis, autophagy (Winslow *et al.,* 2010), mitochondrial function and impair the ER (Mercados *et al.,* 2013).

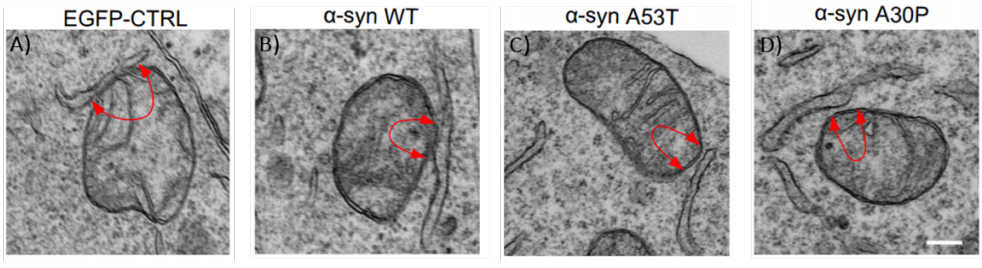

Figure 6.2. Overexpression of Wild-type and familial PD mutation carrying synuclein decreases ER–mitochondrial contacts. ER–mitochondria associations in SH-SY5Y cells. **A)** ER-mitochondrial contact observed in control SH-SY5Y cells, where these are reduced in **B)** EGFP-α-synuclein, **C)** EGFPα-synucleinA53T or **D)** EGFP-α-synucleinA30P expressing cells. Red arrowheads with loops indicate regions of reduced association. Scale bar is 200nM (Figure taken from Paillusson *et al.,* 2017)

This α-syn-ER association may modulate several pathways that are also perturbed within PD, some of which include Ca^{2+} homeostasis, mitochondrial dynamics and mitophagy. Therefore, these findings may provide as useful therapeutic targets and perhaps allowing the discovery of treatments for synucleinopathies including PD and DLB (Figure 6.3).

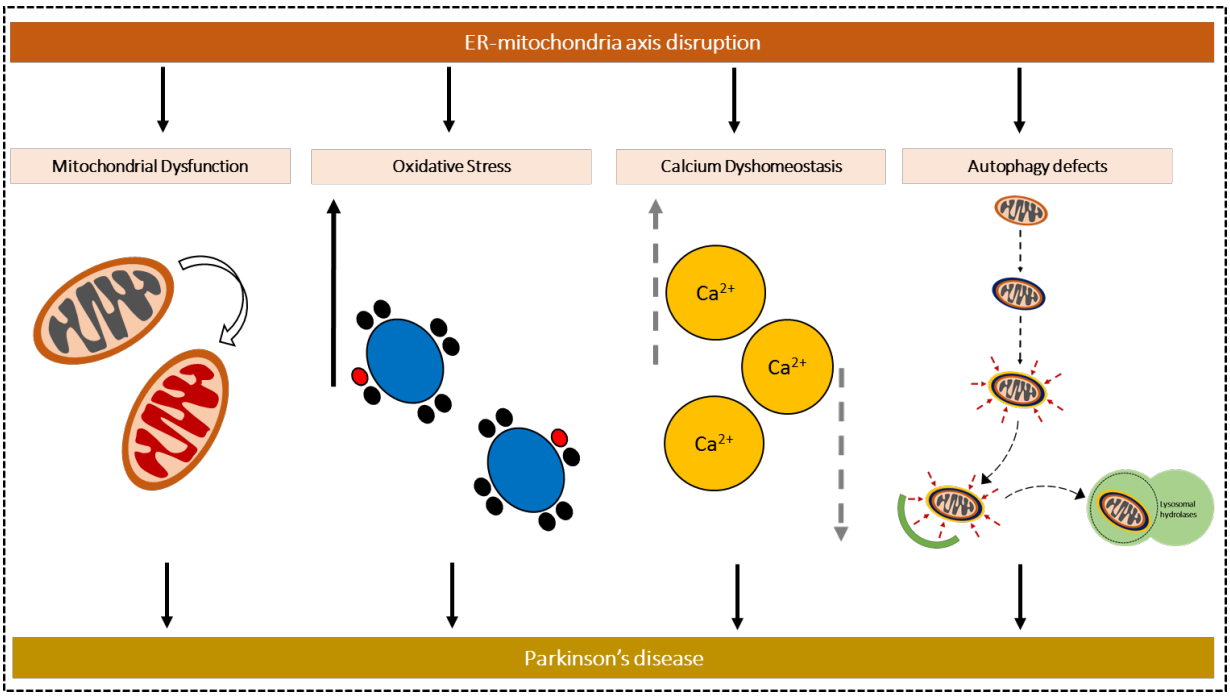

Figure 6.3. ER-mitochondria signalling in PD. The interaction between mitochondria and the MAMs of ER has been linked with different cellular functions. Mitochondrial dysfunction and oxidative stress bring the onset of free radical species (red dots) as a consequence of perturbed ER-mitochondrial Ca^{2+} handling. This Ca^{2+} dyshomeostasis is a standalone contributor to PD pathogenesis possibly effecting pace-making activity of SNpc DA neurons. ER-mitochondrial contacts have shown to be altered within mitochondrial dynamics, altering the mitochondrial motor-adaptor complexes that regulate the transport machinery. Furthermore, studies have described dysfunctional autophagy as a consequence of disrupted ER-mitochondria contacts in PD (Adapted from Gómez-Suaga, 2018).

6.1.3 The NCLX transporter

$_{m}Ca^{2+}$ release in neurons is regulated by a Na^{+}/ Ca^{2+} (NCX) exchanger (Baughman *et al.,* 2011). As the maximal rate of release (via the NCX exchanger) is much lower than the maximal rate of uptake (via MCU), $_{m}Ca^{2+}$ accumulation is observed when the cytosolic Ca^{2+} is high. The net effect of the $_{m}Ca^{2+}$ pathways is that this organelle contains little calcium in resting cells but begins to accumulate large amounts of calcium during stimulated Ca^{2+} entry (such as ischemia) to release this calcium overload in order to recover (Palty *et al.,* 2009). NCX exchange facilitates $_{m}Ca^{2+}$ efflux and is crucial in the maintenance of Ca^{2+} homeostasis (Philipson *et al.,* 2000). The NCKX protein family have a stoichiometry of $4Na^{+}/1Ca^{+}/1K^{+}$, divided into four groups, of which only NCX1–3 and NCKX1–4 are mammalian (Philipson *et al.,* 2000). The two families share a common catalytic core; called alpha 1 and 2 repeating domains (identified in DAergic neurons) which promote their exchange activity (Nicoll *et al.,* 1996, Philipson *et al.,* 2000, Palty *et al.,* 2004, 2010).

Palty *et al., (*2009) identified and characterised a novel NCX exchanger; NCLX, which is enriched in the mitochondria and localised in the cristae (Palty *et al.,* 2009). NCLX catalyses, Na^{+} or Li^{+}-dependent Ca^{2+} transport, with human NCLX expression first observed at the plasma membrane, with further research conducted into whether NCLX is linked to the mitochondrial exchanger. Studies determined that mitochondrial NCLX expressed in the mouse heart and brain exists as in an isoform of 50 and 70kDa respectively, with an additional 100kDa form in the mitochondrial fraction (Palty *et al.,* 2009).

6.1.4 $_{m}Ca^{2+}$ overload in neurons

Adult DAergic neurons in the SNpc lack significant intrinsic Ca^{2+} buffering capacity (Grobaski *et al.,* 1997; Puopolo *et al.,* 2007, Surmeier, 2007) putting them at risk from mitochondrial deficits (Surmeier, 2007). Furthermore, $_{m}Ca^{2+}$ overload renders DA neurons more susceptible to injury (Gandhi *et al.,* 2009), which is thought to occur due to an inability of the $_{m}Ca^{2+}$ shuttling system to handle large loads of Ca^{2+} within the mitochondria (Chan *et al.,* 2007). Recent studies indicate that $_{m}Ca^{2+}$ content is a crucial parameter in regulating mitochondrial transport (Chang *et al.,* 2011). Drugs used to inhibit the MCU complex, have revealed that blocking the MCU complex, in the presence of high cytoplasmic Ca^{2+} maintains mitochondrial movement, indicating an important role for MCU in regulation of Ca^{2+} influx and its effect on mitochondrial motility (Niescier *et al.,* 2013).

Kostic *et al.,* (2015) revealed that impairment of NCLX activity within PINK1 deficient neurons, is rescued by the Protein Kinase A (PKA) signalling pathway. Their study showed this rescue via direct phosphorylation of NCLX by PKA via Forskolin treatment (PKA agonist), which provides a regulatory mode of $_{m}Ca^{2+}$ efflux. Forskolin treatment served as a method to restore $_{m}Ca^{2+}$ efflux under PINK1 deficient conditions, protecting PINK1-deficient neurons from mitochondrial depolarisation via the opening of the permeability transition pore (mPTP) and dopamine-induced cell death (Figure 6.4).

It is therefore of high importance to understand the role of the NCLX transporter on $_{m}Ca^{2+}$ efflux and how this effects mitochondrial movement in neurons with a respiratory chain defect. This study will provide insight into how dysfunctional mitochondria are moved within neurons and how these systems may be altered with disease in order to supply the neuron with ATP.

This study consisted of *in vitro* analyses of mitochondrial transport within neurons differentiated from human induced pluripotent stem cells (IPSC), which harbor a large-scale mtDNA deletion (See chapter 5). Forskolin treatment was used to assess how PKA signalling effects $_{m}Ca^{2+}$ efflux, within neurons, to understand whether stimulation of $_{m}Ca^{2+}$ efflux would alter mitochondrial dynamics within neurons with a large level deletion similar to that observed in PD.

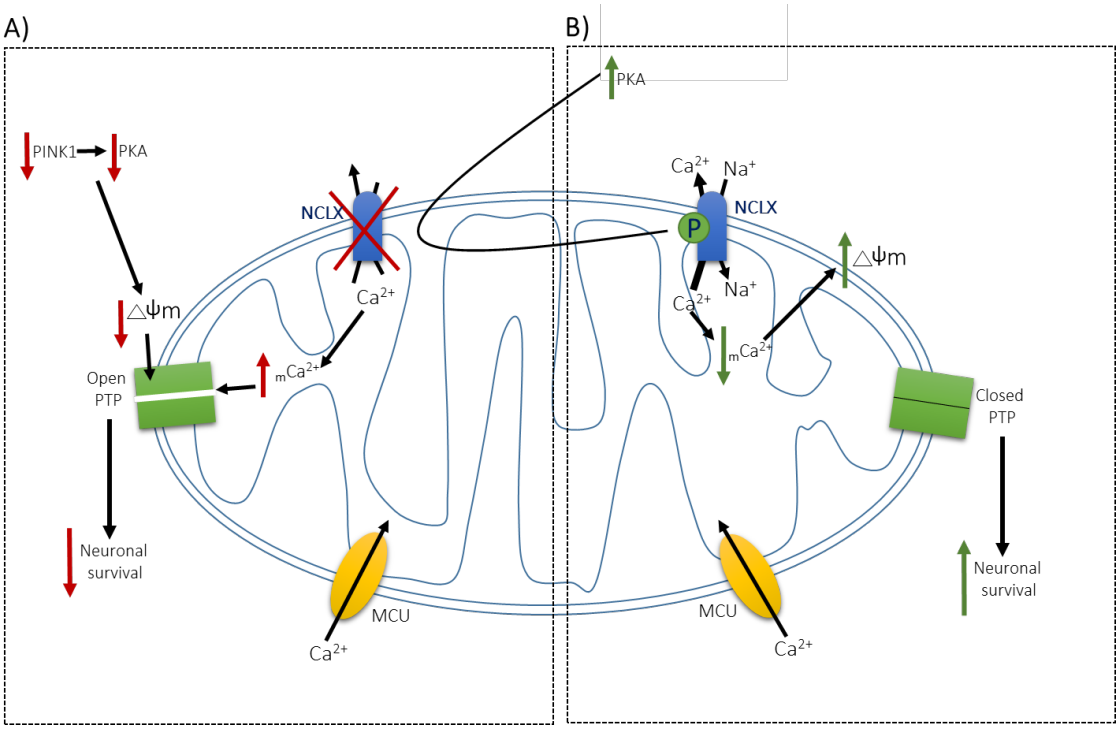

Figure 6.4. The rescue of $_{m}Ca^{2+}$ homeostasis via PKA-Mediated pathway in PINK1 deficient cells. A) PINK1 deficiency can cause mitochondrial damage through mitochondrial depolarisation, inhibiting the NCLX exchanger, which regulates the major Ca^{2+} efflux pathway in mitochondria. The consequential $_{m}Ca^{2+}$ overload, in addition to the mitochondrial depolarisation, opens the mitochondrial permeability transition pore. **B)** PKA activates NCLX via phosphorylation at S258 residue, which rescues its activity in PINK1-deficient neurons and causing a recovery of mitochondrial membrane potential, improving DA neuronal survival (Adapted from Kostic *et al.,* 2015).

6.2 AIMS OF THIS STUDY

After having characterized mitochondrial movements with ageing and in the presence of alpha-synuclein overexpression in a mammalian model (See Chapter 4), it was important to understand whether other effectors of mitochondrial transport i.e. mtDNA deletion and calcium modulation would play a role in a PD-like model. Importantly, this study would also reveal whether modulation of neuronal calcium handling might alter mitochondrial transport in the presence of a mitochondrial defect and whether this might offer therapeutic targets.

As a mitochondrial defect is observed in high heteroplasmy IPSCs (Russell *et al.,* 2018), this study aimed to understand the effect of mitochondrial dysfunction on calcium handling within these neurons and the impact of these changes on mitochondrial transport. Neurons were treated with Forskolin to observe the impact on axonal mitochondrial dynamics of increasing $_{m}Ca^{2+}$ efflux and thus increasing the availability of free calcium. It was hypothesised that mitochondrial transport would be disrupted due to mitochondrial dysfunction and that regulating $_{m}Ca^{2+}$ homeostasis within these neurons would alter these mitochondrial movements. An ability to be able to affect mitochondrial movements within neurons and thus alter their distribution within such cells may have benefit for neurodegenerative diseases.

The aims of this study therefore were to;

1. Understand mitochondrial trafficking in neurons harbouring a large-scale mtDNA deletion.
2. Carry out a Forskolin (PKA agonist) dose response curve to determine optimal dose for INGN2 neurons to observe $_{m}Ca^{2+}$ efflux within neurons harbouring a large scale mtDNA deletion
3. Compare the effects of Forskolin treatment on <10% and ~40% mtDNA deletion differentiated neurons.
4. Observe differences in $_{m}Ca^{2+}$ efflux and whether this alters mitochondrial trafficking by the NCLX transporter in these neurons.

6.3 MATERIALS & METHODS

6.3.1 Neuronal culture

Large-scale mtDNA deletion containing IPSCs were differentiated into neurons according to the methods described in (Chapter 2 – Methods and Materials section 2.1)

6.3.2 Forskolin treatment of neurons

6.3.2.1 Forskolin dose response curve

Stem cells were plated at a seeding density of $3x10^5$ cells/ml in a 24 well matrigel coated plate. A media change (Differentiation media + Forskolin) was conducted 24 hours before passaging, where cells were dosed with Forskolin at 5, 10, 50 and 100µM concentrations (doses determined by Kostic *et al., ,*2015). A media change containing differentiation media with 5nm TMRM was conducted prior to imaging.

6.3.2.2 Forskolin experiments

Once the optimum Forskolin dose was determined, neurons were treated at 10 and 50µM, 30 minutes before imaging. INGN2 neurons were dosed with Forskolin at two time points of neuronal culture firstly, as INGN2 stem cells 24 hours post passaging into differentiation media (Differentiation day 1) and 24 hours prior to fixation as mature neurons (Differentiation day 6). All INGN2 neurons were grown in glass bottom dishes (Ibidi) (seeding density $2.5x10^5$ cells) and were imaged with TMRM on Day 7. The above was repeated using H-89 (PKA inhibitor), though cells were only dosed at Day 1 and Day 6 and imaged on Day 7.

6.3.3 Forskolin western blot in neurons

6.3.3.1 Immunoblot Analysis

Conducted as described in Chapter 5 –Section 5.3.1. NCLX immunoblotting was performed as described previously (Palty *et al.,* 2010) using the following antibodies: custom-made antibody against NCLX (Palty *et al.,* 2004; 1:1,000, gift from Dr Marthe Ludtmann; UCL) and Alpha tubulin (Abcam, 1:500).

6.3.4 Ca^{2+} imaging

6.3.4.1 Fluo-4-am reconstitution

Fluo-4-AM (Thermo Scientific) was reconstituted in 280µl of chloroform (Sigma Aldrich), which was aliquoted into 20µl volumes that were left in the dark for 30minutes to allow the chloroform to evaporate.

6.3.4.2 Loading NGN2 neurons with live imaging dyes

NGN2 neurons were seeded at a density of 300,000 cells/mL in Ibidi glass bottom dishes. On the 7th day of neuronal differentiation, Fluo-4-AM aliquots were thawed and re-suspended in 3µl of DMSO (Sigma Aldrich), 3µl of Pluronic acid (Thermo Scientific) (which facilitates the solubilisation of water-insoluble dyes) of Fluo-4-AM, 5 nm TMRM and 993µl Neurobasal differentiation media. This solution was vortexed and existing media was removed and replaced with the staining solution. The dishes were incubated at 37°C for 10 minutes in the dark, and then at room temperature for another 10 minutes, also in the dark.

6.3.4.3 Ionomycin loading

All videos taken were 10 minutes in length. To determine the Rmax (a maximal increase in intracellular calcium consequently resulting in a maximum increase in fluorescence) (Yoshida and Plant, 1992) of Fluo-4-AM loading, after a measuring fluorescence for 1 minute at baseline, 1µM of ionomycin was added to the dish to induce cytosolic Ca^{2+} influx, where fluorescence was measured for another 5-8 minutes. Videos were captured at 1 frame/second for 5 minutes.

6.3.5 Mitochondrial movement analyses

6.3.5.1 Fluorescent TMRM ΔΨm Imaging **-** Conducted as described in Chapter 4 –Section 3.4.4.1

6.3.5.2 Mitochondrial movement analyses **-** Conducted as described in Chapter 3 –Section 3.4.4

6.3.5.3 Mitochondrial morphology analyses

Aspect ratio and form factor [(perimeter)^2/(4π x area)] analyses were conducted on low heteroplasmy neurons during Forskolin dose response optimisation. These experiments were conducted in low heteroplasmy neurons as an initial study to observe the effect of Forskolin on mitochondrial dynamics (fission/fusion) in these neurons. Results generated from this experiment were then taken and replicated within the high heteroplasmy neurons.

Aspect ratio measures the length-based ratio between the major and minor axes of an ellipse is equivalent for each mitochondrion; determining how round the mitochondria are. Whereas the form factor measures the length and degree of branching of mitochondria. Videos taken were converted into a series of TIFF images in NIS elements software, from which 3 TIFFS were selected, which most accurately represented the neuronal structures, prior to analysis. Cell body mitochondria were then analysed in Image J which comprised of a series of deconvolution steps, where brightness and the contrast of the image were adjusted to optimal levels, and following this sharpening, a binary filter was applied to simplify these images using a deconvolution plugin Image J to even this signal. This allowed the software to identify objects as mitochondria or not, dependant on mitochondrial area. In this way the complexity of the mitochondrial network were analysed via parameters generated according to individual organelles and reticular composites.

6.3.5.4 Statistical Analysis

A mixed-effect regression model was undertaken by Dr Alasdair Blain (Wellcome Centre for Mitochondrial Research) to model the effect of calcium efflux in neurons harbouring a large-scale mtDNA deletion. The data was decided to be plotted as logged values for visual aid only, due to the range in mitochondrial movement.. All data is presented as box and whisker plots that show the distribution of mitochondrial speed and distance values. Raw values for both parameters were logged after defining a moving mitochondrion as travelling above 0.005 μm/s and further than 0.01 μm/s.

6.4 RESULTS

6.4.1 Optimisation of Forskolin treatment in low heteroplasmy cells

Phosphorylation of NCLX via PKA through Forskolin treatment (PKA agonist) provides a method to regulate $_{m}Ca^{2+}$ efflux. Forskolin treatment has been shown to restore $_{m}Ca^{2+}$ efflux under PINK1 deficient conditions (Kostic *et al.,* 2015). This study investigated how PKA signalling effects $_{m}Ca^{2+}$ efflux (via Forskolin treating) in neurons harbouring a single, large-scale mtDNA deletion.

To ensure that Forskolin did not adversely affect mitochondrial function and to test for toxicity in these cell lines, low heteroplasmy stem cells were dosed with 0, 5, 10, 50, and 100µM of Forskolin, 24 hours prior to imaging, and loaded with TMRM, 30 minutes before imaging. In low heteroplasmy stem cells, treatment with Forskolin was not shown to have a significant effect on mitochondrial membrane potential, measured through TMRM intensity (Figure 6.5A).

Since it was thought that mitochondrial morphology in cells with a mitochondrial defect would be affected by Forskolin treatment, assessment of mitochondrial morphology was performed in treated and untreated cells, using aspect ratio (AR) and form factor (FF) analysis. AR determines whether the length based on the ratio between the major and minor axes of an ellipse is equivalent for each mitochondrion; and thus, determines how round mitochondria are, while FF measures the length and degree of branching of the mitochondria. AR analysis on dosed stem cells showed that mitochondrial sphericity was slightly increased in comparison to DMSO treated cells when dosed with 5 and 10µM Forskolin (not significant). While, Forskolin treatment at 50µM and 100µM caused a slight decrease in mitochondrial connectivity (not significant) (Figure 6.5B). FF analyses revealed a slight decrease in branching of mitochondria when dosed with Forskolin (at all concentrations) compared to untreated cells, though these results did not reach significance (Figure 6.5C). These data show that mitochondrial morphology in the low heteroplasmy IPSCs was unaffected by Forskolin doses, this study thus continued with the doses previously used (Kostic *et al.,* 2015) for the remainder of the experiments.

Forskolin treatment (PKA agonist) occurs via direct phosphorylation of serine residues on the NCLX transporter. NCLX which acts to regulate $_{m}Ca^{2+}$ efflux. To ensure NGN2 neurons express the NCLX exchanger protein, western blot analysis was conducted in low heteroplasmy neurons

(Figure 6.5D). NCLX expression in these neurons were observed bands at 55 and 100kDa (reported in brain tissue due to the various isoforms of NCLX) and/or nonspecific antibody binding, Palty *et al.,* 2004 (Figure 6.5E). These experiments used a custom-made antibody against NCLX (Palty *et al.,* 2004; 1:1,000 and 1:2,000), a kind gift from Dr Marthe Ludtmann from the Kostic group (UCL). Though the western blot from iPS cells is not as clear as the blot from isolated mitochondria (Figure 6.5E), taken together with the following calcium data it indicates that NCLX is expressed within experimental iPSC derived neurons.

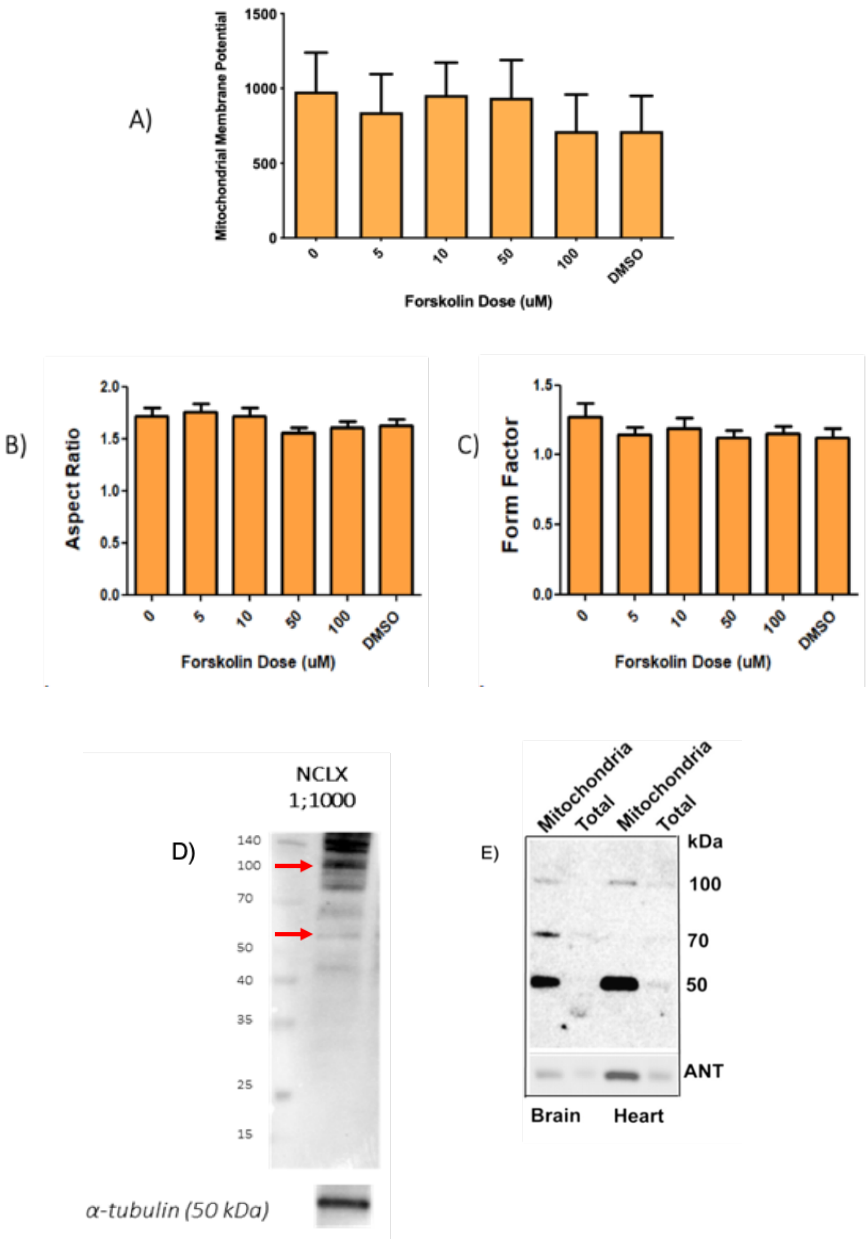

Figure 6.5. Forskolin dose response and NCLX western blot. A) The effect of Forskolin treatment on mitochondrial membrane potential was assessed in low heteroplasmy stem cells. Forskolin treatment had no significant effect in low heteroplasmy stem cells. **B)** Aspect ratio (AR) was found to be unaffected by various doses of Forskolin. **C)** Form factor (FF) analyses showed no significant effect on mitochondrial branching upon Forskolin treatment. **D)** Immunoblot optimisation of NCLX antibody in low heteroplasmy neurons. 20 µg protein was loaded for each sample (NCLX antibody (1;1000). Bands were expected at 55 and 100 kDa. Additional bands were detected at ~140kDa (could either suggest dimerisation and/or nonspecific antibody binding). Alpha tubulin was included as a loading control. **E)** Immunoblot of cellular and mitochondrial fractions of HEK-293-T cells overexpressing mouse NCLX (10 µg) derived from brain and heart tissues. Bands were detected at 50, 70 and 100 kDa (Figure taken for comparison from Palty *et al.,* 2004)

6.4.2 Mitochondrial movement in Forskolin treated neurons harbouring a single, large scale mtDNA deletion

This study utilised IPS cell lines harbouring low (<1%) and high (~40%) levels of a single, large-scale mtDNA deletion (spanning 6017 base pairs from m.7777-13794). As the level of mtDNA deletion was so low in the low heteroplasmy cell line, the line served as an isogenic control.

Mitochondrial dysfunction in PD can be driven by mtDNA deletions (Bender *et al.,* 2006, Kraystberg *et al.,* 2006). The experiments described below aimed to understand whether mitochondrial movement was affected by mtDNA deletion and whether the level of mitochondria Ca^{2+} efflux ($_{m}Ca^{2+}$) further altered these dynamics. Mitochondrial movement parameters: speed, directionality (anterograde and retrograde movement) and distance travelled were analysed and compared for both cell lines via imaging TMRM loaded NGN2 neurons (Figure 6.6A). Mitochondrial motility was quantified via kymograph analyses (Figure 6.6B).

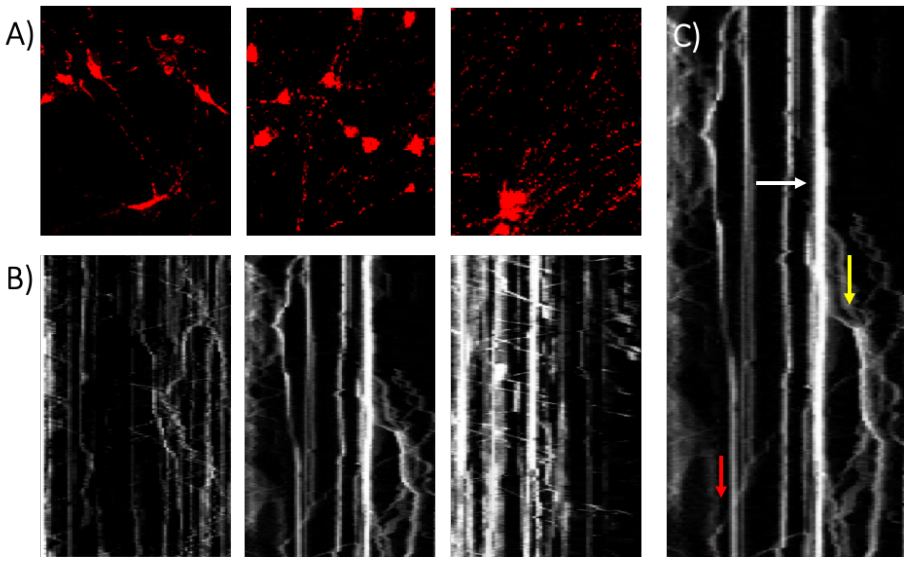

Figure 6.6. Tracking mitochondrial movement after in NGN2 neurons. A) TMRM snapshots of videos taken of low heteroplasmy neurons loaded with 5nm TMRM (Scale bars: 100 µm). **B**) Kymographs generated tracking in vitro mitochondrial movement in low heteroplasmy neurons, which were then analysed for speed and distance values. C) Arrows indicating directionality in mitochondrial movement observed in kymographs: Retrograde (Red), stationary (white) and anterograde (yellow).

6.4.2.1 Static versus moving mitochondria in neurons treated with Forskolin

Similar, to the thresholds set in Chapter 4 (*Ex vivo imaging of mitochondrial trafficking in dopaminergic neurons*) mitochondrial movements in this study were segregated into two populations: 'stationary' (0-0.005µm/s) and 'motile' (0.005µm/s and above). For all the movement parameters mixed model statistics was carried out to observe whether in this study, significant differences were observed between cell lines (mitochondrial movement was altered between both heteroplasmy neurons) and Forskolin dose (differences observed between dosed neurons and untreated controls).

Comparing the total percentage of moving mitochondria between both cell lines, lead to the following observations; i) Cell line with neurons exhibit more moving mitochondria (58.27% moving) than low heteroplasmy neurons (31.59% moving) and ii) in both cell lines, increasing the Forskolin dose, displayed a trend of increased mitochondrial movements (consequently reducing the number of mitochondria that are stationary) when compared to untreated controls. Furthermore, the variability in the number of mitochondria observed in this study does not reflect a reduction in mitochondrial mass in the treated cells, but rather the number of neurons which were suitable for imaging and subsequent analysis (Figure 6.7).

A)

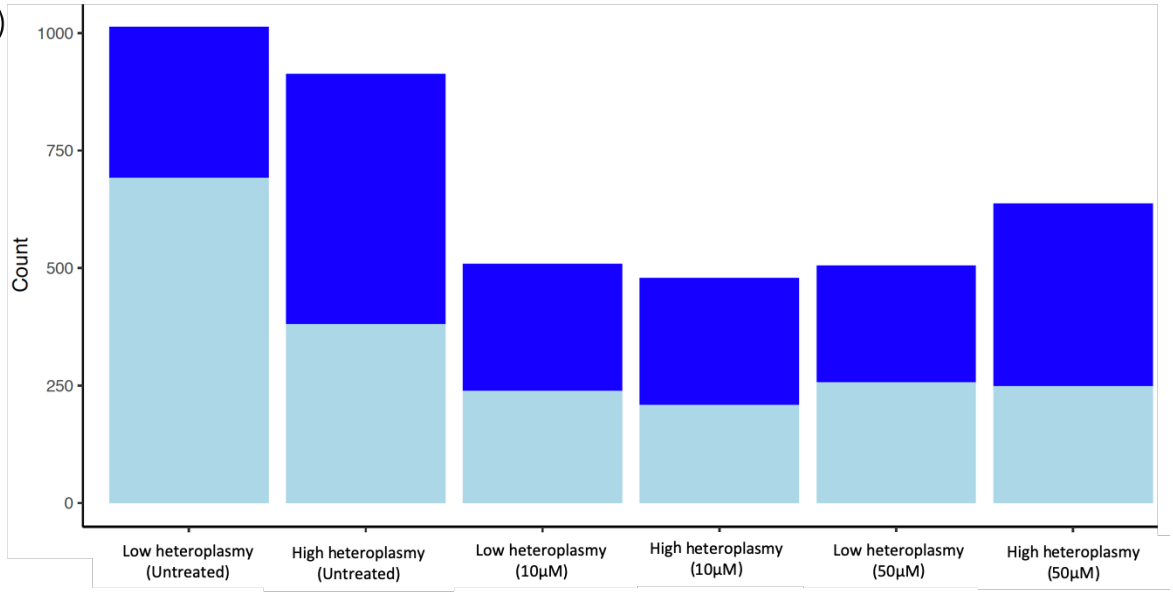

B)

Experiment	N = Total number of mitochondria	Number of moving mitochondria	Moving (%)	Stationery (%)
Low heteroplasmy (Untreated)	1013	320	31.59	68.41
High heteroplasmy (Untreated)	913	532	58.27	41.73
Low heteroplasmy (10µM)	509	270	53.05	46.95
High heteroplasmy (10µM)	479	270	56.37	43.63
Low heteroplasmy (50µM)	505	247	48.91	51.09
High heteroplasmy (50µM)	637	388	60.91	39.09

Figure 6.7. Proportion of mitochondrial movement in Forskolin dosed neurons. A) Plot shows the mean percentage of mitochondria that are stationary (light blue) and moving (dark blue) across three experiments. **B)** Table showing the percentage of stationary versus moving mitochondria for untreated and Forskolin dosed neurons. Overall, less mitochondrial movement was observed in the dosed and control low heteroplasmy neurons compared to high heteroplasmy neurons. N=3 repeats.

6.4.2.2 Mitochondrial Speed

Via kymograph analysis this study found that in untreated cells, the mean mitochondrial speed was significantly lower in high heteroplasmy neurons (0.196 µm/s ± 0.121 (Log -1.950 ± 0.989), [N=532 moving mitochondria]) compared to the low heteroplasmy cells (0.287 µm/s ± 0.329 (Log -2.121 ± 1.582), [N=320 moving mitochondria]) ($p<0.0001$) (Figure 6.8).

When dosed with 10µM Forskolin, the ~40% mtDNA deletion neurons showed reduced mitochondrial speed to (0.057 µm/s ± 0.067, (Log -3.414µm/s ± 1.058) [N=270 moving mitochondria]) compared to their respective untreated controls ($p<0.0001$). Similar reduction was observed in the <10% mtDNA deletion to (0.042µm/s ± 0.071 (Log -3.691 µm/s ± 0.926), [N=270 moving mitochondria]) ($p<0.0001$). Significant differences in mitochondrial speed were also observed between both cell lines ($p<0.0001$) upon Forskolin treatment, with high heteroplasmy neurons showing a higher mean speed (Figure 6.8).

At 50µM Forskolin dose, the average speed of mitochondria in both cell lines were again found significantly decrease to (0.041µm/s ± 0.079 (Log -3.720 µm/s ± 0.922), [N=247 moving mitochondria]) ($p<0.0001$) and (0.079 µm/s ± 0.189 (Log -3.342 µm/s ± 1.161), [N=388 moving mitochondria]) ($p<0.0001$) respectively, compared to untreated controls. Significant differences in mitochondrial speed were observed between the cell lines ($p<0.0001$) (Figure 6.8), with high heteroplasmy neurons again showing faster, mean mitochondrial speeds.

Overall, this indicates that in neurons harbouring a mtDNA deletion, there are significant reductions in the mean speed of mitochondrial movements with Forskolin treatment. Significant differences were also detected between the cell lines at each dose with mitochondria in high heteroplasmy neurons showing a slightly faster speed.

A)

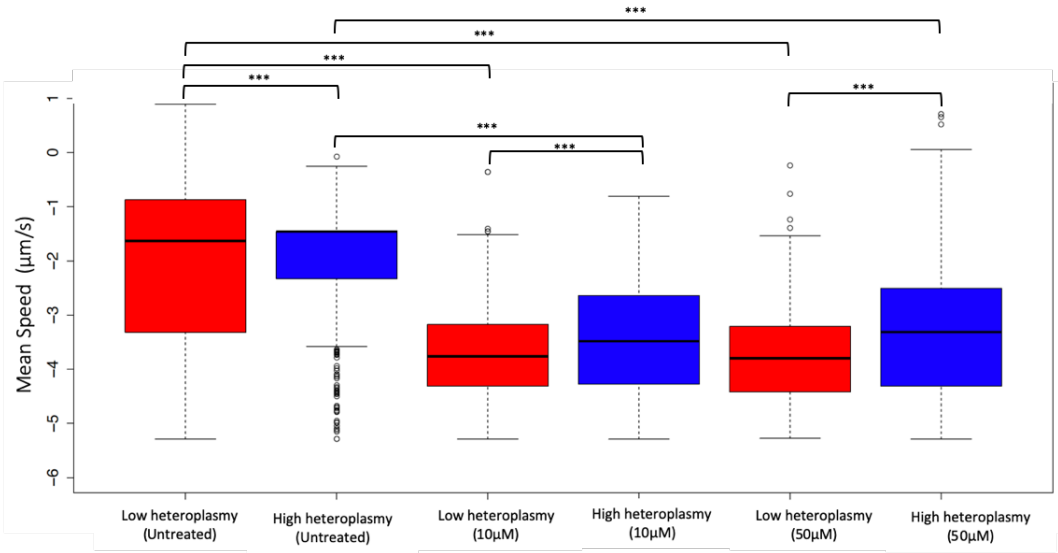

B)

Experiment	Number of moving mitochondria	Mean Speed ± SD (µm/s) (Logged)	Mean Speed ± SD (µm/s)
Low heteroplasmy (Untreated)	320	-2.121 ± 1.582	0.287 ± 0.329
High heteroplasmy (Untreated)	532	-1.950 ± 0.989	0.196 ± 0.121
Low heteroplasmy (10µM)	270	-3.691 ± 0.926	0.042 ± 0.071
High heteroplasmy (10µM)	270	-3.414 ± 1.058	0.057 ± 0.067
Low heteroplasmy (50µM)	247	-3.720 ± 0.922	0.041 ± 0.079
High heteroplasmy (50µM)	388	-3.342 ± 1.161	0.079 ± 0.189

C) Mixed model statistics for speed of mitochondrial movement in Forskolin dosed neurons

	AIC	BIC	LogLik		
	6270.416	6304.09	-3129.208		
	Value	**Standard Error**	**DF**	**T-Value**	**P-Value**
Intercept	-1.9432263	0.07075873	2021	-27.462709	0.0001
Forskolin 10 µM	-1.4815239	0.06292351	2021	-23.544839	0.0001
Forskolin 50 µM	-1.4483936	0.05984375	2021	-24.202923	0.0001
Cell line	-0.2651813	0.05208165	2021	-5.091645	0.0001
Number of observations	2027				
Number of technical repeats	3				

Figure 6.8. Mitochondrial speed in Forskolin dosed neurons. Values are logged to aid visualisation. Box and whisker plot showing the mean (represented by the black line) and spread of data. **A)** Mean mitochondrial speed was significantly lower in high heteroplasmy cells compared to the low heteroplasmy cell line ($p<0.0001$). On 10µM Forskolin treatment, the mean speed of mitochondria in bot cell lines were reduced compared to their respective untreated controls ($p<0.0001$). At 50µM Forskolin dose the average speed of mitochondria in both cell lines was also found to significantly decrease ($p<0.0001$) compared to untreated controls. Significant differences in mitochondrial speed were also observed between the cell lines ($p<0.0001$). **B)** Statistics table for each Forskolin dose for each cell line in this study comparing: number of moving mitochondria of the total mitochondria and their mean speed (logged) and mean speed. N=3 biological repeats for all experiments. **C)** The model intercept represents differences in the speed of mitochondrial movements between the cell lines and Forskolin doses.

6.4.2.3 Distance

In order to understand the how far mitochondria move within the axons of these neurons, the mean distance of mitochondrial movements was calculated.

It was found that the mean distance travelled by ~40% deletion neurons displayed a mean distance of (30.923 µm ± 27.291 (Log 2.746 µm ± 1.412) [N=578 total mitochondria]), significantly higher than in <10% deletion neurons (12.547 µm ± 14.914 (Log 1.757 µm ± 1.377) [N=487 travelling mitochondria]) ($p<0.0001$) (Figure 6.9).

When dosed with 10µM Forskolin, a significant decrease in distance travelled was seen in ~40% deletion neurons (16.119 µm ± 18.968 (Log 2.076 µm ± 1.260) [N=429 travelling mitochondria]) ($p=0.0134$) compared to their respective untreated controls. A significant increase in the distance that mitochondria travelled was observed in the <10% deletion cell line (14.309 µm ± 15.789 (Log 2.035 µm ± 1.197) [N=452 travelling mitochondria]). Further differences in mitochondrial distance were also observed between the cell lines ($p<0.0001$) (Figure 6.9) at this dose.

Finally, upon treatment with 50µM Forskolin, the ~40% deletion neurons displayed a decrease in mean mitochondrial distance travelled to (18.702 µm ± 21.992 (Log 2.219 µm ± 1.287) [N=573 travelling mitochondria]) ($p=0.0037$) compared to their respective untreated controls. In contrast, average distance travelled of mitochondria in the <10% deletion neurons were found to significantly increase to (12.899 µm ± 14.658 (Log 1.871 µm ± 1.242) [N=445 travelling mitochondria]). Significant differences in mitochondrial distance were also observed between the cell lines at this concentration of Forskolin ($p<0.0001$) (Figure 6.9).

Overall, with increased Forskolin concentration, mitochondrial distance travelled was significantly increased within the lower mtDNA deletion cell line, with a decrease in distance travelled observed in the ~40% deletion neurons . Significant changes in mitochondrial distance travelled were also observed between both the cell lines.

A)

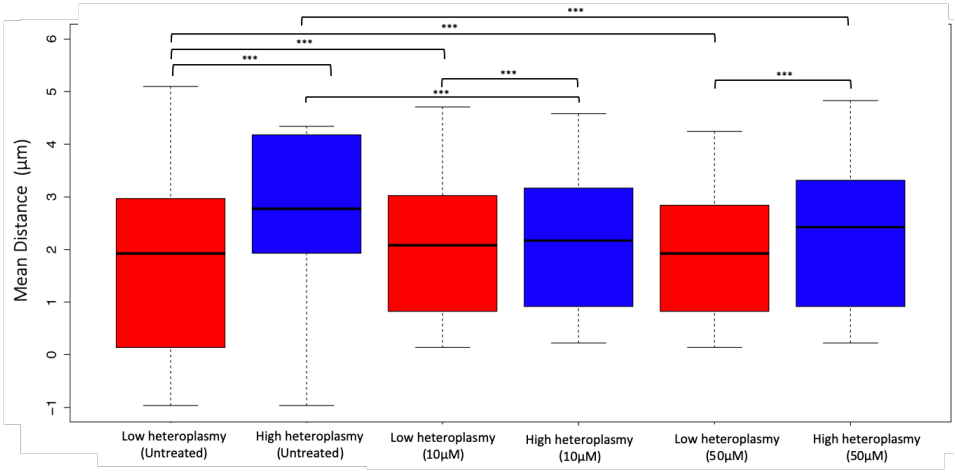

B)

Experiment	N = Number of mitochondria	N = Number of travelling mitochondria	Mean Distance travelled ± SD (µm) (Log)	Mean Distance travelled ± SD (µm)
Low heteroplasmy (Untreated)	1013	487	1.757 ± 1.377	12.547 ± 14.914
High heteroplasmy (Untreated)	913	578	2.746 ± 1.412	30.923 ± 27.291
Low heteroplasmy (10µM)	509	452	2.035 ± 1.197	14.309 ± 15.789
High heteroplasmy (10µM)	479	429	2.076 ± 1.260	16.119 ± 18.968
Low heteroplasmy (50µM)	505	445	1.871 ± 1.242	12.899 ± 14.658
High heteroplasmy (50µM)	637	573	2.219 ± 1.287	18.702 ± 21.992

C) Mixed model statistics for distance of mitochondrial movement in Forskolin dosed neurons

AIC	BIC	LogLik
9977.537	10013.49	-4982.768

	Value	Standard Error	DF	T-Value	P-Value
Intercept	2.4480023	0.18581297	2958	13.174550	0.0001
Forskolin 10 µM	-0.1468414	0.05937269	2958	-2.473214	0.0134
Forskolin 50 µM	-0.1661663	0.05723763	2958	-2.903095	0.0037
Cell line	-0.4695687	0.04809592	2958	-9.763172	0.0001
Number of observations	2964				
Number of groups	3				

Figure 6.9. Mitochondrial distance in Forskolin dosed neurons. Values are logged to aid visualisation. Box and whisker plot showing the mean (represented by the black line) and spread of data. **A)** Mean distance travelled by mitochondria in low heteroplasmy neurons was lower than what was observed in the high heteroplasmy neurons ($p<0.0001$). When dosed with 10µM Forskolin, a significant increase in the distance travelled was observed in the low heteroplasmy cell line, with a significant decrease in distance travelled observed in high heteroplasmy neurons ($p=0.0134$) compared to their respective untreated controls. With 50µM Forskolin, the mean distance travelled of mitochondria in low heteroplasmy neurons increased, in contrast to the high heteroplasmy neurons which again displayed a decrease in mean mitochondrial distance travelled ($p=0.0037$) compared to their respective untreated controls. Significant differences in mitochondrial distance were also observed between the cell lines at this concentration of Forskolin ($p<0.0001$). **B)** Statistics table for each Forskolin dose for each cell line in this study comparing: total number of mitochondria, total number of travelling mitochondria, their mean distance (logged) and mean distance. N=3 biological repeats for all experiments. **C)** The model intercept represents difference in the distance travelled of mitochondrial movement between the cell line and Forskolin doses.

6.4.2.4 Anterograde moving mitochondria – Speed

The motile pool of mitochondria found within both lines was then analysed for directionality, to observe whether the presence of an mtDNA deletion can affect anterograde (+) and retrograde (-) mitochondrial movements.

The percentage of anterograde moving mitochondria (those moving away from the cell body) within low heteroplasmy neurons was 12.14% (mean speed = 0.343 ± 0.323 [Log -1.669 µm/s ± 1.283]). This was slightly higher than for mitochondria within high heteroplasmy neurons exhibiting 11.50% anterograde movement (mean speed= 0.193 µm/s ± 0.153 [Log -2.019 µm/s ± 0.959]), though this increase did not reach significance (Figure 6.10).

When dosed with 10µM Forskolin, in the ~40% deletion neurons, a large decrease in anterograde movements from 11.50% to 3.76% was observed, again followed by a decrease in mean speed (mean speed= 0.074 µm/s ± 0.088 [Log -2.959 µm/s ± 0.769]) compared to untreated controls. In the <10% deletion cell lines anterograde movements increased from 12.14% to 14.34%, though this was associated with a decrease in mitochondrial mean speed (mean speed= 0.052µm/s ± 0.045 [Log -3.258 µm/s ± 0.747]) compared to untreated controls. ($p<0.0001$) (Figure 6.10).

With a 50µM Forskolin dose, ~40% deletion neurons demonstrated a slight increase in anterograde movements to 13.19%, also followed by a decrease in mitochondrial mean speed (mean speed= 0.077 µm/s ± 0.074 (Log -2.936 µm/s ± 0.883). The percentage of anterograde moving mitochondria decreased in <10% deletion cell lines to 9.90%, which was followed by a decrease in speed (mean speed= 0.069µm/s ± 0.118 [Log -3.201µm/s ± 0.881]) compared to untreated controls., both observations were significantly different when compared to untreated controls ($p<0.0001$) (Figure 6.10)

Overall, the speed of anterograde mitochondrial transport was found to be significantly reduced with Forskolin treatment compared to control experiments, although these differences were not observed between both cell lines treated with the same dose.

A)

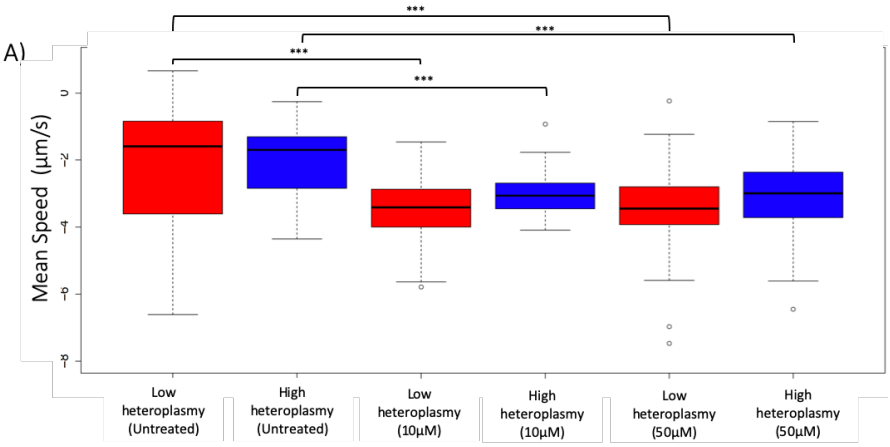

B)

Experiment	Anterograde moving mitochondria (%)	Mean Speed ± SD (µm/s)
Low heteroplasmy (Untreated)	12.14	0.343 ± 0.323
High heteroplasmy (Untreated)	11.50	0.193 ± 0.153
Low heteroplasmy (10µM)	14.34	0.052 ± 0.045
High heteroplasmy (10µM)	3.76	0.074 ± 0.088
Low heteroplasmy (50µM)	9.90	0.069 ± 0.118
High heteroplasmy (50µM)	13.19	0.077 ± 0.074

C) Mixed model statistics for the speed of anterograde mitochondrial movement in Forskolin dosed neurons

	AIC	BIC	LogLik		
	9977.537	10013.49	-4982.768		
	Value	Standard Error	DF	T-Value	P-Value
Intercept	-1.86819	0.08600	449	-21.722	0.0001
Forskolin 10 µM	-1.38729	0.12816	449	-10.825	0.0001
Forskolin 50 µM	-1.19305	0.11137	449	-10.713	0.0001
Cell line	0.07028	0.09996	449	0.703	0.482
Number of observations	453				
Number of groups	3				

Figure 6.10. Mitochondrial speed of anterograde moving mitochondria in Forskolin dosed neurons. Values are logged to aid visualisation. Box and whisker plot showing the mean (represented by the black line) and spread of data **A)** The percentage of anterograde moving mitochondria within low heteroplasmy neurons was higher than for mitochondria within high heteroplasmy neurons exhibiting 11.50% anterograde movement. On 10µM Forskolin, anterograde movements of mitochondria in low heteroplasmy neurons increased from 12.14% to 14.34%, associated with a decrease in mitochondrial mean speed compared to untreated controls. A decrease in anterograde movements 11.50% to 3.76%, was observed in the high heteroplasmy neurons, followed by a decrease in mean speed compared to untreated controls ($p<0.0001$). At 50µM Forskolin dose, the percentage of anterograde moving mitochondria decreased in the low heteroplasmy neurons to 9.90%, which was followed by a decrease in speed compared to untreated controls. High heteroplasmy neurons demonstrated a slight increase in anterograde movements to 13.19%, followed by a decrease in mitochondrial mean speed, significantly different when compared to untreated controls ($p<0.0001$). **B)** Statistics table for each Forskolin dose for each cell line in this study comparing: Percentage anterograde moving mitochondria and their mean speed. N=3 biological repeats for all experiments. **C)** Mixed model intercept represents differences in the speed of anterograde mitochondrial movement.

6.4.2.5 Anterograde moving mitochondria – Distance

Following the observations of the speed of anterograde mitochondrial movements, this study then observed the distance travelled of these mitochondria.

It was found that in the untreated controls, mitochondria within ~40% mtDNA deletion neurons displayed a slightly lower mean distance travelled (mean distance= 13.607 µm ± 12.511 [Log 2.339µm ± 0.704) when compared to the <10% mtDNA deletion neurons (mean distance= 18.527µm ± 18.473 [Log 2.472µm ± 1.061) (Not significant) (Figure 6.11)

On 10µM Forskolin, the distance travelled of anterograde moving mitochondria was found to increase in both cell lines (low (mean distance= 24.359 µm ± 15.832 [Log 2.991 µm ± 0.684) and high (25.996 µm ± 18.982 [Log 2.925µm ± 0.936]) respectively, compared to controls ($P<0.0001$).

Similarly, upon 50µM Forskolin dosing, the distance travelled of anterograde moving mitochondria was found to increase in both cell lines (low (21.571µm ± 14.284 [Log 2.816 µm ± 0.812) and high (28.129 µm ± 19.211 [Log 3.090µm ± 0.754) mtDNA deletion neurons ($P<0.0001$) (Figure 6.11).

Therefore, the distance travelled of anterograde moving mitochondria were found to be significantly increased with Forskolin treatment in neurons compared to controls, though these differences were not observed between the cell lines treated with the same dose. Though anterograde mitochondria are moving slower, they appear to be covering longer lengths; especially the mitochondria within the high heteroplasmy neurons which overall move farther.

A)

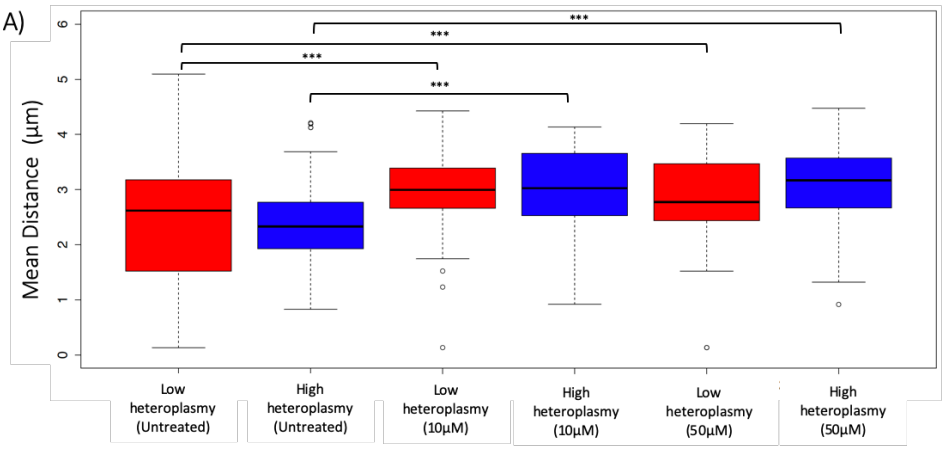

B)

Experiment	Mean Distance travelled ± SD (µm)
Low heteroplasmy (Untreated)	18.527 ± 18.473
High heteroplasmy (Untreated)	13.607 ± 12.511
Low heteroplasmy (10µM)	24.359 ± 15.832
High heteroplasmy (10µM)	25.996 ± 18.982
Low heteroplasmy (50µM)	21.571 ± 14.284
High heteroplasmy (50µM)	28.129 ± 19.211

C) Mixed model statistics for the distance travelled for anterograde mitochondrial movement in Forskolin dosed neurons

	AIC	BIC	LogLik		
	9977.537	10013.49	-4982.768		
	Value	**Standard Error**	**DF**	**T-Value**	**P-Value**
Intercept	2.417180	0.071450	483	33.830	0.0001
Forskolin 10 µM	0.565665	0.103574	483	5.461	0.0001
Forskolin 50 µM	0.571513	0.090240	483	6.333	0.0001
Cell line	-0.004788	0.081454	483	-0.059	0.953
Number of observations	487				
Number of groups	3				

Figure 6.11. Mitochondrial distance travelled of anterograde moving mitochondria in Forskolin dosed neurons. Values are logged to aid visualisation.Box and whisker plot showing the mean (represented by the black line) and spread of data **A)** In the untreated controls low heteroplasmy neurons displayed a slightly higher mean distance travelled compared to the high heteroplasmy (Not significant). On 10µM Forskolin, the distance travelled of anterograde moving mitochondria was found to increase in both cell lines compared to their untreated controls (P<0.0001). On 50µM Forskolin dose, distance travelled of anterograde moving mitochondria was found to increase in both cell lines heteroplasmy neurons (P<0.0001). N=3 biological repeats for all experiments. **C)** Mixed model intercept represents differences in the distance travelled of mitochondrial movement with increased Forskolin dose.

6.4.2.6 Retrograde moving mitochondria – Speed

In the untreated control lines, the percentage of retrograde moving mitochondria was higher (12.04%) and those mitochondria were faster moving within the lower mtDNA cell line (mean speed= 0.347 µm/s ±0.342, [Log -1.612 µm/s ± 1.211]), compared to ~40% mtDNA deletion neurons ; 10.84% (mean speed 0.195 µm/s ±0.174, [Log -2.081 µm/s ± 1.043]), though this did not reach significance (Figure 6.12).

Retrograde mitochondrial movements decreased following 10µM Forskolin treatment, in the ~40% mtDNA deletion neurons to 5.85% accompanied by a decrease in mean speed (mean speed = 0.070 µm/s ±0.052, [Log -2.902 µm/s ±0.723]) when compared to respective untreated control. In the <10% mtDNA deletion neurons, speed increased to 13.56%, also showing reduced mitochondrial mean speed (mean speed= 0.043 µm/s ±0.046, [Log -3.471 µm/s ±0.722]) compared to untreated controls. ($p<0.0001$) (Figure 6.12)

Lastly, following 50µM Forskolin, in the ~40% mtDNA deletion neurons an increase to 13.19% of mitochondria moving in a retrograde direction was observed, with reductions in speed (mean speed= 0.069 µm/s ±0.046, [Log -2.900 µm/s ± 0.696]) whilst the percentage and speed of retrograde moving mitochondria decreased in the lower deletion line to 11.29% (mean speed= 0.045 µm/s ±0.036, [Log -3.349 µm/s ±0.678]) ($p<0.0001$) (Figure 6.12)

The mean speed of retrograde moving mitochondria was found to decrease with Forskolin treatment in both cell lines , though these differences were not observed between the cell lines treated with the same dose.

A)

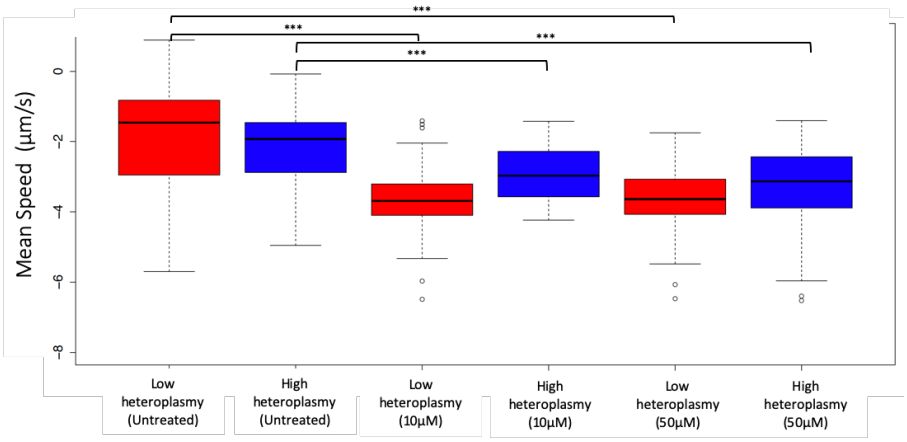

B)

Experiment	Retrograde moving mitochondria (%)	Mean Speed ± SD (µm/s)
Low heteroplasmy (Untreated)	12.04	0.347 ±0.342
High heteroplasmy (Untreated)	10.84	0.195 ±0.174
Low heteroplasmy (10µM)	13.56	0.043 ±0.046
High heteroplasmy (10µM)	5.85	0.070 ±0.052
Low heteroplasmy (50µM)	11.29	0.045 ±0.036
High heteroplasmy (50µM)	13.19	0.069 ±0.046

C) Mixed model statistics for the speed of retrograde mitochondrial movement in Forskolin dosed neurons

	AIC	BIC	LogLik		
	9977.537	10013.49	-4982.768		
	Value	Standard Error	DF	T-Value	P-Value
Intercept	-1.81424	0.08280	455	-21.912	< 2e-16
Forskolin 10 µM	-1.48972	0.11869	455	-12.552	< 2e-16
Forskolin 50 µM	-1.26622	0.10511	455	12.046	< 2e-16
Cell line	-0.00362	0.09281	455	-0.039	0.969
Number of observations	459				
Number of groups	3				

Figure 6.12. Mean mitochondrial speed of retrograde moving mitochondria in Forskolin dosed neurons. Values are logged to aid visualisation. Box and whisker plot showing the mean (represented by the black line) and spread of data **A)** In the untreated control lines, the percentage of retrograde moving mitochondria was higher (12.04%) and those mitochondria were faster moving within the low heteroplasmy neurons compared to the high heteroplasmy neurons (not significant). On 10µM Forskolin treatment, retrograde mitochondrial movement increased in low heteroplasmy neurons, with a reduced mitochondrial mean compared to untreated controls. In the high heteroplasmy neurons, a similar pattern was observed a decrease in retrograde movements, accompanied by a decrease in mean speed when compared to respective untreated control ($p<0.0001$). On 50µM Forskolin, the percentage and speed of retrograde moving mitochondria decreased in the low heteroplasmy, though in the high heteroplasmy neurons an increase in the percentage of mitochondria moving in a retrograde direction was observed, with reduced mean speed compared to both cohorts untreated controls ($p<0.0001$). **B)** Statistics table for each Forskolin dose for each cell line in this study comparing: Percentage retrograde moving mitochondria and their mean speed. N=3 biological repeats for all experiments. **C)** Mixed model intercept represents differences in mitochondrial speed movement with increased Forskolin dose.

6.4.2.7 Retrograde moving mitochondria – Distance

It was found that in the untreated control lines, retrograde moving mitochondria were travelling a slightly shorter distance in the ~40% deletion neurons (mean distance= 10.741µm ± 7.734, [Log 2.128 µm ± 0.749]) compared to the <10% deletion cell line (mean distance= 18.447 µm ± 12.986, [Log 2.629 µm ± 0.837) though this did not reach significance (Figure 6.13).

On 10µM Forskolin treatment, mean distance travelled increased in both cell lines low (mean distance= 23.029 µm ± 15.827, [Log 2.903 µm ± 0.728])) and high (mean distance=37.668 µm ± 26.161, [Log 3.388 µm ±0.726]) mtDNA deletion neurons respectively, when compared to untreated controls ($p<0.0001$) (Figure 6.13).

Lastly, following treatment with 50µM Forskolin, increases in mitochondrial distance travelled were observed in both cell lines, low (mean distance=23.029 µm ± 15.827, [Log 2.882 µm ± 0.769]) and high (mean distance=27.312 µm ± 20.910, [Log 3.036 µm ±0.786]) mtDNA deletion neurons, compared to untreated controls ($p<0.0001$) (Figure 6.13).

Therefore, the distance travelled by retrograde moving mitochondria increased upon Forskolin treatment compared to controls, though these differences were not observed between the both cell lines treated with the same dose. Mitochondria though are moving slower, are covering a longer range of distance, similarly to the anterograde findings.

This study also found that total percentage of anterograde and retrograde moving mitochondria did not total 100%. Mitochondria do not exhibit a uniform pattern of movement and therefore the remaining mitochondria classed as moving could be exhibiting a 'dynamic pause' effect, whereby they are shuffling in the same place of origin, though this study did not quantify this.

A)

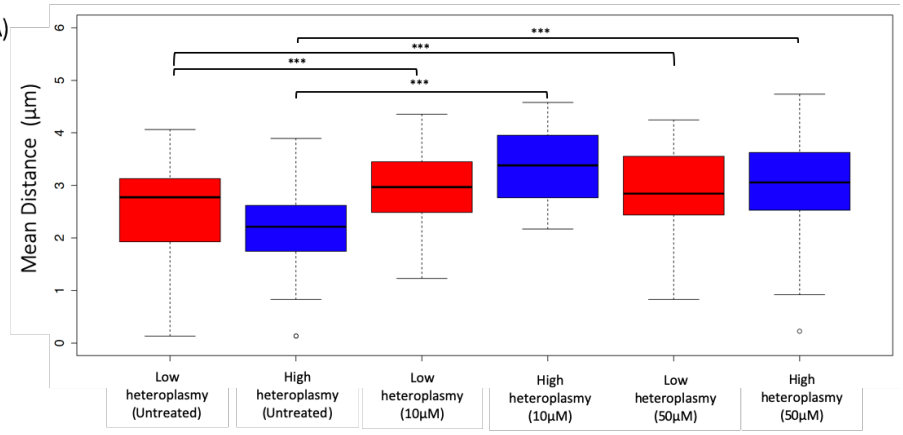

B)

Experiment	Mean Distance travelled ± SD (µm)
Low heteroplasmy (Untreated)	18.447 ± 12.986
High heteroplasmy (Untreated)	10.742 ± 7.734
Low heteroplasmy (10µM)	23.024 ± 15.335
High heteroplasmy (10µM)	37.668 ± 26.161
Low heteroplasmy (50µM)	23.029 ± 15.827
High heteroplasmy (50µM)	27.312 ± 20.910

C) Mixed model statistics for the distance travelled for retrograde mitochondrial movement in Forskolin dosed neurons

	AIC	BIC	LogLik		
	9977.537	10013.49	-4982.768		
	Value	**Standard Error**	**DF**	**T-Value**	**P-Value**
Intercept	2.34780	0.06666	483	35.222	0.0001
Forskolin 10 µM	0.60804	0.09536	483	6.376	0.0001
Forskolin 50 µM	0.58432	0.08194	483	7.131	0.0001
Cell line	0.10614	0.07371	483	1.440	0.151
Number of observations	504				
Number of groups	3				

Figure 6.13. Box and whisker distribution plot of the distance travelled of retrograde moving mitochondria in Forskolin dosed neurons. Values are logged to aid visualisation. Box and whisker plot showing the mean (represented by the black line) and spread of data. **A)** In the untreated control lines, retrograde moving mitochondria were travelling a greater distance in the low heteroplasmy neurons compared to high heteroplasmy neurons (not significant). Following 10µM Forskolin treatment, in both cell lines retrograde moving mitochondria covered a greater distance compared to untreated controls (P<0.0001). On 50µM Forskolin, retrograde moving mitochondria again covered greater distances in both cell lines when compared to controls (P<0.0001). **B)** Statistics table for each Forskolin dose for each cell line in this study comparing: Percentage retrograde moving mitochondria and their mean distance travelled. N=3 biological repeats for all experiments. **C)** Mixed model intercept represents differences in mitochondrial distance with increased Forskolin dose.

6.4.3 Effect of altered calcium efflux on mitochondrial movements

Taken together, these results show that mitochondria harbouring a high level of mtDNA deletion display alterations in their speed, directionality and distance moved after Forskolin treatment; a reagent which allows the opening of the NCLX exchanger allowing calcium ions to exit the mitochondria. Thus, having analysed this mitochondrial movement the following experiments describe how the effect of altered $_{m}Ca^{2+}$ efflux on mitochondrial movement was studied to confirm whether altered cytosolic calcium availability that drives the changes in mitochondrial movement. The theory behind these experiments was to understand whether neurons with a mitochondrial defect have impaired calcium handling and whether Forskolin was capable of restoring this to levels found in the control. Therefore, initial experiments were carried out to observe levels of cytoplasmic Ca^{2+} after Forskolin treatment within control cell lines.

Ionomycin is a calcium ionophore (substance that can cross cellular lipid membranes), which is used to increase cytoplasmic Ca^{2+} influx through direct stimulation of cation entry across the cell membrane. This maximal increase in intracellular calcium consequently results in a maximum increase in fluorescence (Rmax) (Yoshida and Plant, 1992). To determine the Rmax values of Fluo-4-am (a cytosolic calcium indicator which displays and increase in signal when bound to $Ca^{2+)}$ in both cell lines, fluorescence was measured for 60 seconds at the baseline post 1 µM ionomycin treatment, triggering cytosolic Ca^{2+} influx. As Ca^{2+} imaging has not been conducted in these neurons previously, initial optimisation experiments were conducted on the cell lines to obtain the optimum concentrations for the upcoming experiments (Figure 6.14). Following which around 5-10 ROIs were selected per video, of which for each dose approximately 20-30 ROIs were analysed to understand the alterations in Ca^{2+} availability in Forskolin treated neurons loaded with TMRM.

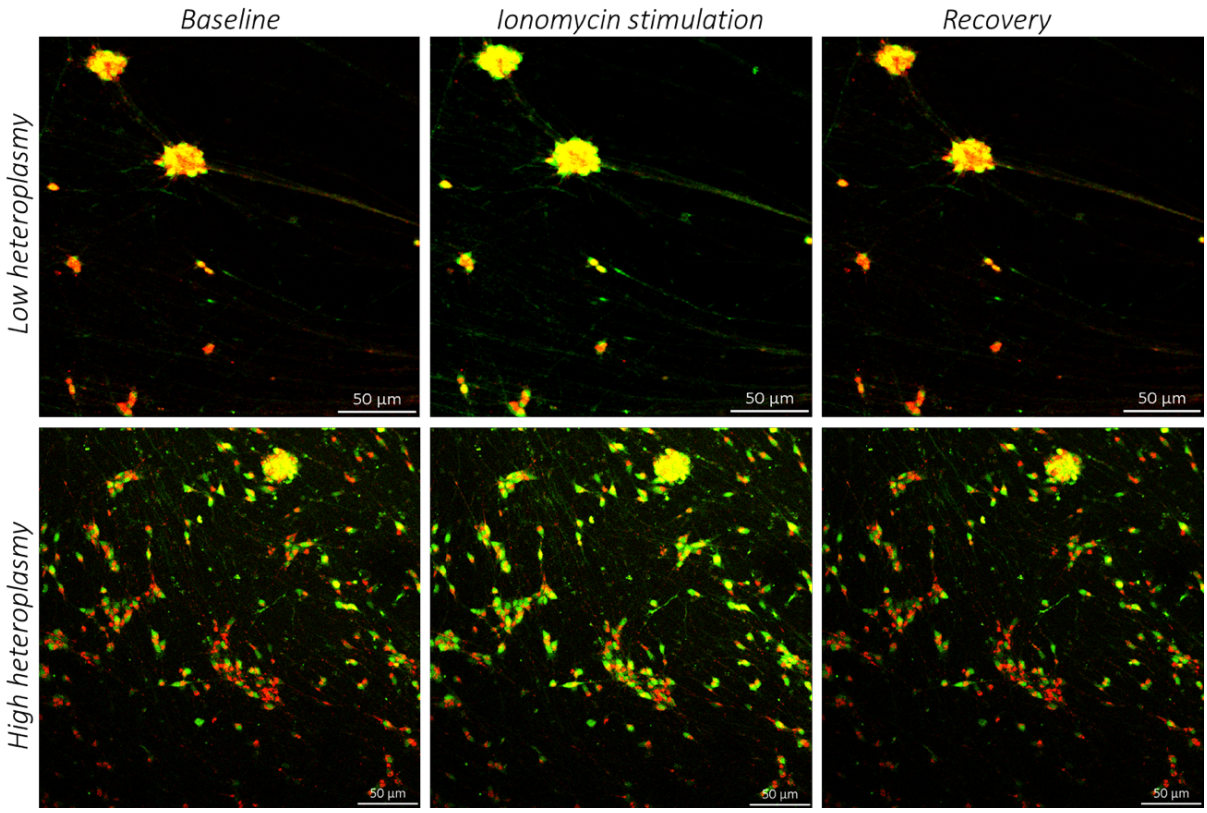

Figure 6.14. Ionomycin stimulation in neurons harbouring mtDNA deletion. Both panels show snapshots of Forskolin treated neurons loaded with TMRM staining (TRITC channel) and Fluo-4-am (FITC). Neurons were stimulated with 1µM ionomycin after 20-30 seconds of imaging (ionomycin stimulation) to induce maximum Ca^{2+} influx into the cell, where after this maximal fluorescence response a shift in signal (to yellow) was observed.

6.4.3.1 Fluo-4-am and TMRM experiments

Neurons were dosed with Forskolin, 30-40 minutes prior to experimentation (Kostic *et al.,* 2015). Measurements of the Fluo-4-AM fluorescence showed that the medians significantly varied between all neurons (p=0.0007). Though reduced available calcium was observed in the untreated ~40% deletion line compared to the untreated <10% deletion line not significant (p=0.4318). When dosed with 10µM Forskolin, both cell lines displayed an increase in Fluo-4-am fluorescence (not significant, p=0.9048). In contrast, 50µM Forskolin treatment demonstrated a large decrease in free Ca^{2+} within <10% deletion when compared to untreated controls, which was found to be significantly different to the ~40% deletion neurons which showed an increase in free Ca^{2+} (p=0.0159) (Figure 6.15A).

Between doses the only significant differences observed were between the untreated high level deletion neurons and 10µM Forskolin high level deletion neurons (p=0.0144) and 10µM and 50µM Forskolin treated lower deletion line (p=0.0042).

It appears that neurons of the high heteroplasmy cell line harbour more free cytosolic Ca^{2+} to as opposed to the low heteroplasmy neurons via the NCLX exchanger through Forskolin treatment. It may be the case that due to fewer damaged mitochondria in the low heteroplasmy cell line, perhaps not as much calcium is needed to be expelled through the NCLX exchanger, due to a decreased $_{m}Ca^{2+}$ overload. The opposite is observed in the high heteroplasmy cell line, which demonstrates increased calcium availability (Figure 6.15A).

As neurons were also stained with TMRM as well as Fluo-4-AM, variations in TMRM intensity were observed in these neurons. An overall decrease in TMRM intensity is observed in the high and low heteroplasmy neurons when Forskolin treated however these did not reach significance. Interestingly though, these findings match the TMRM pattern observed in the previous experiment that analysed dose response in the NGN2 stem cells (Figure 6.15B)

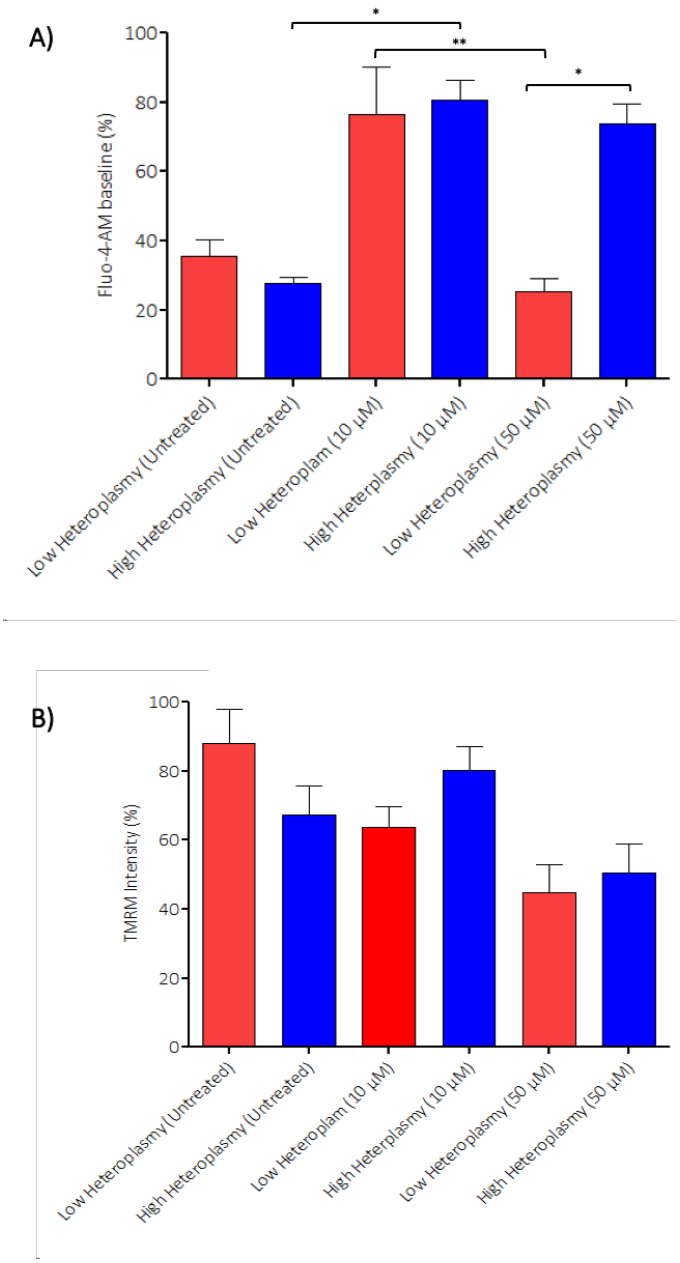

Figure 6.15. Fluo-4-AM and TMRM observations in Forskolin treated neurons. Changes in free Ca^{2+} in low (red) and high (blue) heteroplasmy neurons treated with Forskolin. **A)** Medians significantly varied between all neurons (p=0.0007). Reduced available calcium was observed in the high heteroplasmy neurons compared to low heteroplasmy neurons (not significant). On 10µM Forskolin treatment, low and high heteroplasmy cell lines show increased Fluo-4-am fluorescence (not significant, p=0.9048). On 50µM Forskolin treatment significantly differences in free Ca^{2+} are observed between low and high heteroplasmy neurons (p=0.0159). Further significant differences observed were between the untreated high heteroplasmy neurons and 10µM Forskolin high heteroplasmy neurons (p=0.0144) and 10µM and 50µM Forskolin low heteroplasmy neurons (p=0.0042). **B)** Changes in TMRM intensity representative of mitochondrial membrane potential. Medians were significantly varied between all neurons (p=0.030). Only significant change observed between untreated low heteroplasmy neurons and 50µM Forskolin treated low heteroplasmy neurons (p=0.0261). Calculated using Kruskal Wallis test, with post-hoc Dunn's multiple comparison to allow the testing of comparison of more than two levels. Graphs represented as Mean Fluo-4-AM/TMRM intensity (normalised to ionomycin) ± SEM. 5-10 ROIs were selected per video (approximately containing around 10-20 neurons). N = 3 repeats.

.

6.5 DISCUSSION

6.5.1 Summary of Results

- **Static versus motile mitochondria –** Mitochondria harbouring a higher mtDNA deletion exhibit more mitochondrial movement than the low heteroplasmy neurons. Mitochondrial movement increases with Forskolin treatment in both cell lines.

- **Speed –** Though more mitochondria are moving with Forskolin treatment, the mean mitochondrial speed is significantly reduced with Forskolin treatment.

- **Distance -** Slower moving mitochondria demonstrated a reduced distance in high heteroplasmy neurons, and an increased distance in low heteroplasmy neurons with Forskolin treatment in both dosing experiments and between both cell lines.

- **Directionality -** Overall the speed of anterograde and retrograde mitochondrial transport was found to be significantly reduced in both cell lines with Forskolin treatment though distance travelled was found to be significantly increased compared to controls.

- **Ca^{2+} availability –** Higher heteroplasmy neurons contain more free Ca^{2+} than low heteroplasmy neurons. Forskolin (10 µM) treatment, enhances $_{m}Ca^{2+}$ efflux, causing an almost two fold increase in free calcium availability in both cell lines; sufficient to cause an increase in Ca^{2+} availability through the opening of the NCLX exchanger as a consequence of their mtDNA deletion.

- **Membrane potential –** An overall decrease in TMRM intensity was observed with Forskolin treatment, whereby an increased Ca^{2+} availability might rescue mitochondrial membrane potential via restoring ion flux

Impaired NCLX activity within PINK1 deficient neurons, was found to be rescued by the Protein Kinase A (PKA) signalling pathway via phosphorylation of the serine^{258} NCLX residue. This rescue through direct phosphorylation of NCLX by PKA via Forskolin treatment [PKA agonist]), was described as a regulatory mode of $_{m}Ca^{2+}$ efflux, restoring $_{m}Ca^{2+}$ efflux under PINK1 deficient neurons and protecting these cells from mitochondrial depolarisation via the opening of the PTPs (Figure 6.4. Kostic *et al.,* 2015). Forskolin was used in this experiment to observe whether varying levels of $_{m}Ca^{2+}$ efflux had differential effects on mitochondrial transport. To understand whether $_{m}Ca^{2+}$ efflux affects mitochondrial movement, two concentrations of Forskolin were used.

It has been repeatedly shown that $_{m}Ca^{2+}$ is crucial for mitochondrial health and survival (Palty *et al.,* 2010, Kostic *et al.,* 2015). However, it is still debated whether mitochondrial transport is affected by $_{m}Ca^{2+}$ efflux or the lack of it. Intramitochondrial Ca^{2+} (through Rhod-2-AM) was not observed in this experiment, as this initial experiment was conducted to first understand whether cytosolic Ca^{2+} (Fluo-4-AM) was affected by $_{m}Ca^{2+}$ efflux.

The justification for these experiments were to understand whether increasing $_{m}Ca^{2+}$ efflux (by Forskolin treatment) increased free cytoplasmic calcium within neurons. From here, this study then attempted to understand whether increased intraneuronal Ca^{2+}availability within neurons altered *in vitro* mitochondrial movement, in neurons with a mitochondrial defect.

6.5.2 Impact of $_{m}Ca^{2+}$ efflux on mitochondrial transport within neurons harbouring an mtDNA defect

In this study, it was found that with Forskolin treatment, mitochondria within the high heteroplasmy (~40%) neurons were moving at a lower mean speed and travelled an overall shorter distance in comparison to mitochondria in low heteroplasmy neurons. These findings suggest that, mitochondria within low heteroplasmy neurons, might maintain a steady pace to efficiently supply energy to all regions of the neuron; especially distally, and opposingly high heteroplasmy neuronal mitochondria might be moving too fast, and therefore must need to be reduced to prolong cell survival.

The neuron relies upon a functional OXPHOS system which generates ATP to meet its energy demands (Schwarz, 2013). As the higher heteroplasmy untreated neurons exhibit slower mitochondrial movements, it may indicate that the respiratory chain deficiency; present as a consequence of the large scale mtDNA deletion, may be triggering a defect in motility as ATP generation may be altered. These alterations may then prohibit mitochondrial movement. Furthermore, increased cytoplasmic Ca^{2+} was observed after 10 µM and 50 µM Forskolin treatment in high heteroplasmy neurons compared to controls, where similar findings were observed in the low heteroplasmy neurons though only at 10 µM Forskolin treatment. With Forskolin treatment, cytosolic Ca^{2+} levels may be elevated, explaining the reduced speed/distance of mitochondrial movement.

Mechanistically, the increased level of intracellular calcium identified in high heteroplasmy neurons may be a method to counteract the impaired calcium homeostasis within neurons with a large-scale mtDNA deletion. Ca^{2+} signalling has previously been shown by Wang and Schwarz, (2009) to halt mitochondrial movement in an attempt to adapt and provide for the energy needs of the neuron. This mode of regulation occurs as Ca^{2+} interacts with Miro via Milton. Kinesin exists on both static and moving mitochondria, whereby the EF-hands of Miro regulate Ca^{2+} dependant mitochondrial arrest via binding the kinesin motors directly. This bypasses the step where kinesin dissociates from the mitochondria and therefore becomes 'inactivated' and being bound to Miro stops any further interactions with the microtubule (Wang and Schwarz, 2009).

Recently, live imaging studies have shown an inverse correlation between mitochondrial speed and $_{m}Ca^{2+}$ levels, whereby the lower the $_{m}Ca^{2+}$ content, the faster these organelles move (Chang *et al.,* 2011). In terms of the transport machinery that may be driving this process, it was suggested that as each mitochondrion can bind many miro1 proteins, perhaps mitochondrial speed might be mediated by this binding and consequently its attachment to kinesin motors. Therefore, once a specific $_{m}Ca^{2+}$ threshold is reached, these miro1–kinesin interactions are interrupted, and mitochondria therefore either slow down and/or stop moving, (Chang *et al.,* 2011) supporting a role of $_{m}Ca^{2+}$ on mitochondrial transport.

Moreover, as available cytosolic calcium is higher in the Forskolin treated high heteroplasmy neurons, it may be likely that damaged mitochondria are also expelling $_{m}Ca^{2+}$ at a higher rate (not measured in this study). Once Forskolin treated, the NCLX exchanger may be sufficiently opened to enhance $_{m}Ca^{2+}$ expulsion. $_{m}Ca^{2+}$ may also be released via the mPTP pores (Kostic *et*

al., 2015), as a consequence of the insufficient $_{m}Ca^{2+}$ homeostasis within the dysfunctional mitochondria in high heteroplasmy cell line, which may already be close to opening. Thus, the expelled cytoplasmic Ca^{2+} might in turn prohibit mitochondrial dynamics through the direct increase in cytoplasmic calcium within neurons.

If a high $_{m}Ca^{2+}$ concentration is found within mitochondria it may signal the organelle to halt its movement. This might be so that TCA cycle reactions are promoted to produce ATP, in order provide energy wherever needed. In contrast a lowered $_{m}Ca^{2+}$ concentration might signal for mitochondrial mobility to occur (Chang *et al.,* 2011), and thus to provide ATP supplies to meet the energy demands of the neuron in distal regions. It may be that this is the case in the Forskolin treated NGN2 neurons, as this study observes reduced mitochondrial movement parameters in the neurons harbouring a large scale mtDNA deletion.

Additionally, the medium in which the NGN2s were grown in may alter mitochondrial transport. NGN2 IPSCs are cultured in a medium which contains glucose, where fluctuations in neuronal glucose concentration affect mitochondrial trafficking (Schwarz, 2013). Hence, this suggests that the environment in which these neurons are grown, may have an impact on mitochondrial movement. Repeating these experiments in a glucose-free/low glucose medium i.e. galactose, will force the mitochondria to use their oxidative metabolism to generate energy and will provide a more representative outlook into mitochondrial movement in NGN2 cultured neurons.

6.5.3 Anterograde and retrograde mitochondrial movement in Forskolin treated neurons harbouring a respiratory chain deficiency

This study found that Forskolin significantly altered anterograde and retrograde mitochondrial movement in both cell lines. These mitochondria displayed decreased mitochondrial speed but travelled greater distances when treated with Forskolin compared to untreated controls.

This study identifies alterations in both anterograde and retrograde movement when treated with Forskolin. Though mitochondrial speed is reduced overall with Forskolin treatment, these mitochondria appeared to move farther, indicating that these organelles exhibit slower movement to conserve energy as less ATP is available. This ensures that i) anterograde moving mitochondria can still provide the damaged neuron with ATP in distal regions and ii) the

retrograde moving mitochondria are manoeuvring themselves slower to ensure they reach the lysosomes for degradation.

A mitochondrion rendered as dysfunctional will need to be returned to the soma for lysosomal degradation (Pickrell and Youle, 2015). As this occurs over a longer distance, mitochondria will have to move retrograde and travel further. This study suggests that with increased Forskolin treatment, retrograde mitochondrial distance travelled was increased. As these movement alterations are observed, how directionality is managed via motor protein association will be an interesting follow up study to understand the molecular mechanism of Ca^{2+} regulated mitochondrial movement.

Furthermore, it remains unexplored in this study whether promoting retrograde mitochondrial movement via Forskolin treatment is actually promoting mitophagy of damaged mitochondria/mildly defective mitochondria, as the TMRM data was also inconclusive. Via forskolin treatment it may be the case that (as found in PD patients with defective mitophagy) mitochondria are being targeted to the lysosomes that are not actually undergoing degradation, but instead causing a build up of damaged mitochondria within the cell body. Therefore, though targeting more mitochondria to the lysosomes for degradation is an attractive theory, in this study it is unclear whether i) damaged mitochondria are accumulating in the cell body or ii) whether healthy mitochondria (due to mild phenotype of mtDNA deletion) are being targeted retrograde. These mitochondria may be exacerbating the disease by forcing mitochondrial transport out of the axon and into the cell body. Further studies in regard to answering the above questions will be highly beneficial, if not testing for the detriments of Forskolin treatment and whether mitophagy occurs consequently may be a counterintuitive setup.

As all these trafficking methods are highly energy consuming, mitochondria with a large scale mtDNA deletion may have to move slower in order to prevent organelle death, as they are required to move a long distance. How the mitochondria then regulates its dynamics and what mediates the switches between anterograde and retrograde transport remains a largely debated subject. However, these findings indicate that the the mitochondrial transport machinery is an intricate system constantly undergoing changes to promote cell survival, whereby $_{m}Ca^{2+}$ efflux via Forskolin treatment may be an important regulator.

As a consequence of mtDNA heteroplasmy, not all mitochondria express the large- scale mtDNA deletion. Though quantificational studies show evidence of a ~40% deletion level (See Chapter 5) not all mitochondria will harbour this defect and may therefore be unaffected. The 'healthier' mitochondria may be the population of mitochondria that are moving and also exhibiting directionality, which might explain why the percentage of anterograde moving mitochondria are found to decrease with Forskolin treatment travelling a longer distance in the low heteroplasmy neurons. These mitochondria may not be affected by their mtDNA deletion (<1%) and may have functioning mitochondrial transport systems that maintain mitochondrial dynamics, unlike the high heteroplasmy neurons.

6.5.4 The interplay of mitochondrial dysfunction and calcium handling in neurons in Parkinson's disease

In terms of PD pathology, SN neurons contain damaged mitochondria, in particular those that harbour an mtDNA deletion (Grunewald *et al.,* 2019). The findings in this study illustrate that regulating $_{m}Ca^{2+}$ efflux through Forskolin treatment, mitochondrial transport acts as a novel method to preserve mitochondrial transport within a large-scale mtDNA deletion cell line. These defective mitochondria may be limiting their movement to cater for their genetic damage as a means to conserve energy.

In an attempt to regulate mitochondrial transport this study demonstrated that $_{m}Ca^{2+}$ efflux effects mitochondrial motility. Mitochondria appear to be moving slower i) perhaps in preparation to halt, as cytosolic Ca^{2+} is being altered and/or ii) a depolarised membrane potential (indicated by TMRM intensity) triggers mitochondrial damage and thus reduced mitochondrial transport. Forskolin-dependant mitochondrial transport may be a unique method to rectify the single, large scale mtDNA deletion in a dysfunctional mitochondrial system and mitochondrial transport. It may also be a means as to how damaged mitochondria can be degraded, as a direct consequence of their increased retrograde trafficking to the lysosome.

Within PD, one of the reasons attributed to DAergic neuronal loss is oxidative damage caused by the pace making activity of L-type Ca^{2+} channels (Surmeier *et al.,* 2017). If these calcium channels are therefore causing oxidative damage, perhaps mitochondria in these neurons are

also defective, and also their calcium handling properties. If intraneuronal calcium is reduced, as a consequence of perturbed mitochondrial calcium handling, then perhaps treating DAergic neurons with Forskolin may allow the expulsion of $_{m}Ca^{2+}$ into the cytoplasm, and thus restoring the neurons calcium levels. This is important, as altered cytoplasmic calcium in neurons can increase mitochondrial ROS generation which may be implicated in neurodegenerative mechanisms (Gleichmann and Mattson, 2017).

Therefore, these findings conclude that mitochondrial calcium efflux renders itself a novel target to mediate mitochondrial transport within neurons. This study provides details into alterations of mitochondrial movement within neurons harbouring a single, large-scale mtDNA deletion, a common mutation found in PD and how the NCLX exchanger is a novel target for mediating mitochondrial trafficking through its impact on cytoplasmic calcium (Figure 6.16).

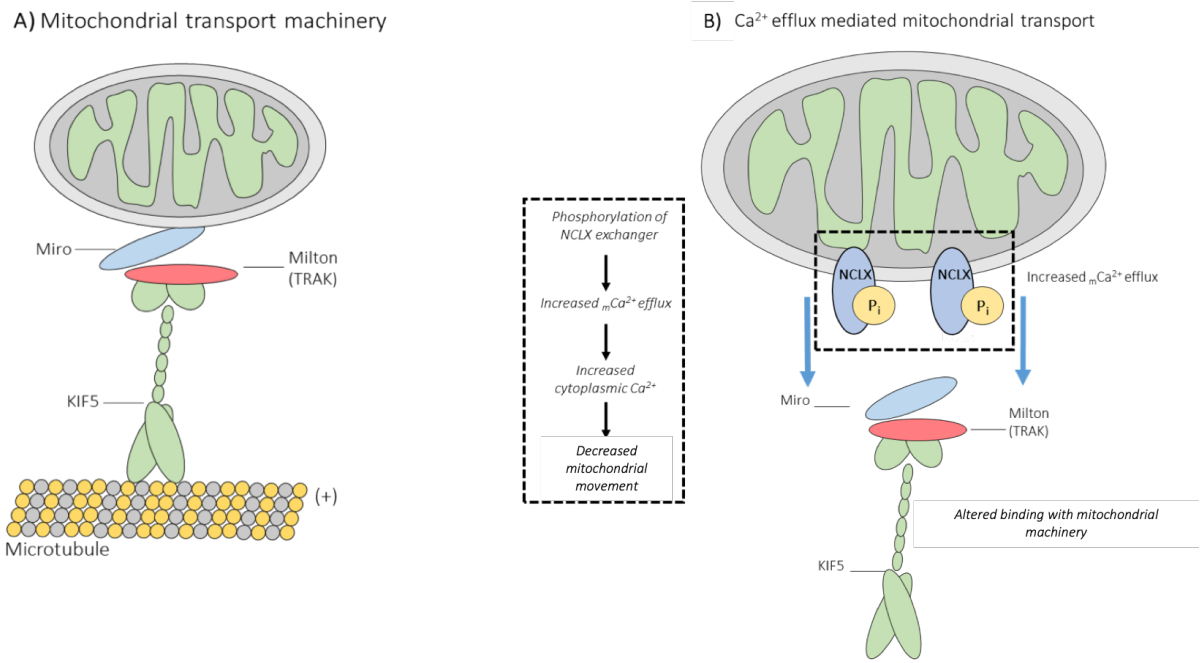

Figure 6.16. Possible $_{m}Ca^{2+}$ efflux mediated mitochondrial transport. A) The well-described mitochondrial transport system which comprises the Miro/Milton – KHC complex. **B)** Phosphorylation of the mitochondrial NCLX exchanger increases $_{m}Ca^{2+}$ efflux permitting more cytoplasmic calcium within the axon which alters mitochondrial trafficking.

6.6 LIMITATIONS OF THIS STUDY

- Similarly, to the previous chapter, this study did not measure mtDNA deletion levels after IPSC differentiation, where it was assumed that the level of deletion would remain the same, which may affect the interpretation of the experimental results.
- No experiments were conducted to assess the viability of the mitochondria in both cell lines once differentiated and treated with Forskolin. Therefore, this must be done to eliminate the possibility of Forskolin having a detrimental effect on mitochondrial health
- Importantly, all untreated control measurements were conducted with a DMSO concentration in the differentiation media, similarly to the Forskolin treated neurons. However, a major limiting factor in this study is that a comparison to neurons differentiated from both cell line, without only differentiation medium and no DMSO were not made in this study at the same time these experiments were conducted. Therefore, though it is suggested the Forskolin can initiate changes in mitochondrial trafficking, there may also be some interplay with the DMSO having an effect.
- Importantly, Russell et al., 2018 demonstrate mitochondrial phenotypes at above 60% mtDNA deletion. The literature also states that phenotypes are observed at above 60& mtDNA deletion. All the experiments conducted in this study were at ~40% mtDNA deletion, as this was largely available in the laboratory. It can be argued that at this lower level of mtDNA deletion perhaps no mitochondrial phenotype will be observed. Therefore, it will be beneficial to repeat thee studies at a higher level of mtDNA deletion.
- Following this, trying to promote mitophagy via Forskolin treatment on healthier mitochondria (40% mtDNA deletion) may have adverse effects. Healthier mitochondria may instead be degraded as opposed to being preserved within the axon to carry out functional mitochondrial movement

6.7 CONCLUSION & FUTURE WORK

This study demonstrated that a significant difference is observed in mitochondrial trafficking between both mtDNA deletion cell lines. The effects of Forskolin were highlighted in this study in neurons with a large-scale mtDNA deletion, indicate that there is interplay between the rate of $_{m}Ca^{2+}$ efflux and mitochondrial trafficking in neurons with a respiratory chain defect. This model provides as a useful tool that provides insight to PD patients, since large-scale mtDNA deletions are seen in affected neurons, as it has not yet been established what the basal mitochondrial trafficking parameters are within the mammalian nigrostriatal pathway for those with PD.

- Future research in this study will observe levels of motor/adaptor complex via western blot within both cell lines to understand the effects of mtDNA deletion on the mitochondrial transport machinery.

- Observe levels of $_{m}Ca^{2+}$ with Rhod-2-AM dyes (increase in fluorescence when bound with mitochondrial calcium) and compare these findings to cytosolic Fluo-4-AM traces in low and heteroplasmy neurons with an mtDNA deletion.

- Administer thapsigargin to inhibit ER involvement, and then then observe Forskolin effects on mitochondrial trafficking via Fluo-4-AM tracing.

- Use FluoVolt™ Membrane Potential Kit to further delve into the mechanisms of how ER-mitochondrial Ca^{2+} handling may mediate mitochondrial trafficking and their localisation.

CHAPTER SEVEN

Final Discussion

7.1 FINAL DISCUSSION

PD pathology comprises the significant loss of dopaminergic neurons from the SNpc of the midbrain however the contribution of mitochondrial trafficking to this loss remains unclear. It has become clear through previous biological studies that mitochondrial movement and mitophagy is perturbed in PD (Spillantini *et al.,* 1998, Whitworth and Pallank, 2009, Youle and Narendra, 2011, Narendra et al., 2012, Pozo Devoto *et al.,* 2017). This study aimed to elucidate how the movements of mitochondria, dynamic organelles that exhibit anterograde and retrograde motion, are altered with disease and how alterations in this trafficking may occur as a response to disease-related mitochondrial dysfunction.

7.1.1 PD models to observe mitochondrial trafficking

The initial focus of this project entailed developing two disease models that encompassed PD pathology to observe mitochondrial movement within these axons. The study developed the imaging of mitochondrial movement within i) *ex vivo* nigrostriatal slices (Chapter 3) and ii) IPSCs harbouring a single, large scale mtDNA deletion (Chapter 5).

The generation of the **mito-Dendra2 - Dat^{IRES}Cre mouse** model provided a unique tool to observe mitochondrial dynamics solely within DAergic neurons of the mouse brain. These mice were then crossed with human wild type alpha synuclein (SNCA) expressing mice to observe the effects of alpha-synuclein on mitochondrial movement. This study observed mitochondrial movement for the first time within a mammalian nigrostriatal slice model and how these dynamics were altered by ageing and alpha-synuclein.

This study aimed to understand the effects of normal ageing on mitochondrial movement as a comparison to what occurs within healthy aged individuals. Furthermore, since ageing is the primary risk factor for the development of PD, such a study would also provide useful data applicable to this condition.

Alpha-synuclein mice were generated to observe the effects of overexpression of this protein on mitochondrial movement to understand how this may be impaired in PD, since SNCA in the last decade has been identified as an effector of mitochondrial movement (Prots *et al.,* 2013). Observing mitochondrial movements within DAergic neurons in the presence of these PD risk

factors, generated novel insight into how mitochondrial dynamics may be altered within the ageing population and PD patients.

In the second model, neurons were cultured from IPSCs harbouring a single, large scale mtDNA deletion which provided insight into the maintenance of mitochondrial movement within a heterogeneous neuronal population. Though it has been shown that mtDNA deletions are the most common mtDNA mutation found in PD, how defects in the mitochondria genome alters mitochondrial motility remains unclear (Reeve *et al.,* 2008). The studies were carried out to understand how mitochondrial trafficking was modified by mitochondrial dysfunction caused by the same mutations detected within SN neurons in PD patients and aged individuals.

Mitochondrial transport within neurons is maintained by motor and adaptor complexes, which are maintained through Ca^{2+} transients (Wang and Schwarz, 2009). Following initial findings from IPSC derived neurons, this study then observed how intramitochondrial calcium affects mitochondrial transport within neurons with a defective respiratory chain due to an mtDNA deletion as observed in PD. Through this model conclusions were drawn with regards to how to basal mitochondrial trafficking was affected within neurons with a mitochondrial defect and also how this movement could be regulated through modulation of mitochondrial calcium efflux.

Both disease models successfully encompassed several aspects of PD pathology and risk factors that may affect mitochondrial movement. The analysis of mitochondrial movement was dissected into three parameters such as speed, the distance of mitochondrial movement and their directionality, to understand how these individual aspects of mitochondrial movement contribute to or may be affected by PD.

7.1.2 The role of alpha-synuclein and mitochondrial trafficking

With increasing evidence of alpha-synuclein localisation with mitochondria (Martin *et al.,* 2006, Li *et al.,* 2007, Devi *et al.,* 2008, Kamp *et al.,* 2010), several studies have since suggested a role for alpha-synuclein in mitochondrial transport.

This study found that within the nigrostriatal pathway, alpha-synuclein plays a role in mitochondrial motility by causing a reduction in overall mitochondrial speed and distance travelled when compared to old aged mice, however this was not aged-matched. Moreover, a role for alpha synuclein in the regulation of mitochondrial motility is not surprising due to the protein's preference to bind curved membranes which render mitochondria a prime binding

site. As research into alpha-synuclein–mitochondrial interactions are still ongoing, the two main questions that remain unanswered are i) where does alpha-synuclein bind the mitochondrion and ii) under which conditions does this interaction occur.

Alpha-synuclein interactions with the mitochondrial transport system have shown that in the presence of increased alpha-synuclein, Miro levels also increase. This may indicate that alpha-synuclein directly binds key mitochondrial transport proteins such as Miro and Milton, in addition to the microtubule-based kinesin motors to control mitochondrial movement (Shaltouki et al., 2018). The upregulation of Miro was shown to further halt mitophagy and consequently alpha-synuclein accumulations are observed within the SN of post mortem PD patient tissue and alpha-synuclein mutant flies. DAergic neurons of the nigrostriatal pathway constantly undergo cellular stress as a result of their unique morphology and pace making activity. These functions are thought to diminish in PD, whereby increased Miro binding and inhibited mitophagy mechanisms might cause more dysfunctional mitochondria and cell death (Shaltouki et al., 2018).

Therefore, it may be that alpha-synuclein mediates mitochondrial transport via two mechanisms. Firstly, the tendency of alpha-synuclein to bind curved membranes such as mitochondria and secondly by being an instigator of mitochondrial transport within neurons via the motor/adaptor transport machinery itself.

7.1.3 The role of mitochondrial calcium efflux on mitochondrial trafficking

The second half of this project was conducted within an *in vitro* setting where the effect of mtDNA deletions and how this defect affects mitochondrial trafficking was investigated.

Ca^{2+} mediates mitochondrial transport in neurons (Sheng, 2014). Within mitochondria, the mitochondrial calcium uniporter (MCU) mediates $_{m}Ca^{2+}$ influx (Baughman et al., 2011; De Stefani et al., 2011), whilst the NCLX exchanger regulates mitochondrial efflux (the rate limiting step) within mitochondrial calcium handling (Kostic *et al.,* 2015). Though the effects of $_{m}Ca^{2+}$ influx and efflux on mitochondrial health are well explored, how these exchangers then mediate mitochondrial movement is not well elucidated.

This study also focused on understanding whether expelling $_{m}Ca^{2+}$ through the NCLX exchanger affects mitochondrial movement. As these neurons harboured an mtDNA deletion, it was

hypothesised that perhaps there may be an accumulation of Ca^{2+} within these damaged mitochondria that was not being released. It was thought that perhaps facilitating $_{m}Ca^{2+}$ release via the NCLX exchanger may affect mitochondrial movement. Indeed, it was shown that regulating the NCLX exchanger reduced mitochondrial speed in both cell lines, as well as altering crucial mitochondrial dynamics parameters such as mitochondrial distance and directionality.

What these findings bring to light is that it may not only be an external motor adaptor complex that plays a role in mitochondrial transport, but also intrinsic factors within the mitochondria that can be manipulated to mediate mitochondrial transport. It may be the case that the available calcium within the axons through expulsion via NCLX exchanger, may regulate mitochondrial starting and stopping.

The conclusions drawn from these studies suggest that $_{m}Ca^{2+}$ efflux via NCLX mediates mitochondrial transport in the axons of mtDNA deletion neurons, highlighting a novel role of $_{m}Ca^{2+}$ efflux mediated mitochondrial movement (Figure 7.1).

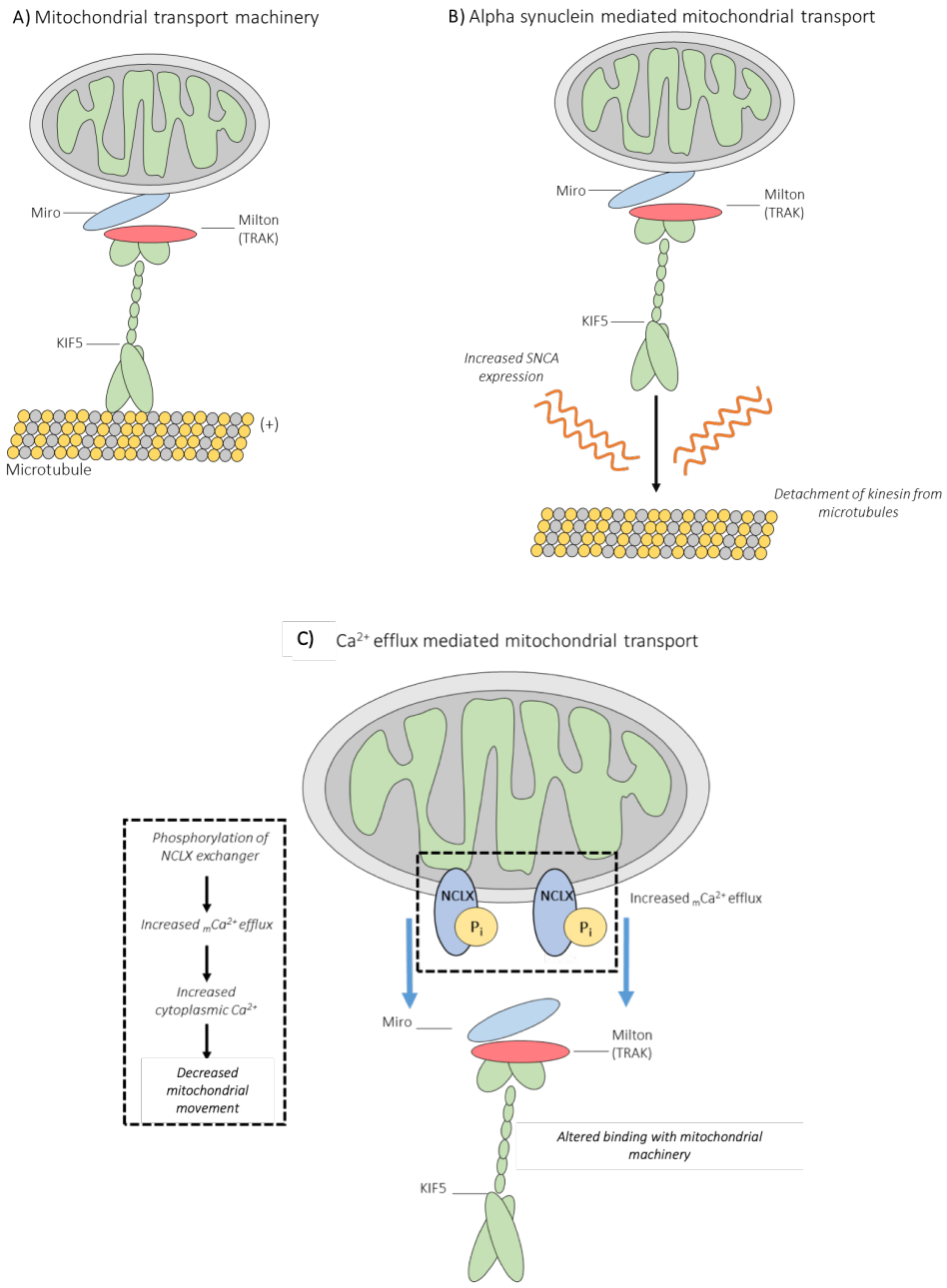

Figure 7.1. Novel regulators of mitochondrial transport in Parkinson's disease. A) The well-described mitochondrial transport system which comprises the Miro/Milton – KHC complex. **B)** Increased alpha synuclein expression which can cause the detachment of kinesin from microtubules limiting mitochondrial speed and distance travelled. **C)** Phosphorylation of the mitochondrial NCLX exchanger which increases $_{m}Ca^{2+}$ efflux permitting more cytoplasmic calcium within the axon which facilitates mitochondrial trafficking.

7.1.4 The effects of mitochondrial transport and the clearance of pathogenic mtDNA through mitophagy

Mitochondria are synthesised within the cell body with their movement surpassing this region to axons. Functional axonal mitochondrial trafficking is crucial to deliver mitochondria to wherever required within neurons (Uittenbogaard and Chiaramello, 2016).

It is believed that retrograde targeted mitochondria are transported towards the cell body for degradation, while anterograde moving mitochondria are 'healthy' mitochondria that are moved to provide energy to regions of the neurons that require the constant influx of ATP (Martin *et al.,* 1999, Hirokawa *et al.,* 2010). *In vitro*, this study found that varying heteroplasmy level altered mitochondrial anterograde and retrograde directionality.

Therefore, in addition to being a provider of energy, it remains unclear how mitochondria are targeted for mitophagy, whereby it may be that these organelles might have a unique system that facilitates this clearing process. For example, an impairment in retrograde movement may cause the halting of damaged mitochondria within the axon i) which may prohibit damaged mitochondrial degradation and also ii) cause an accumulation of stationery damaged mitochondria within the axon which might block the movement of other incoming mitochondria within the axon. These detrimental transport inhibitions may then deprive the neurons of its ATP distribution, to regions required, triggering cell death. Moreover, it is unclear at what time point in a mitochondrion's journey through the axon, the organelle becomes damaged. Can a healthy mitochondrion become depolarised as it is travelling within the axon, or is there a constant circulation of damaged mitochondria within axons that do not undergo degradation? This remains unknown. Therefore, it can be thought that the mitochondrial transport system feeds into the mitophagy machinery whereby it may be useful to generate therapies that identify damaged mitochondria and to help transport them to ensure neurons remain healthy.

In an attempt to clear dysfunctional mitochondria through mitophagic processes Dai *et al.,* (2013) demonstrate that increasing mTOR mediated mitophagy/autophagy selects against damaged mitochondria with increased mutation level. This in turn decreases the mitochondrial mutation level over time, due to an increase in mitophagy within cybrids harbouring the heteroplasmic mtDNA G11778A mutation. The inhibition of the mTOR pathway caused the co-localisation of mitochondria with autophagosomes, reducing the mutation level (Dai *et al.,*

2014). Additionally, a study conducted in *Drosophila* adult fly muscle with a 2,584bp mtDNA deletion, revealed that deleted mtDNA were found to decrease through a few mechanisms: i) reduced mitochondrial fusion as a consequence of decreased mitofusin levels, ii) reducing mitochondrial repolarisation through ATP synthase reversal reactions and iii) increasing key mitophagy proteins; PINK1 or Parkin (Kandul et al., 2016)

Mitochondrial transport occurs to enhance neuronal network connections (Mouli et al., 2009, Patel et a.,2013, Tam et al., 2015). Mitophagy appears to act as a means to remove mtDNA mutations, it will be interesting understand whether mutation level can be rescued within neurons harbouring an mtDNA deletion, and whether changes are observed in mitochondrial directionality and mitochondrial localisation with the autophagosome. Therefore, the interplay of mitochondrial motility and mitophagy provide as implications for new therapies for PD and mitochondrial disease, and maybe other ageing disorders.

7.1.5 Pathways for potential therapeutic targets in this study

Pharmacologically targeting dysfunctional mitochondrial transport appears to be an aspect of mitochondrial damage that is largely unclear. Due to the caveats of understanding disease mechanisms that are help within an intricate pathway such as the nigrostriatal pathway; as well as then reliably quantifying and extracting accurate information from these studies, render assessment of the parameter of mitochondrial damage a challenging task. Furthermore, investigating perturbations in this system and then translating them into a model that is disease relevant is difficult.

This study aimed to observe mitochondrial movements within two disease models, to understand whether mtDNA deletion and alpha-synuclein are mediators of mitochondrial movement. The development of these models and assays i.e. individual tracking of mitochondrial movement to observe membrane potential and mitochondrial morphology, will provide an immense amount of data with regards to why and how damaged mitochondrial are targeted to where they are required.

In these studies, it was found that alpha-synuclein can effect mitochondrial trafficking (not aged-matched observations), and that though the mechanisms behind these effectors still need to be explored, it is still a novel means by which mitochondrial movement can be investigated. Understanding mitochondrial speed and directionality may be imperative in understanding

how and why mitochondria are positioned specifically within particular regions of the neuron. Whether pharmacologically either the addition of healthy mitochondria and/or removal of damaged mitochondria within these regions of dopaminergic neurons may be an advantageous and unique method to targeting and combatting neuronal damage within Parkinson's disease.

7.2 LIMITATIONS OF THIS STUDY

This study utilised mouse and iPSC models: two disease relevant models that provide invaluable insight into PD, however it is important to understand that no disease model is perfect and a few challenges arose which were combatted within these studies.

7.2.1 Limitations of using iPSCs with a large scale mtDNA deletion

Since the discovery of human derived iPSCs, this model has been extremely useful to manipulate pharmacologically to understand neurodegenerative mechanisms. In this study, large scale mtDNA deletion neurons were differentiated from iPSCs in order to record mitochondrial movement. The two major issues that arose within this iPSC model were i) the occasional spontaneous cell death (regardless of passage number) and ii) loss of mtDNA deletion over increased passage number. In both instances, new iPSCs vials at a lower passage number were taken and experiments were repeated. iPSCs are also a highly sensitivity disease model, and very small alterations in their growth environment and/or the addition of pathways altering reagents can alter cell growth and viability. Therefore all experiments were conducted carefully.

7.2.2 Limitations of using a mouse model

The main use for mice as disease model is their large genetic homology, which over decades has allowed the comparison and analysis of disease genotypes and phenotypes from mouse to patients. In this particular study, several challenges were counteracted; the most prominent challenges residing within maintaining tissue viability. From a mouse model nigrostriatal slices were taken and imaged, which required a series of optimisation steps to maintain slice viability. Acute brains slices are a robust method to carry out in vivo studies, where this study modified this technique to observe *ex vivo* mitochondrial dynamics. As with any mouse disease model, especially within PD, observing a PD phenotype cannot always be replicated, and though alterations in mitochondrial movement were observed with alpha synuclein expression, these mice did not exhibit a motor phenotype.

7.3 FURTHER WORK

7.3.1 Ex vivo nigrostriatal slices

Though this study hypothesises that a mitochondrial defect may occur within these mice as a cause of ageing and alpha-synuclein, the mechanism behind these effects remain unidentified. Future work in this area will involve the understanding of kinesin and dynein motors and contributing further evidence into understanding whether alpha-synuclein directly binds kinesin motors and whether this alters mitochondrial movement, as proposed in this thesis. This will generate some insight into alpha-synuclein mediated mitochondrial transport mechanisms specific to PD.

Furthermore, it will be interesting to replicate these studies with a mouse model that demonstrates a mitochondrial defect such as the polymerase gamma (POLG) mouse (Hance *et al.,* 2005). The advantages of this model are that the homozygous mice exhibit a phenotype which includes reduced life span and premature ageing with weight loss. Observing altered mitochondrial dynamics in this mode may shed light into how mitochondrial genetic defects affect mitochondria transport in PD; a similar approach to what was conducted in the iPSC model in this study. The POLG mouse model once crossed and aged with the mito-Dendra/DAT^{IRES}Cre mice will provide information into how ageing and mitochondrial dysfunction perturbs mitochondrial movement within nigrostriatal axons in PD.

7.3.2 Neurons harbouring a single, large scale mtDNA deletion

This study explored the effects of perturbed mitochondrial calcium signalling and how this affects mitochondrial movement. Unlike other organelles, it may be important to understand how mitochondrial trafficking may be regulated by the mitochondrion itself as opposed to external stimuli within the axon, due to their calcium storage properties.

It would also be interesting to explore mitochondria- ER connections and how these are altered with disease. Alterations in mitochondria-ER tethering with disease and how this effect mitochondrial transport machinery will provide large insight into the conditions that trigger mitochondria- ER co-localisation in PD, and how calcium storage is managed within the pace making DAergic neurons of the SNpc.

7.3.3 Removing dysfunctional mitochondria – an alternative to mitophagy?

Though mitophagy is the commonly studied clearance pathway, other degradative pathways have shown to eliminate particular segments of mitochondria. This study did not specifically delve in to mitophagic pathways in PD, however future studies in this area wil provide interesting information regarding mitochondrial clearance. Recently a lot of research has been undertaken to study additional possible 'clearance' pathways in various model organisms.

7.3.3.1 Astrocytic involvement

The role of CNS glial phagocytosis is largely undergoing investigation. Within the optic nerve head (ONH) of wild type mice, cellular protrusions were observed within intact axons, which were engulfed and degraded by neighbouring astrocytes. This is an interesting phenomenon as the original findings indicate that astrocytic phagocytosis occurs post trauma only (al-Ali and al-Hussain, 1996, Bechmann and Nitsch, 1997). These axonal protrusions were found within the ONH and within unmyelinated retinal ganglion cell axons. Though the reason for the onset of these protrusions remain inconclusive it was thought it may be an additional degradative mechanism for retrogradely transported axonal components (Nguyen et al., 2011). Furthermore, the involvement of astrocytes within neuronal mitochondrial populations described that astrocytes might release extracellular mitochondrial particles to neurons following a stroke event. However it still remains unclear through the means by which the organelle enters the neuron and also what mitochondrial dynamics and transport mechanisms occur, on and after release of mitochondria from the astrocyte (Hayakawa *et al.,* 2016).

7.1.5.2 Exophers

After the identification of mitochondrial removal through the formation of axonal protrusions, the idea of mitochondria being able to move into adjacent cells (Lee et al., 2010, Davis et al., 2014) and the possible spread of damaged mitochondria via this mechanism has become an interesting concept. Within adult neurons from *Caenorhabditis elegans*, large membrane-surrounded vesicles extrusions (4µm) referred to as exophers, were identified. Exophers were found to house mitochondria and that the generation of these exophers under neuronal stress demonstrated a healthier function when compared to stressed neurons that did not generate exophers. Thus, exopher production may be an alternative method by which damaged organelles and proteins are removed (Melentijevic et al., 2017).

7.1.5.3 Mitochondrial-derived vesicles (MDVs)

Thought to occur through the 'budding' of the mitochondrial membrane, mitochondrial-derived vesicles (MDVs) formation is thought to arise as a separate function of mitochondrial fission. MDVs are then targeted to the cell body for lysosomal degradation via autophagy (Soubannier et al., 2012, Roberts et al., 2016). These vesicles are created basally but can be triggered under oxidative stress. Interestingly MDV mediated mitochondrial clearance is believed to occur under conditions of mild damage, as a strong depolaristion still triggers PINK1/Parkin-mediated mitophagy (Shlevkov and Schwarz, 2014). It was also shown that MDVs can be secreted as exosomes (Matheoud et al., 2016). These findings suggest that prior to mitophagy, retrograde travelling mitochondria and/or dysfunctional mitochondria may partake in vesicle formation that assists mitophagy, and may be degraded instantly as opposed to having to manoeuvre themselves to the cell body.

For the most part it has been assumed that mitochondria targeted for mitophagy are transported to the cell body. The findings in this thesis demonstrate that in fact mitochondrial movement is largely limited. It may be the case that mitochondria may not have to move so far as they might be directed towards local axonal extrusions perhaps via glial involvement and or exopher formation, allowing dysfunctional mitochondria to be removed instantly. This is an attractive theory, especially within damaged neurons such as those affected in PD, where the neurons possesses a method by which dysfunctional material is instantly degraded and thus maintaining neuronal viability.

7.4 FINAL CONCLUSION

This project successfully optimised the imaging and analysis of mitochondrial movement within Parkinson's disease utilising iPSC and mouse models.

Nigrostriatal slices were taken from mitoDendra2/DATCre^{IRES} mice that were crossed with alpha synuclein (SNCA) over-expressing animals to observe how ageing and SNCA affect mitochondrial movement. It was found that SNCA can impact mitochondrial movement, reducing the speed and distance travelled of mitochondria within nigrostriatal axons when compared to healthy aged mice. However, as these findings were not aged-matched experiments must be repeated to confirm this outcome.

This study then confirmed a respiratory chain defect in iPSCs harbouring a single, large scale mtDNA deletion and explored the effects of $_{m}Ca^{2+}$ efflux on transport. It was revealed that altered $_{m}Ca^{2+}$ efflux alters mitochondrial speed, distance and directionality.

This thesis reports novel findings into how SNCA and $_{m}Ca^{2+}$ efflux can mediate mitochondrial transport within axons. These findings have illustrated a new mechanisms to observe and possibly regulate mitochondrial trafficking in PD, which may perhaps be useful therapeutic targets also.

CHAPTER 8

References

Acin-Perez R, Enriquez JA (2014). The function of the respiratory super complexes: the plasticity model. *Biochimica et Biophysica Acta.;*1837 (4):444–50. 17.

Adam AC, Bornhövd C, Prokisch H, Neupert W, Hell K. (2006), 'The Nfs1 interacting protein Isd11 has an essential role in Fe/S cluster biogenesis in mitochondria' , *EMBO J,* 25, pp.174–183

Aizawa H., Sekine, Y., Takenura, R., Zhang, Z., Nangaku, M. and Hirokawa, N. (1992). Kinesin family in murine central nervous system. J. Cell Biol. 119, 1287-1296.

Akepati, V.R. et al., (2008), 'Characterization of OPA1 isoforms isolated from mouse tissues'. *J. Neurochem.* 106, pp. 372–383

al-Ali SY, al-Hussain SM. (1996), 'An ultrastructural study of the phagocytic activity of astrocytes in adult rat brain'*, J Anat* 188, pp.257–262.

Albin RL, Young AB, Penney JB. (1989), 'The functional anatomy of basal ganglia disorders', *Trends in Neurosciences,* 12, pp. 366–375

Alger BE, Dhanjal SS, Dingledine R, Garthwaite J, Henderson G, King GL, Lipton P, North A, Schwartzkroin PA, Sears TA, Segal M, Whittingham TS, Williams J (1984) 'Brain slice methods. In: Dingledine R (ed) Brain slices.' *Plenum Press*, New York London, pp 381–437

Alle, H., Roth, A., and Geiger, J.R. (2009), 'Energy-efficient action potentials in hippocampal mossy fibres', *Science* 325, pp. 1405–1408

Altmann, R. (1890). Die Elementarorganismen Und Ihre Beziehungen Zu Den Zellen. Leipzig: Veit & comp., 145.

Amiri, M. & Hollenbeck, P. J. (2008), 'Mitochondrial biogenesis in the axons of vertebrate peripheral neurons' , *Dev. Neurobiol.* 68, pp. 1348–1361

Anderson, R.F. et al., (2014) 'Electron-Transfer Pathways in the Heme and Quinone-Binding Domain of Complex II (Succinate Dehydrogenase)', *Biochemistry*, 53(10), pp.1637–1646.

Anderson, S., Bankier, A.T., Barrell, B.G., de Bruijn, M.H., Coulson, A.R., Drouin, J., Eperon, I.C., Nierlich, D.P., Roe, B.A., Sanger, F., Schreier, P.H., Smith, A.J., Staden, R. and Young, I.G. (1981) 'Sequence and organization of the human mitochondrial genome', *Nature*, 290(5806), pp. 457-65.

Ango F, Pin J, Tu J, Xiao B, Worley P, Bockaert J, Fagni L (2000). Dendritic and axonal targeting of type 5 metabotropic glutamate receptor is regulated by Homer1 proteins and neuronal excitation. J. Neurosci. 20, pp. 8710–8716

Arai, T. *et al.* (2006), 'Up-regulation of hMUTYH, a DNA repair enzyme, in the mitochondria of substantia nigra in Parkinson's disease'. *Acta Neuropathol,* 112, pp. 139–145

Ashrafi, G., Schlehe, J.S., LaVoie, M.J., and Schwarz, T.L. (2014). Mitophagy of damaged mitochondria occurs locally in distal neuronal axons and requires PINK1 and Parkin. J. Cell Biol. 206, pp. 655–670.

Athanassiadou A, Voutsinas G, Psiouri L, Leroy E, Polymeropoulos MH, Ilias A, Maniatis GM, Papapetropoulos T (1999). Genetic analysis of families with Parkinson disease that carry the Ala53Thr mutation in the gene encoding α-synuclein. Am J Hum Genet 65: pp.555–558

Attwell, D. and Laughlin, S.B. (2001). An Energy Budget for Signaling in the Grey Matter of the Brain. Journal of Cerebral Blood Flow & Metabolism, 21, pp. 1133-1145.

Augustine, G. J., Santamaria, F., and Tanaka, K. (2003), 'Local calcium signaling in neurons', *Neuron, 40*(2), pp. 331-46..

Babcock DF, Hille B. (1998), 'Mitochondrial oversight of cellular Ca^{2+} signaling', *Curr Opin Neurobiol.*; 8, pp.398–404.

Ballinger, S. W., Shoffner, J. M., Hedaya, E. V., Trounce, I., Polak, M. A., Koontz, D. A. et al. (1992), 'Maternally transmitted diabetes and deafness associated with a 10.4kb mitochondrial DNA deletion', . *Nat. Genet.* 1, pp. 11–15

Baloh RH. (2007), 'Mitochondrial dynamics and peripheral neuropathy', *Neuroscientist* 14, pp. 12–18.

Bandyopadhyay S, Chandramouli K, Johnson MK. (2008), 'Iron–sulfur cluster biosynthesis', *Biochem Soc Trans*, 36, pp. 1112–1119

Bartels, A.L. and Leenders, K.L. (2009) Parkinson's disease: The syndrome, the pathogenesis and pathophysiology, *Cortex*, 45(8), pp. 915–921.

Battelli F and Stern L (1912). Die Oxydationsfermente*. Ergebnisse der Physiologie Biologischen Chemie und Experimentellen Pharmakologie*;15, pp. 96–268.

Baughman, J.M., Perocchi, F., Girgis, H.S., Plovanich, M., Belcher-Timme, C.A., Sancak, Y., Bao, X.R., Strittmatter, L., Goldberger, O., Bogorad, R.L.(2011). Integrative genomics identifies MCU as an essential component of the mitochondrial calcium uniporter. *Nature* 476, pp. 341–345.

Bechmann I, Nitsch R (1997) 'Astrocytes and microglial cells incorporate degenerating fibers following entorhinal lesion: a light, confocal, and electron microscopical study using a phagocytosis-dependent labeling technique', *Glia,* 20, pp. 145–154.

Becker, D. et al. (2012),'Pink1 kinase and its membrane potential (Deltapsi)-dependent cleavage product both localize to outer mitochondrial membrane by unique targeting mode', *J. Biol. Chem.* 287 pp. 22969–22987

Beilina, A. et al. (2005), 'Mutations in PTEN-induced putative kinase 1 associated with recessive parkinsonism have differential effects on protein stability', *Proc. Natl. Acad. Sci. U.S.A.* 102, pp. 5703–5708

Benchoua A., Trioulier Y., Zala D., Gaillard M. C., Lefort N., Dufour N., Saudou F., Elalouf J. M., Hirsch E., Hantraye P., et al. (2006). 'Involvement of mitochondrial complex II defects in neuronal death produced by N-terminus fragment of mutated huntingtin'. *Mol. Biol. Cell* 17, pp. 1652-1663

Benda C (1898) . Ueber die Spermatogenese der Vertebraten und höherer Evertebraten, II. Theil: Die Histiogenese der Spermien. Archive fur Anatomie und Physiologie., 73, pp. 393–8.

Bender, A., Krishnan, K.J., Morris, C.M., Taylor, G.A., Reeve, A.K., Perry, R.H., Jaros, E., Hersheson, J.S., Betts, J., Klopstock, T., Taylor, R.W. and Turnbull, D.M. (2006) 'High levels of mitochondrial DNA deletions in substantia nigra neurons in aging and Parkinson disease - nature genetics', *Nature Genetics*, 38(5), pp. 515–517

Bereiter-Hahn, J. (1978) 'Intracellular motility of mitochondria: role of the inner compartment in migration and shape changes of mitochondria in XTH-cells', *J Cell Sci*, 30, pp. 99-115.

Berg, J., Tymoczko, J. and Stryer, L. (2012) *Biochemsitry 7th edition. Oxidative phosphorylation.* New York: W.H. Freeman and Company.

Berliner E, Mahtani HK, Karki S, Chug LF, JCronan JE, and Gelles J (1994) 'Microtubule Movement by a Biotinated Kinesin Bound to a Streptavidin-coated Surface, *The Journal of Biological Chemistry,* 269(18), pp. 8610-8615.

Bernales, S., Schuck, S., and Walter, P. (2007) 'ER-phagy: selective autophagy of the endoplasmic reticulum' *Autophagy* 3, pp. 285–287

Berridge, M. J. (2002) 'The endoplasmic reticulum: a multifunctional signalling organelle'. *Cell Calcium* 32, pp. 235–249

Berthet A., Margolis E. B., Zhang J. et al. (2014) 'Loss of mitochondrial fission depletes axonal mitochondria in midbrain dopamine neurons.' *J. Neurosci.* 34, pp. 14304–14317.

Bertran-Gonzalez J., Herve D., Girault J. A., Valjent E. (2010) 'What is the degree of segregation between striatonigral and striatopallidal projections?' *Front. Neuroanat* 4 (136), pp, 1-9

Bezprozvanny I (2009),'Calcium signaling and neurodegenerative diseases' , *Trends Mol Med.* 15, pp 89–100.

Biederbick A, Stehling O, Rösser R, Niggemeyer B, Nakai Y, Elsässer HP, Lill R. (2006) 'Role of human mitochondrial Nfs1 in cytosolic iron–sulfur protein biogenesis and iron regulation', *Mol Cell Biol* 26, pp. 5675–5687

Billups, B. & Forsythe, I. D. (2002) 'Presynaptic mitochondrial calcium sequestration influences transmission at mammalian central synapses' *J. Neurosci.* 22, pp. 5840–5847

Bindoff L. A., Birch-Machin M., Cartlidge N. E., Parker Jr W. D. and Turnbull D. M. (1989) 'Mitochondrial function in Parkinson's disease'. Lancet 2 pp. 49.

Bindoff LA, Birch-Machin MA, Cartlidge NE, Parker WD Jr, Turnbull DM (1991) 'Respiratory chain abnormalities in skeletal muscle from patients with Parkinson's disease'*, J Neurol Sci.* 104, pp 203–208

Blanchard, J. L., and M. Lynch, (2000) 'Organellar genes: Why do they end up in the nucleus?', *Trends Genet.*1, pp 315–320.

Bliek A, Shen Q, and Kawajiri S(2013) 'Mechanisms of Mitochondrial Fission and Fusion', *Cold Spring Harbour Perspectives in Medicine,* 5(6), pp. 1-16.

Bock C, Kiskinis E, Verstappen G, Gu H, Boulting G, Smith ZD, Ziller M, Croft GF, Amoroso MW, Oakley DH, Gnirke A, Eggan K, Meissner A. (2011) 'Reference Maps of human ES and iPS cell variation enable high-throughput characterization of pluripotent cell lines' *Cell.* 144, pp. 439–452.

Bogaerts V, Theuns J, Van BC. (2007). Genetic findings in Parkinson's disease and translation into treatment: a leading role for mitochondria? Genes Brain Behav. 7:129–151.

Bogan, N. & Cabot, J. B (1991) 'Light and electron microscopic analyses of intraspinal axon collaterals of sympathetic preganglionic neurons' *Brain Res.* 541, pp. 241–251

Bogenhagen, D. and Clayton, D.A. (1977) 'Mouse L cell mitochondrial DNA molecules are selected randomly for replication throughout the cell cycle', *Cell*, 11(4), pp. 719-27.

Bolam JP, Bennett B. (1995) 'The microcircuitry of the neostriatum In Molecular and Cellular Mechanisms of Neostriatal Functions' Austin, Texas: R.G.Landes Company, pp. 1–19

Bolam JP, Powell JF, Wu JY, Smith AD. (1985) 'Glutamate decarboxylase-immunoreactive structures in the rat neostriatum. A correlated light and electron microscopic study including a combination of Golgi-impregnation with immunocytochemistry', *Journal of Comparative Neurology* 237, pp. 1–20

Bonawitz, N.D., Clayton, D.A. and Shadel, G.S. (2006) 'Initiation and beyond: multiple functions of the human mitochondrial transcription machinery', *Mol Cell*, 24(6), pp. 813-25.

Bossy-Wetzel E., Petrilli A., Knott A. B. (2008) 'Mutant huntingtin and mitochondrial dysfunction' *Trends Neurosci.* 31, pp. 609-616

Boulting GL, Kiskinis E, Croft GF, Amoroso MW, Oakley DH, Wainger BJ et al (2011) 'A functionally characterized test set of human induced pluripotent stem cells'. *Nat Biotechnol* 29:279–286

Bouyer JJ, Miller RJ, Pickel VM (1984) 'Ultrastructural relation between cortical efferents and terminals containing enkephalin-like innunoreactivity in rat neostriatum'. *Regulatory Peptides* 8, pp. 105–115.

Bovè J, Prou D, Perier C, Przedborski S (2005). Toxin-induced models of Parkinson's disease. NeuroRx, 2, pp.484–94.

Boyer, P.D. (1975) 'A model for conformational coupling of membrane potential and proton translocation to ATP synthesis and to active transport', *FEBS Letters*, 58 (1–2), pp.1–6.

Braak H., Del Tredici K., Bratzke H., Hamm-Clement J., Sandmann-Keil D., Rub U. (2002) 'Staging of the intracerebral inclusion body pathology associated with idiopathic Parkinson's disease (preclinical and clinical stages)'. *J. Neurol.* 249 (3), pp. 1–5.

Braak H., Ghebremedhin E., Rub U., Bratzke H., Del Tredici K. (2004). Stages in the development of Parkinson's disease-related pathology. Cell Tissue Res. 318, pp.121–134

Bradford MM (1976). A rapid and sensitive method for the quantitation of microgram quantities of protein utilizing the principle of protein-dye binding', *Analytical Biochemistry,* 72(1-2), pp. 248-254.

Brandt, U. (2006) 'Energy converting NADH:quinone oxidoreductase (complex I)', *Annu Rev Biochem*, 75, pp. 69-92.

Brickley, K. & Stephenson, F. A. (2011). 'Trafficking kinesin protein (TRAK)-mediated transport of mitochondria in axons of hippocampal neurons', *J. Biol. Chem.* 286,pp. 18079–18092

Brickley, K., Smith, M. J., Beck, M. & Stephenson, F. A. (2005) 'GRIF-1 and OIP106, members of a novel gene family of coiled-coil domain proteins: association in vivo and in vitro with kinesin' *J. Biol. Chem.* 280, pp. 14723–14732

Brookes, P.S. et al., (2004) 'Calcium, ATP, and ROS: a mitochondrial love-hate triangle', 287(4), pp. 817–833.

Brown, A., et al. (2014). "Structure of the large ribosomal subunit from human mitochondria." *Science,* 346 (6210), pp. 718-722.

Burre, J. (2015) 'The synaptic function of α-synuclein' *J. Parkinsons Dis.* 5, pp. 699–713.

Burre, J. et al. (2010) 'Alpha-synuclein promotes SNARE-complex assembly in vivo and in vitro' *Science*,329, pp. 1663–1667

Buskila Y , Paul P. Breen , Jonathan Tapson1 , Andre´ van Schaik1 , Matthew Barton2 & John W. Morley1,2 (2014) 'Extending the viability of acute brain slices', *Nature, Scientific Reports,* 4(5309), pp. 1-7.

Bussell R, Jr, Eliezer D. (2004). Effects of Parkinson's disease-linked mutations on the structure of lipid-associated alpha-synuclein. *Biochemistry.* 2004 (43), pp.4810–4818.

Byrd, R.A. and Weissman, A.M. (2013) 'Compact Parkin only: insights into the structure of an autoinhibited ubiquitin ligase'. *EMBO J.* 32, pp. 2087–2089

C. Pacelli, N. Giguere, M.J. Bourque, M. Levesque, R.S. Slack, L.E. Trudeau. (2015) ' Elevated mitochondrial bioenergetics and axonal arborization size are key contributors to the vulnerability of dopamine neurons', *Curr. Biol.* 25, pp.2349-2360.

Cai, Q., Gerwin, C. & Sheng, Z.-H. (2005) 'Syntabulin mediated anterograde transport of mitochondria along neuronal processes'. *J. Cell Biol.* 170, pp. 959–969

Cai, Q., Zakaria, H. M., Simone, A., and Sheng, Z. (2012). 'Spatial parkin translocation and degradation of damaged mitochondria via mitophagy in live cortical neurons', *Curr. Biol.* 22, pp. 545–552.

Caino MC et al., (2015) 'PI3K therapy reprograms mitochondrial trafficking to fuel tumor cell invasion', *PNAS,* 112(28), pp. 8638-8643.

Cali, T., Ottolini, D., Negro, A. & Brini, M. (2012) 'α-Synuclein controls mitochondrial calcium homeostasis by enhancing endoplasmic reticulum–mitochondria interactions', *J. Biol. Chem*. 287, pp. 17914–17929

Campbell, G., Krishnan, K. J., Deschauer, M., Taylor, R. W. & Turnbull, D. M. (2014). Dissecting the mechanisms underlying the accumulation of mitochondrial DNA deletions in human skeletal muscle. *Human molecular genetics* 23, pp.4612-4620.

Carafoli E, Tiozzo R, Lugli G, Crovetti F, Kratzing C (1974) 'The release of calcium from heart mitochondria by sodium', *J Mol Cell Cardiol* 6, pp.361–371.

Carafoli, E. (2003). "The calcium-signalling saga: tap water and protein crystals." *Nat Rev Mol Cell Biol,* 4(4), pp. 326-332.

Cardenas, C. et al. (2010). 'Essential regulation of cell bioenergetics by constitutive InsP3 receptor Ca2+ transfer to mitochondria', *Cell,* 142, pp. 270–283

Carter, B.C., and Bean, B.P. (2009). 'Sodium entry during action potentials of mammalian neurons: incomplete inactivation and reduced metabolic efficiency in fast-spiking neurons', *Neuron*, 64, pp. 898–909.

Cecchini G (2003). Function and structure of complex II of the respiratory chain *Annual Review Biochemistry*.;72 ,pp.77–109. 21.

Chaban Y, Boekema EJ, Dudkinab NV (2014) 'Structures of mitochondrial oxidative phosphorylation supercomplexes and mechanisms for their stabilisation', *Biochimica et Biophysica Acta (BBA) - Bioenergetics,* 1837(4), pp. 418-426.

Chada, S. and Hollenbeck, P. (2003) Mitochondrial movement and positioning in axons: The role of growth factor signalling, *The Journal of experimental biology.*, 206, pp. 1985–92.

Chada, S. R. & Hollenbeck, P. J. (2004). 'Nerve growth factor signaling regulates motility and docking of axonal mitochondria', *Curr. Biol.* 14, pp. 1272–1276

Chan, C.S., Guzman, J.N., Ilijic, E., Mercer, J.N., Rick, C., Tkatch, T., Meredith, G.E., and Surmeier, D.J. (2007). Rejuvenation' protects neurons in mouse models of Parkinson's disease. Nature 447, pp.1081–1086.

Chan, D.C. (2006) 'Mitochondria: dynamic organelles in disease, aging, and 'development'. *Cell,* 125(7), pp. 1241-52.

Chang DT, Honick AS, Reynolds IJ (2006) Mitochondrial trafficking to synapses in cultured primary cortical neurons. J Neurosci 26:7035–7045

Chang, D.D. and Clayton, D.A. (1984) 'Precise identification of individual promoters for transcription of each strand of human mitochondrial DNA', *Cell*, 36(3), pp. 635-43.

Chang K , Niescier RF ,Min K (2011) 'Mitochondrial matrix Ca2+ as an intrinsic signal regulating mitochondrial motility in axons', *Proc Natl Acad Sci U S A,* 108(37), pp. 15456–15461.

Chen Y, Yang M, Deng J, Chen X, Ye Y, Zhu L, Liu J, Ye H, Shen Y, Li Y, Rao EJ, Fushimi K, Zhou X, Bigio EH, Mesulam M, Xu Q, Wu JY (2011). Expression of human FUS protein in Drosophila leads to progressive neurodegeneration. Protein Cell 2(6), pp.477–486

Chen, H., and Chan, D.C. (2009). Mitochondrial dynamics–fusion, fission,movement, and mitophagy–in neurodegenerative diseases. Hum. Mol. Genet. 18 (R2), pp.R169–R176.

Chen, H., Chomyn, A. and Chan, D.C. (2005) 'Disruption of fusion results in mitochondrial heterogeneity and dysfunction', *J Biol Chem*, 280(28), pp. 26185-92.

Chen, H., Vermulst, M., Wang, Y.E., Chomyn, A., Prolla, T.A., McCaffery, J.M. and Chan, D.C. (2010) 'Mitochondrial fusion is required for mtDNA stability in skeletal muscle and tolerance of mtDNA mutations', *Cell*, 141(2), pp. 280-289.

Cheng C, Reynolds IJ (1998) 'Calcium-sensitive fluorescent dyes can report increases in intracellular free zinc concentration in cultured forebrain neurons', *J Neurochem*, 71, pp. 2401–2410.

Cheng XT, Zhou B, Lin MY, Cai Q, Sheng ZH (2015). Axonal autophagosomes recruit dynein for retrograde transport through fusion with late endosomes. J Cell Biol. 2015; 209, pp.377–86.

Chesselet MF (2008) 'In vivo alpha-synuclein overexpression in rodents: A useful model of Parkinson's disease?', *Exp Neurol*, 209, pp.22-27

Cho D. H., Nakamura T., Lipton S. A. (2010). 'Mitochondrial dynamics in cell death and neurodegeneration', *Cell. Mol. Life Sci.* 67, pp. 3435-3447

Choi JM, Woo MS, Ma HI, Kang SY, Sung YH, Yong SW, Chung SJ, Kim JS, Shin HW, Lyoo CH (2008). Analysis of PARK genes in a Korean cohort of early-onset Parkinson disease. Neurogenetics 9: pp.263–269

Chu CT, Ji J, Dagda RK, Jiang JF, Tyurina YY, Kapralov AA, Tyurin VA,Yanamala N, Shrivastava IH, Mohammadyani D, Wang KZQ, Zhu J, Klein-Seetharaman J, Balasubramanian K, et al.,. (2013). 'Cardiolipin externalization to the outer mitochondrial membrane acts as an elimination signal for mitophagy in neuronal cells.' *Nat Cell Biol*. 15 (10), pp.1197-1205.

Chudakov DM, Lukyanov S, Lukyanov KA (2007) 'Tracking intracellular protein movements using photoswitchable fluorescent proteins PS-CFP2 and Dendra2.', *Nature Protocols,* 2(8), pp. 2024-32.

Chung SY, Kishinevsky S, Mazzulli JR, Graziotto J, Mrejeru A, Mosharov EV, Puspita L, Valiulahi P, Sulzer D, Milner TA et al. (2016) 'Parkin and PINK1 patient iPSC-derived midbrain dopamine neurons exhibit mitochondrial dysfunction and alpha synuclein accumulation', *Stem Cell Rep.* 7, pp. 664-677.

Chung-h O. Davis, Keun-Young Kim, Eric A. Bushong, Elizabeth A. Mills, Daniela Boass, Tiffany Shih,Mira Kinebuchi, Sebastien Phan, Yi Zhou, Nathan A. Bihlmeyer, Judy V. Nguyen, Yunju Jin, Mark H. Ellisman and Nicholas Marsh-Armstrong, (2014). Transcellular degradation of axonal mitochondria . *Proc. Natl. Acad. Sci* . 111 (26), pp.9633–9638

Cipolat, S., de Brito, O.M., Dal Zilio, B. and Scorrano, L. (2004) 'OPA1 requires mitofusin 1 to promote mitochondrial fusion', *Proceedings of the National Academy of Sciences of the United States of America*, 101(45), pp. 15927-15932.

Clapham, D. E. (2007) 'Calcium signaling', *Cell,* 131, pp. 1047–1058

Clark AG, Roger AJ (1995). 'Direct evidence for secondary loss of mitochondria in *Entamoeba histolytica*', *Proc Natl Acad Sci* 92, pp. 518–652

Clark IE, Dodson MW, Jiang C, Cao JH, Huh JR, Seol JH, Yoo SJ, Hay BA, Guo M. (2006) 'Drosophila pink1 is required for mitochondrial function and interacts genetically with parkin', *Nature.* 441, pp.1162–1166.

Clark, I., Dodson, M., Jiang, C., Cao, J., Huh, J., Seol, J., Yoo, S., Hay, B. and Guo, M. (2006) Drosophila pink1 is required for mitochondrial function and interacts genetically with parkin, *Nature.*, 441(7097), pp. 1162–6.

Clark, I., Dodson, M., Jiang, C., Cao, J., Huh, J., Seol, J., Yoo, S., Hay, B. and Guo, M. (2006) Drosophila pink1 is required for mitochondrial function and interacts genetically with parkin, Nature., 441(7097), pp. 1162–6.

Clark, I.E. et al. (2006) Drosophila pink1 is required for mitochondrial function and interacts genetically with parkin. *Nature,* 441, pp. 1162–1166

Clayton, D.A. (1982) 'Replication of animal mitochondrial DNA', *Cell*, 28(4), pp. 693-705.

Cleveland, D. W. & Rothstein, J. D.(2001) 'From Charcot to Lou Gehrig: deciphering selective motor neuron death in ALS', *Nature Rev. Neurosci.* 2, pp. 806–819

Cogliati, S., Enriquez, J.A. and Scorrano, L. (2016) 'Mitochondrial Cristae: Where Beauty Meets Functionality', *Trends in Biochemical Sciences*, 41(3), pp. 261-273.

Cohen, G. (2000) Oxidative stress, mitochondrial respiration, and Parkinson's disease, *Annals of the New York Academy of Sciences.*, 899, pp. 112–20.

Cohen, J. E. and R. D. Fields (2004). 'Extracellular calcium depletion in synaptic transmission.' Neuroscientist 10(1), pp. 12-17.

Collier M, Kanaan NM, and Kordower JH (2012) 'Ageing as a primary risk factor for Parkinson's disease: evidence from studies of non-human primates', *Nature Reviews Neuroscience,* 12(6), pp. 359-366.

Corti, O. et al. (2011) 'What genetics tells us about the causes and mechanisms of Parkinson's disease.' *Physiol. Rev.* 91, pp. 1161–1218

Cozzolino, M. & Carri, M. T. (2012) 'Mitochondrial dysfunction in ALS', *Prog. Neurobiol.* 97, pp. 54–66

Crompton, M. (1999). The mitochondrial permeability transition pore and its role in cell death. Journal of Biochemistry. 341, 233–249 Curr. Biol., 26 (2016), pp. 2602-2608

Csordas G et al. (2006) ‘Structural and functional features and significance of the physical linkage between ER and mitochondria’, *J. Cell Biol,* 174 pp. 915–921.

Cui, H., Kong, Y. and Zhang, H. (2012) 'Oxidative Stress, Mitochondrial Dysfunction, and Aging', *Journal of Signal Transduction*, 2012, p. 13.Curr. Biol., 26 (2016), pp. 2602-2608

d'Ydewalle C, Krishnan J, Chiheb DM, Van Damme P, Irobi J, Kozikowski AP, Vanden Berghe P, Timmerman V, Robberecht W, Van Den Bosch L (2011). HDAC6 inhibitors reverse axonal loss in a mouse model of mutant HSPB1-induced Charcot-Marie-Tooth disease. Nat. Med. 17, pp.968–974

Dagda RK, Gusdon AM, Pien I, Strack S, Green S, Li C, Van Houten B, Cherra SJ III, Chu CT. (2011). Mitochondrially localized PKA reverses mitochondrial pathology and dysfunction in a cellular model of Parkinson’s disease. Cell Death Differ; 18, pp.1914–1923.

Dagda RK, Pien I, Wang R, Zhu J, Wang KZ, Callio J, Banerjee TD, Dagda RY, Chu CT. (2014). Beyond the mitochondrion: cytosolic PINK1 remodels dendrites through protein kinase A. Journal of Neurochemistry. 128:864–877.

Dagda, R.K., Gusdon, A.M., Pien, I., Strack, S., Green, S., Li, C., Van Houten, B., Cherra, S.J. and Chu, C.T. (2011) Cell death and differentiation - abstract of article: Mitochondrially localized PKA reverses mitochondrial pathology and dysfunction in a cellular model of Parkinson’s disease, Cell Death & Differentiation, 18(12), pp. 1914–1923.

Dagda, R.K., Gusdon, A.M., Pien, I., Strack, S., Green, S., Li, C., Van Houten, B., Cherra, S.J., III, and Chu, C.T. (2011). Mitochondrially localized PKA reverses mitochondrial pathology and dysfunction in a cellular model of Parkinson’s disease. Cell Death Differences. 18, 1914–1923.

Dai et al., (2013) 'Targeted inhibition of mammalian target of rapamycin (mTOR) enhances radiosensitivity in pancreatic carcinoma cells', *Drug Des Devel Ther,* 7(), pp. 149-159.

Daubner SC, Le T and Wang S (2012) 'Tyrosine Hydroxylase and Regulation of Dopamine Synthesis', *Arch Biochem Biophys,* 508(1), pp. 1-12.

Dauer, W. and Przedborski, S. (2003) Parkinson’s disease: Mechanisms and models, Neuron., 39(6), pp. 889–909.

Davis, C. H. et al. (2014) ‘Transcellular degradation of axonal mitochondria’, *Proc. Natl Acad.* Sci. USA 111, pp. 9633–9638

Dawson, T. and Dawson, V. (2002) Neuroprotective and neurorestorative strategies for Parkinson’s disease, *Nature neuroscience.*, 5, pp. 1058–61.

Dawson, T.M., Dawson, V.L., Institute, Engineering, C., Hopkins, J. and A, U. (2003) Molecular pathways of Neurodegeneration in Parkinson’s disease. Science. 31;302(5646):819-22.

de Grey, A.D. (1997) 'A proposed refinement of the mitochondrial free radical theory of aging', *Bioessays*, 19(2), pp. 161-6.

De Stefani, D., Raffaello, A., Teardo, E., Szabo, I. and Rizzuto, R. (2011) 'A forty-kilodalton protein of the inner membrane is the mitochondrial calcium uniporter', *Nature*, 476(7360), pp. 336-340.

Deas, E., Plun-Favreau, H., Gandhi, S., Desmond, H., Kjaer, S., Loh, S. H. Y., et al. (2011). 'PINK1 cleavage at position A103 by the mitochondrial protease PARL', *Hum. Mol. Genet.* 20, pp. 867–879.

Decuypere, J.-P., Bultynck, G., and Parys, J. B. (2011) 'A dual role for Ca2+ in autophagy regulation', *Cell Calcium,* 50, pp. 242–250

Delong MR. (1990) 'Primate models of movement disorders of basal ganglia origin', *Trends in Neuroscience,* 13 pp. 281–285.

Deng H, Dodson MW, Huang H, Guo M. (2008) 'The Parkinson's disease genes pink1 and parkin promote mitochondrial fission and/or inhibit fusion in Drosophila', 105, pp. 14503–14508.

Detmer SA, Chan DC (2007). Complementation between mouse Mfn1 and Mfn2 protects mitochondrial fusion defects caused by CMT2A disease mutations. *J Cell Biol.* ;176:405–414.

Devi L, Raghavendran V, Prabhu BM, Avadhani NG, Anandatheerthavarada HK (2008). Mitochondrial import and accumulation of alpha-synuclein impair complex I in human dopaminergic neuronal cultures and Parkinson disease brain. *J Biol Chem;*283(14):pp.9089-100.

Devine MJ, Ryten M, Vodicka P, Thomson AJ, Burdon T, Houlden H et al. (2011) 'Parkinson's disease induced pluripotent stem cells with triplication of the a-synuclein locus.' *Nat Commun,* 2, pp. 440.

Diaz, F., Garcia, S., Padgett, K.R. and Moraes, C.T. (2012). A defect in the mitochondrial complex III, but not complex IV, triggers early ROS-dependent damage in defined brain regions. Human Molecular Genetics.1;21(23):5066-77.

Dietrich M.O., Liu Z.W., Horvath T.L. (2013). 'Mitochondrial dynamics controlled by mitofusins regulate Agrp neuronal activity and diet-induced obesity.' *Cell,* 155, pp. 188–199

Dodson MW, Guo M (2007) 'Pink1, Parkin, DJ-1 and mitochondrial dysfunction in Parkinson's disease', Curr Opin Neurobiol, 17(3), pp. 331-337

Dölle et al., (2016) 'Defective mitochondrial DNA homeostasis in the substantia nigra in Parkinson disease', *Nature Communications,* 7(13548), pp. 1-11.

Dora Games et al. (1995). 'Alzheimer-type neuropathology in transgenic mice overexpressing V717F β-amyloid precursor protein',*Nature* . 373, pp.523–527

Drin G, Antonny B. (2010), 'Amphipathic helices and membrane curvature.', *FEBS Lett,* 584, pp.1840–1847.

Dukes A et al., (2017) 'Live imaging of mitochondrial dynamics in CNS dopaminergic neurons in vivo demonstrates early reversal of mitochondrial transport following MPP+ exposure', *Neurobiology of disease,* 95, pp. 238-249.

Dunn, W. A. Jr., Cregg, J. M., Kiel, J. A., van der Klei, I. J., Oku, M., Sakai, Y., et al. (2005). 'Pexophagy: the selective autophagy of peroxisomes' , *Autophagy* 1, pp. 75–83.

Duve D, C. & Wattiaux, R. Functions of lysosomes. Annu. Rev. Physiol. 28, 435–492 (1966)

Ebbing b, Mann k, Starosta A, Jaud J, Schöls L, Schüle R , Woehlke G (2008). Effect of spastic paraplegia mutations in KIF5A kinesin on transport activity. Hum. Mol. Genet., 1, pp. 1245-1252

Edwards FA, Konnerth A, Sakmann B, Takahashi T (1989). A thin slice preparation for patch clamp recordings from neurones of the mammalian central nervous system. Pflugers Arch ;414, pp.600–612.

Efremov RG, Baradaran R, Sazanov LA (2010). The architecture of respiratory complex I. *Nature*.;465 (7297),pp.441–445.

El-Husseini Ael, D., Craven, S. E., Brock, S. C. & Bredt, D. S. (2001) 'Polarized targeting of peripheral membrane proteins in neurons.' *J. Biol. Chem.* 276, pp. 44984–44992

Elmore S. P., Qian T., Grissom S. F., Lemasters J. J. (2001). The mitochondrial permeability transition initiates autophagy in rat hepatocytes. *FASEB J.* 15, pp. 2286-2287

Elson, J.L., Samuels, D.C., Turnbull, D.M. and Chinnery, P.F. (2001) 'Random intracellular drift explains the clonal expansion of mitochondrial DNA mutations with age', *Am J Hum Genet*, 68(3), pp. 802-6.

Embley TM, Hirt RP (1998) 'Early branching eukaryotes?', *Curr Opin Genet Dev* 8, pp. 624–629

Embley TM, Martin W. Eukaryotic evolution, changes and challenges (2006). *Nature*.;440(7084),pp.623–30

Exner N., Treske B., Paquet D., Holmstrom K., Schiesling C., Gispert S., Carballo-Carbajal I., Berg D., Hoepken H. H., Gasser T., et al. (2007). Loss-of-function of human PINK1 results in mitochondrial pathology and can be rescued by parkin. *J. Neurosci.* 27, pp. 12413-12418

Fabricius, C., Berthold, C. H. & Rydmark, M. (1993). 'Axoplasmic organelles at nodes of Ranvier. II. Occurrence and distribution in large myelinated spinal cord axons of the adult cat', *J. Neurocytol.* 22, pp. 941–954

Faccenda, D. Choon H Tan, Michael R Duchen, and Michelangelo Campanella (2013). 'Mitochondrial IF1 preserves cristae structure to limit apoptotic cell death signalling. Cell cycle, 12(16), pp. 2530-2532

Fahn S, Sulzer D. (2004) 'Neurodegeneration and neuroprotection in Parkinson disease.' *Neuro Rx* , 1, pp. 139–154.

Faits MC, Zhang C, Soto F, Kerschensteiner D (2016) Dendritic mitochondria reach stable positions during circuit development., *ELife,* 7(5), pp. 1-17.

Falkenberg, M., Gaspari, M., Rantanen, A., Trifunovic, A., Larsson, N.G. and Gustafsson, C.M. (2002) 'Mitochondrial transcription factors B1 and B2 activate transcription of human mtDNA', *Nat Genet*, 31(3), pp. 289-94.

Fang D, Qing Y, Yan S, Chen D, and Yan SS (2016) 'Development and Dynamic Regulation of Mitochondrial Network in Human Midbrain Dopaminergic Neurons Differentiated from iPSCs', *Stem Cell Reports,* 7(4), pp. 678-692.

Fasano CA, Chambers SM, Lee G, Tomishima MJ, Studer L. (2010) 'Efficient derivation of functional floor plate tissue from human embryonic stem cells.' *Cell Stem Cell*, 6, pp. 336–347.

Fattorini G, Verderio C, Melone M, Giovedì S, Benfenati F, Matteoli M, Conti F. (2009) 'VGLUT1 and VGAT are sorted to the same population of synaptic vesicles in subsets of cortical axon terminals.', *J Neurochem.* 110, pp. 1538–1546

Ferguson SJ. ATP synthase: what dictates the size of a ring? (2000) *Currents topics in Biology*.;10(21), pp.804–8.

Fibiger, H.C., Pudritz, R.E., McGeer, P.L. & McGeer, E.G. (1972) 'Axonal transport in nigro-striatal and nigro-thalamic neurons: effects of medial forebrain bundle lesions and 6-hydroxydopamine.' *J. Neurochem.*, 19, pp, 1697 – 1708.

Fiesel FC, Ando M, Hudec R, Hill AR, Castanedes-Casey M, Caulfield TR, Moussaud-Lamodiere EL, Stankowski JN, Bauer PO, Lorenzo-Betancor O, (2015). 'Patho-physiological relevance of PINK1- dependent ubiquitin phosphorylation.' *EMBO. Rep.* 16, pp.1114-1130.

Filadi R*, et al.* (2015) 'Mitofusin 2 ablation increases endoplasmic reticulum-mitochondria coupling', *Proc. Natl.Acad.Sci.USA,* 112 (17), pp. 2174-2181

Fischer, F. et al. (2012) 'Mitochondrial quality control: an integrated network of pathways.' *Trends Biochem. Sci.* 37, pp. 284–292

Fleischer, S., Klouwen, H. and Brierley, G. (1961) 'Studies of the electron transfer system. 38. Lipid composition of purified enzyme preparations derived from beef heart mitochondria', *J Biol Chem*, 236, pp. 2936-41.

Fode, C., Gradwohl, G., Morin, X., Dierich, A., LeMeur, M., Goridis, C. and Guillemot, F. (1998). 'The bHLH protein NEUROGENIN 2 is a determination factor for epibranchial placode-derived sensory neurons.', *Neuron,* 20, pp. 483-494

Fontecave, M (2006) 'Iron-sulfur clusters: ever-expanding roles', *Nature Chemical Biology*, 2(4), pp.171–174.

Fowler JS, Volkow N, Wang GJ, Logan J, Pappas N, Shea C, MacGregor R. (1997) 'Age-related increases in brain monoamine oxidase B in living healthy human subjects.' *Neurobiol Aging.* 18, pp.431– 435.

Francesconi, A. & Duvoisin, R. M (2002). Alternative splicing unmasks dendritic and axonal targeting signals in metabotropic glutamate receptor 1. J. Neurosci. 22, pp.2196–2205

Fransson, A., Ruusala, A. & Aspenström, P. (2003) 'Atypical Rho' GTPases have roles in mitochondrial homeostasis and apoptosis.' *J. Biol. Chem*. 278, pp. 6495–6502

Frederick, R. L., McCaffery, J. M., Cunningham, K. W., Okamoto, K. & Shaw, J. M. (2004) 'Yeast Miro GTPase, Gem1p, regulates mitochondrial morphology via a novel pathway.' *J. Cell Biol.* 167, pp. 87–98

Freund TF, Powell J, Smith AD (1984) 'Tyrosine hydroxylase-immunoreactive boutons in synaptic contact with identified striatonigral neurons, with particular reference to dendritic spines.', *Neuroscience,* 13, pp. 1189–1215.

Frey, T.G. and Mannella, C.A. (2000) 'The internal structure of mitochondria', *Trends Biochem Sci*, 25(7), pp. 319-24.

Fridovich I. (1989) 'Superoxide dismutases. An adaptation to a paramagnetic gas.' *J Biol Chem.* 264, pp. 7761–7764.

Friedman, J.R. et al. (2011). 'ER tubules mark sites of mitochondrial division.' *Science (New York, N.Y.)*, 334 (6054), pp.358–62.

Friel DD. (2000). 'Mitochondria as regulators of stimulus-evoked calcium signals in neurons.' Cell Calcium. 2000; 28:307–316.

G.A Perkins and T.G Frey (2000) 'Recent structural insight into mitochondria gained by microscopy.', *Micron,* 31(1), pp. 97-111.

Galvani, L. (1791). De viribus electricitatis in motu musculari: commentarius. Bononiae : Ex Typographia Instituti Scientiarium.

Gandhi, S., Wood-Kaczmar, A., Yao, Z., Plun-Favreau, H., Deas, E., Klupsch, K., Downward, J., Latchman, D.S., Tabrizi, S.J., Wood, N.W., Duchen, M.R. and Abramov, A.Y. (2009) Article PINK1-Associated Parkinson's disease is caused by neuronal vulnerability to calcium-induced cell death, *Molecular Cell*, 33, pp. 627–638.

Garofalo, T. et al. (2016). 'Evidence for the involvement of lipid rafts localized at the ER–mitochondria associated membranes in autophagosome formation.', *Autophagy* 12, pp. 917–935

Gautier C.A., Kitada T., Shen J. (2008) 'Loss of PINK1 causes mitochondrial functional defects and increased sensitivity to oxidative stress.' *Proc. Natl. Acad. Sci. U.S.A.* 105, pp. 11364–11369.

Gautier, C. A. et al. (2016) 'The endoplasmic reticulum–mitochondria interface is perturbed in PARK2 knockout mice and patients with PARK2 mutations.' *Hum. Mol. Genet*. 25, pp. 2972–2984

Geisler, S., Holmström, K.M., Skujat, D., Fiesel, F.C., Rothfuss, O.C., Kahle, P.J. and Springer, W. (2010) PINK1/Parkin-mediated mitophagy is dependent on VDAC1 *Nature Cell Biology*, 12(2), pp. 119–131.

Gelmetti, V. et al. (2017) ;PINK1 and BECN1 relocalize at mitochondria associated membranes during mitophagy and promote ER–mitochondria tethering and autophagosome formation.', *Autophagy,* 13, pp. 654–669

Genova ML, Lenaz G. (2014) Functional role of mitochondrial respiratory supercomplexes. Biochim Biophys Acta.;1837(4), pp. 427–43.

Gerfen, C.R., Herkenham, M. & Tribault, J. (1987) 'The neostriatal mosaic: II. Patch and matrix-directed mesostriatal dopaminergic and non-dopaminergic systems.', *J. Neurosci.*, **7**, 3915 – 3934.

Ghavami, S. et al. (2014) 'Autophagy and apoptosis dysfunction in neurodegenerative disorders.' *Prog. Neurobiol.* 112, pp. 24–49

Giasson, B.I., Duda, J.E., Quinn, S.M., Zhang, B., Trojanowski, J.Q., Lee, V.M., (2002). Neuronal alpha-synucleinopathy with severe movement disorder in mice expressing A53T human alpha-synuclein. Neuron 34, pp. 521 – 533

Gibson GE, Starkov A, Blass JP, Ratan RR, Beal MF. (2010). 'Cause and consequence: mitochondrialdysfunction initiates and propagates neuronal dysfunction, neuronal death and behavioralabnormalities in age-associated neurodegenerative diseases.', *Biochim Biophys Acta.* 1802, pp. 122–134.

Gilkerson, R.W., Selker, J.M.L. & Capaldi, R.A. (2003) 'The cristal membrane of mitochondria is the principal site of oxidative phosphorylation.', *FEBS letters*, 546(2–3), pp.355–8.

Gispert S., Ricciardi F., Kurz A., Azizov M., Hoepken H.H., Becker D., Voos W., Leuner K., Muller W.E., Kudin A.P., et al. (2009). 'Parkinson phenotype in aged PINK1-deficient mice is accompanied by progressive mitochondrial dysfunction in absence of neurodegeneration.' *PLoS ONE.* 4, pp. 5777.

Gispert, S., Del Turco, D., Garrett, L., Chen, A., Bernard, D.J., Hamm, Clement, J., Korf, H.W., Deller, T., Braak, H., Auburger, G., Nussbaum, R.L., (2003). Transgenic mice expressing mutant A53T human alphasynuclein show neuronal dysfunction in the absence of aggregate formation. Mol. Cell. Neurosci. 24, pp. 419 – 429.

Gispert, S., Del Turco, D., Garrett, L., Chen, A., Bernard, D.J., HammClement, J., Korf, H.W., Deller, T., Braak, H., Auburger, G., Nussbaum, R.L. (2003) 'Transgenic mice expressing mutant A53T human alphasynuclein show neuronal dysfunction in the absence of aggregate formation.', *Mol. Cell. Neurosci* 24, pp. 419 – 429.

Glater, E. E., Megeath, L. J., Stowers, R. S. & Schwarz, T. L.(2006) 'Axonal transport of mitochondria requires milton to recruit kinesin heavy chain and is light chain independent.', *J. Cell Biol.* 173,pp. 545–557

Glater, E.E., Megeath, L.J., Stowers, S.R. and Schwarz, T.L. (2006) Axonal transport of mitochondria requires milton to recruit kinesin heavy chain and is light chain independent, *The Journal of Cell Biology*, 173(4), pp. 545–557.

Gleichmann M and Mattson MP (2011) 'Neuronal Calcium Homeostasis and Dysregulation', *Antioxidants & Redox Signalling,* 14(7), pp. 1261 - 1272.

Glenn Friedrich and Phillipe Soriano (1991). Promoter traps in embryonic stem cells: a genetic screen to identify and mutate developmental genes in mice.', *Genes and development, cold spring harbour,* 5, pp. 1513-1523.

Godement P, Vanselow J, Thanos S, F (1987). A study in developing visual systems with a new method of staining neurones and their processes in fixed tissue. *Development*, 101, pp. 697-713

Goldberg, A. V et al. (2008). 'Localization and functionality of microsporidian iron-sulphur cluster assembly proteins.' *Nature*, 452 (7187), pp.624–628.

Gomez-Isla, T., Irizarry, M.C., Mariash, A., Cheung, B., Soto, O., Schrump, S., Sondel, J., Kotilinek, L., Day, J., Schwarzschild, M.A., Cha, J.H., Newell, K., Miller, D.W., Ueda, K., Young, A.B., Hyman, B.T., Ashe, K.H., (2003). Motor dysfunction and gliosis with preserved dopaminergic markers in human alpha-synuclein A30P transgenic mice. Neurobiol. Aging 24, pp. 245 – 258.

Gomez-Sa´ nchez, R., Gegg, M.E., Bravo-San Pedro, J.M., Niso-Santano, M., Alvarez-Erviti, L., Pizarro-Estrella, E., Gutie´rrez-Martı´n, Y., Alvarez-Barrientos, A., Fuentes, J.M., Gonza´ lez-Polo, R.A., and Schapira, A.H. (2014). Mitochondrial impairment increases FL-PINK1 levels by calcium-dependent gene expression. Neurobiol. Dis. 62, 426–440.

González-Hernández T, Barroso-Chinea P, Acevedo A, Salido E, Rodríguez M (2004). 'Response of the GABAergic and Dopaminergic Mesostriatal Projections to the Lesion of the Contralateral Dopaminergic Mesostriatal Pathway in the Rat.' *Movement Disorders*. 19 (9), pp. 1029 –1042.

Górska-Andrzejak, J. et al. (2003) 'Mitochondria are redistributed in Drosophila photoreceptors lacking milton, a kinesin-associated protein.' *J. Comp. Neurol.* 463, pp. 372–388

Grace, A. A. & Bunney, B. S. (1983) 'Intracellular and extracellular electrophysiology of nigral dopaminergic neurons Evidence for electrotonic coupling.', *Neuroscience* 10, pp. 333–348

Graham D. (1978) 'Pathways for catecholamines in the genesis of neuromelanin and cytotoxic quinones.' *Mol Pharmacol.* 14, pp. 633–643.

Gray MW (1992). The endosymbiont hypothesis revisited. *International Review of Cytology*.; 5, pp.233–357

Gray, M.W., Burger, G. & Lang, B.F. (1999). 'Mitochondrial evolution.' *Science,* 283 (5407), pp.1476–81.

Gray, M.W., Burger, G. & Lang, B.F. (2001). 'The origin and early evolution of mitochondria.', *Genome biology*, 2(6), pp. 1018.

Greene, A. W., Grenier, K., Aguileta, M. A., Muise, S., Farazifard, R., and Haque, M. E. (2012). 'Mitochondrial processing peptidase regulates PINK1 processing, import and Parkin recruitment.', *EMBO Rep.* 13, pp. 378–385

Greene, J.C., Whitworth, A.J., Kuo, I., Andrews, L.A., Feany, M.B., and Pallanck, L.J. (2003). Mitochondrial pathology and apoptotic muscle degeneration in Drosophila parkin mutants. *Proceedings of. National Academy of Sciences.*100, pp.4078– 4083.

Greengard P., Allen P. B., Nairn A. C. (1999). 'Beyond the dopamine receptor: the DARPP-32/protein phosphatase-1 cascade.', *Neuron* 23, pp. 435–447

Grenier, K., McLelland, G.-L., and Fon, E. A. (2013). 'Parkin- and PINK1- dependent mitophagy in neurons: will the real pathway please stand up?, *Front. Neurol,* 4, pp. 100.

Gresser MJ , Myers J, Boyer PD (1982)' Catalytic site cooperativity of beef heart mitochondrial F_1 adenosine triphosphatase. Correlations of initial velocity, bound intermediate, and oxygen exchange measurements with an alternating three-site model' J Biol Chem, 257 (20), pp.12030-12038

Grishin, A., Li, H., Levitan, E. S. & Zaks-Makhina, E. (2006). 'Identification of γ-aminobutyric acid receptorinteracting factor 1 (TRAK2) as a trafficking factor for the K+ channel Kir2.1.', *J. Biol. Chem,* 281 pp. 30104–30111

Grobaski KC, Ping H, DaSilva HM, NG Bowery, ST Connelly, PD Shepard (1997). Responses of rat substantia nigra dopamine-containing neurones to (-)-HA-966 in vitro. Br J Pharmacol, 120. pp. 575–580

Gross NJ, Getz GS, Rabinowitz M. (1969) 'Apparent turnover of mitochondrial deoxyribonucleic acid and mitochondrial phospholipids in the tissues of the rat' , *J Biol Chem.* 244, pp. 1552–62.

Guardia-Laguarta, C. et al. (2014) 'α-Synuclein is localized to mitochondria-associated ER membranes.', *J. Neurosci.* 34, pp. 249–259

Guardia-Laguarta, C., Area-Gomez, E., Schon, E. A. & Przedborski, S. (2015) 'Novel subcellular localization for alpha-synuclein: possible functional consequences.' Front. Neuroanat. 9 (17), pp.1-7

Guillaud, L., Setou, M. & Hirokawa, N (2003). KIF17 dynamics and regulation of NR2B trafficking in hippocampal neurons. J. Neurosci. 23, pp.131–140 (2003).

Guo, X. et al. (2005) 'The GTPase dMiro is required for axonal transport of mitochondria to Drosophila synapses, *Neuron* 47, pp. 379–393

Gupta A, Dawson VL, Dawson TM. (2008) 'What causes cell death in Parkinson's disease?', *Ann Neurol* 64, pp. 3-15.

Gurskaya NG1, Verkhusha VV, Shcheglov AS, Staroverov DB, Chepurnykh TV, Fradkov AF, Lukyanov S, Lukyanov KA. (2006) 'Engineering of a monomeric green-to-red photoactivatable fluorescent protein induced by blue light.', *Nature Biotechnology,* 24(4), pp. 461–465.

Gutiérrez, R., Romo-Parra, H., Maqueda, J., Vivar, C., Ramírez, M., Morales M. A., et al. (2003). 'Plasticity of the GABAergic phenotype of the "glutamatergic" granule cells of the rat dentate gyrus.' *J. Neurosci.* 23, pp. 5594–5598

Guzman JZ, Sanchez-Padilla J, Wokosin D, Kondapalli J, Ilijic E, et al. (2010) 'Oxidant stress evoked by pacemaking in dopaminergic neurons is attenuated by DJ-1.' *Nature,* 468, pp 696–700

Guzman, K. M., Jing, L. & Patwardhan, A. (2010) 'Effects of changes in the L-type calcium current on hysteresis in restitution of action potential duration.', *Pacing Clin. Electrophysiol.* 33, pp. 451–459

Haas R. H., Nasirian F., Nakano K., Ward D., Pay M., Hill R. and Shults C. W. (1995) 'Low platelet mitochondrial complex I and complex II/III activity in early untreated Parkinson's disease.' *Ann. Neurol.* 37, pp. 714–722.

Haber, J.E. (2000) 'Partners and pathways repairing a double-strand break.' *Trends Genet.* 16, 259–264

Haghnia, M. et al. (2007) 'Dynactin is required for coordinated bidirectional motility, but not for dynein membrane attachment.' *Mol. Biol. Cell*, 18, pp. 2081–2089

Halestrap AP. (2009) 'Mitochondrial calcium in health and disease.', *Biochim Biophys Acta.* 1878 (11), pp. 1289-12990

Halliwell, B. (1992). 'Reactive oxygen species and the central nervous system.', *J. Neurochem. 5*9, pp. 1609–1623

Hamasaki, M. et al. (2013). 'Autophagosomes form at ER–mitochondria contact sites', *Nature* 495, pp. 389–393

Handschin, C., Chin, S., Li, P., Liu, F., Maratos-Flier, E., Lebrasseur, N.K., Yan, Z. and Spiegelman, B.M. (2007) 'Skeletal muscle fiber-type switching, exercise intolerance, and myopathy in PGC-1alpha muscle-specific knock-out animals', *J Biol Chem*, 282(41), pp. 30014-30021.

Hanekamp, T. & Thorsness, P.E. (1999) 'YNT20, a bypass suppressor of yme1 yme2, encodes a putative 3′-5′ exonuclease localized in mitochondria of *Saccharomyces cerevisiae*.' *Curr. Genet.* 34, pp. 438–448

Hanley JJ, Bolam JP. (1997) 'Synaptology of the nigrostriatal projection in relation to the compartmental organization of the neostriatum in the rat.', *Neuroscience* 81, PP. 353–370

Hara, T., Nakamura, K., Matsui, M., Yamamoto, A., Nakahara, Y., SuzukiMigishima, R., et al. (2006). 'Suppression of basal autophagy in neural cells causes neurodegenerative disease in mice.' ,Nature 441, PP. 885–889.

Harris, J.J., and Attwell, D. (2012). 'The energetics of CNS white matter.' *J. Neurosci.* 32, pp 356–371.

Hartfield, E.M., Yamasaki-Mann, M., Ribeiro Fernandes, H.J., Vowles, J., James, W.S., Cowley, S.A. and Wade-Martins, R. (2014) 'Physiological Characterisation of human iPS-derived Dopaminergic Neurons', *PLoS ONE*, 9(2), pp. e87388.

Hastings TG. (1976) ‘Enzymatic oxidation of dopamine: The role of prostaglandin H synthase.’ *J Neurochem.* 64, pp 919–924.

Hatefi, Y. (1976) 'The Enzymes and the Enzyme Complexes of the Mitochondrial Oxidative Phosphorylation System', *The Enzymes of Biological Membranes: Volume 4: Electron Transport Systems and Receptors*. Boston, MA: Springer US, pp. 3-41.

Hattori, T., Takada, M., Moriizumi, T. & Van der Kooy, D. (1991) ‘Single dopaminergic nigrostriatal neurons from two chemically distinct synaptic types: possible transmitter segregation within neurons.’, *J. Comp. Neurol.*, 309, pp. 3910 – 3401.

Hayashi T, Rizzuto R, Hajnoczky G, Su TP. MAM: more than just a housekeeper. Trends Cell Biol. 2009;19:81–88.

Hayashi, J.I., Ohta, S., Kikuchi, A., Takemitsu, M., Goto, Y.I. and Nonaka, I. (1991) 'Introduction of disease-related mitochondrial DNA deletions into HeLa cells lacking mitochondrial DNA results in mitochondrial dysfunction', *Proceedings of the National Academy of Sciences of the United States of America*, 88(23), pp. 10614-10618.

He L, Chinnery PF, Durham SE, Blakely EL, Wardell TM, Borthwick GM, Taylor RW, Turnbull DM (2002) ‘Detection and quantification of mitochondrial DNA deletions in individual cells by real-time PCR.’ Nucleic Acids Res. 30 (14), pp. 68

Helena Bros, Anja Hauser, Friedemann Paul, Raluca Niesner and Carmen Infante-Duarte ,(2015). ‘Assessing Mitochondrial Movement Within Neurons: Manual Versus Automated Tracking Methods.’ *Traffic* . 16, pp.906–917

Henderson, N.S. et al. (2000) ‘Separation of intact pyruvate dehydrogenase complex using blue native agarose gel electrophoresis.’, *Electrophoresis*, 21(14), pp. 2925–2931.

Herrmann, J.M. and Neupert, W. (2000) 'Protein transport into mitochondria', *Current Opinion in Microbiology*, 3(2), pp. 210-214.

Hink E, Bevan MD, Bolam JP, Smith y (1996) ‘The subthalamic nucleus and the external pallidum: two tightly interconnected structures that control the output of the basal ganglia in the monkey.’ *Neuroscience* 73, PP. 335–357

Hirokawa, N. (1982) ‘Cross-linker system between neurofilaments, microtubules, and membranous organelles in frog axons revealed by the quick-freeze, deep-etching method.’, *J. Cell Biol.* 94, pp. 129–142

Hirokawa, N. & Takemura, R (2005) ‘Molecular motors and mechanisms of directional transport in neurons.’ 6, pp. 201-214

Hirokawa, N. & Takemura, R. in Molecular Motors (ed. Schliwa, M.) 79–109 (Wiley-VCH, Weinheim, 2003).

Hirokawa, N., Niwa, S. & Tanaka, Y. (2010) 'Molecular motors in neurons: transport mechanisms and roles in brain function, development, and disease.' *Neuron* 68, pp. 610–638

Hirokawa, N., Sato-Yoshitake, R., Yoshida, T. & Kawashima, T. (1990) 'Brain dynein (MAP1C) localizes on both anterogradely and retrogradely transported membranous organelles in vivo.' *J. Cell Biol.* 111, pp. 1027–1037

Hodgkin, A. and Huxley, A. (1939). 'Action Potentials Recorded from Inside a Nerve Fibre.' *Nature*, 144(3651):710.

Hollenbeck M, Grabensee B (1993) 'Hemolytic-uremic syndrome and thrombotic thrombocytopenic purpura in the adult.' *Deutsche medizinische Wochenschrift* 118, pp. 69–75

Hollenbeck PJ, Saxton WM. (2005). 'The axonal transport of mitochondria.' *J Cell Sci* 118, pp. 5411–5419.

Hollenbeck, P.J. (1993) 'Products of endocytosis and autophagy are retrieved from axons by regulated retrograde organelle transport.' *J. Cell Biol.* 121, pp.305– 315.

Holt, I.J. & Reyes, A., (2012) 'Human Mitochondrial DNA Replication.' *Cold Spring Harbor Perspectives in Biology*, 4 (12), pp.012971

Holt, I.J., Harding, A.E., and Morgan-Hughes, J.A. (1988). 'Deletions of muscle mitochondrial DNA in patients with mitochondrial myopathies.' *Nature,* 331, pp. 717–719.

Holt, I.J., Lorimer, H.E. and Jacobs, H.T. (2000) 'Coupled Leading- and Lagging-Strand Synthesis of Mammalian Mitochondrial DNA', *Cell*, 100(5), pp. 515-524.

Honig, M.G. and Hume, R.I. (1986) Fluorescent Carbocyanine dyes allow living Neurons of identified origin to be studied in long-term cultures. *The Journal of Cellular Biology*, 103(1): pp.171–187.

Houlden, H. and Singleton, A.B. (2012) 'The genetics and neuropathology of Parkinson's disease.' *Acta Neuropathol.* 124, pp.325– 338

Hu BY, Weick JP, Yu J, Ma LX, Zhang XQ, Thomson JA, Zhang SC. (2010) 'Neural differentiation of human induced pluripotent stem cells follows developmental principles but with variable potency.' *Proc Natl Acad Sci U S A*. 107. pp. 4335–40.

Hu, Y., Massen, S., Terenzio, M., Lang, V., Chen-Lindner, S., Eils, R., et al. (2013). 'Modulation of serines 17 and 24 in the LC3-interacting region of Bnip3 determines pro-survival mitophagy versus apoptosis.' *J. Biol. Chem.* 288, pp. 1099–1113

Hubley, M. J., Locke, B. R. & Moerland, T. S. (1996) 'The effects of temperature, pH, and magnesium on the diffusion coefficient of ATP in solutions of physiological ionic strength.' *Biochim. Biophys. Acta* 1291, pp. 115–121

Hunte C, Zickermann V, Brandt U (2010). Functional Modules and Structural Basis of Conformational Coupling in Mitochondrial Complex I', *Science,* 329(5990), pp. 448-451.

Hurd DD, Saxton WM. (1996). Kinesin mutations cause motor neuron disease phenotypes by disrupting fast axonal transport in Drosophila. Genetics 144, pp.1075–1085.

Hyman S. E., Malenka R. C. (2001). 'Addiction and the brain: the neurobiology of compulsion and its persistence.' *Nat. Rev. Neurosci.* 2, pp. 695–703

Imai Y, Kanao T, Sawada T, Kobayashi Y, Moriwaki Y, Ishida Y, Takeda K, Ichijo H, Lu B, Takahashi R. (2010) 'The loss of PGAM5 suppresses the mitochondrial degeneration caused by inactivation of PINK1 in Drosophila.' *PLoS Genet.* 6, pp. 1001229.

Imai, Y. et al. (2002) 'CHIP is associated with Parkin, a gene responsible for familial Parkinson's disease, and enhances its ubiquitin ligase activity.' *Mol. Cell,* 10, pp. 55–67

Inazu M, Takeda H, Ikoshi H, Uchida Y, Kubota N, Kiuchi Y, Oguchi K, Matsumiya T. (1999) 'Regulation of dopamine uptake by basic fibroblast growth factor and epidermal growth factor in cultured rat astrocytes.' *Neurosci Res,* 34, pp.235–244

Itoh, K. et al. (2013) 'Mitochondrial dynamics in neurodegeneration.' *Trends Cell Biol.* 23, pp. 64–71

Iwai A, Masliah E, Yoshimoto M, Ge N, Fianagan L, Rohan de Silva HA, Kittei A and Saitoh T *(*1995a*)* The precursor protein of non-A β component of Alzheimer's disease amyloid is a presynaptic protein of the central nervous system. *Neuron* 14*:pp.*467–475*.*

Iwai A, Yoshimoto M, Masliah E, Saitoh T *(*1995b*)* Non-A β component of Alzheimer's disease amyloid (NAC) is amyloidogenic. *Biochemistry* 34*:pp.*10139–10145*.*

Iwata S, Lee JW, Okada K, Lee JK, Iwata M, Rasmussen B (1998). Complete structure of the 11-subunit bovine mitochondrial cytochrome bc1 complex. *Science*, 281(5373): pp.64–71. 22.

Izzo PN, Bolam JP (1988) 'Cholinergic synaptic input to different parts of spiny striatonigral neurons in the rat.' *Journal of Comparative Neurology,* 269, pp. 219–234.

Jackson D. M., Westlind-Danielsson A. (1994). 'Dopamine receptors: molecular biology, biochemistry and behavioural aspects.' *Pharmacol. Ther.* 64, pp. 291–370

Jackson, J.G., O'Donnell, J.C., Takano, H., Coulter, D.A., and Robinson,M.B. (2014). Neuronal activity and glutamate uptake decrease mitochondrial mobility in astrocytes and position mitochondria near glutamate transporters. J. Neurosci. 34, pp.1613–1624.

Jenner P (2003). Oxidative stress in Parkinson's disease. Annals of Neurology. 53: Suppl 3S26–36.P.

Jenner P, Langston JW. (2011) 'Explaining adagio: A critical review of the biological basis for the clinical effects of rasagiline.' *Mov Disord.* 26, pp. 2316–2323.

Jensen MB, Bhatia VK, Jao CC, Rasmussen JE, Pedersen SL, Jensen KJ, Langen R, Stamou D. (2011) 'Membrane curvature sensing by amphipathic helices: a single liposome study using α-synuclein and annexin B12.' *J Biol Chem,* 286, pp. 42603–42614.

Jeppesen, M.G., Navratil, T., Spremulli, L.L. and Nyborg, J. (2005) 'Crystal structure of the bovine mitochondrial elongation factor Tu.Ts complex', *J Biol Chem*, 280(6), pp. 5071-81.

Jin, S. M., Lazarou, M., Wang, C., Kane, L. A., Narendra, D. P., and Youle, R. J. (2010). 'Mitochondrial membrane potential regulates PINK1 import and proteolytic destabilization by PARL' *J. Cell Biol,* 191, pp. 933–942.

Jin, S.M. et al. (2010) 'Mitochondrial membrane potential regulates PINK1 import and proteolytic destabilization by PARL.' *J. Cell Biol.* 191 pp. 933–942

Jo E, Fuller N, Rand RP, St George-Hyslop P, Fraser PE (2002) 'Defective membrane interactions of familial Parkinson's disease mutant A30P alpha-synuclein', *J Mol Biol*, 315 (4), pp. 799-807

Johns, D. R., Rutledge, S. L., Stine, O. C. & Hurko, O (1989) 'Directly repeated sequences associated with pathogenic mitochondrial DNA deletions.' *Proc. Natl Acad. Sci. USA.* 86, pp. 8059–8062

Johnson DC, Dean DR, Smith AD, Johnson MK (2005). 'Structure, function and formation of biological iron–sulfur clusters.' *Ann Rev Biochem* 74, pp. 247–281

Johnson MA, Weick JP, Pearce RA, Zhang SC. (2007) 'Functional neural development from human embryonic stem cells: accelerated synaptic activity via astrocyte coculture.' *J Neurosci,* 27, pp. 3069–3077.

Jonckheere, A.I., Smeitink, J.A.M. and Rodenburg, R.J.T. (2012) 'Mitochondrial ATP synthase: architecture, function and pathology', *Journal of Inherited Metabolic Disease*, 35(2), pp. 211-225.

Judy V. Nguyen, Ileana Soto, Keun-Young Kim, Eric A. Bushong, Ericka Oglesby, Francisco J. Valiente-Soriano, (2011). 'Myelination transition zone astrocytes are . *Proc. Natl. Acad. Sci.* . 108 (3), pp.1176–1181

Jung, D., Filliol, D., Miehe, M. & Rendon, A (1993) 'Interaction of brain mitochondria with microtubules reconstituted from brain tubulin and MAP2 or TAU.' *Cell Motil. Cytoskeleton* 24, pp. 245–255

Kahle, P.J., Neumann, M., Ozmen, L., Muller, V., Jacobsen, H., Schindzielorz, A., Okochi, M., Leimer, U., van Der Putten, H., Probst, A., Kremmer, E., Kretzschmar, H.A., Haass, C., (2000). Subcellular localization of wild-type and Parkinson's disease-associated mutant alpha -synuclein in human and transgenic mouse brain. J. Neurosci. 20, pp. 6365 – 6373.

Kamp F, Beyer K. 'Binding of α-synuclein affects the lipid packing in bilayers of small vesicles.' (2006), *J Biol Chem,* 281, pp. 9251–9259.

Kamp F, Exner N, Lutz AK, Wender N, Hegermann J, Brunner B, Nuscher B, Bartels T, Giese A, Beyer K, Eimer S, Winklhofer KF, Haass C (2010). Inhibition of mitochondrial fusion by α-synuclein is rescued by PINK1, Parkin and DJ-1.*EMBO J.* 2010 Oct 20; 29(20):pp.3571-89.

Kanai, Y. et al. (2000) 'KIF5C, a novel neuronal kinesin enriched in motor neurons.' *J. Neurosci.* 20, pp. 6374–6384

Kandul NP, Zhang T, Hay B, and Guoa M, (2016) 'Selective removal of deletion-bearing mitochondrial DNA in heteroplasmic Drosophila', *Nature Communications,* 7(13100), pp. 1-11.

Kang, J. S. et al. (2008) 'Docking of axonal mitochondria by syntaphilin controls their mobility and affects short term facilitation.' *Cell,* 132, pp. 137–148

Kao YH, Lassová L, Bar-Yehuda T, Edwards RH, Sterling P, Vardi N. (2004) 'Evidence that certain retinal bipolar cells use both glutamate and GABA.' *J Comp Neurol.* 478, pp. 207–218

Katz, B. & Miledi, R. (1968) 'The role of calcium in neuromuscular facilitation.' *J. Physiol.* 195, pp. 481–492

Kaushal, P. S., et al. (2014). "Cryo-EM structure of the small subunit of the mammalian mitochondrial ribosome." *Proc Natl Acad Sci U S A,* 111(20), pp. 7284-7289.

Kawaguchi Y (1997) 'Neostriatal cell subtypes and their functional roles.' *Neuroscience Research* 27, pp. 1–8.

Kawaguchi Y, Wilson CJ, Augood SJ, Emson PC (1995) 'Striatal interneurones: chemical, physiological and morphological characterization.' *Trends in Neurosciences,* 18, pp. 527–535.

Kazlauskaite, A., Kelly, V., Johnson, C., Baillie, C., Hastie, C.J., Peggie, M., Macartney, T., Woodroof, H.I., Alessi, D.R., Pedrioli, P.G., and Muqit, M.M. (2014a). Phosphorylation of Parkin at Serine65 is essential for activation: elaboration of a Miro1 substrate-based assay of Parkin E3 ligase activity. *Open Biology*. 4, pp. 130213.

Kebabian J. W., Calne D. B. (1979). 'Multiple receptors for dopamine.' *Nature* 277, pp. 93–96

Keeling, P.J. & Palmer, J.D., (2008). 'Horizontal gene transfer in eukaryotic evolution.' *Nat Rev Genet*, 9(8), pp. 605–618.

Kemp JM, Powell TPS (1971a) 'The structure of the caudate nucleus of the cat: light and electron microscopy.' *Philosophical Transactions of the Royal Society of London*, 262, pp.383–401.

Kemp, J. M., and Powell, T. P. (1971a). The site of termination of afferent fibres in the caudate nucleus. *Philos. Trans. R. Soc. Lond. B Biol. Sci.* 262, 413–427.

Khaidakov, M., Heflich, R. H., Manjanatha, M. G., Myers, M. B. & Aidoo, A. (2003). 'Accumulation of point mutations in mitochondrial DNA of aging mice.' *Mutation Research/Fundamental and Molecular Mechanisms of Mutagenesis* 526, pp. 1-7.

Ki CS, Stavrou EF, Davanos N, Lee WY, Chung EJ, Kim JY, Athanassiadou A (2007). The Ala53Thr mutation in the α-synuclein gene in a Korean family with Parkinson disease. Clin Genet 71: pp.471–473

Kim et al., (2012) CRIF1 Is Essential for the Synthesis and Insertion of Oxidative Phosphorylation Polypeptides in the Mammalian Mitochondrial Membrane', *Cell Metabolism,* 16(2), pp. 274-283.

Kim et al.,. (2007). 'Selective degradation of mitochondria by mitophagy.' *Arch Biochem. Biophys.* 462, pp. 245-253

Kimelberg HK, Katz DM. (1986) 'Regional differences in 5-hydroxytryptamine and catecholamine uptake in primary astrocyte cultures.' *J Neurochem.* 47, pp. 1647–1652.

King, S. J. & Schroer, T. A. (2000) 'Dynactin increases the processivity of the cytoplasmic dynein motor.' *Nature Cell Biol.* 2, pp. 20–24

Kirk, E., Chin, L. S. & Li, L. (2006) 'GRIF1 binds Hrs and is a new regulator of endosomal trafficking' *J. Cell Sci.* 119, pp. 4689–4701

Kirkeby A, Grealish S, Wolf DA, Nelander J, Wood J, Lundblad M et al (2012) 'Generation of regionally specified neural progenitors and functional neurons from human embryonic stem cells under defined conditions.' *Cell Rep* 1, pp.703–714.

Kirkinezos IG, Moraes CT. (2001) 'Reactive oxygen species and mitochondrial diseases.' *Semin Cell Dev Biol*.12. pp.449–457.

Kiryu-Seo, S., N. Ohno, G.J. Kidd, H. Komuro, and B.D. Trapp. (2010). Demyelination increases axonal stationary mitochondrial size and the speed of axonal mitochondrial transport. J. Neurosci. 30, pp.6658–6666.

Kispal G, Csere P, Prohl C, Lill R (1999). 'The mitochondrial proteins Atm1p and Nfs1p are required for biogenesis of cytosolic Fe/S proteins'. *EMBO J* 18, pp. 3981–3989

Kitada T., Pisani A., Porter D.R., Yamaguchi H., Tscherter A., Martella G., Bonsi P., Zhang C., Pothos E.N., Shen J. (2007) 'Impaired dopamine release and synaptic plasticity in the striatum of PINK1-deficient mice.' *Proc. Natl. Acad. Sci. U.S.A. 2007*. 104, pp. 11441–11446.

Kitada, T., Asakawa, S., Hattori, N., Matsumine, H., Yamamura, Y., Minoshima, S., Yokochi, M., Mizuno, Y. and Shimizu, N. (1998) 'Mutations in the parkin gene cause autosomal recessive juvenile parkinsonism',*Nature.*, 392(6676), pp. 605–8.

Klein C and Westenberger A (2012) 'Gene tics of Parkinson's Disease', *Cold Spring Harbour Perspectives in Medicine,* 2(1), pp. 1-15.

Klionsky, D. J., Abdelmohsen, K., Abe, A., Abedin, M. J., Abeliovich, H., Acevedo Arozena, A., et al. (2016). 'Guidelines for the use and interpretation of assays for monitoring autophagy' (3rd Edn). *Autophagy* 12, pp. 1–222.

Komatsu, M., Waguri, S., Chiba, T., Murata, S., Iwata, J. I., Tanida, I., et al. (2006). 'Loss of autophagy in the central nervous system causes neurodegeneration in mice.' *Nature* 441, pp. 880–884.

Koopman WJ, Nijtmans LG, Dieteren CE, Roestenberg P, Valsecchi F, Smeitink JA (2010) Mammalian mitochondrial complex I: biogenesis, regulation, and reactive oxygen species generation. *Antioxidant Redox Signal,* 12(12):pp.1431–70.

Kornmann B, et al. (2009) 'An ER–mitochondria tethering complex revealed by a synthetic biology screen.' *Science.* 325, pp. 477–481.

Kornmann B, Osman C, & Walter P (2011) 'The conserved GTPase Gem1 regulates endoplasmicreticulum-mitochondria connections.' *Proceedings of the National Academy of Sciences of the United States of America,* 108(34) pp. 14151-14156.

Korr H, Kurz C, Seidler TO, Sommer D, Schmitz C.(1998) 'Mitochondrial DNA synthesis studied autoradiographically in various cell types in vivo.' *Braz J Med Biol Res.* 31, pp. 289–98.

Kostic, M., Ludtmann, M., Bading, H., Hershfinkel, M., Steer, E., Chu, C., Abramov, A. and Sekler, I. (2015) 'PKA Phosphorylation of NCLX reverses Mitochondrial calcium overload and Depolarization, promoting survival of PINK1-Deficient Dopaminergic Neurons', *Cell reports.*, 13(2), pp. 376–86.

Koyano, F. (2014) 'Ubiquitin is phosphorylated by PINK1 to activate parkin', *Nature*, .1. Not final proof.

Kraytsberg, Y., Kudryavtseva, E., McKee, A. C., Geula, C., Kowall, N. W. & Khrapko, K. (2006). 'Mitochondrial DNA deletions are abundant and cause functional impairment in aged human substantia nigra neurons.' *Nature genetics* 38, pp. 518-520.

Krige D, Carroll MT, Cooper JM, Marsden CD, Schapira AH. (1992) 'Platelet mitochondrial function in Parkinson's disease.' The Royal Kings and Queens Parkinson disease research group. *Ann Neurol*. 32, pp. 782–788.

Kriks S et al (2011) 'Dopamine neurons derived from human ES cells efficiently engraft in animal models of Parkinson's disease.', *Nature,* 480, pp. 547–551

Krishnan, K.J., Reeve, A.K., Samuels, D.C., Chinnery, P.F., Blackwood, J.K., Taylor, R.W., Wanrooij, S., Spelbrink, J.N., Lightowlers, R.N. and Turnbull, D.M. (2008) 'What causes mitochondrial DNA deletions in human cells?', *Nat Genet*, 40(3), pp. 275-9.

Kroeger, K. M., Hashimoto, M., Kow, Y. W., and Greenberg, M. M. (2003) 'Crosslinking of 2deoxyribono lactone and its betaelimination product by base excision repair enzymes', *Biochemistry,* 42, pp. 2449- 2455.

Kühlbrandt, W., (2015). Structure and function of mitochondrial membrane protein complexes. *BMC Biology*, 13(1), p.89.

Kumar MJ, Andersen JK. (2004) 'Perspectives on MAO-B in aging and neurological disease - where do we go from here?' *Mol Neurobiol.* 30, pp. 77–89.

Kuroda, Y. et al. (2006) 'Parkin enhances mitochondrial biogenesis in proliferating cells.' *Hum. Mol. Genet.* 15, pp. 883–895

LaMonte, B.H., K.E. Wallace, B.A. Holloway, S.S. Shelly, J. Ascaño, M. Tokito, T. Van Winkle, D.S. Howland, and E.L. Holzbaur. (2002). Disruption of dynein/dynactin inhibits axonal transport in motor neurons causing lateonset progressive degeneration. Neuron. 34, pp.715–727.

Langston JW, Ballard P, Tetrud JW, Irwin I, (1983). Chronic Parkinsonism in humans due to a product of meperidine-analog synthesis. Science 219: pp.979–980

Lawrence, C. J et al., (2004). A standardized kinesin nomenclature. J. Cell Biol. 167, 1pp. 9-22.

Lazarou, M., Sliter, D. A., Kane, L. A., Sarraf, S. A., Wang, C., Burman, J. L., et al. (2015). 'The ubiquitin kinase PINK1 recruits autophagy receptors to induce mitophagy.' *Nature*, 524, pp. 309–314.

ldfors A., Larsson N.G., Lindberg C., Holme E. (1993) 'Mitochondrial DNA deletions in inclusion body myositis.' *Brain.* 116, pp. 325–336.

Lee S, Sato Y, Nixon RA (2011). Lysosomal proteolysis inhibition selectively disrupts axonal transport of degradative organelles and causes an Alzheimer's-like axonal dystrophy. J Neurosci. 31:pp.7817–30

Lee, M.K., Stirling, W., Xu Y., Xu X, Qui D., Mandir, A.S., Dawson, T.M., Copeland, N.G., Jenkins, N.A., Price, D.L., (2002). Human alphasynuclein-harboring familial Parkinson's disease-linked Ala-53YThr mutation causes neurodegenerative disease with alpha-synuclein aggregation in transgenic mice. Proc. Natl. Acad. Sci. U. S. A. 99, pp. 8968 – 8973.

Lee, S. J., Desplats, P., Sigurdson, C., Tsigelny, I. & Masliah, E. (2010) 'Cell-to-cell transmission of non-prion protein aggregates.' *Nat. Rev. Neurol.* 6, pp.702–706

Legesse-Miller, A., Massol, R.H. and Kirchhausen, T. (2003) 'Constriction and Dnm1p Recruitment Are Distinct Processes in Mitochondrial Fission', *Molecular Biology of the Cell*, 14(5), pp. 1953-1963.

Lehman JJ, Barger PM, Kovacs A, Saffitz JE, Medeiros DM, Kelly DP. (2000). 'Peroxisome proliferator-activated receptor γ coactivator-1 promotes cardiac mitochondrial biogenesis.' *J Clin Invest,* 106, pp. 847–856.

Lennie, P. (2003). The cost of cortical computation. Curr. Biol. 13, pp.493–497.

Letts, J.A., Fiedorczuk, K. and Sazanov, L.A. (2016) 'The architecture of respiratory supercomplexes', *Nature*, 537(7622), pp. 644-648.

Lewis TL Jr, Turi GF, Kwon SK, Losonczy A, Polleux F. (2016). Progressive decrease of mitochondrial motility during maturation of cortical axons *in vitro* and *in vivo.* Current biology. Cell press 26 (19), pp. 2602-2608.

Li, Z., Okamoto, K., Hayashi, Y. & Sheng, M. (2004) 'The importance of dendritic mitochondria in the morphogenesis and plasticity of spines and synapses.' *Cell*, 119, pp. 873–887

Liao P, Tandarich LC, Hollenbeck PJ, (2017). 'ROS regulation of axonal mitochondrial transport is mediated by Ca2+ and JNK in Drosophila'. *PLOS one*. 12 (5), pp.1-21

Lieberthal, W., Menza, S.A. & Levine, J.S., (1998). 'Graded ATP depletion can cause necrosis or apoptosis of cultured mouse proximal tubular cells.' *The American journal of physiology*, 274 (2 Pt 2), pp. 315-27.

Lightowlers, R. N., et al. (2014). "Mitochondrial protein synthesis: Figuring the fundamentals, complexities and complications, of mammalian mitochondrial translation." *Febs Letters* 588(15), pp. 2496-2503.

Ligon LA, Steward O. (2000). 'Movement of mitochondria in the axons and dendrites of cultured hippocampal neurons.' *J Comp Neurol* 427,pp 340 –350.

Ligon, L. A., Tokito, M., Finklestein, J. M., Grossman, F. E. & Holzbaur, E. L. (2004) 'A direct interaction between cytoplasmic dynein and kinesin I may coordinate motor activity.' J*. Biol. Chem.* 279, pp. 19201–19208

Lill, R. (2009). 'Function and biogenesis of iron-sulphur proteins.' *Nature*, 460(7257), pp.831–838.

Lim KL, Ng CH (2009) 'Genetic models of Parkinson disease.' *Biochim Biophys Acta* 1792, pp. 604 –615

Litonin, D., Sologub, M., Shi, Y., Savkina, M., Anikin, M., Falkenberg, M., Gustafsson, C.M. and Temiakov, D. (2010) 'Human mitochondrial transcription revisited: only TFAM and TFB2M are required for transcription of the mitochondrial genes in vitro', *J Biol Chem*, 285(24), pp. 18129-33.

Liu S, Sawada T, Lee S, Yu W, Silverio G, Alapatt P, Millan I, Shen A, Saxton W, Kanao T, et al. (2012). Parkinson's disease-associated kinase PINK1 regulates Miro protein level and axonal transport of mitochondria. PLoS Genet 8, pp.e1002537.

Liu X, Weaver D, Shirihai O, Hajnoczky G. (2009). Mitochondrial "kiss-and-run": Interplay between mitochondrial motility and fusion–fission dynamics. EMBO J 28: pp.3074–3089.

Liu, S., Sawada, T., Lee, S., Yu, W., Silverio, G., Alapatt, P., et al. (2012). 'Parkinson's disease-associated kinase PINK1 regulates miro protein level and axonal transport of mitochondria.' PLoS Genet. 8, pp. 1002537

Liu, X., et al. (1996). "Induction of apoptotic program in cell-free extracts: requirement for dATP and cytochrome c." *Cell,* 86(1), pp. 147-157.

Lloyd-Evans E, Platt FM (2011) 'Lysosomal Ca(2+) homeostasis: role in pathogenesis of lysosomal storage diseases.' Cell Calcium, 50 (2), pp. 200-205

Loson, O.C., Song, Z., Chen, H. and Chan, D.C. (2013) 'Fis1, Mff, MiD49, and MiD51 mediate Drp1 recruitment in mitochondrial fission', *Mol Biol Cell*, 24(5), pp. 659-67.

Lutz, A.K. et al. (2009) 'Loss of parkin or PINK1 function increases Drp1-dependent mitochondrial fragmentation.' *J. Biol. Chem.* 284, pp. 22938–22951

Lytton J (2007) 'Na+/Ca2+ exchangers: three mammalian gene families control Ca2+ transport.' *Biochem J* 406, pp. 365–382.

Ma, Q., Fode, C., Guillemot, F. and Anderson, D. J. (1999). 'Neurogenin1 and neurogenin2 control two distinct waves of neurogenesis in developing dorsal root ganglia.' *Genes Dev.* 13, pp. 1717-1728.

Macaskill AF, Rinholm JE, Twelvetrees AE, Arancibia-Carcamo IL, Muir J, Fransson A, Aspenstrom P, Attwell D, Kittler JT. (2009). Miro1 is a calcium sensor for glutamate receptor-dependent localization of mitochondria at synapses. Neuron. Feb 26;61(4), pp.541-55.

MacAskill, A. F. & Kittler, J. T (2012) 'Control of mitochondrial transport and localization in neurons.' *Trends Cell Biol.* 20, pp. 102–112

Maday, S., and Holzbaur, E.L. (2014). Autophagosome biogenesis in primary neurons follows an ordered and spatially regulated pathway. Dev Cell.30(1),pp.71-85.

Mai Z, Ghosh S, Frisardi M, Rosenthal B, Rogers R, Samuelson J (1999). 'Hsp60 is targeted to a cryptic mitochondrion-derived organelle ("crypton") in the microaerophilic protozoan parasite *Entamoeba histolytica*.' *Mol Cell Biol* 19, pp. 2198–2205

Mai, N., Chrzanowska-Lightowlers, Z.M.A. and Lightowlers, R.N. (2016) 'The process of mammalian mitochondrial protein synthesis', *Cell and Tissue Research*, pp. 1-16.

Maler, L., Fibiger, H.C. & McGeer, P.L. (1973) 'Demonstration of the nigrostriatal projection by silver staining after nigral injections of 6-hydroxydopamine.' *Exp. Neurol.*, 40, pp. 501 – 515.

Mallajosyula JK, Kaur D, Chinta SJ, Rajagopalan S, Rane A, Nicholls DG, Di Monte DA, Macarthur H, Andersen JK. (2008) 'MAO-B elevation in mouse brain astrocytes results in Parkinson's pathology.' *PLoS One.* 3, pp. 1616.

Mandelkow, E. M., Stamer, K., Vogel, R., Thies, E. & Mandelkow, E. (2003) 'Clogging of axons by tau, inhibition of axonal traffic and starvation of synapses' *Neurobiol. Aging*, 24, pp.1079–1085

Manfredi, G., Vu, T., Bonilla, E., Schon, E. A., DiMauro, S., Arnaudo, E. et al. (1997) 'Association of myopathy with large-scale mitochondrial DNA duplications and deletions: which is pathogenic?' *Ann. Neurol.* 42, pp.180–188

Marcia G. Honig and Richard I. Hume, (1989). 'DiI and diO: versatile fluorescent dyes for neuronal labelling and pathway tracing.'*Trends in Neurosciences*. 12, pp.333-341

Margulis, L., (1971). 'Symbiosis and evolution'. *Scientific American*, 225(2), pp.48–57.

Marta Martinez-Vicente (2017). 'Neuronal Mitophagy in Neurodegenerative Diseases', *Frontiers in Molecular Neuroscience* . 10 (64), pp.1-13

Martin and Muller, M. (1998) 'The hydrogen hypothesis for the first eukaryote', *Nature*, 392(6671), pp. 37-41.

Martin LJ, Pan Y, Price AC, Sterling W, Copeland NG, Jenkins NA, Price DL, Lee MK (2006). Parkinson's disease alpha-synuclein transgenic mice develop neuronal mitochondrial degeneration and cell death. *J Neurosci;* 26(1):pp.41-50.

Martin, I. et al. (2011) 'Recent advances in the genetics of Parkinson's disease.' *Annu. Rev. Genomics Hum. Genet.* 12, pp. 301–325

Martin, M. et al. (1999) 'Cytoplasmic dynein, the dynactin complex, and kinesin are interdependent and essential for fast axonal transport.' *Mol. Biol. Cell*, 10, pp.3717–3728

Martinez-Vicente, M. (2015). 'Autophagy in neurodegenerative diseases: from pathogenic dysfunction to therapeutic modulation.' *Semin. Cell Dev. Biol.* 40, pp. 115–126.

Masliah E, Rockenstein E, Veinbergs I, et al. (2000) 'Dopaminergic loss and inclusion body formation in alpha-synuclein mice: implications for neurodegenerative disorders.' *Science,* 287,pp. 1265–9.

Matsuda et al., (2009) 'Single Nigrostriatal Dopaminergic Neurons Form Widely Spread and Highly Dense Axonal Arborizations in the Neostriatum', *Journal of Neuroscience,* 29(2), pp. 444-453.

Matsuoka, Y., Vila, M., Lincoln, S., McCormack, A., Picciano, M., LaFrancois, J., Yu, X., Dickson, D., Langston, W.J., McGowan, E., Farrer, M., Hardy, J., Duff, K., Przedborski, S., Di Monte, D.A., (2001). Lack of nigral pathology in transgenic mice expressing human alpha synuclein driven by the tyrosine hydroxylase promoter. Neurobiol. Dis. 8, pp.535 – 539.

Matthews MR, Raisman G. (1972) 'A light and electron microscopic study of the cellular response to axonal injury in the superior cervical ganglion of the rat.' 181 (1062), pp. 43-79

Mattson MP, Gleichmann M, Cheng A (2008) 'Mitochondria in neuroplasticity and neurological disorders', 60 (5), pp. 748-766

Mattson, M. P. (2004) 'Pathways towards and away from Alzheimer's disease.' *Nature*, 430, pp. 631–639

Mauro-Lizcano, M., Esteban-Martínez, L., Seco, E., Serrano-Puebla, A., GarciaLedo, L., Figueiredo-Pereira, C., et al. (2015). 'New method to assess mitophagy flux by flow cytometry'. *Autophagy* 11, pp.833–843.

McKinney, E.A. & Oliveira, M.T., (2013). 'Replicating animal mitochondrial DNA'. *Genetics and Molecular Biology*, 36(3), pp.308–315.

Mears, J.A., Lackner, L.L., Fang, S., Ingerman, E., Nunnari, J. and Hinshaw, J.E. (2011) 'Conformational changes in Dnm1 support a contractile mechanism for mitochondrial fission', *Nat Struct Mol Biol*, 18(1), pp. 20-6.

Meier, T. and D. Pogoryelov (2013). 'ATP Synthase Structure' *Encyclopedia of Biophysics.* G. C. K. Roberts. Berlin, Heidelberg, Springer Berlin Heidelberg: pp. 129-134.

Meissner, C., Lorenz, H., Hehn, B., and Lemberg, M. K. (2015). 'Intramembrane protease PARL defines a negative regulator of PINK1- and PARK2/Parkindependent mitophagy.' *Autophagy* 11, pp. 1484–1498

Mekhoubad S, Bock C, de Boer AS, Kiskinis E, Meissner A, Eggan K. (2012) 'Erosion of dosage compensation impacts human iPSC disease modeling'. *Cell Stem Cell,* 10, pp. 595–609.

Meldolesi J & Pozzan T (1998) 'The endoplasmic reticulum Ca2+ store: a view from the lumen.' *Trends Biochem Sci*,23 pp. 10–14.

Melentijevic et al., (2017) 'C. elegans neurons jettison protein aggregates and mitochondria under neurotoxic stress'. *Nature Letter*. 542 (1), pp. 367–371.

Mercado, G., Valdes, P. & Hetz, C. (2013) 'An ERcentric view of Parkinson's disease.' *Trends Mol. Med.* 19, pp. 165–175

Michael W. Gray (2012) 'Mitochondrial Evolution', *Cold Spring Harbour Perspectives in Medicine,* 4(9), pp. 1-16.

Michikawa, Y., Mazzucchelli, F., Bresolin, N., Scarlato, G. & Attardi, G. (1999). 'Aging-dependent large accumulation of point mutations in the human mtDNA control region for replication.' *Science* 286,pp. 774-779.

Middleton ER, Rhoades E. 'Effects of curvature and composition on α-synuclein binding to lipid vesicles'. *Biophys J,*99, pp. 2279–2288.

Millecamps S, Julien JP. (2013) 'Axonal transport deficits and neurodegenerative diseases'. *Nat Rev Neurosci,* 14, pp. 161–76.

Miller KE, Sheetz MP. (2004). 'Axonal mitochondrial transport and potential are correlated'. *J Cell Sci,* 117, pp. 2791– 2804.

Miller, F.J., Rosenfeldt, F.L., Zhang, C., Linnane, A.W. and Nagley, P. (2003) 'Precise determination of mitochondrial DNA copy number in human skeletal and cardiac muscle by a PCR-based assay: lack of change of copy number with age', *Nucleic Acids Research*, 31(11), pp. 61.

Miller, K. E. & Sheetz, M. P. (2006) 'Direct evidence for coherent low velocity axonal transport of mitochondria' *J. Cell Biol.* 173, pp. 373–381

Minczuk M et al., (2011) 'TEFM (c17orf42) is necessary for transcription of human mtDNA.', *Nucleic Acids Research,* 39(10), pp. 4284-4299.

Mink JW, Thach WT (1993) 'Basal ganglia intrinsic circuits and their role in behavior' *Current Opinion in Neurobiology* 3, pp. 950–957.

Misgeld T. & Schwarz T.L. (2017). Mitostasis in Neurons: Maintaining Mitochondria in an Extended Cellular Architecture. Neuron 96,pp. 651-66.

Misgeld T., Kerschensteiner, M., Bareyre, F. M., Burgess, R. W. & Lichtman, J. W. (2007) 'Imaging axonal transport of mitochondria in vivo' *Nature Methods* 4, pp. 559–561

Misko A, Jiang S, Wegorzewska I, Milbrandt J, & Baloh RH (2010) 'Mitofusin 2 is necessary for transport of axonal mitochondria and interacts with the Miro/Milton complex', 30 (12), pp. 4232 -4230

Missale C., Nash S. R., Robinson S. W., Jaber M., Caron M. G. (1998). 'Dopamine receptors: from structure to function.' *Physiol. Rev.* 78, pp. 189–225

Mitchell, P. (1961) 'Coupling of phosphorylation to electron and hydrogen transfer by a chemi-osmotic type of mechanism', *Nature*, 191, pp. 144-8.

Mitchell, P. (1976) 'Possible molecular mechanisms of the protonmotive function of cytochrome systems', *J Theor Biol*, 62(2), pp. 327-67.

Miwa S, Lawless C, von Zglinicki T. (2008) 'Mitochondrial turnover in liver is fast in vivo and is accelerated by dietary restriction: application of a simple dynamic model.' *Aging Cell*. 7, pp. 920–23.

MJ Berridge. (1998). Neuronal calcium signalling. Neuron, 21 pp. 13–26

Montero M, Alonso MT, Carnicero E, Cuchillo-Ibanez I, Albillos A, Garcia AG, Garcia-Sancho J,Alvarez J. (2000) 'Chromaffin-cell stimulation triggers fast millimolar mitochondrial Ca2+ transients thatmodulate secretion'. *Nat Cell Biol.* 2, pp. 57–61.

Montoya, J., Gaines, G.L. and Attardi, G. (1983) 'The pattern of transcription of the human mitochondrial rRNA genes reveals two overlapping transcription units', *Cell*, 34(1), pp. 151-9.

Moore, D. J., West, A. B., Dawson, V. L. & Dawson, T. M. (2005) 'Molecular pathophysiology of Parkinson's disease.' *Annu. Rev. Neurosci.* 27, pp.57–87

Moraes, C. T., DiMauro, S., Zeviani, M., Lombes, A., Shanske, S., Miranda, A. F. et al. (1989) 'Mitochondrial DNA deletions in progressive external ophthalmoplegia and Kearns-Sayre syndrome.' *N. Engl. J. Med.* 320,pp. 1293–1299

Moreira, P. I., Carvalho, C., Zhu, X., Smith, M. A. & Perry, G. (2010) 'Mitochondrial dysfunction is a trigger of Alzheimer's disease pathophysiology'. *Biochim. Biophys. Acta* 1802, pp. 2–10

Morozov, Y.I., Agaronyan, K., Cheung, A.C.M., Anikin, M., Cramer, P. and Temiakov, D. (2014) 'A novel intermediate in transcription initiation by human mitochondrial RNA polymerase', *Nucleic Acids Research*, 42(6), pp. 3884-3893.

Morozov, Y.I., Parshin, A.V., Agaronyan, K., Cheung, Alan C.M., Anikin, M., Cramer, P. and Temiakov, D. (2015) 'A model for transcription initiation in human mitochondria', *Nucleic Acids Research*, 43(7), pp. 3726-3735.

Morris RL, Hollenbeck PJ (1995). Axonal transport of mitochondria along microtubules and F-actin in living vertebrate neurons. J Cell Biol 131:pp.1315–1326

Morris RL, Hollenbeck PJ. (1993). The regulation of bidirectional mitochondrial transport is coordinated with axonal outgrowth. J Cell Sci 104: pp.917–927.

Morrison, B. M., Hof, P. R. & Morrison, J. H. (1998) 'Determinants of neuronal vulnerability in neurodegenerative diseases' *Ann. Neurol,* 44, pp. S32–S44

Mortiboys H., Thomas K.J., Koopman W.J., Klaffke S., Abou-Sleiman P., Olpin S., Wood N.W., Willems P.H., Smeitink J.A., Cookson M.R., et al. (2008) 'Mitochondrial function and morphology are impaired in parkin-mutant fibroblasts.' *Ann. Neurol,*64, pp. 555–565.

Mosharov et al., (2009). 'Interplay between cytosolic dopamine, calcium, and alpha-synuclein causes selective death of substantia nigra neurons.' *Neuron,* 62, pp. 218-229.

Moslemi A.R., Lindberg C., Oldfors A (1997) 'Analysis of multiple mitochondrial DNA deletions in inclusion body myositis' *Hum. Mutat,* 10, pp.381–386.

Mouli P. K., Twig G. & Shirihai O. S. (2009) 'Frequency and selectivity of mitochondrial fusion are key to its quality maintenance function.' *Biophys. J.* 96, pp. 3509–3518

Mühlenhoff U, Gerber J, Richhardt N, Lill R (2003). 'Components involved in assembly and dislocation of iron–sulfur clusters on the scaffold protein Isu1p.' *EMBO J* 22, pp. 4815–4825

Müller, S.K., Bender, A., Laub, C., Högen, T., Schlaudraff, F., Liss, B., Klopstock, T. and Elstner, M. (2013) 'Lewy body pathology is associated with mitochondrial DNA damage in Parkinson's disease', *Neurobiology of Aging*, 34(9), pp. 2231–2233

Munoz P, Huenchuguala S, Paris I, Segura-Aguilar J. (2012) 'Dopamine oxidation and autophagy' *Parkinsons Di.* Pp.920953.

Murakawa, T., Yamaguchi, O., Hashimoto, A., Hikoso, S., Takeda, T., Oka, T., et al. (2015). 'Bcl-2-like protein 13 is a mammalian Atg32 homologue that mediates mitophagy and mitochondrial fragmentation.' *Nat. Commun*. 6, pp.7527

Murphy MP. (2009) 'How mitochondria produce reactive oxygen species.' *Biochem J*. 417, pp.1–13.

Mutsaers, S. E. & Carroll, W. M. (1998) 'Focal accumulation of intra-axonal mitochondria in demyelination of the cat optic nerve.' *Acta Neuropathol.* 96,pp. 139–143

Myasnikov, A.G. et al., (2009).'Structure–function insights into prokaryotic and eukaryotic translation initiation'. *Current Opinion in Structural Biology*, 19(3), pp.300–309.

Nagatsu T, Sawada M (2006) 'Molecular mechanism of the relation of monoamine oxidaes inhibitors to Parkinson's disease: Possible implications of glial cells.' *J Neural Transm.* 71, pp. 53–65.

Naisbitt, S. et al. (2000) 'Interaction of the postsynaptic density-95/guanylate kinase domain-associated protein complex with a light chain of myosin-V and dynein.' *J. Neurosci.* 20, pp. 4524–4534

Nakatogawa, H., Ichimura, Y. & Ohsumi, Y. (2007) 'Atg8, a ubiquitin-like protein required for autophagosome formation, mediates membrane tethering and hemifusion.' *Cell,* 130, pp. 165–178

Narendra, D., Jin, S., Tanaka, A., Suen, D., Gautier, C., Shen, J., Cookson and Youle, R. (2010) 'PINK1 is selectively stabilized on impaired mitochondria to activate Parkin', *PLoS biology.*, 8(1). e1000298

Narendra, D., Kane, L. A., Hauser, D. N., Fearnley, I. M., and Youle, R. J. (2010). 'p62/SQSTM1 is required for Parkin-induced mitochondrial clustering but not mitophagy; VDAC1 is dispensable for both.' *Autophagy,* 6,pp. 1090–1106.

Narendra, D., Tanaka, A., Suen, D.-F. and Youle, R.J. (2008) 'Parkin is recruited selectively to impaired mitochondria and promotes their autophagy', *The Journal of Cellular Biology* 1;183(5):pp.795-803.

Narendra, D.P. et al. (2010) 'PINK1 is selectively stabilized on impaired mitochondria to activate Parkin.' PLoS Biol. 8, pp. 1000298

Natalia B. Pivovarova and S. Brian Andrews (2010). 'Calcium-dependent mitochondrial function and dysfunction in neurons.' *The FEBS journal* . 277, pp. 3622–3636

Neuhoff H, Neu A, Liss B, Roeper J. (2002), 'I(h) channels contribute to the different functional properties of identified dopaminergic subpopulations in the midbrain', *The Journal of Neuroscience*. 22, pp. 1290-1302.

Neupert W, Herrmann JM. Translocation of proteins into mitochondria (2007). *Annual Review of Biochemistry*.;76,pp.723–49*. Neuroreport;* 18(15):pp.1543-6.

Nguyen, H., Byers, B., Cord, B., Shcheglovitov, A., Byrne, J., Gujar, P., Kee, K., Schüle, B., Dolmetsch, R., Langston, W., Palmer, T. and Pera, R. (2011) 'LRRK2 mutant iPSC-derived DA neurons demonstrate increased susceptibility to oxidative stress', *Cell stem cell.*, 8(3), pp. 267–80.

Nguyen, L.H., Erzberger, J.P., Root, J. & Wilson, D.M., III. (2000) 'The human homolog of *Escherichia coli* Orn degrades small single-stranded RNA and DNA oligomers.' *J. Biol. Chem.* 275, pp. 25900–25906

Nicholls, D.G., and Budd, S.L. (2000). Mitochondria and neuronal survival. *Physiol. Rev*. 80, pp.315–360.

Nicholls, T.J., Rorach, J. & Minczuk, M., (2013). 'Mitochondria: Mitochondrial RNA metabolism and human disease.' *The International Journal of Biochemistry & Cell Biology*, 45(4), pp.845–849.

Nicoll RA, Alger BE (1979). A simple chamber for recording from submerged brain slices. *Journal of* Neuroscience; 1: pp.323-325

Nicoll, D.A., Ottolia, M., Goldhaber, J.I., and Philipson, K.D. (2013). 20 years from NCX purification and cloning: milestones. Advances in Experimental Medicine and Biology., 961, 17–23

Niescier RF, Hong K, Park D, Min X (2018). MCU Interacts with Miro1 to Modulate Mitochondrial Functions in Neurons. , *The Journal of Neuroscience,* 38(20), pp. 4666 – 4677.

Noda, N. N., Ohsumi, Y. & Inagaki, F. 'Atg8-family interacting motif crucial for selective autophagy.' *FEBS Lett.* 584, pp. 1379–1385

Noji, H., Yasuda, R., Yoshida, M. and Kinosita, K. (1997) 'Direct observation of the rotation of F1-ATPase', *Nature*, 386(6622), pp. 299-302.

Nuscher B, Kamp F, Mehnert T, Odoy S, Haass C, Kahle PJ, Beyer K. (2004) 'Alpha-synuclein has a high affinity for packing defects in a bilayer membrane: a thermodynamics study.' *J Biol Chem*. 279, pp. 21966–21975.

O'Toole M, Latham R, Baqri RM, Miller KE (2008) 'Modeling mitochondrial dynamics during in vivo axonal elongation.' *J Theor Biol.* 255, pp. 369–77.

Obashi K. and Okabe S. (2013) 'Regulation of mitochondrial dynamics and distribution by synapse position and neuronal activity in the axon' *Eur. J. Neurosci.* 38, pp.2350–2363.

Ogawa F*,* Malavasi EL, Crummie DK, Eykelenboom JE, Soares DC, Mackie S, Porteous DJ, Millar JK. (2014) 'DISC1 complexes with TRAK1 and Miro1 to modulate anterograde axonal mitochondrial trafficking', *Hum Mol Genet,* 23 (4), pp. 906-919

Ohno, N., Kidd, G.J., Mahad, D., Kiryu-Seo, S., Avishai, A., Komuro, H.,and Trapp, B.D. (2011). 'Myelination and axonal electrical activity modulate the distribution and motility of mitochondria at CNS nodes of Ranvier' *J. Neurosci.* 31, pp. 7249–7258.

Ojala, D., Montoya, J. and Attardi, G. (1981) 'tRNA punctuation model of RNA processing in human mitochondria', *Nature*, 290(5806), pp. 470-4.

Oldfors A., Moslemi A.R., Jonasson L., Ohlsson M., Kollberg G., Lindberg C. (2006) 'Mitochondrial abnormalities in inclusion-body myositis' *Neurology.* 66, pp. S49–S55.

Ono Y, Nakatani T, Sakamoto Y, Mizuhara E, Minaki Y, Kumai M *et al* (2007) 'Differences in neurogenic potential in floor plate cells along an anteroposterior location: midbrain dopaminergic neurons originate from mesencephalic floor plate cells.' *Development,* 134, pp. 3213–3225.

Osafune K, Caron L, Borowiak M, et al. (2008) 'Marked differences in differentiation propensity among human embryonic stem cell lines.' *Nature Biotechnol.* 26, pp. 313–315.

Overly CC, Rieff HI, Hollenbeck PJ (1996) 'Organelle motility and metabolism in axons vs dendrites of cultured hippocampal neurons.' *J Cell Sci,* 109(5), pp.971–980

Paillusson S. et al. (2017) 'α-Synuclein binds to the ER–mitochondria tethering protein VAPB to disrupt Ca^{2+} homeostasis and mitochondrial ATP production.' *Acta Neuropathol*. 134, 129–149

Palacino J.J., Sagi D., Goldberg M.S., Krauss S., Motz C., Wacker M., Klose J., Shen J. (2004) 'Mitochondrial dysfunction and oxidative damage in parkin-deficient mice.' *J. Biol. Chem,* 279, pp.18614–18622.

Palade GE (1952). The fine structure of mitochondria. The Anatomical Record. 114(3):427–51. 9.

Palade, G.E. (1953) 'An electron microscope study of the mitochondrial structure', *J Histochem Cytochem*, 1(4), pp. 188-211.

Palty R, Ohana E, Hershfinkel M, Volokita M, Elgazar V, Beharier O, Silverman WF, Argaman M, Sekler I. (2004). Lithium-calcium exchange is mediated by a distinct potassium-independent sodium calcium exchanger. J Biol Chem. 279:25234–25240.

Palty, R., Silverman, W.F., Hershfinkel, M., Caporale, T., Sensi, S.L., Parnis, J., Nolte, C., Fishman, D., Shoshan-Barmatz, V., Herrmann, S., Khananshvili, D. and Sekler, I. (2010) 'NCLX is an essential component of mitochondrial Na+/Ca2+ exchange', *Proc Natl Acad Sci U S A*, 107(1), pp. 436-41.

Panov A. V., Gutekunst C. A., Leavitt B. R., Hayden M. R., Burke J. R., Strittmatter W. J., Greenamyre J. T. (2002). 'Early mitochondrial calcium defects in Huntington's disease are a direct effect of polyglutamines.' *Nat. Neurosci.* 5, pp. 731-736

Park J, Lee SB, Lee S, Kim Y, Song S, Kim S, Bae E, Kim J, Shong M, Kim JM, Chung J. (2006). Mitochondrial dysfunction in Drosophila PINK1 mutants is complemented by parkin. *Nature*. 29;441(7097), pp.1157-61

Parker WD, Boyson SJ, Parks JK. (1989) 'Abnormalities of the electron transport chain in idiopathic Parkinson's disease.' *Ann Neurol.* 26, pp. 719–723.

Patel P. K., Shirihai O. & Huang K. C. (2013) 'Optimal dynamics for quality control in spatially distributed mitochondrial networks' *PLoS Comput. Biol.* 9, pp. 103- 108

Patricia Gómez-Suaga, José M Bravo-San Pedro, Rosa A. González-Polo, José M. Fuentes and Mireia Niso-Santano, (2018). 'ER–mitochondria signaling in Parkinson's disease.' *Cell Death and Disease* . 9, pp.1-12

Perier, C., Bender, A., García-Arumí, E., Melià, M.J., Bové, J., Laub, C., Klopstock, T., Elstner, M., Mounsey, R.B., Teismann, P., Prolla, T., Andreu, A.L., Vila, M., Friedrich-Baur-Institute and Sciences, M. (2013) Accumulation of mitochondrial DNA deletions within dopaminergic neurons triggers neuroprotective mechanisms. *Brain*. 136; pp. 2369–2378

Pfefferkorn CM, Jiang Z, Lee JC. (2012) 'Biophysics of α-synuclein membrane interactions.' *Biochim Biophys Acta*. 1818, pp.162–171.

Pfister K et a., (2006) 'Genetic analysis of the cytoplasmic dynein subunit families.', *PLOS Genetics,* 2(1), pp. 0011-0026.

Pham AH, McCaffery JM, Chan DC (2012) 'Mouse lines with photoactivatable mitochondria to study mitochondrial dynamics'. *Genesis,* 50, pp. 833–843

Phillips, J. et al. (2016) 'Development of passive CLARITY and immunofluorescent labelling of multiple proteins in human cerebellum: understanding mechanisms of neurodegeneration in mitochondrial disease.' *Sci. Rep.* 6, pp.26013

Pickel VM, Chan J (1990) 'Spiny neurons lacking choline acetyltransferase immunoreactivity are major targets of cholinergic and catecholaminergic terminals in rat striatum.' *Journal of Neuroscience Research,* 25, pp,263–280.

Pickrell AM, Huang CH, Kennedy SR, Ordureau A, Sideris DP, Hoekstra JG, Harper JW, Youle RJ (2015) 'Endogenous Parkin preserves dopaminergic substantia nigral neurons following mitochondrial DNA mutagenic stress.' *Neuron,* 87, pp. 371-381.

Pickrell, A.M. and Youle, R.J. (2015) 'The roles of PINK1, Parkin, and Mitochondrial fidelity in Parkinson's disease', Cell 85(2), pp. 257–273.

Pilling, A. D., Horiuchi, D., Lively, C. M. & Saxton, W. M. (2006) 'Kinesin-1 and Dynein are the primary motors for fast transport of mitochondria in Drosophila motor axons.' *Mol. Biol. Cell,* 17, pp.2057–2068

Pivovarova NB, Hongpaisan J, Andrews SB, Friel DD (1999) 'Depolarization-induced mitochondrial Caaccumulation in sympathetic neurons: spatial and temporal characteristics.' *J Neurosci.* 19, pp. 6372–6384.

Plucińska G, Paquet D, Hruscha A, Godinho L, Haass C, Schmid B, Misgeld T.(2012). 'In vivo imaging of disease-related mitochondrial dynamics in a vertebrate model system.', *J Neurosci*. 32 (46), pp.16203- 16212.

Polymeropoulos MH, Lavedan C, Leroy E, Ide SE, Dehejia A, Dutra A, Pike B, Root H, Rubenstein J, Boyer R (1997). Mutation in the α-synuclein gene identified in families with Parkinson's disease. Science 276: pp.2045–2047

Ponnalagu, D. and Singh, H. (2016) 'Anion Channels of Mitochondria', *Handb Exp Pharmacol*. 240, pp. 71-101

Poole A. C., Thomas R. E., Andrews L. A., McBride H. M., Whitworth A. J., Pallanck L. J. (2008). The PINK1/Parkin pathway regulates mitochondrial morphology. *Proc. Natl. Acad. Sci. USA* 105, pp. 1638-1643

Poston, C. N., Krishnan, S. C. & Bazemore-Walker, C. R. (2013) 'In-depth proteomic analysis of mammalian mitochondria-associated membranes (MAM)'. *J. Proteomics* 79, pp. 219–230

Pozo Devoto VM and Falzone TL (2017). 'Mitochondrial dynamics in Parkinson's disease: a role for α-synuclein?', *Disease Models and Mechanisms* . 10 (9), pp.1075–1087

Pozzan T, Rudolf R. (2009) 'Measurements of mitochondrial calcium in vivo.' Biochim Biophys Acta. 1787 (11), pp. 1317-23

Pozzo-Miller LD, Pivovarova NB, Leapman RD, Buchanan RA, Reese TS, Andrews SB (1997) 'Activity dependent calcium sequestration in dendrites of hippocampal neurons in brain slices' *J Neurosci,* 17, pp. 8729–8738.

Pranke IM, Morello V, Bigay J, Gibson K, Verbavatz JM, Antonny B, Jackson CL (2011) 'Alpha-synuclein and ALPS motifs are membrane curvature sensors whose contrasting chemistry mediates selective vesicle binding.' *J Cell Biol.*194, pp. 89–103.

Price, R. L., Lasek, R. J. & Katz, M. J. (1991) 'Microtubules have special physical associations with smooth endoplasmic reticula and mitochondria in axons'. *Brain Res.* 540, pp. 209–216

Prithivirajsingh, S. *et al.* (2004) 'Accumulation of the common mitochondrial DNA deletion induced by ionizing radiation.' *FEBS Lett.* 571, pp. 227–232

Puigserver P, Wu Z, Park CW, Graves R, Wright M, Spiegelman BM. (1998). 'A cold-inducible coactivator of nuclear receptors linked to adaptive thermogenesis.' *Cell* 92, pp. 829–839.

Puopolo M, Raviola E, Bean BP. (2007). Roles of subthreshold calcium current and sodium current in spontaneous firing of mouse midbrain dopamine neurons. *Journal of Neuroscience*. 27 pp. 645–656

Puschmann A, Ross OA, Vilarino-Guell C, Lincoln SJ, Kachergus JM, Cobb SA, Lindquist SG, Nielsen JE, Wszolek ZK, Farrer M (2009). A Swedish family with de novo α-synuclein A53T mutation: Evidence for early cortical dysfunction. Parkinsonism Relat Disord 15: pp.627–632

Py B, Barras F (2010). 'Building Fe-S proteins: Bacterial strategies'. *Nat Rev Microbiol* 8, pp. 436–446

R Rizzuto, T Pozzan. (2006). Microdomains of intracellular Ca2+: molecular determinants and functional consequences. Physiol Rev, 86, pp. 369–408

R. Dingledine (Ed.), Brain Slices, Plenum Press, New York (1984), pp. 381-437

Radad K, Rausch WD, Gille G (2006) 'Rotenone induces cell death in primary dopaminergic culture by increasing ROS production and inhibiting mitochondrial respiration.' *Neurochem Int*. 49, pp. 379– 386

Radad K, Rausch WD, Gille G (2006). Rotenone induces cell death in primary dopaminergic culture by increasing ROS production and inhibiting mitochondrial respiration. Neurochem Int 49:pp.379– 386

Rakovic, A., Shurkewitsch, K., Seibler, P., Grünewald, A., Zanon, A., Hagenah, J., et al. (2013). Phosphatase and tensin homolog (PTEN)-induced Putative Kinase 1 (PINK1)-dependent ubiquitination of endogenous parkin attenuates mitophagy: study in human primary fibroblasts and induced pluripotent stem cell-derived neurons. *J. Biol. Chem.* 288,pp. 2223–2237.

Rangaraju, V., Calloway, N. & Ryan, T. A. (2014) 'Activity-driven local ATP synthesis is required for synaptic function'. *Cell,* 156, pp. 825–835

Rappold P. M., Cui M., Grima J. C., Fan R. Z., de Mesy-Bentley K. L., Chen L., Zhuang X., Bowers W. J. and Tieu K. (2014) 'Drp1 inhibition attenuates neurotoxicity and dopamine release deficits in vivo.' *Nat. Commun.* 5, pp. 5244.

Reddy PH, and Reddy TP (2011). Mitochondria as a therapeutic target for aging and neurodegenerative diseases., *Current Alzheimer's Research,* 8(4), pp. 393-409.

Reeve A, Simcox E, and Turnbull D. (2014) ‘Ageing and Parkinson's disease: Why is advancing age the biggest risk factor?;, *Ageing Research Reviews*. 14 (100), pp.19–30

Reeve, A., Meagher, M., Lax, N., Simcox, E., Hepplewhite, P., Jaros, E. & Turnbull, D. (2013). The impact of pathogenic mitochondrial DNA mutations on substantia nigra neurons. *The Journal of Neuroscience* 33, 10790-10801.

Reeve, A.K., Krishnan, K.J., Duchen, M.R., Turnbull, D.M (2016). Mitochondrial dysfunction in Neurodegenerative disorders. Available at: http://www.springer.com/us/book/9780857297006

Reeve, A.K., Krishnan, K.J., Elson, J.L., Morris, C.M., Bender, A., Lightowlers, R.N. and Turnbull, D.M. (2008) 'Nature of mitochondrial DNA deletions in substantia nigra neurons', *Am J Hum Genet*, 82(1), pp. 228-35.

Rehling, P., Brandner, K. and Pfanner, N. (2004) 'Mitochondrial import and the twin-pore translocase', *Nat Rev Mol Cell Biol*, 5(7), pp. 519-530.

Reyes, S., Fu, Y., Double, K., Thompson, L., Kirik, D., Paxinos, G. and Halliday, G.M. (2012) ‘GIRK2 expression in dopamine neurons of the substantia nigra and ventral tegmental area’, *The Journal of Comparative Neurology*, 520(12), pp. 2591–2607.

Richfield, E.K., Thiruchelvam, M.J., Cory-Slechta, D.A., Wuertzer, C., Gainetdinov, R.R., Caron, M.G., Di Monte, D.A., Federoff, H.J., (2002). ‘Behavioral and neurochemical effects of wild-type and mutated human alpha-synuclein in transgenic mice.’ *Exp. Neurol.* 175, pp. 35 – 48

Riederer P, Konradi C, Schay V, Kienzl E, Birkmayer G, Danielczyk W, Sofic E, Youdim MB (1987) ‘Localization of MAO-A and MAO-B in human brain: A step in understanding the therapeutic action of L-deprenyl’ *Adv Neurol.* 45, pp. 111–118.

Rintoul G et al., (2003) 'Glutamate Decreases Mitochondrial Size and Movement in Primary Forebrain Neurons', *Journal of Neuroscience,* 23(21), pp. 7881-7888.

Rivera, J. F., Ahmad, S., Quick, M. W., Liman, E. R. & Arnold, D. B (2003). An evolutionarily conserved dileucine motif in Shal K+ channels mediates dendritic targeting. Nature Neurosci. 6, pp.243–250

Rivero-Rios, P., Gomez-Suaga, P., Fdez, E. & Hilfiker, S. (2014) ‘Upstream deregulation of calcium signaling in Parkinson’s disease.’ *Front. Mol. Neurosci.* 7, pp. 53

Rizzuto R, et al. (1998) ‘Close contacts with the endoplasmic reticulum as determinants of mitochondrial Ca^{2+} responses’ *Science.* 280, pp. 1763–1766.

Rizzuto R, T Pozzan. (2006). Microdomains of intracellular Ca2+: molecular determinants and functional consequences. *Physiol Rev*, 86, pp. 369–408

Rizzuto, R. et al., (2012). ‘Mitochondria as sensors and regulators of calcium signalling.’ *Nature Reviews Molecular Cell Biology*, 13(9), pp.566–578.

Robberson, D.L., Kasamatsu, H. and Vinograd, J. (1972) 'Replication of Mitochondrial DNA. Circular Replicative Intermediates in Mouse L Cells', *Proceedings of the National Academy of Sciences of the United States of America*, 69(3), pp. 737-741.

Rockenstein, E., Mallory, M., Hashimoto, M., Song, D., Shults, C.W., Lang, I., Masliah, E., (2002). Differential neuropathological alterations in transgenic mice expressing alpha-synuclein from the platelet-derived growth factor and Thy-1 promoters. J. Neurosci. Res. 68, pp. 568 – 578.

Rodríguez, M. & González-Hernández, T. (1999) 'Electrophysiological and morphological evidence for a GABAergic nigrostriatal pathway'.' *J. Neurosci.*, 19, pp. 4682 – 4694.

Rossignol, R., Faustin, B., Rocher, C., Malgat, M., Mazat, J.P. and Letellier, T. (2003) 'Mitochondrial threshold effects', *Biochem J*, 370(Pt 3), pp. 751-62.

Rouault, T.A., (2012). 'Biogenesis of iron-sulfur clusters in mammalian cells: new insights and relevance to human disease.' *Disease models & mechanisms*, 5(2), pp.155–64.

Rowland AA, Voeltz GK (2012) 'Endoplasmic reticulum–mitochondria contacts: function of the junction.' *Nat. Rev. Mol. Cell Biol.*13, pp. 607–625.

Rudolf R, Mongillo M, Rizzuto R, Pozzan T. (2003) 'Looking forward to seeing calcium' *Nat Rev Mol Cell Biol,* 4, pp.579–586.

Russell, O.M. (2018). 'Preferential amplification of a human mitochondrial DNA deletion in vitro and in vivo.' *Scientific Reports*, 1799(8), pp. 1-10

Russo GJ, Louie K, Wellington A, Macleod GT, Hu F, Panchumarthi S, Zinsmaier KE. (2009). Drosophila Miro is required for both anterograde and retrograde axonal mitochondrial transport. J Neurosci 29: pp.5443–5455.

Ruthel, G. & Hollenbeck, P. J. (2003) 'Response of mitochondrial traffic to axon determination and differential branch growth.' *J. Neurosci.* 23, pp. 8618–8624

Ryu, E. J. et al. (2002) 'Endoplasmic reticulum stress and the unfolded protein response in cellular models of Parkinson's disease.' *J. Neurosci.* 22, pp. 10690–10698

Safiulina, V. F., Fattorini, G., Conti, F., and Cherubini, E. (2006). 'GABAergic signaling at mossy fiber synapses in neonatal rat hippocampus.' *J. Neurosci.* 26,pp. 597–608.

Sagan, L. (1967) 'On the origin of mitosing cells', *Journal of Theoretical Biology*, 14(3), pp. 225-IN6.

Sajic, M., Mastrolia, V., Lee, C.Y., Trigo, D., Sadeghian, M., Mosley, A.J., Gregson, N.A., Duchen, M.R., and Smith, K.J. (2013).'Impulse conduction increases mitochondrial transport in adult mammalian peripheral nerves in vivo' *PLoS Biol.* 11, pp. 1001754.

Sandoval, H., Thiagarajan, P., Dasgupta, S. K., Schumacher, A., Prchal, J. T., Chen, M., et al. (2008). 'Essential role for Nix in autophagic maturation of erythroid cells.' *Nature* 454, pp. 232–235.

Santorelli F.M., Sciacco M., Tanji K., Shanske S., Vu T.H., Golzi V., Griggs R.C., Mendell J.R., Hays A.P., Bertorini T.E., et al. (1996) 'Multiple mitochondrial DNA deletions in sporadic inclusion body myositis: a study of 56 patients.' *Ann. Neurol,* 39, pp.789–795.

Saotome, M. et al. (2008) 'Bidirectional Ca2+-dependent control of mitochondrial dynamics by the Miro GTPase.' *Proc. Natl Acad. Sci. USA*, 105, pp. 20728–20733

Sarraf, S.A., Raman, M., Guarani-Pereira, V., Sowa, M.E., Huttlin, E.L., Gygi, S.P., and Harper, J.W. (2013). Landscape of the PARKIN-dependent ubiquitylome in response to mitochondrial depolarization. *Nature* 496, pp.372–376.

Scardigli, R., Schuurmans, C., Gradwohl, G. and Guillemot, F. (2001). 'Cross regulation between Neurogenin2 and pathways specifying neuronal identity in the spinal cord.' *Neuron* 31, pp. 203-217.

Schapira A. H. (2007) 'Mitochondrial dysfunction in Parkinson's disease.' *Cell Death Differ.* 14, pp. 1261–1266.

Schapira A. H., Cooper J. M., Dexter D., Clark J. B., Jenner P. and Marsden C. D. (1990) 'Mitochondrial complex I deficiency in Parkinson's disease.' J*. Neurochem,* 54, pp.823–827.

Schapira, A., Holt, I., Sweeney, M., Harding, A., Jenner, P. and Marsden, C. (1990) 'Mitochondrial DNA analysis in Parkinson's disease', *Movement disorders : official journal of the Movement Disorder Society.*, 5(4), pp. 294–7.

Schneeberger M., Dietrich M.O., Sebastian D., Imbernon M., Castano C., Garcia A., Esteban Y., Gonzalez-Franquesa A., Rodriguez I.C., Bortolozzi A., et al. (2013) 'Mitofusin 2 in POMC neurons connects ER stress with leptin resistance and energy imbalance.' Cell, 155, pp.172–187

Schon, E.A., and Przedborski, S. (2011). Mitochondria: the next (neurode)generation. Neuron 70, pp.1033–1053.

Schousboe A, Waagepetersen HS (2007). "GABA: homeostatic and pharmacological aspects". *Prog. Brain Res*, 160, pp. 9–19.

Schwartz, W. (2007) *Lynn Margulis, origin of Eukaryotic cells. Evidence and research implications for a theory of the origin and evolution of microbial, plant, and animal cells on the Precambrian earth. XXII u. 349 S., 89 Abb., 49 tab. New Haven-London 1970: Yale university*. (13 Vols). Wiley-Blackwell.

Schwarz TL (2013) 'Mitochondrial trafficking in neurons.' *Cold Spring Harb Perspect Biol*, 5m, pp. 11304

Schwarzer, C., Barnikol-Watanabe, S., Thinnes, F. P. & Hilschmann, N. (2002) 'Voltage-dependent anion-selective channel (VDAC) interacts with the dynein light chain Tctex1 and the heat-shock protein PBP74.' *Int. J. Biochem. Cell Biol.* 34, pp. 1059–1070

Schweers, R. L., Zhang, J., Randall, M. S., Loyd, M. R., Li, W., Dorsey, F. C., et al. (2007). 'NIX is required for programmed mitochondrial clearance during reticulocyte maturation'. *Proc. Natl. Acad. Sci. U S A,* 104, pp. 19500–19505.

Sciacco M., Bonilla E., Schon E.A., DiMauro S., Moraes C.T (1994) 'Distribution of wild-type and common deletion forms of mtDNA in normal and respiration-deficient muscle fibers from patients with mitochondrial myopathy' *Hum. Mol. Genet,* 3, pp. 13–19.

Selosse, M.-A., B. Albert and B. Godelle (2001). 'Reducing the genome size of organelles favours gene transfer to the nucleus.' *Trends Ecol. Evol.* 16, pp. 135–141.

Semenoff D, Kimelberg H. (1985) 'Autoradiography of high affinity uptake of catecholamines by primary astrocyte cultures.' *Brain Res*. 385, pp. 125–136.

Sengupta, B., Stemmler, M., Laughlin, S.B., and Niven, J.E. (2010). Action potential energy efficiency varies among neuron types in vertebrates and invertebrates. PLoS Comput. Biol. 6, e1000840.

Seo A Y, Joseph A, Dutta D, Hwang JCY , Aris JP and Leeuwenburgh C. (2010) 'New insights into the role of mitochondria in aging: mitochondrial dynamics and more' *Journal of Cell Science*. 123 (15), PP. 2533–2542.

Seog D, Lee D, and Lee S (2004) 'Molecular motor proteins of the kinesin superfamily proteins (KIFs): structure, cargo and disease.', *Journal of Korean Medical Science,* 19(1), pp. 1-7.

Setou, M. et al. (2002) 'Glutamate-receptor-interacting protein GRIP1 directly steers kinesin to dendrites.' *Nature,* 417,pp. 83–87

Setou, M., Nakagawa, T., Seog, D. H. & Hirokawa, Nv (2000). Kinesin superfamily motor protein KIF17 and mLin-10 in NMDA receptor-containing vesicle transport. Science 288, pp. 1796–1802

Shaltouki A, Hsieh C, Kim M, Wang X , (2018)' Alpha-synuclein delays mitophagy and targeting Miro rescues neuron loss in Parkinson's models' . *Acta Neuropathologica*. 136, pp.607–620

Sheftel AD, Stehling O, Pierik AJ, Netz DJ, Kerscher S, Elsässer HP, Wittig I, Balk J, Brandt U, Lill R (2009). 'Human Ind1, an iron–sulfur cluster assembly factor for respiratory complex *I' Mol Cell Biol,* 29, 6059–6073

Sheng, Z.-H. and Cai, Q. (2012) 'Mitochondrial transport in neurons: Impact on synaptic homeostasis and neurodegeneration:. *Nature Reviews Neuroscience*, 13(2), pp. 77–93

Sherer TB, Betarbet R, Testa CM, Seo BB, Richardson JR, et al. (2003). Mechanism of toxicity in rotenone models of Parkinson's disease. *Journal of Neuroscience.* 23: 10756–10764.TB

Shi Y, Ghosh MC, Tong WH, Rouault TA (2009). 'Human ISD11 is essential for both iron–sulfur cluster assembly and maintenance of normal cellular iron homeostasis.' *Hum Mol Genet* 18, pp. 3014–3025

Shiota T et al.,(2015) 'Molecular architecture of the active mitochondrial protein gate', *Science,* 349(6255), pp. 1544-1548.

Shoffner, J. M., Lott, M. T., Voljavec, A. S., Soueidan, S. A., Costigan, D. A. & Wallace, D. C. (1989) 'Spontaneous Kearns-Sayre/chronic external ophthalmoplegia plus syndrome associated with a mitochondrial DNA deletion: a slip-replication model and metabolic therapy.' *Proc. Natl Acad. Sci. USA,* 86, pp.7952–7956

Sieradzan, K. A. & Mann, D. M. (2001) 'The selective vulnerability of nerve cells in Huntington's disease.' *Neuropathol. Appl. Neurobiol.* 27, pp. 1–21

Singh, R., Kaushik, S., Wang, Y., Xiang, Y., Novak, I., Komatsu, M., et al. (2009). 'Autophagy regulates lipid metabolism.' *Nature,* 458,pp. 1131–1135.

Sjöstrand, F. S. (1956). 'The Ultrastructure of Cells as Revealed by the Electron Microscope. International Review of Cytology'. *G. H. Bourne and J. F. Danielli, Academic Press*. Volume 5: 455-533.

Slomovic, S., Laufer, D., Geiger, D. and Schuster, G. (2005) 'Polyadenylation and Degradation of Human Mitochondrial RNA: the Prokaryotic Past Leaves Its Mark', *Molecular and Cellular Biology*, 25(15), pp. 6427-6435.

Smirnova, E., Griparic, L., Shurland, D.L. and van der Bliek, A.M. (2001) 'Dynamin-related protein Drp1 is required for mitochondrial division in mammalian cells', *Mol Biol Cell*, 12(8), pp. 2245-56.

Smit-Rigter, L. et al. (2016) 'Mitochondrial dynamics in visual cortex are limited in vivo and not affected by axonal structural plasticity.' *Curr. Biol*. 26, pp. 2609–2616

Smith Y, Bennett BD, Bolam JP, Parent A, Sadikot AF (1994) 'Synaptic relationships between dopaminergic afferents and cortical or thalamic input in the sensorimotor territory of the striatum in monkey.' *Journal of Comparative Neurology*, 344, pp. 1–19.

Smith Y, Bevan MD, Shink E, Bolam JP (1998) 'Microcircuitry of the direct and indirect pathways of the basal ganglia.' *Neuroscience,* 86, pp. 353–387.

Smith, D. E., Saji, M., Joh, T. H., Reis, D. J. & Pickel, V. M. (1987) 'Ibotenic acid-induced lesions of striatal target and projection neurons: ultrastructural manifestations in dopaminergic and non-dopaminergic neurons and in glia.' *Histol. Histopathol.* 2, pp. 251–263

Smith, M. J., Pozo, K., Brickley, K. & Stephenson, F. A. (2006) 'Mapping the GRIF-1 binding domain of the kinesin, KIF5C, substantiates a role for GRIF-1 as an adaptor protein in the anterograde trafficking of cargoes.' *J. Biol. Chem.* 281, pp. 27216–27228

Snead D and Eliezer D (2014) 'Alpha-Synuclein Function and Dysfunction on Cellular Membranes', *Experimental Neurobiology,* 23(4), pp. 292-313.

Sokoloff, L. (1960). 'The metabolism of the central nervous system in vivo.' In Handbook of Physiology, Section I, *Neurophysiology*, Volume 3, J. Field, H.W. Magoun, and V.E. Hall, eds. (Washington D.C.: American Physiological Society), pp. 1843–1864.

Sorbara, C.D., Wagner, N.E., Ladwig, A., Niki_c, I., Merkler, D., Kleele, T.,Marinkovi_c, P., Naumann, R., Godinho, L., Bareyre, F.M., et al. (2014). Pervasive axonal transport deficits in multiple sclerosis models. Neuron84, pp.1183–1190.

Spillantini MG, Crowther RA, Jakes R, Hasegawa M, Goedert M. (1998) 'alpha-Synuclein in filamentous inclusions of Lewy bodies from Parkinson's disease and dementia with lewy bodies', *Proc. Natl. Acad. Sci,* 95(11), pp. 6469-6473.

Spira PJ, Sharpe DM, Halliday G, Cavanagh J, Nicholson GA (2001). Clinical and pathological features of a Parkinsonian syndrome in a family with an Ala53Thr α-synuclein mutation. Ann Neurol49:pp. 313–319

Squitieri F., Cannella M., Sgarbi G., Maglione V., Falleni A., Lenzi P., Baracca A., Cislaghi G., Saft C., Ragona G., et al. (2006). 'Severe ultrastructural mitochondrial changes in lymphoblasts homozygous for Huntington disease mutation.' *Mech. Ageing Dev.* 127, pp. 217-220

Stefanatos R and Sanz A (2017) 'The role of mitochondrial ROS in the aging brain', *FEBS Letters,* 292(5), pp. 743-758.

Stefanis, L. (2012) 'A-synuclein in Parkinson's disease'.Cold Spring Harbour Perspectives in Medicine. 2(2):a009399.

Stefely JA & Pagliarini D (2017) .Biochemistry of Mitochondrial Coenzyme Q Biosynthesis, *Trends in Biochemical Sciences,* 42(10), pp. 824-843.

Stehling O and Lill R (2013) 'The role of mitochondria in cellular iron-sulfur protein biogenesis: mechanisms, connected processes, and diseases.', *Cold Spring Harbour Perspectives in Medicine,* 5(8), pp. 1-17.

Sterky, F. H., Lee, S., Wibom, R., Olson, L., and Larsson, N.G. (2011). Impaired mitochondrial transport and Parkin-independent degeneration of respiratory chain-deficient dopamine neurons *in vivo*. *Proc. Natl. Acad. Sci. U S A* 108, 12937–12942.

Stoica R, et al. (2016) 'ALS/FTD-associated FUS activates GSK-3beta to disrupt the VAPB-PTPIP51 interaction and ER–mitochondria associations.' *EMBO Rep.* 17, pp. 1326–1342.

Stork CJ, Li YV. (2006) 'Intracellular zinc elevation measured with a 'calcium-specific' indicator duringischemia and reperfusion in rat hippocampus: a question on calcium overload.' *J Neurosci,* 26, pp. 10430–10437.

Stowell, J. N. & Craig, A. M. (1999) 'Axon/dendrite targeting of metabotropic glutamate receptors by their cytoplasmic carboxy-terminal domains.', *Neuron,* 22, pp. 525–536

Stowers, R. S., Megeath, L. J., Górska-Andrzejak, J., Meinertzhagen, I. A. & Schwarz, T. L. (2002) 'Axonal transport of mitochondria to synapses depends on milton, a novel Drosophila protein', *Neuron,* 36, pp. 1063–1077

Subramaniam S & Chesselet M (2013) 'Mitochondrial dysfunction and oxidative stress in Parkinson's disease', *Prog Neurobiol*, pp. 17-32

Sulzer D, Surmeier DJ. (2013) ‘Neuronal vulnerability, pathogenesis, and Parkinson’s disease.’ *Mov Disord.* 28, pp. 41–50.

Sun T, Qiao H, Pan PY, Chen Y, Sheng ZH (2013) ‘Motile axonal mitochondria contribute to the variability of presynaptic strength.’ *Cell Rep,* 4, pp. 413–419.

Surmeier D et al., (2017). ‘Calcium and Parkinson's disease’, *Biochemical and Biophysical Research Communications*. 483, pp.1013-1019

Surmeier D. J., Song W. J., Yan Z. (1996). ‘Coordinated expression of dopamine receptors in neostriatal medium spiny neurons.’ *J. Neurosci.* 16, pp. 6579–6591

Swanson, L.W. (1982) ‘The projections of the ventral tegmental area and adjacent regions: a combined fluorescent retrograde tracer and immunofluorescence study in the rat.’ *Brain Res. Bull.*, 9, pp.321 – 353.

Szabadkai G, Bianchi K, Várnai P, De Stefani D, Wieckowski MR, Cavagna D, Nagy AI, Balla T, and Rizzuto R (2006) 'Chaperone-mediated coupling of endoplasmic reticulum and mitochondrial Ca2+ channels', *Journal of Cell Biology,* 175, pp. 901-911.

Szabo, I. and M. Zoratti (2014). "Mitochondrial channels: ion fluxes and more." Physiol Rev 94(2), pp. 519-608.

Takihara, Y. et al. (2015) ‘In vivo imaging of axonal transport of mitochondria in the diseased and aged mammalian CNS.’ *Proc. Natl Acad. Sci. USA,* 112,pp. 10515–10520

Takihara, Y., Inatani, M., Eto, K., Inoue, T., Kreymerman, A., Miyake, S.,Technikova-Dobrova Z, Sardanelli AM, Speranza F, Scacco S, Signorile A, Lorusso V, Papa S. (2001). Cyclic adenosine monophosphate-dependent phosphorylation of mammalian mitochondrial proteins: enzyme and substrate characterization and functional role. Biochemistry. 20;40(46):pp.13941-7.

Tam Z. Y., Gruber J., Halliwell B. & Gunawan R. (2015) ‘Context-dependent role of mitochondrial fusion-fission in clonal expansion of mtDNA mutations.’ *PLoS Comput. Biol.* 11, pp. e1004183

Tanaka, Y. et al. (1998) ‘Targeted disruption of mouse conventional kinesin heavy chain, kif5B, results in abnormal perinuclear clustering of mitochondria.’, *Cell,* 93, pp.1147–1158 (1998).

Tang, Y. & Zucker, R. S. (1997) ‘Mitochondrial involvement in post-tetanic potentiation of synaptic transmission.’, *Neuron* 18, pp. 483–491

Tawil R., Griggs R.C. (2002) ‘Inclusion body myositis’ *Curr. Opin. Rheumatol*, 14, pp. 653–657.

Taylor, R. W., Barron, M. J., Borthwick, G. M. & other authors (2003).’ Mitochondrial DNA mutations in human colonic crypt stem cells’. *Journal of Clinical Investigation* 112, pp. 1351.

Taylor, R.W. and Turnbull, D.M. (2005) 'Mitochondrial DNA Mutations in Human Disease', *Nature reviews. Genetics*, 6(5), pp. 389-402.

Technikova-Dobrova Z, Sardanelli AM, Speranza F, Scacco S, Signorile A, Lorusso V, Papa S. (2001). Cyclic adenosine monophosphate-dependent phosphorylation of mammalian mitochondrial proteins: enzyme and substrate characterization and functional role. Biochemistry. 20;40(46):13941-7.

Thanos S & Mey J (1995). Type-specific stabilization and target-dependent survival of regenerating ganglion cells in the retina of adult rats. Journal of Neuroscience, 15 (2) , pp. 1057-1079

Thanos, J. Mey (1995) 'Type-specific stabilization and target-dependent survival of regenerating ganglion cells in the retina of adult rats.' *Journal of Neuroscience,* 15, pp. 1057-1079

Thanos, S. & Bonhoeffer, F. (1987). 'Axonal arborization in the developing chick retinotectal system.' *J. comp. Neurol.* 261, pp. 155-164.

Thomas G McWilliams and Miratul MK Muqit (2017) 'PINK1 and Parkin: emerging themes in mitochondrial homeostasis', *Current Opinon in Cell Biology,* 45(), pp. 83-91.

Thompson, L., Andersson, E., Jensen, J. B., Barraud, P., Guillemot, F., Parmar, M. and Björklund, A. (2006). 'Neurogenin 2 identifies a transplantable dopamine neuron precusor in the developing ventral mesencephalon.' *Exp. Neurol.* (in press)

Trifunovic, A., Wredenberg, A., Falkenberg, M. et al., (2004). 'Premature ageing in mice expressing defective mitochondrial DNA polymerase.' *Nature,* 429, pp. 417-423.

Tsukihara T, Aoyama H, Yamashita E, Tomizaki T, Yamaguchi H, Shinzawa-Itoh K (1996). The whole structure of the 13-subunit oxidized cytochrome c oxidase at 2.8 A. *Science.* 272(5265), pp.1136–44.

Tucker, E.J. et al., (2011). 'Mutations in MTFMT Underlie a Human Disorder of Formylation Causing Impaired Mitochondrial Translation.' *Cell Metabolism*, 14(3), pp.428–434.

Turrens JF (2003) 'Mitochondrial formation of reactive oxygen species.' *J Physiol.* 552, pp. 335–344.

Turrens JF, Boveris A. (1980) 'Generation of superoxide anion by the NADH dehydrogenase of bovine heart mitochondria.' *Biochem J.* 191,pp. 421–427.

Twig, G., Elorza, A., Molina, A.J., Mohamed, H., Wikstrom, J.D., Walzer, G., Stiles, L., Haigh, S.E., Katz, S., Las, G., Alroy, J., Wu, M., Py, B.F., Yuan, J., Deeney, J.T., Corkey, B.E. and Shirihai, O.S. (2008) 'Fission and selective fusion govern mitochondrial segregation and elimination by autophagy', *Embo j*, 27(2), pp. 433-46.

Uittenbogaard M and Chiaramello A (2016) 'Mitochondrial Biogenesis: A Therapeutic Target for Neurodevelopmental Disorders and Neurodegenerative Diseases', *Current Pharmaceutical Design,* 20(35), pp. 5574-5593.

Valente EM, Abou-Sleiman PM, Caputo V, Muqit MM, Harvey K, Gispert S, Ali Z, Del Turco D, Bentivoglio AR, Healy DG, Albanese A, Nussbaum R, González-Maldonado R, Deller T, Salvi S, Cortelli P, Gilks WP, Latchman DS, Harvey RJ, Dallapiccola B, Auburger G, Wood NW. (2004). Hereditary early-onset Parkinson's disease caused by mutations in PINK. . *Science.* May 21;304(5674):pp.1158-60.

Valente L, et al. (2007) Infantile encephalopathy and defective mitochondrial DNA translation in patients with mutations of mitochondrial elongation factors EFG1 and EFTu. *Am J Hum Genet*80(1):pp.44-58

Valente et al. (2004) 'Hereditary early-onset Parkinson's disease caused by mutations in PINK1.', *Science,* 304, pp. 1158–1160

Valero T. (2014) 'Mitochondrial biogenesis: pharmacological approaches.' *Curr. Pharm. Des.* 20, pp. 5507–5509.

Valjent E., Bertran-Gonzalez J., Herve D., Fisone G., Girault J. A. (2009). 'Looking BAC at striatal signaling: cell-specific analysis in new transgenic mice.' *Trends Neurosci.* 32, pp. 538–547

Van der Kooy, D., Coscina, D.V. & Hattori, T. (1981) 'Is there a non-dopaminergic nigrostriatal pathway?' *Neuroscience*, 6, pp.345 – 357

Van der Putten, H., Wiederhold, K.H., Probst, A., Barbieri, S., Mistl, C., Danner, S., Kauffmann, S., Hofele, K., Spooren, W.P., Ruegg, M.A., Lin, S., Caroni, P., Sommer, B., Tolnay, M., Bilbe, G., (2000). 'Neuropathology in mice expressing human alpha-synuclein.' *J. Neurosci.* 20, pp. 6021 – 6029.

Van Laar V and Berman s (2009) 'Mitochondrial dynamics in Parkinson's disease', *Experimental Neurology,* 218(2), pp. 247-256.

Van Laar, V. S., Arnold, B., Cassady, S. J., Chu, C. T., Burton, E. A., and Berman, S. B. (2011). 'Bioenergetics of neurons inhibit the translocation response of Parkin following rapid mitochondrial depolarization.' *Hum. Mol. Genet*. 20, pp. 927–940.

Vance JE (2015) 'Phospholipid synthesis and transport in mammalian cells.' , *Traffic,* 16, pp. 1–18.

Vance JE. (1990) 'Phospholipid synthesis in a membrane fraction associated with mitochondria'. *J. Biol. Chem*. 265, pp. 7248–7256

Verstreken, P. et al. (2005) 'Synaptic mitochondria are critical for mobilization of reserve pool vesicles at Drosophila neuromuscular junctions.' *Neuron*, 47,pp. 365–378

Vogel, H. (2001) 'Mitochondrial myopathies and the role of the pathologist in the molecular era', *J Neuropathol Exp Neurol*, 60(3), pp. 217-27.

Volpicelli-Daley LA, Gamble KL, Schultheiss CE, Riddle DM, West AB, Lee VM (2014) 'Formation of alpha-synuclein Lewy neurite-like aggregates in axons impedes the transport of distinct endosomes.' *Mol Biol Cell*, 25, pp. 4010–4023

Wakoto Matsuda, Takahiro Furuta, Kouichi C. Nakamura,Hiroyuki Hioki, Fumino Fujiyama,Ryohachi Arai and Takeshi Kaneko, (2009). 'Single Nigrostriatal Dopaminergic Neurons Form Widely Spread and Highly Dense Axonal Arborizations in the Neostriatum.' *The Journal of Neuroscience*. 29 (2), pp.444–453

Walker, M. C., Ruiz, A., and Kullmann, D. M. (2001). 'Monosynaptic GABAergic signaling from dentate to CA3 with a pharmacological and physiological profile typical of mossy fiber synapses.' *Neuron*, 29, pp. 703–715

Wallace, D. C. (1989). 'Mitochondrial DNA mutations and neuromuscular disease.' *Trends in Genetics* 5, 9-13.

Wallace, D. C. (2005) 'A mitochondrial paradigm of metabolic and degenerative diseases, aging, and cancer: a dawn for evolutionary medicine.' *Annu. Rev. Genet,* 39, pp.359–407 (2005).

Wallace, D.C. (1989) 'Mitochondrial DNA mutations and neuromuscular disease', *Trends Genet*, 5(1), pp. 9-13.

Wallace, D.C., Singh, G., Lott, M.T., Hodge, J.A., Schurr, T.G., Lezza, A.M., Elsas, L.J., 2nd, and Nikoskelainen, E.K. (1988). 'Mitochondrial DNA mutation associated with Leber's hereditary optic neuropathy.' *Science,* 242, pp. 1427–1430.

Wang PT, Garcin PO, Fu M, Masoudi M, St-Pierre P, Pante N, Nabi IR (2015) 'Distinct mechanisms controlling rough and smooth endoplasmic reticulum–mitochondria contacts.', *J Cell Sci* 128, pp. 2759–2765

Wang T, Martin S, Papadopulos A, Harper CB, Mavlyutov TA, Niranjan D, Glass NR, Cooper-White JJ, Sibarita JB, Choquet D, Davletov B, Meunier FA. (2015). Control of autophagosome axonal retrograde flux by presynaptic activity unveiled using botulinum neurotoxin type a. J Neurosci. 2015; 35:pp. 6179–94.

Wang X*, et al.* (2011) PINK1 and Parkin target Miro for phosphorylation and degradation to arrest mitochondrial motility. *Cell,* 147(4), pp. 893-906.

Wang X, Schwarz TL (2009a) Chapter 18. Imaging axonal transport of Mitochondria. Methods Enzymol 457:pp.319–333

Wang, C. and Youle, R.J. (2009) 'The role of mitochondria in apoptosis, *Annu Rev Genet*, 43, pp. 95-118.

Wang, W. *et al.,* 2011. 'FeS/S/FeS(2) redox system and its oxidoreductase-like chemistry in the iron-sulfur world.' *Astrobiology*, 11(5), pp.471–6.

Wang, X. & Schwarz, T. L. (2009) 'The mechanism of Ca2+-dependent regulation of kinesin-mediated mitochondrial motility.',*Cell,* 136, pp. 163–174

Wang, X., Winter, D., Ashrafi, G., Schlehe, J., Wong, Y.L., Selkoe, D., Rice, S., Steen, J., LaVoie, M.J. and Schwarz, T.L. (2011) 'PINK1 and Parkin target Miro for Phosphorylation and degradation to arrest Mitochondrial Motility', *Cell.,* 147(4), pp. 893–906.

Wanrooij, S. and Falkenberg, M. (2010) 'The human mitochondrial replication fork in health and disease', *Biochim Biophys Acta*, 1797(8), pp. 1378-88.

Watanabe S, Ilieva H, Tamada H, Nomura H, Komine O, Endo F, Jin S, Mancias P, Kiyama H, Yamanaka K (2016) 'Mitochondria-associated membrane collapse is a common pathomechanism in SIGMAR1- and SOD1-linked ALS.' *EMBO Mol Med.*

Watt, I.N., Montgomery, M.G., Runswick, M.J., Leslie, A.G.W. and Walker, J.E. (2010) 'Bioenergetic cost of making an adenosine triphosphate molecule in animal mitochondria', *Proceedings of the National Academy of Sciences*, 107(39), pp. 16823-16827.

Wauer, T. (2015) 'Mechanism of phospho-ubiquitin-induced PARKIN activation', *Nature*, 524(7565), pp. 370–374.

Webber, E., Li, L. & Chin, L. S. (2008) 'Hypertonia-associated protein Trak1 is a novel regulator of endosometo-lysosome trafficking', *J. Mol. Biol.* 382,pp. 638–651

Weber, K., Wilson, J.N., Taylor, L., Brierley, E., Johnson, M.A., Turnbull, D.M. and Bindoff, L.A. (1997) 'A new mtDNA mutation showing accumulation with time and restriction to skeletal muscle', *American Journal of Human Genetics*, 60(2), pp. 373-380.

Weihofen, A., Thomas, K.J., Ostaszewski, B.L., Cookson, M.R. and Selkoe, D.J. (2009) 'Pink1 forms a Multiprotein complex with Miro and Milton, linking pink1 function to Mitochondrial trafficking ', Biochemistry, 48(9), pp. 2045–2052.

Welte, M. A. 'Bidirectional transport along microtubules'. *Curr. Biol.* 14, pp. 525–537

Wendou Yu, Yaping Sun, Su Guo and Bingwei Lu , (2011). 'The PINK1/Parkin pathway regulates mitochondrial.' *Human Molecular Genetics.* 20 (16), pp.3227–3240

Werth, J. L. & Thayer, S. A. (1994) 'Mitochondria buffer physiological calcium loads in cultured rat dorsal root ganglion neurons.' *J. Neurosci.* 14,pp. 348–356

Whatley JM, John P, Whatley FR (1979). 'From extracellular to intracellular: The establishment of mitochondria and chloroplasts.' *Proc R Soc Lond B Biol Sci*, 204, pp. 165–187

Whittaker et al., (2015) 'Epilepsy in Adults With Mitochondrial Disease: A Cohort Study', *Annals of Neurology,* 78(1), pp. 949-957.

Whitworth, A.J. and Pallanck, L.J. (2009) 'The PINK1/Parkin pathway: A mitochondrial quality control system?', *Journal of Bioenergetics and Biomembranes*, 41(6), pp. 499–503.

Wieckowski MR, Giorgi C, Lebiedzinska M, Duszynski J, Pinton P (2009). 'Isolation of mitochondria-associated membranes and mitochondria from animal tissues and cells' *Nat Protoc,* 4, pp. 1582–1590

Wiedemann N, Urzica E, Guiard B, Müller H, Lohaus C, Meyer HE, Ryan MT, Meisinger C, Mühlenhoff U, Lill R, et al. (2006). 'Essential role of Isd11 in iron–sulfur cluster synthesis on Isu scaffold proteins.' *EMBO J,* 25, pp. 184–195

Wilkens, V., Kohl, W. and Busch, K. (2013) 'Restricted diffusion of OXPHOS complexes in dynamic mitochondria delays their exchange between cristae and engenders a transitory mosaic distribution', *Journal of Cell Science*, 126(1), p. 103.

Winklhofer, K. F. & Haass, C. (2010) 'Mitochondrial dysfunction in Parkinson's disease.' *Biochim. Biophys. Acta*, 1802,pp. 29–44

Winslow AR, Chen CW, Corrochano S, Acevedo-Arozena A, Gordon DE, Peden AA, Lichtenberg M, Menzies FM, Ravikumar B, Imarisio S et al (2010) 'alpha-Synuclein impairs macroautophagy: implications for Parkinson's disease.', *J Cell Biol,* 190, pp. 1023–1037.

Winslow, A. R. et al. (2010) 'α-Synuclein impairs macroautophagy: implications for Parkinson's disease.', *J. Cell Biol*. 190,pp. 1023–1037
Wittig & Schägger (2008). Structural organization of mitochondrial ATP synthase.. *Biochimica et Biophysica Acta*. 1777 (7-8), pp. 592 -598.

Wohlgemuth S. E., Seo A. Y., Marzetti E., Lees H. A., Leeuwenburgh C. (2010). 'Skeletal muscle autophagy and apoptosis during aging: Effects of calorie restriction and life-long exercise.' *Exp. Gerontol.* 45, pp. 138-148

Wong ED, Wagner JA, Gorsich SW, McCaffery JM, Shaw JM, Nunnari JM. (2000) 'The dynamin-related GTPase, Mgm1p, is an intermembrane space protein required for maintenance of fusion competent mitochondria.' *J. Cell Biol,*151, pp. 341–352

Wong, E. & Cuervo, A. M. (2010) 'Autophagy gone awry in neurodegenerative diseases.' *Nat. Neurosci.* 13, pp. 805–811

Wong, L. J., Perng, C. L., Hsu, C. H., Bai, R. K., Schelley, S., Vladutiu, G. D. et al. (2003) 'Compensatory amplification of mtDNA in a patient with a novel deletion/duplication and high mutant load.' *J. Med. Genet.* 40, pp. 125

Wong, R. W., Setou, M., Teng, J., Takei, Y. & Hirokawa, N. (2002) 'Overexpression of motor protein KIF17 enhances spatial and working memory in transgenic mice.' *Proc. Natl Acad. Sci. USA,* 99, pp.14500–14505

Wood-Kaczmar A., Gandhi S., Yao Z., Abramov A. Y., Miljan E. A., Keen G., Stanyer L., Hargreaves I., Klupsch K., Deas E., et al. (2008). 'PINK1 is necessary for long term survival and mitochondrial function in human dopaminergic neurons.' *PLoS One* 3, pp. 2455

Wray S, Self M, Lewis PA, Taanman JW, Ryan NS, Mahoney CJ, Liang Y, Devine MJ, Sheerin UM, Houlden H et al (2012) 'Creation of an open-access, mutation-defned fbroblast resource for neurological disease research.' *PLoS ONE,* 7, pp. 43099.

Wu H, Xu J, Pang ZP, Ge W, Kim KJ, Blanchi B, Chen C, Südhof TC, Sun YE (2007) 'Integrative genomic and functional analyses reveal neuronal subtype differentiation bias in human embryonic stem cell lines', *Proc Natl Acad Sci U S A,*104, pp. 13821–138266.

Wu, H., Wei, H., Sehgal, S. A., Liu, L., and Chen, Q. (2016). 'Mitophagy receptors sense stress signals and couple mitochondrial dynamic machinery for mitochondrial quality control.' *Free Radic. Biol. Med.* 100,pp. 199–209.

Wu, W. et al. (2016) 'FUNDC1 regulates mitochondrial dynamics at the ER–mitochondrial contact site under hypoxic conditions.' *EMBO J.* 35, pp. 1368–1384

Xia, D., Yu, C.A., Kim, H., Xia, J.Z., Kachurin, A.M., Zhang, L., Yu, L. and Deisenhofer, J. (1997) 'Crystal structure of the cytochrome bc1 complex from bovine heart mitochondria', *Science*, 277(5322), pp. 60-6.

Xie W, Chung KK (2012) 'Alpha-synuclein impairs normal dynamics of mitochondria in cell and animal models of Parkinson's disease.' *J Neurochem,* 122, pp. 404–414.

Xu, W., Tan, L. & Yu, J. T. (2015) 'Link between the SNCA gene and parkinsonism.' *Neurobiol. Aging,* 36, pp. 1505–1518

Yamamoto, A., and Simonsen, A. (2011). 'The elimination of accumulated and aggregated proteins: a role for aggrephagy in neurodegeneration.' *Neurobiol. Dis,* 43,pp. 17–28.

Yamano, K., and Youle, R. J. (2013). 'PINK1 is degraded through the N-end rule pathway.', *Autophagy,* 9, pp. 1758–1769.

Yamauchi K et al., (2009) 'FGF8 signaling regulates growth of midbrain dopaminergic axons by inducing semaphorin 3F.', *Journal of Neuroscience,* 29(13), pp. 4044-4055.

Yang Y, Gehrke S, Imai Y, Huang Z, Ouyang Y, Wang JW, Yang L, Beal MF, Vogel H, Lu B. (2006) 'Mitochondrial pathology and muscle and dopaminergic neuron degeneration caused by inactivation of Drosophila Pink1 is rescued by Parkin.', *Proc Natl Acad Sci U S A.* 103, pp. 10793–10798.

Yang Y, Ouyang Y, Yang L, Beal MF, McQuibban A, Vogel H, Lu B (2008) 'Pink1 regulates mitochondrial dynamics through interaction with the fission/fusion machinery.' *Proc Natl Acad Sci U S A.* 105, pp. 7070–7075.

Yang, C . (2009). *A drosophila melanogaster model of pink1-associated Parkinson's disease*. Available at: https://searchworks.stanford.edu/view/7949319 (Accessed: 24 April 2016).

Yang, J. Y. & Yang, W. Y. (2013) 'Bit-by-bit autophagic removal of parkin-labelled mitochondria.' *Nat. Commun.* 4, pp. 2428

Yang, M. Y., et al. (2002). "Biased incorporation of ribonucleotides on the mitochondrial L-strand accounts for apparent strand-asymmetric DNA replication." Cell 111(4), pp. 495-505.

Yang, Y. et al. (2006) 'Mitochondrial pathology and muscle and dopaminergic neuron degeneration caused by inactivation of Drosophila Pink1 is rescued by Parkin.' *Proc. Natl. Acad. Sci. U.S.A,* 103, pp.10793–10798

Yang, Y. et al. (2008) 'Pink1 regulates mitochondrial dynamics through interaction with the fission/fusion machinery.', *Proc. Natl. Acad. Sci. U.S.A.* 105, pp. 7070–7075

Yi M, Weaver D, and Hajnóczky G (2004) 'Control of mitochondrial motility and distribution by the calcium signal a homeostatic circuit', *Journal of Cell Biology,* 167(4), pp. 661–672.

Yoshida M, Muneyuki E, Hisabori T (2001). ATP synthase – a marvellous rotary engine of the cell. *Nature Reviews Molecular Cell Biology*. 2(9):pp.669–77

Yoshida S and Plant S, (1992). 'Mechanism of release of Ca2+ from intracellular stores in response to ionomycin in oocytes of the frog Xenopus laevis.' *The Journal of Physiology*, 458, pp. 307–318.

Youdim MB, Edmondson D, Tipton KF. (2006) 'The therapeutic potential of monoamine oxidase inhibitors.', *Nat Rev Neurosci,* 7, pp. 295–309.

Youle RJ & Strasser A(2008) 'The BCL-2 protein family: opposing activities that mediate cell death.', *Nature Reviews,* 9(), pp. 47-59.

Youle, R.J. and van der Bliek, A.M. (2012) 'Mitochondrial fission, fusion, and stress.', *Science* 337, pp. 1062–1065

Yue Z (2007). Regulation of neuronal autophagy in axon: implication of autophagy in axonal function and dysfunction/degeneration. Autophagy. 2007; 3:pp.139–41.

Yung KL, Bolam JP,Smith AD, Hersch SM, Ciliax BJ, Levey AI (1995) 'Ultrastructural localisation of D1 and D2 dopamine receptors in the basal ganglia of the rat by light and electron microscopic immunocytochemistry.' *Neuroscience,* 65, pp. 709–730.

Yuste R, Denk W. (1995). 'Dendritic spines as basic functional units of neuronal integration.' *Nature,* 375, pp. 682–684.

Zander JF, Münster-Wandowski A, Brunk I, Pahner I, Gómez-Lira G, Heinemann U, Gutiérrez R, Laube G, Ahnert-Hilger G. (2010). 'Synaptic and vesicular coexistence of VGLUT and VGAT in selected excitatory and inhibitory synapses.' *J Neurosci.* 30, pp. 7634–7645.

Zeviani, M., Moraes, C. T., DiMauro, S., Nakase, H., Bonilla, E., Schon, E. A. et al. 91988) 'Deletions of mitochondrial DNA in Kearns-Sayre syndrome.' *Neurology*, 38, pp.1339–1346

Zhang X, Zhou JY, Chin MH, Schepmoes AA, Petyuk VA, Weitz KK, Petritis BO, Monroe ME, Camp DG, Wood SA, Melega WP, Bigelow DJ, Smith DJ, Qian WJ, Smith RD (2010) Region-specific protein abundance changes in the brain of MPTP-induced Parkinson's disease mouse model. Journal of proteome research 9:PP.1496–1509.

Zhang, C. L., Ho, P. L., Kintner, D. B., Sun, D. & Chiu, S. Y. (2010) 'Activity-dependent regulation of mitochondrial motility by calcium and Na/K-ATPase at nodes of Ranvier of myelinated nerves.' *J. Neurosci*. 30, pp.3555–3566

Zhang, J., and Ney, P. A. (2009). 'Role of BNIP3 and NIX in cell death, autophagy, and mitophagy.' *Cell Death Differ.* 16, pp. 939–946.

Zhang, X. et al., (2009). 'Ochratoxin A induces apoptosis in neuronal cells.' *Genes & nutrition*, 4(1), pp.41–8.

Zhou R, Yazdi AS, Menu P, Tschopp J. (2011) ‘A role for mitochondria in NLRP3 inflammasome activation.’ *Nature*, 469, pp. 221–225

Zhou, B. et al. (2016) ‘Facilitation of axon regeneration by enhancing mitochondrial transport and rescuing energy deficits.’ *J. Cell Biol.* 214, pp 103–119

Zhou, C. et al. (2008) ‘The kinase domain of mitochondrial PINK1 faces the cytoplasm.’ *Proc. Natl. Acad. Sci. U.S.A.* 105, pp. 12022–12027

Zhou, C., Huang, Y., Shao, Y., Jessica, Prou, D., Perier, C., Dauer, W., Schon, E.A., Przedborski, S. (2008) The kinase domain of mitochondrial PINK1 faces the cytoplasm. *Proceedings of. National Academy of Sciences.* 105(33):12022-7

Zhu X , Perry G, Smith M, Wang X (2014) 'Abnormal mitochondrial dynamics in the pathogenesis of Alzheimer's isease.', *Journal of Alzheimer's Disease,* 33(01), pp. 253–S262.

Zhu, J., Vinothkumar, K.R. and Hirst, J. (2016) 'Structure of mammalian respiratory complex I', *Nature*, 536(7616), pp. 354-358.

Ziviani, E. et al. (2010) ‘Drosophila parkin requires PINK1 for mitochondrial translocation and ubiquitinates mitofusin.’ *Proc. Natl. Acad. Sci. U.S.A*. 107, pp.5018–5023

Zollo, O., Tiranti, V. and Sondheimer, N. (2012) 'Transcriptional requirements of the distal heavy-strand promoter of mtDNA', Proc Natl Acad Sci U S A, 109 (17), PP. 6508-6512

Zu-Hang Sheng Z and Qian Cai. (2012). Mitochondrial transport in neurons: impact on synaptic homeostasis and neurodegeneration. *Nature Reviews Neuroscience*. 13 (1), 77-93.